



BIBLIOTHÈQUE

CÉGEP DE L'ABITIBI-TÉMISCAMINGUE
UNIVERSITÉ DU QUÉBEC EN ABITIBI-TÉMISCAMINGUE

Mise en garde

La bibliothèque du Cégep de l'Abitibi-Témiscamingue et de l'Université du Québec en Abitibi-Témiscamingue (UQAT) a obtenu l'autorisation de l'auteur de ce document afin de diffuser, dans un but non lucratif, une copie de son œuvre dans [Depositum](#), site d'archives numériques, gratuit et accessible à tous. L'auteur conserve néanmoins ses droits de propriété intellectuelle, dont son droit d'auteur, sur cette œuvre.

Warning

The library of the Cégep de l'Abitibi-Témiscamingue and the Université du Québec en Abitibi-Témiscamingue (UQAT) obtained the permission of the author to use a copy of this document for nonprofit purposes in order to put it in the open archives [Depositum](#), which is free and accessible to all. The author retains ownership of the copyright on this document.

POLYTECHNIQUE MONTRÉAL

affiliée à l'Université de Montréal

et

l'Université du Québec en Abitibi-Témiscamingue

et

Universidad de Antofagasta

**Flotation Process of Porphyry Copper Ore to Prevent Acid Mine Drainage
from Tailings and Waste Rock: A Cleaner Production Approach**

YESICA LORENA BOTERO

Département des génies civil, géologique et des mines

Thèse présentée en vue de l'obtention du diplôme de *Philosophiae Doctor*

Génie minéral

Avril 2023

© Yesica Lorena Botero, 2023.

POLYTECHNIQUE MONTRÉAL

affiliée à l'Université de Montréal

et

l'Université du Québec en Abitibi-Témiscamingue

et

Universidad de Antofagasta, Chile

Cette thèse intitulée:

Flotation Process of Porphyry Copper Ore to Prevent Acid Mine Drainage from Tailings and Waste Rock: A Cleaner Production Approach

présenté par **Yesica Lorena BOTERO**

en vue de l'obtention du diplôme de *Philosophiae Doctor*

a été dûment accepté par le jury d'examen constitué de :

Richard SIMON, président

Isabelle DEMERS, membre et directrice de recherche

Luis CISTERNAS, membre et directeur de recherche

Mostafa BENZAAZOUA, membre et codirecteur de recherche

Lucie COUDERT, membre

Ricardo JELDRES, membre

Kristian WATERS, membre externe

ACKNOWLEDGEMENTS

This work was developed under a double degree agreement between the University of Antofagasta (Chile) and University of Quebec in Abitibi Temiscamingue (Canada).

I would like to express my deepest appreciation to Professor Luis Cisternas for being my supervisor and for encouraging me to pursue a double degree with the University of Quebec in Abitibi Temiscamingue (UQAT), Canada.

I would like also to express my sincere gratitude to Professor Isabelle Demers, who was my supervisor at UQAT, for her support and guidance during the realization of the double degree for my PhD studies.

I would like also to express my sincere gratitude to Professor Mostafa Benzaazoua, who was my co-advisor at UQAT, for encouraging me to pursue a double degree with the UQAT, and also for his support and guidance during the realization of the double degree for my Ph.D. studies.

I also thank Project Anillo ACM 170005 “Tailings & Sea Water: From end-of-pipe toward cleaner production, Project Anillo ACT210027 “Integrating circular economy strategies in mineral processing”, ANID scholarship Grant 21210801, UQAT scholarship, and the foundation J.A. DeSève scholarship.

To my mother, my best friend and confidant.

RÉSUMÉ

Cette thèse vise à approfondir les connaissances sur la prévention du drainage minier acide (DMA) des minerais de cuivre porphyriques basée sur la flottation dans une perspective de production plus propre. Ainsi, il a été proposé d'étudier des alternatives qui génèrent des déchets solides avec de faibles niveaux d'espèces acidifiantes responsables de la génération de DMA. Considérant que les principaux déchets solides sont les résidus et les stériles (WR), deux aspects ont été étudiés: le premier était la concentration d'un minéral avec la génération de résidus à faible teneur en espèces acidifiantes, et le second était l'extraction de métaux précieux et espèces acidifiantes de WR par désulfuration (voir Graphic Abstract).

Pour obtenir des résidus à faible teneur en espèces acidifiantes, deux types de stratégies de flottation ont été proposées, la flottation en vrac et la flottation sélective. À cette fin, le premier objectif était axé sur la flottation en vrac et sélective des minéraux purs covellite et pyrite, et d'un minerai de cuivre porphyrique provenant de l'exploitation minière de Chuqicamata au Chili. La flottation de la covellite pure a fait l'objet de l'étude non seulement parce que le comportement de la covellite est peu étudié mais aussi parce que le minerai de cuivre porphyrique utilisé dans ce travail était minéralogiquement composé de covellite (0,22%), chalcocite (0,21%), chalcopirite (0,06) et pyrite (0,69%). Il a donc fallu approfondir la connaissance du comportement de la covellite lors de sa flottation pour reproduire les résultats obtenus avec le minerai de cuivre porphyrique. La méthode utilisée pour atteindre cet objectif consistait à utiliser deux types de collecteurs, le thionocarbamate d'O-isopropyl-N-éthyle (IPETC) et le xanthate d'amyle de potassium (PAX), pour évaluer l'effet de ces collecteurs en vrac et en flottation sélective. Le résultat permet d'obtenir les paramètres optimaux pour exécuter la flottation en vrac et la flottation sélective, permettant des récupérations de covellite et de pyrite par flottation en vrac de 93,4 et 90,2 %, respectivement, et pour la flottation sélective, des récupérations de covellite et de pyrite de 80,5 et 20,3 %, respectivement. Les résultats de la flottation du minerai de cuivre porphyrique confirment que l'IPETC a une meilleure affinité pour le cuivre, tandis que le PAX a une meilleure affinité pour le fer. Néanmoins, l'IPETC peut être utilisé comme collecteur sélectif ou vrac en ne faisant varier que le pH et en utilisant de faibles concentrations (2×10^{-5}). Après tout, il n'est pas nécessaire d'utiliser différents collecteurs pour la flottation en vrac et sélective.

Lors de l'étude de la flottation de la covellite, il a été nécessaire d'étudier les mécanismes d'adsorption des collecteurs à la surface de la covellite. Par conséquent, le deuxième objectif s'est concentré sur l'étude de l'adsorption des collecteurs IPETC et PAX sur la surface de la covellite. Des méthodes expérimentales et de simulation ont été utilisées pour atteindre cet objectif. Les méthodes expérimentales comprenaient des techniques de caractérisation telles que la spectroscopie infrarouge à transformée de Fourier (FT-IR) et la spectroscopie photoélectronique à rayons X (XPS). Dans la méthode de simulation, la théorie fonctionnelle de la densité (DFT) a été appliquée pour l'analyse de surface de covellite. Les résultats montrent que les mécanismes d'adsorption de l'IPETC et du PAX dans la surface de la covellite étaient différents. Le FT-IR nous permet d'identifier que le mécanisme d'adsorption de PAX sur la surface de la covellite passe par la formation de Cu-amylxanthate (CuAX) et de dixantogène (AX)₂. Le mécanisme d'adsorption de l'IPETC suggère que la liaison est facilitée par le S du collecteur avec des atomes de Cu à la surface de la covellite. Les spectres XPS ont montré que le mécanisme d'adsorption de PAX sur la surface de la covellite passe principalement par C 1s et S 2p. Le mécanisme d'adsorption de l'IPETC sur la surface de la covellite suggère que la liaison est activée par l'élément—S du collecteur avec des atomes de Cu à la surface de la covellite. Enfin, les calculs DFT prédisent que pour l'IPETC, la liaison avec le cuivre ne s'est produite qu'à travers le groupe C—S. Pour PAX, la liaison avec le cuivre s'est produite via les groupes C = S et C – S. Ces résultats nous ont permis de comprendre le comportement du collecteur et de choisir le bon collecteur en fonction du type de flottation, flottation en vrac ou flottation sélective.

L'introduction de la désulfuration dans le processus de flottation transforme le processus en un processus de concentration polymétallique. L'analyse et la conception de ce type de procédé sont rares dans la littérature. Ainsi, cette question a été considérée dans le troisième objectif, la conception de circuits de flottation pour les minéraux polymétalliques incluant la désulfuration. Deux aspects ont été étudiés ; premièrement, l'adaptation de la méthodologie basée sur l'optimisation pour les minéraux monométalliques aux minéraux polymétalliques ; deuxièmement, les données de flottation fournies par le minerai Cu-Ni-EGP de la mine Kevitsa ont été utilisées pour déterminer la conception optimale des circuits de flottation séquentiels et intégrés pour ce minerai polymétallique. Le concentrateur Kevitsa utilise un circuit de flottation séquentiel cuivre-nickel. Par conséquent, l'idée était de reconcevoir ce circuit en utilisant différentes stratégies et analyses de celui-ci. Dans tous les cas étudiés, la désulfuration a été incluse comme sujet pertinent.

Les résultats montrent que la stratégie utilisée pour les minéraux monométalliques peut être appliquée aux minéraux polymétalliques. Cela a été possible car, comme dans le cas des minéraux monométalliques, il a été observé qu'il existe peu de conceptions optimales pour un problème donné pour des variations importantes dans les récupérations des étapes de flottation. Ceci a été analysé en flottation fractionnée sélective et en vrac. Dans ces cas, il existe un produit intermédiaire (concentré ou résidus) qui est ensuite traité. De plus, une nouvelle idée a été introduite au niveau conceptuel : les circuits de flottation intégrés. Dans un circuit de flottation intégré, il n'y a pas de flottation fractionnée ni de produit intermédiaire et les étapes de flottation sélective et en vrac sont combinées pour atteindre l'objectif de séparation. L'étude de ces configurations possibles de circuit de flottation nous donne une vision plus globale de la meilleure stratégie d'un point de vue économique et environnemental.

Par ailleurs, abordant le traitement des WR, le quatrième objectif était d'évaluer la faisabilité du retraitement des WR d'un minerai de cuivre porphyrique par le procédé de désulfuration et d'étudier le comportement géochimique des matériaux désulfurés. L'objectif était de classer le WR en fractions réactives et non réactives, sur la base du concept du diamètre d'encapsulation physique des sulfures (DPLS), en utilisant la taille des particules des fractions sélectionnées et le degré de libération des sulfures pour l'analyse. Par conséquent, six fractions ont été évaluées F6 (>5 mm) désignées de grande taille, F5 (-5 mm à +2,4 mm), F4 (-2,4 mm à +850 μm), F3 (-850 μm à +300 μm), F2 (-300 μm à +53 μm) et F1 (-53 μm). Les résultats montrent que le DPLS était < 2,4 mm ; ainsi, une taille de particule supérieure à 2,4 mm a été considérée comme non réactive. Pour la fraction réactive, le procédé de désulfuration a été utilisé. La cellule de Denver a été utilisée pour la fraction fine (<212 μm), et la technologie de flottation en lit fluidisé (Hydrofloat) pour la fraction grossière (-850 μm à +212 μm). Le comportement géochimique a également été étudié à l'aide des essais en colonne et de mini-cellules d'altération pour la grande granulométrie et le WR désulfuré, respectivement. Les résultats géochimiques montrent que les WR de grande taille (>5mm) et désulfurés ne produiront pas de DMA puisque les valeurs de pH étaient comprises entre 7 et 8. De plus, les contaminants lessivés (Fe, Cu, Zn, Pb) sont restés en dessous des limites réglementaires fixées par Directive 019 (Québec, Canada).

Cette thèse fournit de nouvelles connaissances pour améliorer la gestion des résidus et des WR dans l'exploitation minière du cuivre porphyrique. La nouveauté de cette étude consiste à considérer le traitement de désulfuration des résidus et des WR d'un minerai polymétallique à un

stade précoce du processus de flottation encadré dans le concept de production plus propre. Par conséquent, les études fondamentales, la flottation de minerais réels et l'utilisation de modèles mathématiques pour optimiser les circuits de flottation nous permettent d'évaluer le circuit de flottation du point de vue de la chimie, de l'équipement et opérationnel, permettant l'analyse du problème de manière intégrée. L'importance de cette thèse repose sur l'apport de connaissances et d'outils pour la recherche future qui vise à travailler avec des minerais de cuivre porphyrique.

Mots clés : résidus, stériles, drainage minier acide, flottation, production plus propre, optimisation, valorisation des métaux, désulfuration, minerai de cuivre porphyrique, minerai polymétallique.

ABSTRACT

This dissertation aims to deepen knowledge in relation to the prevention of the acid mine drainage (AMD) of porphyry copper ores based on flotation from a cleaner production perspective. Thus, it was proposed to investigate alternatives that generate solid waste with low levels of acidifying species responsible for the generation of AMD. Considering that the main solid waste from mining comprises tailings and waste rock (WR), two aspects were investigated: the concentration of a mineral through the generation of tailings with low acidifying species content, and the extraction of valuable metallic species and acidifying species from WR by desulfurization (see Graphic Abstract).

To obtain tailings with low acidifying species content, two types of flotation strategies were proposed: bulk and selective flotation. For this purpose, the first objective was focused on the bulk and selective flotation of the pure minerals covellite and pyrite and a porphyry copper ore from the Chuqicamata mining operation in Chile. Flotation of the pure covellite was the focus of the study not only because the behavior of covellite has barely been studied, but also because the porphyry copper ore used in this work was mineralogically composed of covellite (0.22%), chalcocite (0.21%), chalcopyrite (0.06%), and pyrite (0.69%). Therefore, it was necessary to deepen knowledge in relation to the behavior of covellite during its flotation to reproduce the results obtained with the porphyry copper ore. The method used to accomplish this goal involved using two types of collectors, O-isopropyl-N-ethyl thionocarbamate (IPETC) and potassium amyl xanthate (PAX), to assess the effect of these collectors in bulk and selective flotation. The results enabled determination of the optimum parameters to run the bulk and selective flotation, providing covellite and pyrite recoveries of 93.4 and 90.2%, respectively, for bulk flotation, and recoveries of 80.5 and 20.3%, respectively, for selective flotation. The results of the porphyry copper ore flotation confirm that IPETC has a better affinity for copper, whereas PAX has a better affinity for iron. Nevertheless, IPETC can be used as a selective or bulk collector varying only the pH and using low concentrations (2×10^{-5}). After all, it is not necessary to use different collectors for bulk and selective flotation.

During the study of covellite flotation, it was necessary to investigate the adsorption mechanisms of collectors on the covellite surface. Therefore, the second objective was focused on studying the adsorption of the collectors IPETC and PAX on the covellite surface. Both experimental and

simulation methods were used to achieve this goal. Experimental methods included characterization techniques such as Fourier-transform infrared spectroscopy (FT-IR) and X-ray photoelectron spectroscopy (XPS). In the simulation method, density functional theory (DFT) was applied for covellite surface analysis. The results show that the adsorption mechanisms of IPETC and PAX on the covellite surface were different. FT-IR enabled us to identify that the adsorption mechanism of PAX on the covellite surface is through the formation of Cu-amyloxanthate (CuAX) and dixantogen (AX)₂. The adsorption mechanism of IPETC suggests the binding is facilitated by the S of the collector with Cu atoms on the covellite surface. The XPS spectra show that the adsorption mechanism of PAX on the covellite surface is principally through C 1s and S 2p. The adsorption mechanism of IPETC on the covellite surface suggests that the bonding is enabled through the —S element of the collector with Cu atoms on the covellite surface. Finally, the DFT calculations predict that for IPETC, the bonding with copper only occurred through the C—S group. For PAX, the bonding with copper occurred through the C=S and C—S groups. These results enable us to understand the collector's behavior and to choose the right collector depending on the flotation type, i.e., either bulk or selective flotation.

Introducing desulfurization within the flotation process transforms the process into one of polymetallic concentration. The analysis and design of this type of process are scarce in the literature. As a result, this issue was considered in the third objective by designing flotation circuits for polymetallic minerals that include desulfurization. Two aspects were studied: first, the adaptation of the optimization-based methodology for monometallic minerals to polymetallic minerals; second, flotation data provided by the Kevitsa mine Cu-Ni-PGE ore were utilized to determine the optimal design for sequential and integrated flotation circuits for this polymetallic ore. The Kevitsa concentrator employs a copper–nickel sequential flotation circuit. Therefore, the idea was to redesign this circuit using different strategies and analyses of it. In all the cases studied, desulfurization was included as a relevant topic. The results show that the strategy utilized for monometallic minerals can be applied to polymetallic minerals. This was possible because, as in the case of monometallic minerals, it was observed that there are few optimal designs for a given problem that provide significant variations in the flotation stage recoveries. This was analyzed in both selective and bulk fractional flotation. In these cases, there is an intermediate product (concentrate or tailings) that is further processed. In addition, a new idea was introduced at the conceptual level: integrated flotation circuits. In an integrated flotation circuit, there is no fractional

flotation or intermediate product, and both selective and bulk flotation stages are combined to reach the separation goal. Studying these possible flotation circuit configurations gives us a more comprehensive view of the best strategy from an economic and cleaner production point of view.

Addressing the treatment of WR, the fourth objective was to evaluate the feasibility of reprocessing the WR of a porphyry copper ore through the desulfurization process and to study the geochemical behavior of the desulfurized materials. The aim was to classify the WR into reactive and non-reactive fractions, based on the concept of the diameter of the physical locking of sulfides (DPLS), using the particle sizes of the selected fractions and sulfides and their liberation degree for the analysis. Therefore, six fractions were assessed, with F6 (>5mm) designating large particle sizes, followed by F5 (-5 mm to +2.4mm), F4 (-2.4mm to +850 μm), F3 (-850 μm to +300 μm), F2 (-300 μm to +53 μm) and F1 (-53 μm). The results show that the DPLS was < 2.4mm; thus, a particle size larger than 2.4 mm was considered non-reactive. For the reactive fraction, the desulfurization process was conducted. A Denver flotation cell was used for the fine fraction (<212 μm), and fluidized bed flotation technology (HydroFloat) was used for the coarse fraction (-850 μm to +212 μm). The geochemical behavior was also studied using column and weathering cell tests for the large particle size and the desulfurized WR, respectively. The geochemical results show that the large size (>5mm) and desulfurized WR did not produce AMD, since the pH values were between 7 and 8. In addition, the leached contaminants (Fe, Cu, Zn, and Pb) remained below the regulatory limits set by Directive 019 (Quebec, Canada).

This dissertation provides new knowledge to improve tailings and WR management in porphyry copper mining. The study's novelty lies in its consideration of the desulfurization treatment of both the tailings and WR of a polymetallic ore in an early stage of the flotation process, framed by the concept of cleaner production. Therefore, fundamental studies, the flotation of real ores, and the use of mathematical models for optimizing flotation circuits enable us to assess the flotation circuit from chemistry, equipment, and operational perspectives, allowing for the analysis of the problem in an integrated way. The importance of this dissertation relies on providing knowledge and tools for future research that seeks to focus on porphyry copper ores.

Keywords: tailings, waste rock, acid mine drainage, flotation, cleaner production, optimization, metal valorization, desulfurization, porphyry copper ore, polymetallic ore.

RESUMEN

Esta disertación tiene como objetivo profundizar en el conocimiento de la prevención del drenaje ácido de mina (DAM) de minerales de pórfido de cobre basados en flotación desde una perspectiva de producción más limpia. Por lo tanto, se propuso investigar alternativas que generen residuos sólidos con bajos niveles de especies acidificantes responsables de la generación de DAM. Teniendo en cuenta que los principales residuos sólidos son los relaves y los desmontes (WR), se investigó dos aspectos: el primero fue la concentración de un mineral con la generación de relaves con bajo contenido de especies acidificantes, y el segundo fue la extracción de metales valiosos y especies acidificantes de WR por desulfuración (ver Graphic abstract).

Para obtener relaves con bajo contenido de especies acidificantes, se propusieron dos tipos de estrategias de flotación, flotación bulk y flotación selectiva. Para ello, el primer objetivo se centró en la flotación bulk y selectiva de los minerales puros covelita y pirita, y un mineral de pórfido de cobre de la operación minera Chuqicamata en Chile. La flotación de la covelita pura fue el foco del estudio no solo porque el comportamiento de la covelita es poco estudiado sino también porque el mineral de pórfido de cobre utilizado en este trabajo estaba compuesto mineralógicamente por covelita (0,22%), calcocita (0,21%), calcopirita (0,06) y pirita (0,69%). Por lo tanto, fue necesario profundizar en el conocimiento del comportamiento de la covelita durante su flotación para reproducir los resultados obtenidos con el mineral de pórfido de cobre. El método utilizado para lograr este objetivo fue el uso de dos tipos de colectores, O-isopropil-N-etil tionocarbamato (IPETC) y amilxantato de potasio (PAX), para evaluar el efecto de estos colectores en flotación bulk y selectiva. Los resultados permitieron obtener los parámetros óptimos para ejecutar la flotación bulk y selectiva, proporcionando para la flotación bulk recuperaciones de covelita y pirita del 93,4 y 90,2%, respectivamente, y para la flotación selectiva, recuperaciones de covelita y pirita del 80,5 y 20,3%, respectivamente. Los resultados obtenidos en la flotación del mineral de pórfido de cobre confirman que IPETC tiene una mejor afinidad por el cobre, mientras que PAX tiene una mejor afinidad por el hierro. No obstante, el IPETC se puede utilizar como colector selectivo o bulk variando solo el pH y utilizando bajas concentraciones (2×10^{-5}). Después de todo, no es necesario utilizar diferentes colectores para la flotación bulk y selectiva.

Durante el estudio de la flotación de covelita, fue necesario investigar los mecanismos de adsorción de los colectores en la superficie de la covelita. Por tanto, el segundo objetivo se centró en estudiar

la adsorción de los colectores IPETC y PAX sobre la superficie de la covelita. Se utilizaron métodos tanto experimentales como de simulación para alcanzar este objetivo. Los métodos experimentales incluyeron técnicas de caracterización como la espectroscopia infrarroja por transformada de Fourier (FT-IR) y la espectroscopia fotoelectrónica de rayos X (XPS). En el método de simulación, se aplicó la teoría funcional de la densidad (DFT) para el análisis de la superficie de la covelita. Los resultados muestran que los mecanismos de adsorción de IPETC y PAX en la superficie de la covelita fueron diferentes. El FT-IR nos permite identificar que el mecanismo de adsorción de PAX en la superficie de la covelita es a través de la formación de Cu-amilxantato (CuAX) y dixantógeno (AX)₂. El mecanismo de adsorción de IPETC sugiere que la unión es facilitada por el S del colector con átomos de Cu en la superficie de la covelita. Los espectros de XPS mostraron que el mecanismo de adsorción de PAX en la superficie de la covelita es principalmente a través de C 1s y S 2p. El mecanismo de adsorción de IPETC en la superficie de la covelita sugiere que el enlace se activa a través del elemento —S del colector con átomos de Cu en la superficie de la covelita. Finalmente, los cálculos de DFT predicen que para IPETC el enlace con el cobre solo ocurrió a través del grupo C—S. Para PAX, el enlace con el cobre ocurrió a través de los grupos C=S y C—S. Estos resultados nos permitieron entender el comportamiento del colector y elegir el colector adecuado dependiendo del tipo de flotación, ya sea flotación bulk o selectiva.

Introducir la desulfuración dentro del proceso de flotación transforma el proceso en uno de concentración polimetálica. El análisis y diseño de este tipo de procesos son escasos en la literatura. Luego, este tema fue considerado en el tercer objetivo, diseñar circuitos de flotación para minerales polimetálicos que incluyan desulfuración. Se estudiaron dos aspectos; primero, la adaptación de la metodología basada en la optimización de minerales monometálicos a minerales polimetálicos; en segundo lugar, se utilizaron los datos de flotación proporcionados por el mineral Cu-Ni-PGE de la mina Kevitsa para determinar el diseño óptimo de los circuitos de flotación integrados y secuenciales para este mineral polimetálico. El concentrador Kevitsa emplea un circuito de flotación secuencial de cobre-níquel. Por lo tanto, la idea fue rediseñar este circuito utilizando diferentes estrategias y análisis del mismo. En todos los casos estudiados se incluyó la desulfuración como tema relevante. Los resultados muestran que la estrategia utilizada para los minerales monometálicos se puede aplicar a los minerales polimetálicos. Esto fue posible porque, al igual que en el caso de los minerales monometálicos, se observó que existen pocos diseños óptimos para un problema dado para variaciones significativas en las recuperaciones de las etapas

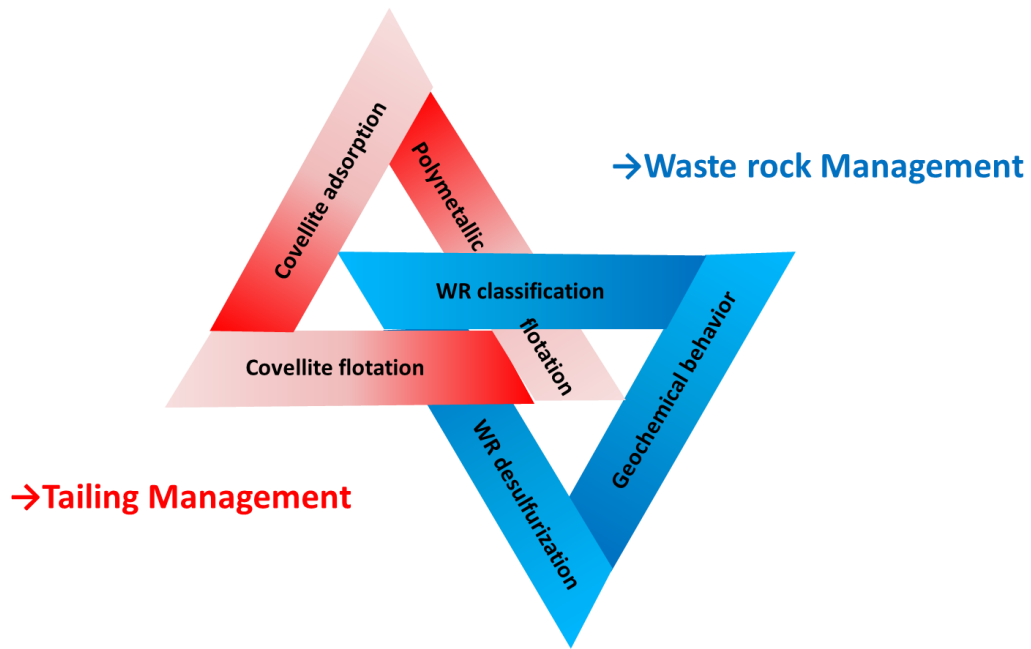
de flotación. Esto se analizó tanto en flotación fraccionada selectiva como bulk. En estos casos, hay un producto intermedio (concentrado o relave) que se procesa en otra etapa del proceso. Además, se introdujo una nueva idea a nivel conceptual: los circuitos integrados de flotación. En un circuito de flotación integrado, no hay flotación fraccionada ni producto intermedio, y las etapas de flotación selectiva y bulk se combinan para alcanzar el objetivo de separación. El estudio de estas posibles configuraciones de circuitos de flotación nos brinda una visión más completa de la mejor estrategia desde un punto de vista económico y de producción más limpia.

Además, abordando el tratamiento de WR, el cuarto objetivo fue evaluar la factibilidad de reprocesar el WR de un mineral de pórfido de cobre mediante el proceso de desulfuración y estudiar el comportamiento geoquímico de los materiales desulfurados. El objetivo fue clasificar el WR en fracciones reactivas y no reactivas, con base al concepto del diámetro del bloqueo físico de sulfuros (DPLS), utilizando el tamaño de partícula de las fracciones seleccionadas y el grado de liberación de sulfuros para el análisis. Por lo tanto, se evaluaron seis fracciones F6 (>5 mm) designadas de gran tamaño, F5 (-5 mm a +2,4 mm), F4 (-2,4 mm a +850 μm), F3 (-850 μm a +300 μm), F2 (-300 μm a +53 μm) y F1 (-53 μm). Los resultados muestran que el DPLS fue < 2,4 mm; por lo tanto, el tamaño de partícula superior a 2,4 mm se consideró no reactivo. Para la fracción reactiva se realizó el proceso de desulfuración. Se utilizó celda Denver para la fracción fina (<212 μm), y la tecnología de flotación en lecho fluidizado (Hydrofloat) para la fracción gruesa (-850 μm a +212 μm). También se estudió el comportamiento geoquímico mediante los ensayos de columna y de meteorización para el gran tamaño de partícula y el WR desulfurado, respectivamente. Los resultados geoquímicos muestran que el WR de gran tamaño (>5 mm) y desulfurado no producirá DMA ya que los valores de pH estaban entre 7 y 8. Además, los contaminantes lixiviados (Fe, Cu, Zn, Pb) permanecieron por debajo de los límites reglamentarios establecidos por Directiva 019.

Esta disertación proporciona nuevos conocimientos para mejorar la gestión de relaves y WR en la minería de pórfidos de cobre. La novedad de este estudio consiste en considerar el tratamiento de desulfuración tanto de relaves como de WR de un mineral polimetálico en una etapa temprana del proceso de flotación enmarcado en el concepto de producción más limpia. Por lo tanto, los estudios fundamentales, la flotación de minerales reales y el uso de modelos matemáticos para optimizar los circuitos de flotación nos permiten evaluar el circuito de flotación desde la perspectiva química, de equipos y operativa, lo que permite analizar el problema de manera integrada. La importancia

de esta tesis radica en brindar conocimientos y herramientas para futuras investigaciones que busquen trabajar con minerales de pórfido de cobre.

Palabras clave: relaves, estéril, drenaje ácido de mina, flotación, producción más limpia, optimización, valorización de metales, desulfuración, mineral de pórfido de cobre, mineral polimetálico.



Graphic abstract: Thesis main elements.

PREFACE

This dissertation is based in four journal articles. The author is the principal researcher and corresponding author in the four articles. The articles included in this dissertation are the following:

1. Yesica L. Botero, Rodrigo Serna-Guerrero, Alejandro López-Valdivieso, Mostafa Benzaazoua and Luis A. Cisternas. New insights related to the flotation of covellite in porphyry ores. *Minerals Engineering*, 2021. (Doi:10.1016/j.mineng.2021.107242).
2. Yesica L. Botero, Andrés Canales-Mahuzier, Rodrigo Serna-Guerrero, Alejandro López-Valdivieso, Mostafa Benzaazoua and Luis A. Cisternas. Physical-chemical study of IPETC and PAX collector's adsorption on covellite surface. *Applied Surface Science*, 2022. (Doi:10.1016/j.apsusc.2022.154232).
3. Yesica L. Botero, Isabelle Demers, Luis A. Cisternas and Mostafa Benzaazoua. Application of characterization techniques for the prevention of AMD for waste rock from a Chilean porphyry copper mine. Conference paper, presented in the 6th International Symposium on Process Mineralogy (Process Mineralogy '22), Sitges, Spain, 2022.
4. Yesica L. Botero, Luis A. Cisternas, Isabelle Demers and Mostafa Benzaazoua. Insights into the design of polymetallic flotation circuits, including tailing desulfurization. *Separation and Purification Technology*, 2023. (Submitted, Doi: 10.2139/ssrn.4366523).

In addition, the author published the following articles during her time as doctoral student, but they are not related to the objectives of this dissertation.

5. Luiza Texeira, Daniel Calisaya-Azpilcueta, Constanza Cruz, Yesica L. Botero and Luis A. Cisternas. Impact of the use of seawater on acid mine drainage from mining wastes. *Cleaner Production*, 2023. (Doi:10.1016/j.jclepro.2022.135516).
6. Constanza Cruz, Yesica L. Botero, Ricardo I. Jeldres, Lina Uribe and Luis A. Cisternas. Current Status of the Effect of Seawater Ions on Copper Flotation: Difficulties, Opportunities, and Industrial Experience. *Mineral Processing and Extractive Metallurgy Review*, 2021. (Doi: 10.1080/08827508.2021.1900175).

7. Luis A. Cisternas, Freddy A. Lucay, and Yesica L. Botero. Trends in Modeling, Design and Optimization of Multiphase Systems in Minerals Processing. Minerals, 2020. (Doi: 10.3390/min10010022).
8. Yesica. L. Botero, D. Ramírez, Jorge Eliécer López-Rendón and Franklin Jaramillo. From clayey minerals to Al₂O₃ nanoparticles: synthesis and colloidal stabilization for opto-electronic applications. Minerals, 2020. (Doi: 10.3390/min10020118).

From the point of view of dissemination, the Author participated in different conferences during her time as doctoral student, the results presented in these conferences were related to the develop of this dissertation.

1. 6th International Symposium on Process Mineralogy (Process Mineralogy '22), Sitges, Spain, 2022. Oral: "Application of characterization techniques for the prevention of AMD for waste rock from a Chilean porphyry copper mine". Yesica. L. Botero, Isabelle Demers, Mostafa Benzaazoua and Luis A. Cisternas.
2. Integration, Optimisation & Design of Mineral Processing Circuits (IntegratedMinPro '22), UK, 2022. Oral: "Design and integration for environmentally benign processes: analysis of flotation circuits". Yesica. L. Botero, Isabelle Demers and Luis A. Cisternas.
3. Flotation '21 (MEI), UK, 2021. Oral: "Study of thionocarbamate and amyl xanthate collector's adsorption on covellite and pyrite surface: experiments and DFT simulations". Yesica. L. Botero, Andrés Canales-Mahuziera, Mostafa Benzaazoua and Luis A. Cisternas.
4. 17th International conference on Mineral Processing and Geometallurgy (PROCEMIN-GEOMET), Chile, 2021. Oral: "Physical-chemical study of thiocarbamate and xanthate influence on covellite flotation". Yesica. L. Botero, Rodrigo Serna-Guerrero, Alejandro López-Valdivieso, M. Benzaazoua and Luis A. Cisternas.
5. International Mineral Processing Congress (IMPC), Cape Town, South Africa, 2020. Oral: "Flotation flowsheet for eliminating pyrite in tailings: a cleaner production solution". Yesica. L. Botero, Luis A. Cisternas and Alejandro López-Valdivieso.
6. International Symposium on Sustainable Mining and Mineral Processing Technology, Wuhan, China, 2019. Poster: "Integrated design of polymetallic flotation circuit:

- Application to cleaner production”. Yesica. L. Botero, Lorena Cortés, Luis A. Cisternas and Alejandro López-Valdivieso.
7. 7th International Computational Modelling Symposium (Computational Modelling '19), National Maritime Museum, Falmouth, Cornwall, UK. 2019. Oral: “Design of polymetallic flotation circuit based on optimization”. Luis A. Cisternas and Yesica. L. Botero.
 8. International Conference on Foundation of mineral processing and extractive metallurgy (FoMPEM) 2019, Chile. Poster: “Selective separation of copper and iron sulfides to obtain tailings with low pyrite content”. Yesica L. Botero, Luis A. Cisternas, Alejandro López-Valdivieso.

TABLE OF CONTENTS

ACKNOWLEDGEMENTS	I
RÉSUMÉ.....	II
ABSTRACT.....	VI
RESUMEN.....	IX
PREFACE	XIV
LIST OF TABLES	XX
LIST OF FIGURES.....	XXI
LISTE OF SYMBOLS AND ABBREVIATIONS	XXIII
LIST OF APPENDICES	XXIV
1. INTRODUCTION	1
1.1 Background.....	1
1.2 Motivation of the Study and Scope	4
1.3 Definition of the Problem.....	4
1.4 Research Hypothesis and Objectives.....	5
1.4.1 Hypotheses	5
1.4.2 Objectives.....	7
1.5 Research Contribution	7
1.6 Overview of the Chapters and Structure of the Dissertation	9
2. LITERATURE REVIEW	10
2.1 Covellite.....	10
2.2 Pyrite.....	12
2.2.1 Effect of oxidation.....	13

2.2.2	Effect of pH.....	14
2.2.3	Depressants.....	15
2.2.4	Activators	22
2.3	Mining Waste	25
2.3.1	Generation of acid mine drainage (AMD)	27
2.3.2	Management of AMD from tailings.....	28
2.4	Environmental Desulfurization of Tailings and Waste Rock.....	30
2.4.1	Desulfurization of tailings.....	36
2.4.2	Desulfurization of waste rock	38
2.5	Desulfurization of Tailings Using Bulk and Selective Circuit Design Based on Advanced Computational Optimization	45
2.6	Mineral Characterization	53
3.	RESEARCH DESIGN AND METHODS	55
4.	ARTICLES AND REVIEW OF THE RESULTS	59
4.1	Article I: New Insights Related to the Flotation of Covellite in Porphyry Ores.	59
4.1.1	Overview	59
4.1.2	Research objective.....	60
4.1.3	Contributions.....	60
4.2	Article II: Physical–Chemical Study of IPETC and PAX Collector’s Adsorption on Covellite Surface	62
4.2.1	Overview	62
4.2.2	Research objective.....	63
4.2.3	Contributions.....	63
4.3	Article III: Insights into the Design of Polymetallic Flotation Circuits, Including Tailing Desulfurization.	64

4.3.1	Overview	64
4.3.2	Research objective.....	66
4.3.3	Contributions.....	67
4.4	Article IV: Conference Paper: Application of Characterization Techniques for the Prevention of AMD for Waste Rock from a Chilean Porphyry Copper Mine.....	68
4.4.1	Overview	69
4.4.2	Research objective.....	70
4.4.3	Contributions.....	71
5.	GENERAL DISCUSSION	73
5.1	Other results.....	73
5.1.1	Desulfurization results (flotation using Denver cell and HydroFloat).....	74
5.1.2	WR geochemical behavior	78
5.2	Discussion and contributions of the study	82
5.3	Limitations of the study	83
6.	CONCLUSIONS AND RECOMMENDATION	85
6.1	Conclusions	85
6.2	Recommendations	87
	REFERENCES.....	89
	APPENDICES.....	116

LIST OF TABLES

Table 2.1 Advantages and limitations of fine- and coarse-particle flotation.	42
Table 2.2 Fluidized-bed flotation advantages for treating coarse particles.....	44
Table 2.3 Origin-destination matrix for concentrates (x) and tails (o).....	48
Table 5.1 Results for Denver cell flotation (particle size < 212 μm).....	74
Table 5.2 Mineralogical composition of concentrates C4-3 and C5-1.	76
Table 5.3 Results for HydroFloat® flotation (-850 μm to + 212 μm).	77

LIST OF FIGURES

Figure 1.1 Structure of the dissertation.	9
Figure 2.1 Structure of covellite (adapted from (Morales-García et al., 2014)). Spheres represent S(2) (dark yellow), S(1) (light yellow), Cu(2) (dark blue), and Cu(1) (light blue).....	12
Figure 2.2 Eh-pH diagram of the pyrite–water system at 25 °C. (Taken from Moslemi and Gharabaghi, 2017).....	14
Figure 2.3 Galvanic interaction between pyrite and chalcopyrite. (Adapted from Ekmekçi and Demirel, 1997.)	16
Figure 2.4 Mechanisms of adsorption of polymers on pyrite surface (taken from (Mu et al., 2015)).	20
Figure 2.5 Pyrite flotation as a function of the pH with the collector (adapted from Sun and Wang, 2009).....	23
Figure 2.6 Strategies for waste and AMD management.	27
Figure 2.7 AMD generation mechanism (adapted from Botero et al., 2021).	28
Figure 2.8 Static method used for the prediction of acid generation potential.	32
Figure 2.9 Floatability of sulfide minerals using conventional flotation (Lynch et al., 1981).	40
Figure 2.10 Results of mechanical and fluidized bed flotation cells for a sample of galena (Adapted from Jowett, 1980).	41
Figure 2.11 Schematic of the HydroFloat® separator with bubble–particle aggregates (Taken from Eriez, 2021).	43
Figure 2.12 Optimal configurations of recovery for species 1 and 2. (a) Low price and low feed grade. (b) Low Price and high feed grade. (c) High price and low feed grade. (d) High price and high feed grade. Flotation plant with three stages (Cisternas et al., 2015).....	51
Figure 2.13 Optimal flotation circuits of Figure 2.12 (Cisternas et al., 2015).....	52
Figure 3.1 The general methodology proposed for the thesis project.	55

Figure 3.2 Flowsheet proposed for kinetic tests.....	57
Figure 3.3 Activities conducted to develop each objective proposed in the thesis project.	58
Figure 4.1 Graphical abstract of the methodologies implemented to study the flotation of covellite and porphyry copper ore.	61
Figure 4.2 Graphical abstract of the methodologies implemented to study the adsorption mechanisms between collectors and the covellite surface.	63
Figure 4.3 Graphical abstract of Insights into the design of polymetallic flotation circuits, including tailing desulfurization.....	66
Figure 4.4 Graphical abstract of the methodologies implemented to conduct WR management.	71
Figure 5.1 Analysis of desulfurized WR via ABA testing.....	76
Figure 5.2 Pareto chart of standardized effect on sulfide recoveries.	78
Figure 5.3 Column test results for particle sizes > 5mm. a) pH and Eh evolution, b) conductivity evolution, c) acidity and alkalinity evolution, d) elemental cumulative charge, dashed lines refer to left y-axis while solid lines refer to right y-axis.	80
Figure 5.4 a) pH, b) Eh, and c) conductivity results of weathering cells for F4, F5, and desulfurized samples T5-1 and T4-3.....	82
Figure 5.5 Cumulative charge of elements Fe, Cu, Zn, Ca, and Mg, and sulfate of weathering cell results for a) F5, b) F4, and desulfurized samples c) T4-3 and d) T5-1. Dashed lines refer to the right y-axis while solid lines refer to the left y-axis.....	83

LISTE OF SYMBOLS AND ABBREVIATIONS

AMD	Acid mine drainage
AP	Acid potential
ABA	Acid-Base-Accounting
AGP	Acid generating potential
DFT	Density functional theory
DPLS	Diameter of the physical locking
DDTP	Diisobutyl dithiophosphate
FTIR	Fourier transform infrared spectroscopy
IPETC	O-isopropyl-N-ethyl thionocarbamate
ICP-AES	Inductively coupled plasma atomic emission spectroscopy
MO	Optic microscopy
NNP	Net neutralizing potential
NPR	Neutralizing potential ratio
NP	Neutralizing potential
QEMSCAN	Quantitative evaluation of minerals by scanning electron microscopy.
PAX	Potassium Amyl Xanthate
SEM-EDS	Scanning Electron Microscopy with Energy Dispersive Spectroscopy
WR	Waste Rock
XPS	X-ray photoelectron spectroscopy
XRF	X-ray fluorescence
XRD	X-ray diffraction

LIST OF APPENDICES

APPENDIX A Article 1: New insights related to the flotation of covellite in porphyry ores.....	116
APPENDIX B Article 2: Physical-chemical study of IPETC and PAX collector's adsorption on covellite surface.....	144
APPENDIX C Article 3: Insights into the design of polymetallic flotation circuits, including tailing desulfurization.....	178
APPENDIX D Article 4: Application of characterization techniques for the prevention of AMD for waste rock from a Chilean porphyry copper mine.....	212

CHAPTER 1 INTRODUCTION

1.1 Background

Copper is mainly supplied from primary inputs, and future demand can only be met by increasing primary inputs despite efforts to increase secondary sources by improving end-of-life recycling (Dong et al., 2020). This is a significant issue in the mining industry because the global reserves of copper are expected to decrease dramatically by 2050, with a corresponding ore grade decline of approximately 0.1%. Thus, as copper demand increases, the ore grade decreases (Elshkaki et al., 2016). The high demand for copper is correlated with the growth of the global population and economic development, which increases the consumption of this metal in several economic sectors, notably plumbing, wiring, and electricity. The latter two sectors are related mainly to the global desire for greener economies and the expansion of electric vehicle sales; electric vehicles use four times as much copper as petroleum-fueled cars. This growth requires greater infrastructure to provide adequate charging stations (MINING-DOT-COM, 2021). Thus, with a greater copper demand and ore grade decreases, a larger amount of copper mining is necessary to meet the demand, resulting in large quantities of solid waste such as waste rock (WR) and tailings being produced during the extraction of economically valuable minerals. Both types of waste are generally enriched with sulfide minerals such as pyrite, pyrrhotite, and arsenopyrite, which have no economic value and are reactive. These can oxidize due to surrounding water and oxygen exposure, generating acid mine drainage (AMD).

Currently, various methodologies have been developed for the treatment of AMD in tailings. These are known as "end-of-pipe technology," and focus on remediation rather than prevention of AMD. Accordingly, methodologies have not yet been developed that allow the total elimination of AMD from the early stages of the concentration process. Therefore, a future practice that could be implemented for the prevention of AMD would be to identify the source of potential AMD generation in the process and implement methods that enable the separation of acidifying sulfides at an early stage. This strategy, referred to herein as "in-process technology", will produce tailings with low sulfide content. In-process technology, which focuses on modifying stages of the flotation process, can be considered a cleaner production approach. In this sense, this work presents a number of investigations, including flotation tests, fundamental adsorption studies, and flotation circuit design and analysis.

Covellite is a sulfide copper mineral that is usually present in low concentrations and accompanies the chalcopyrite in porphyry copper ores. It is well known that the vast majority of studies focus on chalcopyrite flotation, as it currently represents the primary source of copper. Therefore, covellite is considered of limited relevance for the industry because of its low grade in ore, tailings, and WR (Camus, 1975; Kelm et al., 2009; Lam et al., 2020; Smuda et al., 2014). However, Voisin (2012) analyzed several samples from different Chilean copper mines and found that covellite concentration was between 0.6 and 17 % wt. It is noteworthy that the copper content in covellite is 66.5%, whereas in chalcopyrite it is 34.6%. Furthermore, due to the decrease in ore grade and high demand, it is inevitable to investigate other sources of copper to maintain the same level of copper production. In addition, covellite is poorly recovered by flotation finishing in tailings. Consequently, in recent years there has been growing interest in processing WR and tailings, and the recovery of valuable components such as covellite (Araya et al., 2020). There are few studies related to covellite flotation. Some studies have examined covellite behavior in flotation with different reagents, and ab initio calculations have been implemented to study the adsorption mechanism of collectors on the covellite surface. However, covellite floatability behaves differently depending on the reagents used. To deepen knowledge in respect of covellite flotation, flotation tests and fundamental studies were conducted using pure minerals and porphyry ore with thionocarbamates and PAX as collectors. The porphyry copper ore utilized was mainly composed of covellite, chalcocite, and pyrite. The fundamental studies correspond to adsorption studies undertaken to better understand the phenomena on the covellite surface and further use this information in the flotation of porphyry copper ore. Both selective and bulk flotation were included because tailings produced with or without a low grade of sulfur is a general goal (Ackerman et al., 2000, 1999; Porento and Hirva, 2004; Raju and Forsling, 1991; Roos et al., 1990).

Concentration by flotation is rarely performed in one stage. Therefore, flotation circuits must be included if tailings with a low grade of sulfur are wanted. In respect of flotation circuit design, polymetallic ore is usually separated by sequential or fractional flotation circuits for each base metal. The methodologies proposed in the literature for flotation circuit design consider only one base metal. Another issue with using sequential circuits is related to acid mine drainage (AMD) production, since the tailings usually include sulfide ores, notably pyrite (Bulatovic, 2007; Fuerstenau, M.C.; Jameson, G.J.; Yoon, 2007). There are some studies on tailings desulfurization and valorization by flotation to prevent the generation of AMD (Nuorivaara et al., 2019; Santander

and Valderrama, 2019). These studies focus on end-of-pipe technology; that is, tailings desulfurization is analyzed after the process has been developed. There is no information about flotation flowsheeting to produce a concentrate rich in copper sulfides, another rich in iron sulfides, and a tailing with low sulfide content, all produced or analyzed simultaneously. In other words, there is no methodology for flotation circuit design for polymetallic ores that enables resolution of the problem in an integrated way. Hence, there is a need to propose methodologies for flotation circuit design and analyses of polymetallic minerals. This new perspective could provide alternatives to processing ore with a cleaner production methodology.

In Chile, most copper mines operate open-pit mining, which generates large volumes of WR that are generally stored in large unsaturated piles on the land surface at the mine site. These WR stockpiles present an environmental risk and financial liability to mining companies. Managing WR stockpiles requires a thorough understanding of the physical, chemical, and microbial processes occurring within the stockpiles (Amos et al., 2015). However, not enough attention has been paid to this issue. Still, some studies have been conducted in other locations. For instance, WR collected from the waste dump at Langlois mine in Lebel-sur-Quévillon (Quebec, Canada) has been studied for polymetallic recovery and to prevent AMD (Amar et al., 2021). Given the decrease in copper ore grade and the need to valorize solid waste and prevent AMD, studies that help to recover copper from the waste have become necessary. In addition, the proper recovery of copper from WR and tailings could help to decrease the cost of waste management and limit the production of AMD (Amar et al., 2021). For this reason, this project also focuses on the treatment of WR, framed within the concept of cleaner production. Desulfurization is an alternative to treating WR, and the concept of bulk and selective flotation can be applied. However, another flotation technology must be considered because the WR usually has a large particle size distribution, which is a significant issue in the flotation process due to the degree of liberation of the particles and the effect of particle size on flotation. In this work we propose identifying the particle size from which WR can generate AMD. For the fractions that cause AMD, desulfurization is proposed based on particle size. For coarse particles larger than 250 μm , fluidized bed flotation technology (HydroFloat) is examined. For fine particles, conventional flotation is observed. Finally, regarding the concept of cleaner production, focusing on this issue from the onset of a mine's operation allows preventive management and thus limits the environmental impact. Therefore, the results obtained in this research will allow us to better understand the flotation behavior of WR and tailings derived

from porphyry copper ore, identify optimal conditions for their processing, and learn about the stabilization and management of this solid waste.

1.2 Motivation of the Study and Scope

The motivation for this thesis was the prevention of AMD from tailings and WR, and the valorization of metals within this solid waste. To address these issues, gaps in different flotation components such as chemistry, circuit design, and operational conditions were identified, as mentioned in the background, and the processing of porphyry copper ore by flotation was studied. In addition, the concept of cleaner production was utilized to develop strategies to address these issues. Cleaner production involves reducing waste by employing process change rather than end-of-pipe approaches. In fact, the central difference between pollution control and cleaner production is that pollution control is an after-the-event, react-and-treat approach. In comparison, cleaner production looks forward and attempts to anticipate and prevent (Rankin, 2014).

These gaps enabled us to identify that alternative copper sources must be considered, especially those that end up in the tailings. This is the reason why covellite flotation was studied; in addition, due to a lack of information on how this mineral behaves during the flotation process, it was necessary to conduct fundamental studies. However, solid waste must be free of sulfur after the flotation process to avoid AMD. Therefore, a methodology to design flotation circuits for polymetallic minerals, including desulfurization, was proposed. WR management must guarantee that mines do not generate AMD and that the process to be used is economically and environmentally feasible. Therefore, a method was developed to identify, on the one hand, the fraction that does not generate AMD and can be deposited in piles on the land surface, and on the other hand, the fraction that needs to be desulfurized and eventually valorized. Finally, it is noteworthy that these methods had not yet been developed with porphyry copper ore before this thesis. Therefore, this research contributes to knowledge on this topic and provides some tools with which to address the processing of porphyry copper ore and its geochemical stabilization.

1.3 Definition of the Problem

Two types of porphyry copper ore were used to conduct this research. The first was from Chuquicamata mine, Chile, and was mineralogically composed of covellite (0.22%), chalcocite (0.21%), chalcopyrite (0.06%), and pyrite (0.69%). First, microflotation testing was used to study

the physicochemical behavior of pure covellite as it was the main mineral in this ore. Then, flotation testing of the ore was conducted based on the experimental results obtained from microflotation results. Moreover, circuits based on optimization were developed using bulk and selective circuits to obtain a flowsheet that represents the best circuit for metal valorization and tailings desulfurization.

The second ore used comprised the WR of a porphyry copper ore from Centinela mine. The Centinela mine is located in the Atacama Desert (northern Chile). The Atacama Desert is known worldwide for hosting numerous world-class porphyry Cu deposits. The Centinela mine exposes several porphyry Cu deposits affected by supergene mineralization. The WR was mainly composed of pyrite, chalcopyrite, covellite, anhydrite, and quartz. The sulfide mineralogy was dominated by pyrite (6.3%). Moreover, this WR has different issues, high heterogeneity, large particle size distribution, low neutralizing species, and a low liberation degree. As a result, the ore could create environmental problems due to its high pyrite concentration. In addition, its large particle size distribution makes it challenging to assess the geochemical behavior. Thus, the ore was classified into fractions. Then, the fractions were separated into reactive and non-reactive fractions. The reactive fractions were further processed using the desulfurization process by flotation.

This dissertation focuses on the prevention of AMD from tailings and WR from a cleaner-production perspective. Therefore, during the development of this thesis, the principles of clean production were considered, especially the idea of identifying problems at their source instead of actions at the end of the process. The central separation technology utilized in this research was flotation. Four articles were developed, which correspond to each objective of the thesis.

1.4 Research Hypothesis and Objectives

The hypothesis and objectives of this dissertation are set out below.

1.4.1 Hypotheses

Since the solid waste to be studied comprises tailings and WR, this research project was based on the following two hypotheses:

Hypothesis #1

The production of tailings with a minimum content of acidifying species is possible using bulk and selective flotation.

Research questions:

- To obtain bulk and selective flotation of the covellite, what type of collector, collector concentration, and pH must be used?
- Is the collector's adsorption on the covellite surface affected by the pH?
- What are the adsorption mechanisms of the collectors on the covellite surface?
- Is it possible to design optimized bulk and selective flotation circuits to obtain tailings with low pyrite content?
- What are the advantages, disadvantages, and issues associated with the traditional desulfurization method and desulfurization into the flotation process using sequential or integrated circuits?

Hypothesis # 2

It is possible to avoid AMD and extract valuable metal species from WR using fluidized-bed flotation.

Research questions:

- What is the particle size for which the WR of the porphyry copper ore can be considered reactive or non-reactive?
- Is fluidized-bed flotation suitable for desulfurization of the reactive coarse-size fraction of WR?
- How must the chemical stability of desulfurized WR be evaluated?
- Could the desulfurization of WR be a sustainable management alternative to limit its long-term environmental impacts?

1.4.2 Objectives

The general objective of this thesis project was to deepen the knowledge of a porphyry copper ores using flotation technology for the prevention of AMD from tailings and WR, and the valorization of metals.

The specific objectives were as follows:

1. Evaluate the performances of different collectors in the flotation bulk and selective of pure minerals (covellite, pyrite), and porphyry copper ore from the Chuqicamata mining operation in northern Chile.
2. To investigate the adsorption mechanisms of IPETC and PAX collectors on the covellite surface.
3. To design flotation circuits for polymetallic minerals including desulfurization based on bulk and selective flotation using an optimization-based method.
4. To evaluate the feasibility of processing the WR derived from porphyry copper ore using the desulfurization process and study the geochemical behavior of desulfurized materials.

1.5 Research Contribution

During the development of this thesis, different contributions were made since four articles were written to fulfill the four objectives mentioned previously.

Article I makes the following contributions. We investigated whether covellite can be considered another source of copper. Covellite was the focus of this study. This article enabled us to determine the behavior of covellite during the flotation process. We identified the operational conditions and the influence of collector type, collector concentration, and pH in covellite recovery. This was valuable information since the flotation of porphyry copper ore was conducted using the same conditions, and high values of copper recovery were achieved. Therefore, this article provides valuable knowledge and tools regarding how the porphyry copper ore present mainly in covellite can be processed. Another significant contribution is that the optimal conditions by which to obtain bulk and selective flotation with porphyry copper ore were identified. This enabled us to introduce the desulfurization process as an important method to be implemented from a cleaner-production perspective. This article fulfills Objective 1.

Article II investigates the adsorption mechanism between the selected collector (IPETC and PAX) and the covellite surface. This article offers valuable knowledge about the physicochemical interactions between collectors and the mineral surface. This information enabled us to understand why the IPECT could be used as a selective collector in covellite flotation and how the PAX collector could be used for both selective and bulk flotation depending on the collector concentration and pH used. Knowing how the collector interacts with covellite surface enabled us to determine the best reagents and optimal conditions by which to run the flotation process, which made the flotation process more efficient. This article fulfills Objective 2.

Following articles I and II, article III develops flotation flowsheets that represent the optimal circuit by which to obtain valuable concentrates and tailings with low acidifying species, framed in the clean production concept. Therefore, this article designs and analyzes different conceptual flotation circuits to treat polymetallic ores, including desulfurization. Selective fractional circuits and bulk fractional circuits are assessed. In addition, integrated circuits are proposed as a new type of separation circuit for polymetallic minerals. The advantages, disadvantages, and costs are also analyzed. The results show that 1) the strategy utilized for monometallic mineral circuit design can be applied to polymetallic minerals; 2) a bulk fractional circuit has a lower cost and better environmental behavior than a selective fractional circuit; 3) an integrated circuit can present some advantages, but obtaining the adequate behavior in each flotation stage can be challenging; 4) the simultaneous design of the whole polymetallic circuit is the best way to address the design of these complex systems. Article III also demonstrates that thinking in alternative ways to develop a flotation flowsheet is viable and should be studied further in the future. This article fulfills Objective 3.

Finally, article IV combines two areas of research—flotation and geochemical behavior of WR—to better manage WR. We aimed to assess the effects of the mineralogy, particle size, and liberation degree of the WR in AMD production. The characterization techniques enabled the identification of the diameter of physical locking of sulfides (DPLS) to separate the reactive and non-reactive fractions. Then, the reactive fractions were desulfurized using different technologies (Denver cell and HydroFloat) based on particle size. The kinetic testing (column tests and weathering cells) showed that the WR was non-acid-generating; therefore, the methods implemented to avoid AMD from WR were successful. Article IV provides tools by which to set the standard to treat WR from porphyry copper ore. This article fulfills Objective 4.

1.6 Overview of the Chapters and Structure of the Dissertation

This dissertation is divided into two main parts. Figure 1.1 summarizes the structure of the dissertation. Part I presents an overview of the study divided into six chapters. Chapter 1 presents the introduction, which contains the background, motivation, definition of the problem, hypothesis, objectives, and research contributions. Chapter 2 describes the literature review; here, an overview of the current state of the flotation process, solid waste management, and AMD prevention practices is presented. Chapter 3 introduces the methodology used to fulfill each objective proposed. Chapter 4 summarizes each article, including the key results. Chapter 5 presents the general discussion: other results obtained, discussion and contributions of the study, and limitations of the study. Chapter 6 presents the conclusions and recommendations. It should be noted that the section "other results" in Chapter 5 was necessary because some results were not included in paper IV, and some experiments still need to be finished to complete this research. Therefore, the research associated with Objective 4 was divided into three parts: WR characterization, flotation tests, and kinetic tests. The WR characterization results were summarized and presented in a conference (conference paper), and preliminary results of flotation and kinetic testing are shown in the other results in Chapter 5. Finally, part II of this dissertation provides the full version of the article that shaped this study.

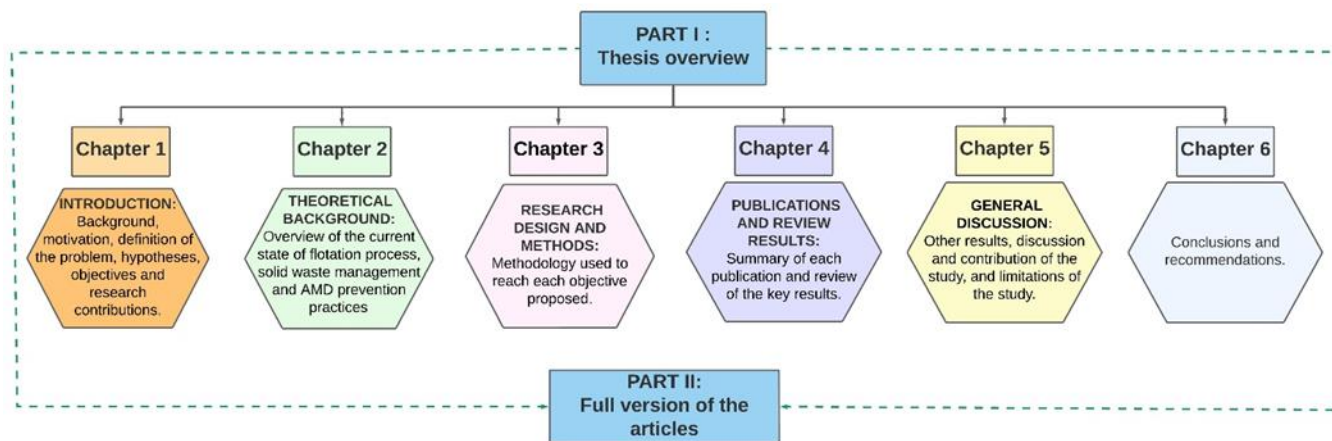


Figure 1.1 Structure of the dissertation.

CHAPTER 2 LITERATURE REVIEW

The literature on flotation and solid waste management was carefully reviewed. This section explains the main concepts used in the dissertation that enabled us to identify gaps and propose possible solutions applicable to the current situation in the mining industry.

2.1 Covellite

In the flotation process, chalcopyrite is the leading mineral source of copper. A possible method by which to enhance copper supply is to exploit other minerals such as covellite. Burrows et al. (2020) reported a copper-gold deposit in Eastern Sumbawa, Indonesia, in which the copper occurred entirely as covellite associated with pyrite (with 0.6% Cu). Interest in covellite has increased because it is widely used in optical applications, thanks to its excellent semiconductor properties, and as a cathode material (Lotter et al., 2016; Yin et al., 2019). Despite this, few studies have been undertaken concerning covellite flotation. For instance, Porento and Hirva, (2004) performed theoretical research using ab initio calculations on the interaction of sulfhydryl surfactants (1,1,1-butanetriethiol, diethyldithiocarbamate and ethyl xanthate) with covellite surfaces. They compiled data regarding all of the possible covellite–collector interactions. They suggested that it is more straightforward to study covellite using computational methods than to carry out flotation tests because the flotation process comprises highly complex behavior. The results show that 1,1,1-butanetriethiol interacts more strongly than diethyldithiocarbamate or ethyl xanthate, making it a promising collector for covellite flotation. However, this methodology only provided a limited analysis of the specific interaction between the covellite surface and the chosen collectors. In a real flotation process, multiple parameters modify the covellite behavior, including the effect of pH, interactions with other minerals, and the redox potential (Eh). In this sense, it is better to complement this kind of result with a real flotation test.

Another study was carried out by Raju and Forsling (1991), who studied the adsorption of diethyldithiocarbamate (DTC) on covellite, cuprite, and tenorite surfaces. In this case, the research focused only on the adsorption mechanism of each collector for each type of mineral using the UV–visible spectrophotometric technique. The effects of different collector concentrations and pH on the adsorption on the mineral surface were evaluated. Various copper-DTC complexes that formed on each mineral surface were identified, but flotation tests were not performed. Roos et al. (1990) studied the electrochemical behavior of chalcocite and covellite. Their study involved a

microflotation-electrochemical cell, and the effect of the electrochemical potential on the covellite flotation was investigated. They identified that the range between +50 and + 200 mV represents the potential at which the hydrophobization of covellite is possible.

Two further studies were carried out to study the effects of xanthogen formate and chelating agents on the flotation of copper sulfides (Ackerman et al., 2000, 1999). The first study was based on the flotation of pure chalcopyrite, chalcocite, covellite, bornite, and pyrite minerals by varying the alkyl group of xanthogen formate. It was found that xanthogen formates are excellent collectors of most copper sulfides and that the xanthogen chain length decreases the recovery of chalcopyrite, while remaining constant for the other minerals. However, for pyrite, long chain substituents influence the reactive clustering, which makes the position more favorable as a good collector for pyrite (Ackerman et al., 2000). The second study evaluated the effectiveness of different chelating agents in the flotation of copper sulfides and pyrite. The best collector for copper sulfides was imidazoline (1-Hydroxyethyl-2-Heptadecenyl). It was also shown to be a good collector of pyrite (Ackerman et al., 1999).

Recently, Yin et al. (2019) analyzed covellite and pyrite separation using pure minerals. Their work focused on calcium hypochlorite ($\text{Ca}(\text{ClO})_2$) as a pyrite depressant on the flotation separation. The results show that $\text{Ca}(\text{ClO})_2$ strongly inhibits pyrite flotation, while covellite is unaffected by this depressant. Even though such work provides some valuable insights into covellite flotation, it was focused on enhancing pyrite depression. For this reason, infrared (IR) spectroscopy and X-ray photoelectron spectroscopy (XPS) analyses were carried out to characterize the $\text{Ca}(\text{ClO})_2$ adsorption on the pyrite surface.

Although the abovementioned works discuss interesting aspects of covellite properties and their behavior in froth flotation, there is insufficient information to properly evaluate and design feasible operations dedicated to covellite concentration. To understand all the chemical interactions between covellite and collectors, it is necessary to enhance our knowledge regarding the properties and structure of covellite. Several papers have studied the topological and electronic properties of covellite using the density functional theory (DFT) method (Karikalan et al., 2017; Soares et al., 2016).

Covellite has a complex structure with hexagonal symmetry described as tetrahedral (CuS_4) and trigonal (CuS_3) (see Figure 2.1). The arrangements of atoms are analyzed along the (001) direction,

where the trigonal planar arrangement is attributed to Cu(1)-S(1) binding, and the tetrahedral arrangement is attributed to Cu(2)-S(2) binding; these are connected by sequences (Cu(2)-S(2)₄)-(Cu(1)-S(1)₃)-(Cu(2)-S(2)₄). The Cu(1), Cu(2), S(1), and S(2) correspond to Cu(I), Cu(II), S²⁻, and S₂²⁻, respectively. The disulfide bond (S(2)-S(2)) involves covalent bonding, and Cu-S involves ionic bonding. The cleavage energy is a value between 0.1 and 1 Jm⁻², and it is used to identify the most favored cleavage plane of a bulk surface. The smaller value is associated with the cleavage plane. This energy was calculated for the bulk surface of covellite along the (001) direction. A lower energy ($\gamma=0.30 \text{ J.m}^{-2}$) was found in Cu(2)-S(1) bond. Later, Cu(2) acquires trigonal planar geometry (Cu(1)-S(1)₃); this could be the reason why the oxidation state of covellite is defined as Cu(I) (Karikalan et al., 2017; Rosso and Hochella, 1999; Soares et al., 2016). Thus, Cu(I) could interact differently with the collectors and pH.

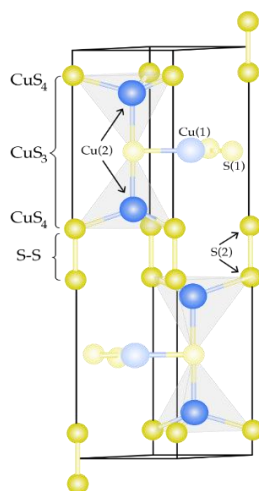


Figure 2.1 Structure of covellite (adapted from (Morales-García et al., 2014)). Spheres represent S(2) (dark yellow), S(1) (light yellow), Cu(2) (dark blue), and Cu(1) (light blue).

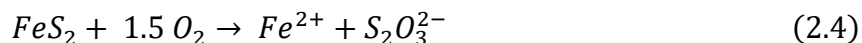
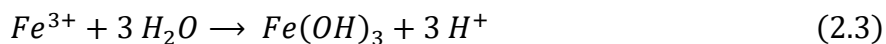
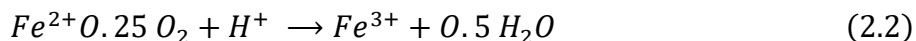
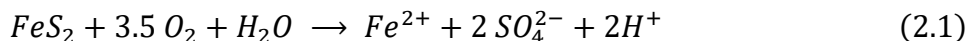
2.2 Pyrite

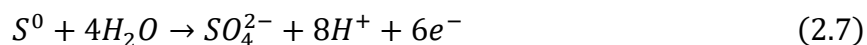
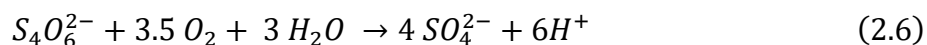
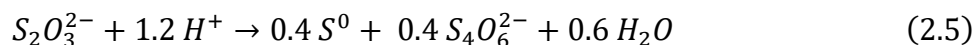
Pyrite is considered in the copper flotation process as the main sulfide gangue mineral, which decreases the grade of valuable minerals in the concentrate. Since pyrite is the most common and most widely studied metal sulfide, it is useful to review the chemistry of pyrite as a starting point for understanding its behavior and assessing its environmental impact. In this sense, the environmental impact will be studied using two approaches: 1. end-of-pipe technology, since pyrite is the principal species that remains in tailings after the flotation process; 2. in-process technology, since the pyrite is considered to be separated in an early stage of processing. Pyrite's behavior

depends on controlling the pulp potential. The pulp potential is strongly affected by the oxidation level and pH. Thus, these parameters are responsible for the floatability of pyrite (Cruz et al., 2021; Moslemi and Gharabaghi, 2017).

2.2.1 Effect of oxidation

Oxidation comprises a very complex process involving several electrochemical reactions. The most important reactions in pyrite oxidation comprise the formation of ions such as Fe^{2+} and SO_4^{2-} after complete oxidation of pyrite, as represented by Equation 2.1 (Egiebor and Oni, 2007). Fe^{2+} can be further oxidized, producing more reactions (Equations 2.2 and 2.3) (Chernyshova, 2003; Janzen et al., 2000). The third equation shows the formation of ferric hydroxide, which can precipitate, and is responsible for pyrite depression due to the formation of a coating on the pyrite surface. This phenomenon becomes more critical with an increase in the pH. However, high oxidation also incorporates breaking between the iron and sulfur atoms producing the thiosulfate ion ($S_2O_3^{2-}$) (see Equation 2.4) (Kelsall et al., 1999). This thiosulfate is unstable in acidic conditions and produces elemental sulfur and tetrathionate ions ($S_4O_6^{2-}$) (see Equation 2.5) (Descostes et al., 2004; Kelsall et al., 1999). $S_4O_6^{2-}$ further produces hydrophilic species (SO_4^{2-}) responsible for pyrite depression (see Equation 2.6) (Descostes et al., 2004; Kelsall et al., 1999). There is strong evidence that an increase in sulfate ions on the pyrite surface results in a decrease in surface hydrophobicity and, therefore, a reduction in pyrite flotation. Another reaction that occurs is the oxidation of elemental sulfur (hydrophobic entity) into the sulfate species (hydrophilic entity) (see Equation 2.7) (Hicyilmaz et al., 2004). In conclusion, extensive oxidation brings with it the formation of hydrophilic species such as $Fe(OH)_3$, SO_3^{2-} , SO_4^{2-} , and $S_2O_3^{2-}$, which affect the floatability of pyrite (Ekmekçi and Demirel, 1997; Peng et al., 2003a).





2.2.2 Effect of pH

Regarding the effect of pH, Figure 2.2 shows the behavior of pyrite as a function of the pH. It can be seen that pyrite has natural floatability at very acidic pH values thanks to the formation of elemental sulfur (S^0). Nevertheless, the formation of elemental sulfur (S^0) occurs in a narrow potential range. Then, a higher potential SO_4^{2-} is formed, affecting the natural floatability of pyrite. However, by analyzing the floatability of pyrite at an alkaline pH, it can be seen that the species formed are $Fe(OH)_3$ and SO_4^{2-} after the oxidation process becomes more abundant. Therefore, the formation rate and the stability of these hydrophilic species strongly depend on pH. $Fe(OH)_3$ is electrochemically very stable, causing passivation of the pyrite surface (Cruz et al., 2021; Moslemi and Gharabaghi, 2017). Thus, the alkaline pH inhibits the floatability of pyrite.

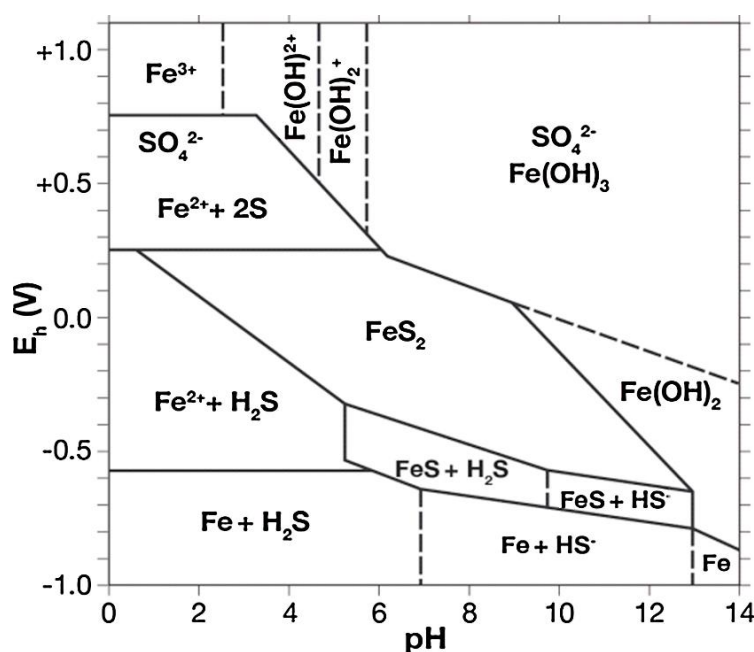


Figure 2.2 Eh-pH diagram of the pyrite–water system at 25 °C. (Taken from Moslemi and Gharabaghi, 2017).

2.2.3 Depressants

Pyrite depression has been extensively studied because pyrite must be separated from copper sulfides. Thus, methods other than pH adjustment are implemented to carry out pyrite depression. For instance, depressants are commonly used to reach selective copper flotation against pyrite. Several depressants have been used, including inorganic reagents, organic reagents, and non-xanthate collector's reagents. Mu et al. (2016) reviewed fundamental studies of the depression of pyrite and the common reagents used. Their work also discusses aspects related to the adsorption mechanism of these reagents on the pyrite surface.

2.2.3.1 Inorganic depressants

pH modifiers, oxidants, cyanide, and sulfoxyl are used as inorganic depressants. The depression of pyrite as a function of pH was shown earlier in Figure 2.2. The reagents commonly used are sodium hydroxide and lime. In the case of sodium hydroxide (NaOH), the species formed is hydrophilic iron hydroxide, which avoids the adsorption of the collector on the pyrite surface. The mechanism of adsorption suggests competition between hydroxyl and xanthate anion adsorption. Therefore, a high iron-hydroxyl concentration leads to the desorption of the collector from the pyrite surface (Fuerstenau et al, 1985). In respect of lime (CaO), the dissolution of lime in water produces Ca^{2+} and OH^- . Then, at an alkaline pH, $\text{Ca}(\text{OH})^+$ is the main species in the solution. The mechanism of adsorption of lime on the pyrite surface is due to $\text{Ca}(\text{OH})^+$ losing electrons from its surface, resulting in electron transfer from the donor $\text{Ca}(\text{OH})^+$ species to the acceptor mineral (pyrite) (Chen et al., 2011; Fornasiero and Ralston, 1992; Li et al., 2012). $\text{Ca}(\text{OH})^+$ has a higher affinity to the pyrite surface, which is why pyrite can be depressed at lower pH values using this reagent. Finally, these reagents are extensively used in the flotation process. Nevertheless, some issues appear, since the depression of pyrite by adjusting pH decreases the recovery of chalcopyrite. This is due to the hydroxide inhibiting the adsorption of the collector on the chalcopyrite surface, reducing the plant performance (Leppinen, 1990; Shen et al., 1998).

According to the above, oxidants have been studied as another alternative for pyrite depression. In a highly oxidizing environment between (+500 mV and +800 mV) (Moslemi and Gharabaghi, 2017), pyrite recovery decreases due to the formation of hydrophilic oxide/hydroxide species, which are highly stable and form coatings on pyrite surfaces. Thus, oxygenation of the pulps allows controlling the formation of species essential either for pyrite depression or pyrite flotation (Houot

and Duhamet, 1990). Another factor that influences the separation of pyrite is the grinding medium (Martin et al., 1991; Peng et al., 2003b). Galvanic interactions (see Figure 2.3) take place between minerals and grinding media, which modify the pulp potential influencing the selectivity. As a result, several interactions take place. For instance, the pyrite surface is activated due to the adsorption of copper ions dissolved from copper sulfide (copper-activated pyrite). In addition, other species are formed, such as $Fe(OH)_2$, $Fe(OH)_3$, and hydrophilic species such as $Cu(OH)_2$ and SO_4^{2-} on the copper sulfide surface, affecting its floatability (Ekmekçi and Demirel, 1997; Huang and Grano, 2006). To avoid this issue, combination of an oxygen conditioning time and the addition of depressants is good practice since it significantly reduces pyrite flotation (Boulton et al., 2001; He et al., 2006). For instance, López-Valdivieso et al. (2018) determined that oxidation enhances the formation of ferric oxyhydroxide species on the pyrite surface, which promotes the adsorption of depressants such as dextrin.

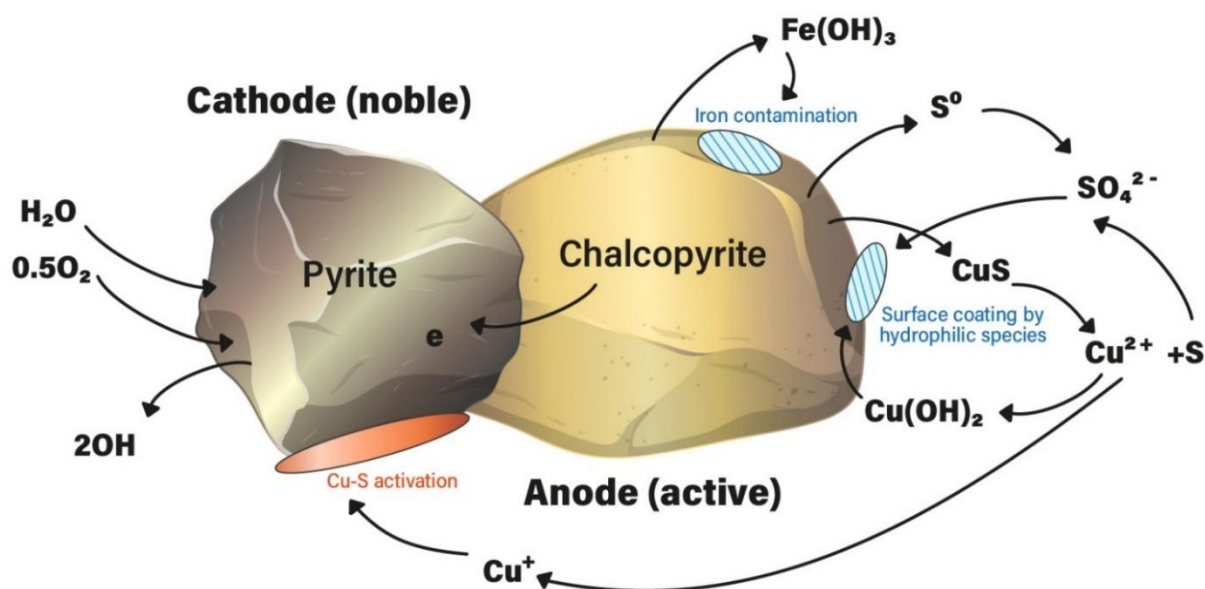


Figure 2.3 Galvanic interaction between pyrite and chalcopyrite. (Adapted from Ekmekçi and Demirel, 1997)

Cyanides are also employed to depress pyrite. The adsorption mechanisms of cyanides on the pyrite surface are as follows: firstly, by the desorption of xanthate ions on the pyrite surface due to competition between cyanide complexes formed and xanthate anions, as in the case of hydroxyl ions (Prestidge et al., 1993). Secondly, through the formation of insoluble iron cyanide, which precipitates on the pyrite surface, making the pyrite surface hydrophilic (Guo et al., 2014; Wang

and Forssberg, 1996). Thirdly, sulfur or polysulfides are also produced due to surface oxidation. Then, the cyanide may react with the species forming the hydrophilic thiocyanate, which depresses the pyrite (Prestidge et al., 1993). Fourthly, the reduction of potential inhibits the electrochemical activity on the pyrite surface, avoiding oxidation of the xanthate collector and, therefore, its adsorption (de Wet et al., 1997; Guo et al., 2015). Finally, as mentioned earlier, the pyrite surface is activated due to the adsorption of copper ions dissolved from the copper sulfide. Then, the cyanide can be used as a deactivating agent in copper-activated pyrite thanks to the cyanide removing the copper from the pyrite surface through the formation of strong cuprous cyanide complexes, such as CuCN , $\text{Cu}(\text{CN})_3^{2-}$ and $\text{Cu}(\text{CN})_4^{3-}$ (Bulatovic, 2007). However, using this reagent creates an environmental issue since it is highly toxic, and using excessive amounts of cyanide can be poisonous because this reagent ends up in the tailings, which contaminate surrounding water sources (Mehrabani et al., 2011). Therefore, using cyanide is not the most suitable option by which to depress pyrite because the tailings produced are composed of a high amount of pyrite, which is the principal species responsible for AMD, and the process also involves a hazardous reagent that worsens its environmental impact.

Due to the great environmental impact of cyanide, other reagents such as sulfoxyl have been developed. As mentioned in Section 2.2.1, there is evidence that an increase in sulfate ions on the pyrite surface results in a decrease in surface hydrophobicity (Equations 2.4, 2.5, 2.6, and 2.7). Therefore, some sulfoxyl species such as sulfite (SO_3^{2-}), bisulfite (HSO_3^-), metabisulfite ($\text{S}_2\text{O}_5^{2-}$), and sulfur dioxide (SO_2) have been used in the flotation at neutral or mildly alkaline pH levels as pyrite depressants (Chandra and Gerson, 2009; Khmeleva et al., 2002). For instance, sodium sulfide depresses pyrite flotation by introducing an additional anodic reaction, which means that the sodium sulfate consumes the dissolved oxygen available in the pulp, reducing the mixed potential, which avoids xanthate oxidation. As a consequence, dixanthogen is not formed, and pyrite cannot float (Janetski et al., 1977). Another interesting property of sulfoxyl is shown in Equation 2.8 (reaction mechanism between iron, isopropyl xanthate, and bisulfite (Khmeleva et al., 2003, 2002)). The presence of the bisulfite (HSO_3^-) leads to the desorption of dixantogen from the pyrite surface and, therefore, the formation of hydrophilic species such as FeSO_3 . Finally, it appears that sulfoxyl is suitable for use as a depressant. However, a high dosage of sulfoxyl species is required for pyrite depression. Thus, the relatively high cost of these reagents and high consumption limit their application in the flotation process (Bulut et al., 2011).



2.2.3.2 Organic depressants

The study of biodegradable depressants as an environmentally friendly alternative has attracted the attention of researchers due to the global desire to implement methodologies that allow decreasing the environmental impact generated by the flotation process. The organic depressants implemented for pyrite depression include polysaccharide polymers (starch, dextrin, guar gum, carboxymethyl cellulose (CMC), and chitosan), lignosulfonate, polyacrylamides (PAMs), and diethylenetriamine (DETA) (Bulatovic, 1999). The interaction between organic depressants and the pyrite surface is very complex due to the heterogeneity of the pyrite surface and the complex structure of the polymers. However, some mechanisms of adsorption have been proposed. Figure 2.4 shows the possible interaction mechanisms of organic depressants on the mineral surface. Firstly, there is electrostatic attraction between the negative charge of the polymer and the mineral surface (see Figure 2.4a). Secondly, hydrophobic interactions occur between the hydrophobic sites of mineral and polymer chains, which allow the accumulation of polymers on the pyrite surface (see Figure 2.4b). Thirdly, hydrogen bonding can occur through the hydroxyl groups of the polymer and the hydrophilic sites on the mineral surface. This interaction can be improved at alkaline pH levels (see Figure 2.4c). Finally, chemical interactions can occur between polymers (anionic functional groups) and metallic surfaces (cations), resulting in the binding of polymers (see Figure 2.4d) (Boulton et al., 2001; Gregory and Barany, 2011).

The polysaccharides starch, dextrin, and guar gum contain hydroxyl groups on C-2 and C-3 carbon atoms in each unit. Thus, all of these polysaccharides can form complexes with metal hydroxides through hydrogen bonding. These reactions are pH-dependent (Laskowski et al., 2007; Liu et al., 2000; Rath and Subramanian, 1999). Therefore, the depression of pyrite using polysaccharides occurs through the selective adsorption of these organic reagents on the pyrite surface. For instance, the effectiveness of starch as a depressant was studied by Bulut et al. (2011). They found that using a low dosage (1.7 mg/L^{-1}) and high pH (10), the starch adsorption on the pyrite surface was higher. The mechanism of starch adsorption was through the metal-hydroxylated species. However, when they carried out this procedure with pyritic copper ore, the starch also affected the flotation of copper sulfides. López Valdivieso et al. (2004) studied the adsorption of dextrin on the pyrite

surface. They reported that adsorption between dextrin and the pyrite surface occurs through the ferric oxyhydroxide species present on the pyrite surface. It was also demonstrated that dextrin adsorption on the pyrite surface improves with an increase in the level of pyrite surface oxidation (Lopez Valdivieso et al., 2007). The effect of guar gum on pyrite flotation was investigated by Bicak et al. (2007); they found that low doses of guar gum had a substantial impact on pyrite flotation since the recovery decreased dramatically. Pyrite depression with guar gum occurred through the formation of a hydrophilic iron oxyhydroxy coating, which was improved by increasing the pH. CMC contains a carboxyl group (negative charge), which increases its selectivity. Unlike starch and dextrin, CMC is adsorbed not only by hydroxyl groups but also through carboxyl groups. The hydroxyl groups only interact with metal hydroxyl species, and the carboxyl groups interact with various metallic species formed on the mineral surface (Bicak et al., 2007). Feng et al. (2013) studied the mechanism of adsorption–desorption of the collector and CMC on the pyrite surface. They found that the depression of pyrite occurs through the competition between adsorption of CMC and desorption of the collector from pyrite surfaces. Thus, CMC inhibits the adsorption of collectors on the pyrite surface. Chitosan contains amine, hydroxyl, and acetamide groups (Gylienė et al., 2015). Amine and hydroxyl allow the chitosan to chelate with metal ions (Gylienė et al., 2015; Huang et al., 2013). XPS spectra have demonstrated that both amine and hydroxyl groups are adsorbed on the pyrite surface, forming a complex, probably through a chemisorption mechanism (Huang et al., 2013). Finally, it can be concluded that in most of these cases, organic depressants were complemented using inorganic depressants, since it was necessary to control the pH to improve the selective separation of the pyrite in the flotation process.

Lignosulfonates are anionic polyelectrolyte polymers obtained during the sulfite pulping process in cellulose production (Lebo and Gargulak, 2004; Ouyang et al., 2010). The molecular structure of lignosulfonates includes hydroxyl groups in the sulfonic ($\text{S}(\text{OH})_3$) and carboxylic acid groups (RCOOH) (Ouyang et al., 2006). These chelating agents improve the ability of lignosulfonates to be adsorbed on the surface of the minerals. Therefore, a higher content of functional groups enhances the hydrophilicity of the pyrite surface, which facilitates its depression. Polyacrylamide (PAM) is another organic depressant that is commonly used. It is a synthetic polymer that contains the chelating group amide. Again, as in the case of lignosulfonates, this chelating group gives the PAM a good affinity for the pyrite surface (Huang et al., 2014). Finally, diethylenetriamine (DETA) has the chemical formula $\text{NH}_2\text{-CH}_2\text{-CH}_2\text{-NH-CH}_2\text{-CH}_2\text{-NH}_2$. It contains similar chelating

agents to chitosan (Liu et al., 2008). The depression mechanism of DETA can be explained through two aspects. Firstly, the cleaning mechanism means that DETA can remove activating ions such as copper from the pyrite surface. Secondly, the blocking mechanism implies that a complex Cu-DETA is formed, which adsorbs back to the pyrite surface, competing with collectors for their adsorption on mineral surfaces (Agorhom et al., 2014; Rashchi et al., 2004; Sui et al., 1998).

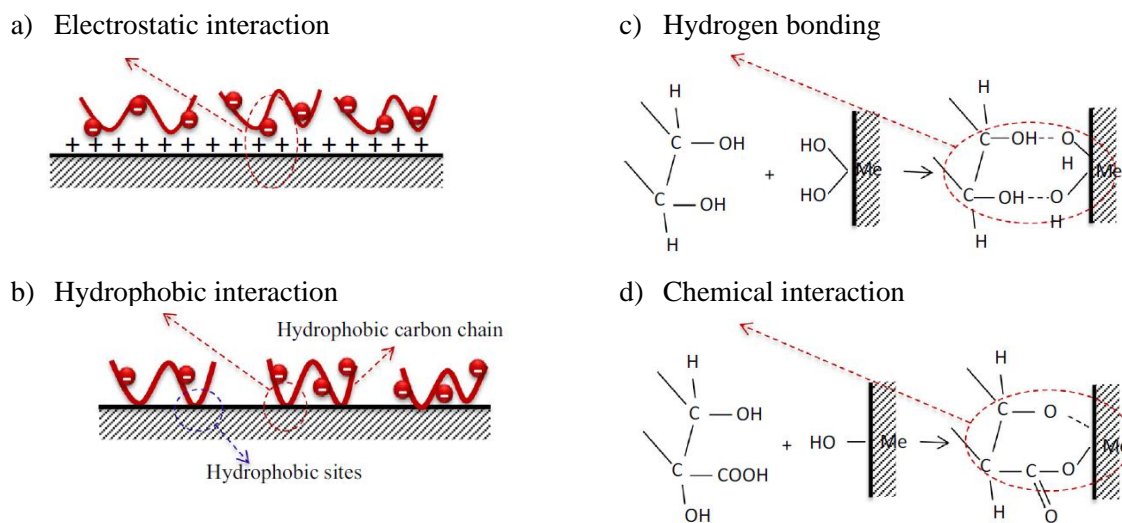


Figure 2.4 Mechanisms of adsorption of polymers on pyrite surface (taken from Mu et al., 2015).

Recently, more research has been published related to the study of novel depressants. For instance, Khoso et al. (2019) studied the selective separation of chalcopyrite from pyrite using a novel non-hazardous biodegradable polyglutamic acid (PGA) as a depressant. The PGA is a homo-polyamide biopolymer composed of chelating agents of glutamic acid units connected by amide linkages between amino- and carboxylic-acid groups (Luo et al., 2016; Ogawa et al., 1997; Zhang et al., 2018). It was found that PGA more strongly depresses pyrite than chalcopyrite in the pH range of 8-12. The recoveries obtained were 85% for copper and 20% for pyrite, demonstrating that PGA reduces the collector's adsorption on the pyrite surface. FT-IR characterization was used to study the mechanism of adsorption of the PGA on the pyrite surface. It was found that the leading bands of PGA corresponding to -COOH, -CONH, -CH₂, and -CH₃ were visible in the spectrum of PGA-treated pyrite, demonstrating PGA adsorption. Additionally, hydrophilic species such as ferric hydroxide and ferric sulfate were identified on the pyrite surface after treatment with PGA.

Another study was carried out by Khoso et al. (2021). They used a tricarboxystarch micromolecule as a pyrite depressant. Tricarboxystarch is a sodium salt; the chelating agents are R-COOH, R-

COH, and R-OH. Batch flotation experiments were conducted on sulfur-rich copper sulfide ore. It was found that adding a low dosage of tricarboxystarch under acidic conditions (pH 6) yielded high-grade copper. The concentrate contained approximately 21.9% Cu and 33.8% S.

Finally, Zhang et al. (2021) used galactomannan (GM) to replace traditional depressants such as guar gum, polyacrylamide (PAM), dextrin, carboxymethylcellulose (CMC), sodium, and hexametaphosphate (SHMP) for pyrite depression. GM is a polysaccharide with a high molecular weight. Its structure comprises a large number of hydroxyl groups, which strongly react with metal ions adsorbing on mineral surfaces, generating surfaces that are highly hydrophilic. The adsorption mechanism of GM on pyrite surfaces was studied using Fourier-transform infrared spectroscopy (FT-IR) measurements and X-ray photoelectron spectroscopy (XPS) analyses. The FT-IR spectrum of GM-treated pyrite shows a new band caused by the stretching vibration -OH in GM, indicating strong adsorption of GM on the pyrite surface. XPS confirms these results, since the S2p high-resolution spectrum shows that the pyrite spectrum was almost unchanged after adding GM and xanthate, indicating that the collector could not be adsorbed on the pyrite surface in the presence of GM. Thus, pyrite is strongly depressed by GM.

2.2.3.3 Non-xanthate collectors

It is well known that xanthate collectors do not have good selectivity against pyrite during the flotation process. That is why so-called non-collectors such as dithiophosphate (DTP), dithiophosphinate (DTPI), and thionocarbamate (TC) are commonly used in the flotation of sulfide minerals (Bulatovic, 2007). These collectors are chemically composed of chelating groups that provide them with high affinity with specific metal ions. They are very efficient in selectivity against pyrite (Pecina-Treviño et al., 2003). Collector adsorption on the pyrite surface is an aspect with significant relevance. In this work, we study the behavior in the flotation process of the non-xanthate collector O-isopropyl-N-ethyl Thionocarbamate (IPETC) and the collector potassium amyl xanthate (PAX). The latter will be discussed further in Section 2.2.4. Thus, IPETC is used as a selective collector, which means that it has higher selectivity against gangue iron sulfides, notably pyrite, and also exhibits high chemical stability in a wide pH range due to it having a $pK_a \geq 12$ (Fairthorne et al., 1996). In addition, IPETC contains N and S functional groups for chelation, making it an effective collector in terms of high copper recovery and pyrite rejection (Buckley et al., 2014). Another characteristic of IPETC is that the O-alkyl group present in its composition

influences the hydrophobicity of the collector, and the N-alkyl group controls the degree of the reactive center that approaches the copper surface, and therefore its steric accessibility (Zhao et al., 2016). In summary, the action of pyrite depressants can involve desorbing either the collector or the activator from the pyrite surface, deactivating the activating ions, preventing collector adsorption on pyrite, or making the pyrite surface hydrophilic to reach selectivity against the pyrite in the flotation process.

2.2.4 Activators

The activation of the pyrite surface is one of the most important phenomena associated with flotation. There are different ways that pyrite can be activated. The first involves collector adsorption on a non-activated surface. The second involves forming metal species such as copper, which can be adsorbed on the mineral surface, creating suitable sites for further collector adsorption; this is commonly called copper-activated pyrite. As previously mentioned, collector-type xanthates are commonly used as sulfide mineral activators. The mechanisms of adsorption of collector-type xanthates on the pyrite surface involve different electrochemical stages, which can be explained by Equations 2.9–2.11. The reactions start with the charge transfer in the adsorption of xanthate (X^-) (see Equation 2.9), followed by the oxidation of xanthate to dixanthogen (X_2); this oxidation is essential for xanthate adsorption on sulfide mineral surfaces (see Equation 2.10). The final step involves the formation of metal xanthate (FeS_2+X_2) (Mu et al., 2016).

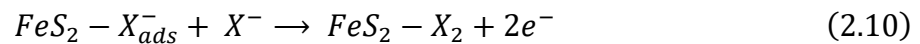
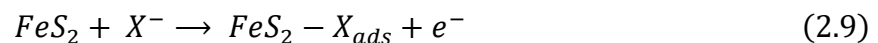


Figure 2.5 shows pyrite flotation as a function of the pH with the collector. Here, it can be seen that pyrite floatability occurs primarily when dixanthogen is formed (delimited red area). Thus, under slightly oxidizing conditions (from +0.2 to +0.4V), it is possible to achieve pyrite flotation in the range of pH values between 6 and 9 (Cruz et al., 2021; Sun and Wang, 2009). Hence, pyrite floatability will depend directly on the pulp potential and pH selected for each test. However,

several studies have demonstrated that the adsorption of ferric xanthate also occurs on the pyrite surface, but the quantity of this species is lower than that of dixanthogen (Chandra et al., 2012; Chandra and Gerson, 2009; Leppinen, 1990; Wang and Eric Forssberg, 1991).

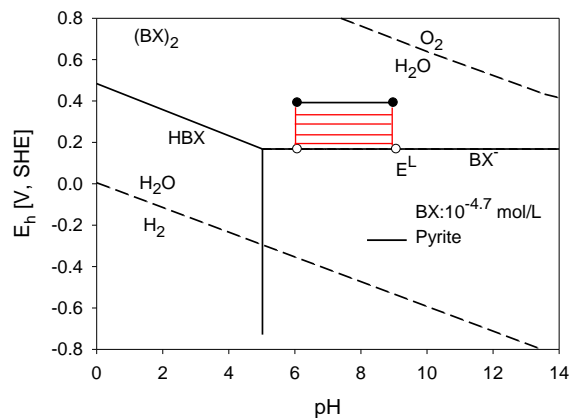
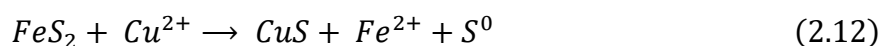


Figure 2.5 Pyrite flotation as a function of the pH with the collector (adapted from Sun and Wang, 2009).

So far, it seems that pyrite is easily floatable. Nevertheless, two issues exist that limit pyrite flotation: the effect of the oxygen content and the pH in the collector adsorption. These two aspects were discussed in Sections 2.2.1 and 2.2.2 in relation to the hydrophilic species formed on the pyrite surface. Concerning the effect of pH in the collector adsorption on the pyrite surface, Janetski et al. (1977) showed that at a lower pH (3) (see Figure 2.5), the pyrite surface is oxidized to more positive potentials than the potential formation of dixanthogen. Thus, oxygen reduction and xanthate oxidation are the dominant electrochemical reactions in the system. As a result, the pyrite surface will be hydrophobic through the adsorption of dixanthogen. However, when the pH increases, the potential required for pyrite oxidation decreases < 0.2 V (see Figure 2.5); below this potential, the oxidation of xanthate to dixanthogen is not possible. Therefore, under such conditions, the rate of xanthate oxidation decreases, and the pyrite surface remains hydrophilic. In addition, the oxidation potentials of pyrite and xanthate are cathodically displaced by an increase in pulp pH and xanthate concentration, respectively. However, the change caused by increasing the xanthate concentration by one order of magnitude is greater than that caused by increasing the pH by one unit. Therefore, it is possible to reverse the effect of pH by increasing the collector concentration (Janetski et al., 1977).

Several studies have investigated the effect of oxygen content on collector adsorption on the pyrite surface. It has been demonstrated that oxygen improves xanthate adsorption on the pyrite surface since there is an increase in the dissolved oxygen in the pulp, which increases the pulp potential. Therefore, more oxygen is available for the oxidation of xanthate to dixanthogen (Fuerstenau et al., 1990b, 1990a; Göktepe, 2010; Kuopanportti et al., 2000, 1997). However, the level of oxidation should not be taken lightly, because it is well known that under high oxidative conditions, hydrophilic species are formed on the pyrite surface. Thus, a common practice during flotation testing is the use of a nitrogen atmosphere. Nitrogen inhibits the formation of hydrophilic species, and as a result, xanthate adsorption on the pyrite surface is enabled (Miller et al., 2002). In this work we use the collector potassium amyl xanthate (PAX), which belongs to the xanthate family and is commonly used as a bulk or non-selective collector. PAX is prepared by reacting n-amyl alcohol, carbon disulfide, and potassium hydroxide. Carbon disulfide promotes the hydrophobicity of the collector, and the long alkyl chain increases its collecting power (Ma et al., 2017; Mielczarski et al., 1989).

Pyrite activation by copper is due to galvanic interactions between minerals and grinding media, which modify the pulp potential influencing the selectivity. As a result, the pyrite surface is activated due to the adsorption of copper ions dissolved from copper sulfide. The reaction mechanism between pyrite and copper ions is given by the spontaneous reduction of Cu^{2+} into Cu^{1+} and sulfur oxidation (see Equation 2.12). In addition, as can be seen in Figure 2.3 and Equation 2.12, it has been suggested that covellite is the major compound responsible for copper-activated pyrite. This fact was validated by XPS analysis and voltammetry studies (Finkelstein, 1997; Hicyilmaz et al., 2004; Laajalehto et al., 1999; Weisener and Gerson, 2000).



pH also has an effect on copper-activated pyrite. It has been reported that under slightly acidic pH conditions, pyrite activation by Cu^{2+} is strongly affected by the electrochemical pulp potential. Increasing the pulp potential decreases the adsorption of Cu^{2+} , causing a decrease in the surface area available for the copper adsorption due to oxidation of the pyrite surface. Under alkaline pH, it has been found that Cu^{2+} is first adsorbed on the surface as $\text{Cu}(\text{OH})_2$. Then, $\text{Cu}(\text{OH})_2$ reacts

with sulfide (S_2^{2-}) on the pyrite surface and is later reduced to form Cu(I)S species through the oxidation of polysulfides (Voigt et al., 1994). Therefore, under alkaline conditions and with a high oxidation level, the rate of copper adsorption on the pyrite surface is lower, since the copper must penetrate the passivated coat formed on the pyrite surface. The pyrite floatability strongly depends on the formation of Cu^{1+} . Thus, to maintain reducing conditions that prevent the oxidation of Cu^{1+} to Cu^{2+} species, we must allow a more favorable medium for pyrite activation. Finally, another phenomenon that occurs during the flotation process is collector adsorption on the pyrite's activated surface. The reaction mechanism starts with copper-activated pyrite, followed by the chemical reaction with the xanthate forming the cuprous xanthate species. This compound is a hydrophobic entity formed as a coating on the pyrite surface (Chandra and Gerson, 2009; He et al., 2005; Laajalehto et al., 1999; Leppinen, 1990).

Finally, these data allow us to determine the behavior of pyrite and covellite in the flotation process and how collectors behave differently with different minerals. Therefore, it is possible to suggest how to carry out the bulk and selective flotation process for the copper concentration process, producing tailings with low pyrite content and allowing the desulfurization of WR. Even though IPETC and PAX collectors have been commonly used in mineral processing, some unresolved questions exist concerning the type of species adsorbed, its adsorption mechanism, and the relationship between the species adsorbed and floatability. In addition, the mineralogical composition of each mineral is different, which makes its study more challenging.

2.3 Mining Waste

Copper porphyry deposits are most often mined in open-pit operations. These deposits have relatively low ore grades; therefore, high-tonnage exploitation is necessary. One consequence is that significant amounts of solid waste are produced compared with the units of copper recovered. Approximately 98% of the material extracted from these mines comprises waste. This waste can be subdivided into three major categories: leach rock, WR, and tailings. In this work, we focus on WR and tailings.

WR is removed during development and production as a means to gain access to the ore. For this reason, WR usually has a low concentration of valuable minerals. In addition, WR has a heterogeneous mineralogical and chemical composition and physical characteristics due to the deposition of waste from different mine sources (Amar et al., 2021; Amos et al., 2015; Elghali et

al., 2019, 2018; Jamieson et al., 2015; Matinde, 2018). WR generally comprises coarse material, but can have a wide range of sizes from very large particle sizes to dust-sized particles. The size and shape of the material depend on the characteristics of the rock (e.g., hardness) and extraction methods (ripping, drilling, and blasting) (Elghali et al., 2019; Fala et al., 2005). The particle size distribution of WR from various mining sites has been studied. It was demonstrated that WR corresponds to relatively coarse material. The D_{10} of WR was found to be between 0.2 and 3 mm, and the D_{60} was between 1 and 80 mm (McKeown et al., 2000; Peregoedova, 2012). Its uniformity coefficient ($CU = D_{60}/D_{10}$) can reach 30 or more. High values of this coefficient indicate well-graded soil.

Tailings are generated after the beneficiation process of copper ore. During this process, ores are first crushed and finely ground and then treated in flotation cells with chemicals to recover copper concentrates. Tailings consist predominantly of fine particles that are rejected from the flotation process. They are generally considered homogenous materials with homogeneous particle-size distributions. Bussière (2007) demonstrated that D_{10} was between 0.001 and 0.004 mm and D_{60} was between 0.01 and 0.05 mm; the uniformity coefficient CU was between 8 and 18.

WR and tailings can contain minerals such as pyrrhotite, arsenopyrite, gersdorffite, and pyrite. The last of these is present in a significant proportion of this waste. These minerals can have a major environmental impact because, in the presence of oxygen and water, they are oxidized and can produce AMD. The potential generation of AMD depends on mineralogy waste and the dissolution rates of the minerals. Therefore, the behavior of these types of waste can be very different. For this reason, the assessment and management of waste is challenging for the mining industry (Blowes et al., 2014; Paktunc and Davé, 2000). Traditionally, WR is deposited in unsaturated piles, which can cover thousands of hectares, and tailings are often stored in dams and impoundments (Elghali et al., 2019). The current strategy implemented for waste management is known as end-of-pipe technology, and consists of AMD mitigation. These methodologies are focused on waste that already contains an acidifying species. Therefore, reprocessing the waste seems to be a good alternative. However, reprocessing the waste means consuming more reagents, energy, and water, increasing costs and environmental effects. Framed in the context of cleaner production, we incorporated the concept of in-process technology into our research. This strategy aims to remove the species responsible for AMD at an early stage of the flotation process, using bulk and selective flotation as a method of desulfurization. This methodology allows us to obtain two desulfurized

minerals, one from the WR and the other named tailings with low pyrite content, from the flotation of porphyry copper ore. Therefore, in this work, desulfurization is a methodology used in in-process technology rather than end-of-pipe technology (see Figure 2.6).

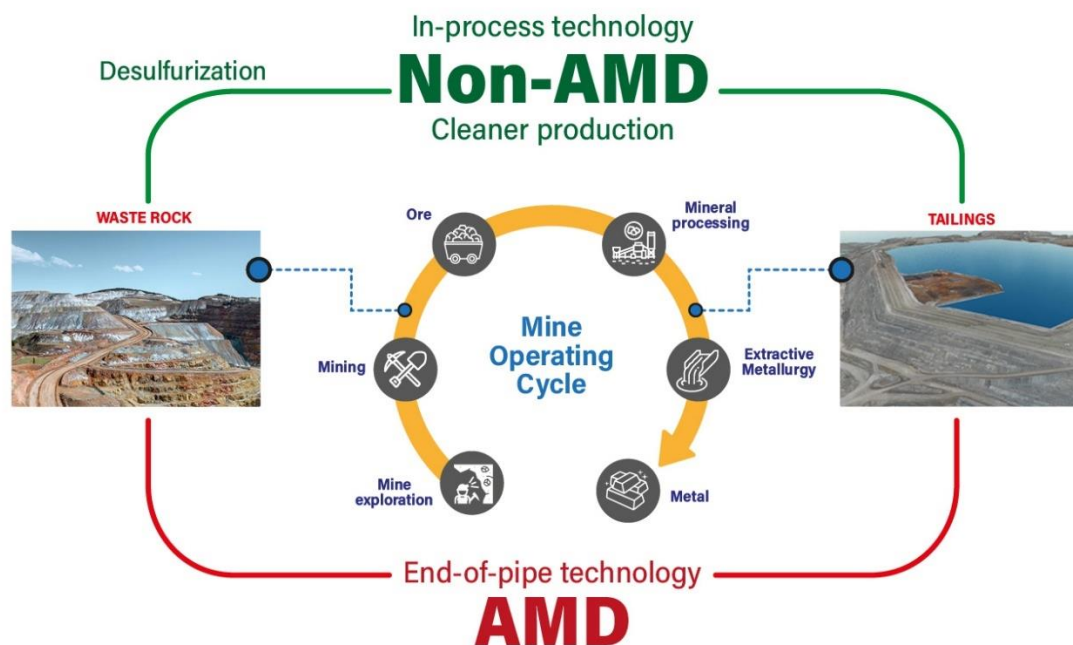


Figure 2.6 Strategies for waste and AMD management.

2.3.1 Generation of acid mine drainage (AMD)

AMD is an acidic water flow ($\text{pH} < 6$) generated by mining activity. It is formed when solid waste contains sulfide minerals, such as pyrite (FeS_2). AMD affects the chemical stability of solid waste by dissolving heavy metalloids such as As, Cd, Co, Pb, and Zn, which are toxic species that can migrate to surrounding ecosystems, contaminating groundwater and surface water (Gascón et al., 2015; Jain et al., 2016; Naidu et al., 2019). Pyrite is a common iron sulfide in mining activity solid waste, and it is reactive in oxidizing media. Therefore, the formation of AMD from pyrite is the most studied mechanism. The main factors that affect the formation of AMD are oxygen, water, microbial activity, and particle size (Gascón et al., 2015). From the point of view of water–oxygen and bacteria interaction, the process starts with the chemical reaction of pyrite (FeS_2) with the surrounding water and oxygen, producing sulfuric acid (H_2SO_4). H_2SO_4 is responsible for water acidification and, at the same time, dissolves other heavy metals (Gascón et al., 2015; Ginocchio and León-Lobos, 2011; Jain et al., 2016; Naidu et al., 2019). Additionally, it produces Fe^{2+} , which

reacts with oxygen and bacteria, producing Fe^{3+} . Fe^{3+} can generate $\text{Fe}(\text{OH})_{3(s)}$ and H^+ , which contribute to the formation of more acid. Furthermore, Fe^{3+} can react again with pyrite, generating more acid and Fe^{2+} . The latter reaction is usually fast because Fe^{3+} is highly oxidative (see Figure 2.7). Additionally, Fe^{3+} facilitates the leaching of other compounds such as As, Pb, and Cu (Murray et al., 2014).

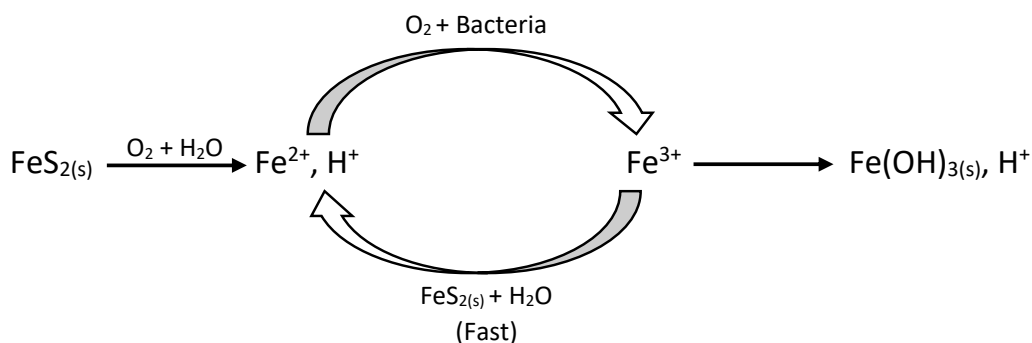


Figure 2.7 AMD generation mechanism (adapted from Botero et al., 2021).

According to the above, the processes currently implemented for the concentration of valuable minerals result in the production of tailings with a high content of iron sulfide minerals and metals/metalloids, which generate AMD. In this context, various methodologies have been developed for the mitigation of AMD.

2.3.2 Management of AMD from tailings

The current technologies used to treat AMD from tailings can be categorized as end-of-pipe technology. End-of-pipe technology methodologies look for solutions for AMD generation in the last phase of the process. They can be classified as AMD prevention, AMD mitigation, and recovery of valuable species from the AMD. The prevention methodology focuses on identifying the source of generation; this includes adopting actions before starting the extractive activity to determine the potential contaminant and predict the method that is more convenient to be implemented for AMD prevention. One example is the dry cover method. This method consists of covering the tailings with one or more layers of materials that are permeable to water and oxygen. Some materials used for dry cover include rock-neutralizing materials such as lime and dolomite, which have low sulfur contents. These layers of permeable material form a capillary barrier that

helps retain water within the clay layer. Therefore, the limited supply of water and O_2 suppresses the oxidation of pyrite and the formation of AMD (Lottermoser, 2007).

Another example is the wet cover method, which consists of controlled flooding of the tailings disposal areas. The water cover must have enough height to isolate the tailings from contact with the air to guarantee the minimum oxygen diffusion. This approach can be complex and expensive to implement, particularly for older deposits and in arid zones where the water is scarce (MEND, 1998). Therefore, these methodologies are not suitable because large areas of tailings must be covered. This is why mitigation of AMD is largely implemented rather than prevention.

Mitigation activities are actions taken when it is verified that preventive measures cannot work and there is a possibility of AMD generation. These measures aim to satisfy environmental quality criteria, reducing the impacts of mining activities. AMD mitigation methods can be classified as active and passive. Active methods require the continuous addition of chemical reagents, constant monitoring, and mechanical devices to mix reagents with the water. An example of these methods is the neutralization technique. This technique consists of a physical–chemical process where a neutralizing agent is added to the tailings. Traditionally, limestone ($CaCO_3$) and hydrated lime ($Ca(OH)_2$) are used as neutralizing agents. The addition of these materials raises the pH level. Thus, the dissolved metals in the water will form insoluble metal hydroxides and will precipitate. Even though this is a good alternative for AMD mitigation, it involves increased operational costs due to the high consumption of reagents and energy (Gascón et al., 2015; Lottermoser, 2007).

Passive techniques do not require reagents or mechanical devices for their operation. These methods use natural processes such as gravity, the metabolic process, microbial activity, and photosynthesis to reduce the concentration of dissolved metals and neutralize the acidity of AMD. For instance, the limestone drains technique is a physicochemical method that uses shallow trenches filled with crushed limestone and covered with impermeable plastic soil or sediment, through which AMD is filtered. The acid drainage water must permanently make contact with the limestone throughout the entire canal. The dissolution of limestone consumes acidity and establishes a mitigating capacity by forming bicarbonate ions in the water, neutralizing acidity from AMD (Gascón et al., 2015; Lottermoser, 2007). Finally, it is worth mentioning that in this section we have only presented the more common strategies used for AMD mitigation; there are several more. Therefore, the best treatment for AMD mitigation will depend on AMD mineralogical

composition, pH, and economic factors. Furthermore, mitigation implies the construction of a complex system to manage the tailings (e.g., new facilities, new technologies), increasing the cost. From an environmental point of view, the way the flotation process is conducted does not allow the complete elimination of AMD from tailings because they contain acidic species permanently. Consequently, this brief review regarding the traditional practices of tailings AMD management suggests that prevention of AMD is the best option rather than mitigation and is required in many jurisdictions. In this sense, incorporating the concept of cleaner production in mining processes is a future practice, and the strategy involves the desulfurization of minerals through the flotation process.

2.4 Environmental Desulfurization of Tailings and Waste Rock

The environmental desulfurization of mine waste using various mineral processing techniques has been reviewed by Ait-Khouia et al. (2021). They presented a critical analysis of the advantages and limitations of implementing different physical techniques for removing the sulfide minerals responsible for generating AMD. They concluded that the application of each mineral processing method depends strongly on the physical–chemical properties of minerals, such as specific gravity, mineralogical composition, particle size distribution, liberation grade, magnetism, optical properties, hydrophobicity, hydrophilicity, and others. Some of these techniques are conventional gravimetric concentration, centrifugal gravimetric concentration, magnetic separation, electrical separation, sensor-based sorting, and flotation. For instance, conventional gravimetric concentration is carried out in shaking tables. This technique allows the treatment of tailings and WR with particle sizes between 75 μm and 15mm. No chemical reagents are required, allowing low investment and operating costs. Nevertheless, some issues are related to the use of this technique. The difference in densities between the sulfide minerals and gangue must be $>1 \text{ g/cm}^3$, and the degree of liberation must be high. This technique is ineffective for fine particles ($< 75 \mu\text{m}$), and the performance is limited when the waste contains clay minerals $>30\%$ (Ndlovu et al., 2017; Wills and Finch, 2016; Yıldırım Gülsoy and Gülcan, 2019).

Centrifugal gravimetric concentration using a Knelson concentrator is another widely used technique. This technique enables a high separation efficiency and recovery rate. However, wastewater treatment is complex due to very fine particles, which require special filters or thickeners (Das and Sarkar, 2018; Koppalkar, 2010; Zhu et al., 2017). Another technology used in

centrifugal gravimetric concentration is the Kelsey jig; the advantages of this technology are that it has high capacity, is capable of handling fine particle sizes (10 μm) and accepts a narrow specific gravity. However, it has relatively high investment and operating costs (Das and Sarkar, 2018).

Magnetic separation is also a good alternative for mineral beneficiation, it is respectful to the environment, but a medium liberation degree (particle size $>75 \mu\text{m}$) and high investment and operation costs are required (Rezvanipour et al., 2018; Rikers et al., 1998; Wills and Finch, 2016). Electrical separation can be used for particle sizes between 60 and 500 μm . This method has a good processing performance, and it is environmentally friendly. Nevertheless, some issues related to the particle moisture and liberation degree make it challenging to use because the moisture alters the behavior of the particles, and the liberation degree must be high, with a marked difference in electrical conductivity (Halder, 2018; Wills and Finch, 2016).

Sensor-based sorting is generally used for WR because it can be applied for coarse particles (0.5-350mm). The purpose of ore sorting is to remove coarse barren material before energy- and cost-intensive downstream processing and handling. Fewer tons of ore are treated per ton of product, reducing the cost, energy, and water consumption per ton of product. Thus, ore sorting has the potential to improve profitability and reduce the environmental impact of a mining operation. However, this practice depends on the ore characteristics, distribution of grade throughout the deposit, and the efficiency of the sorter. In addition, this technology requires extensive testing and evaluation on a case-by-case basis. These aspects impact the operating capital and operating costs for the operation. Therefore, the additional costs associated with ore sorting must be outweighed by the reduction in downstream processing costs and/or increased production (Dalm et al., 2014; Robben and Wotruba, 2019).

Finally, flotation is commonly used to accomplish environmental desulfurization. This technique has been successfully carried out on numerous mine tailings around the world from small to industrial scale (Benzaazoua et al., 2017, 2000; Nadeif et al., 2019; Skandrani et al., 2019). The flotation process takes advantage of the surface properties of minerals, such as hydrophobicity and hydrophilicity, to separate sulfide minerals from gangue. The method involves a physicochemical interaction between several reagents, such as collectors, activators, frothers, and pH, and mineral surfaces, with the aim to make the sulfide mineral surfaces hydrophobic and separate them from gangue minerals. However, the slurry formed during the flotation process is a complex system

depending on multiple variables such as pulp potential, redox reactions, particle size, pH, collector concentration, making the control of parameters and the study of the process challenging. Despite this, flotation remains the most widely used technique for desulfurization of tailings because high recoveries are obtained. In addition, this technique has been implemented successfully for WR desulfurization (Amar et al., 2020).

The acid generation potential assessment of WR and tailings is another relevant aspect in the desulfurization process. For predicting the net neutralizing potential (NNP) and neutralizing potential ratio (NPR), several static methods have been developed based on parameters and criteria that differ from one method to another. Static prediction tests attempt to determine the balance between the acid potential (AP) of the material, derived by quantifying the acid-producing components, and the neutralizing potential (NP), determined by measuring the quantities of acid-consuming components (Lawrence and Scheske, 1997). The NNP and NPR can be interpreted via the criteria of the acid–base accounting (ABA) diagram to determine the acid generation potential (AGP) of the ore studied (see Figure 2.8).

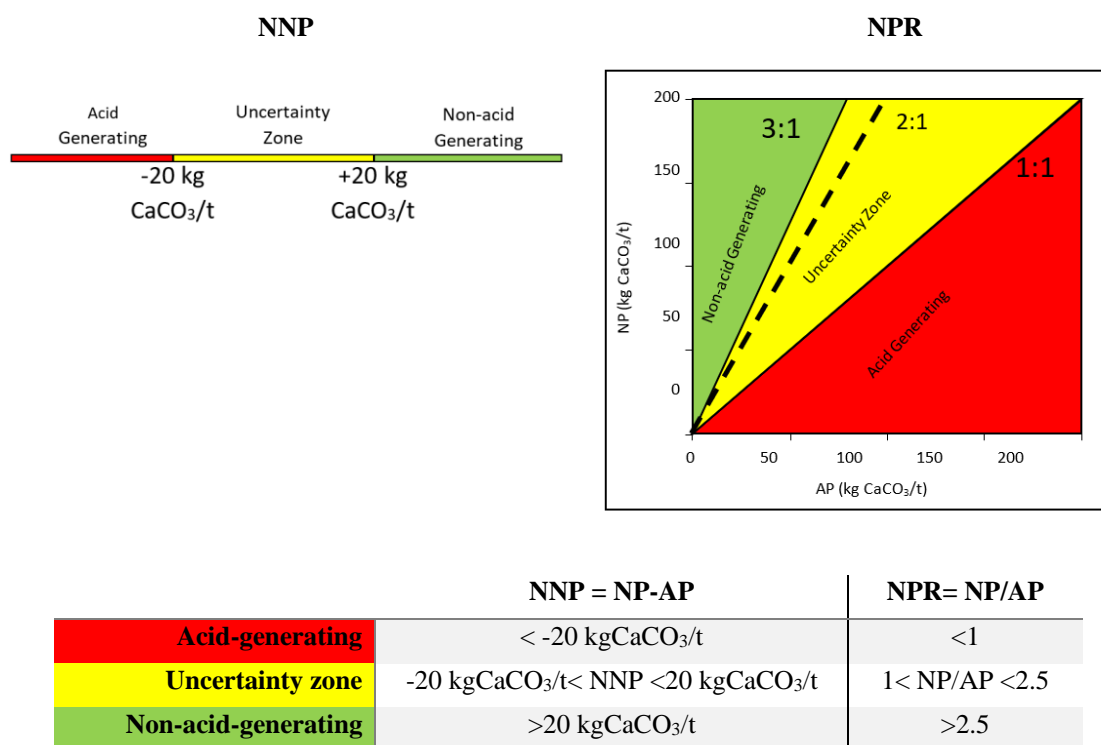


Figure 2.8 Static method used for the prediction of acid generation potential.

The NNP is calculated by subtracting the AP from the NP ($NNP = NP - AP$). If the NNP value is lower than 20 kg $CaCO_3/t$, the sample is classified as acid-generating. An uncertainty zone is characterized by NNP values between -20 and 20 kg $CaCO_3/t$ (Miller, S., Jeffery, J., Wong, J., 1991). The neutralization potential ratio ($NPR = NP/AP$) constitutes another index by which to evaluate the AMD production potential. Characteristically, a sample is considered acid-generating if $NPR < 1$, uncertain if $1 < NPR < 2.5$, and non-acid-generating if $NPR > 2.5$ (Benzaazoua et al., 2017, 2004; Elghali et al., 2018).

The static methods are classified into two categories: chemical and mineralogical tests. The static chemical method involves the test of Sobek (1978), which is based on the total sulfur (wt% S) and total carbon (wt% C). Then, the AP and carbonate neutralization potential (NP) are calculated as follows:

$$AP \left(Kg \frac{CaCO_3}{t} \right) = 31.25 * \% Stotal \quad (2.13)$$

$$NP \left(Kg \frac{CaCO_3}{t} \right) = 83.3 * \% Cttotal \quad (2.14)$$

This method generates some discrepancies in the measurement of AP and NP because AP is calculated based on the total sulfur content instead of the sulfide content of the sample. Furthermore, for NP, the total carbon used in the Sobek test also includes non-neutralizing carbon (Paktunc, 1999). Therefore, the importance of mineralogical characterization in AMD prediction has become more relevant in identifying all the minerals that can contribute to effective NP and AP calculations (Lawrence and Scheske, 1997). In this sense, the static mineralogical method is used for the determination of AP and NP based on the mineralogy of the sample (Lawrence and Scheske, 1997; Paktunc, 1999). Lawrence and Scheske (1997) proposed that NP calculations could be carried out using each neutralizing mineral stoichiometrically. The Paktunc (1999) method proposes calculations based on the sum of the individual contribution of each mineral in the production of acidity and its neutralization, according to the following two equations:

$$AP = 10 \sum_{i=0}^k \frac{n_{M,a} X_i W_a}{W_i} \quad (2.15)$$

$$NP = 10 \sum_{i=0}^k \frac{X_i W_a}{n_{M,i} W_i} \quad (2.16)$$

where 10 is a conversion factor; X_i is the amount of mineral i in wt%; W_a and W_i are the molecular weights of H_2SO_4 and mineral i , respectively; $n_{M,a}$ and $n_{M,i}$ are stoichiometric factors of acid generation and neutralization; and k denotes the number of sulfide minerals and neutralizing minerals in the sample.

These equations improve AP and NP predictions by considering sulfides other than pyrite and other carbonate minerals. However, some studies have recommended reviewing the reactivity factor for AP determination. This was implemented later by Bouzahzah et al. (2013) based on Paktunc's equation. They suggested a modified equation to attempt to include the reaction kinetics of each sulfide for AP calculations. The relative acidity production factor was determined experimentally by calculating the average of the total acidity produced by each sulfide in the leachates of the kinetic tests. The relative experimental acidity production of each sulfide was used to calculate a relative reactivity factor (r_s). Then, the equation used for AP calculation was:

$$AP = 10 \sum_{i=0}^k \left(\frac{n_{M,a} X_i W_a}{W_i} \right) r_s \quad (2.17)$$

It was determined that r_s is 1 for pyrite and pyrrotite, and 0.06, 0.23, 0.26, and 2.54 for galena, chalcopyrite, sphalerite, and arsenopyrite, respectively. These values mean that arsenopyrite produces about 2.5 times more acidity than pyrite (Chopard et al., 2017). Thus, this is a better approach compared with the methods proposed by Sobek and Lawrence–Paktunc. However, this factor does not consider the oxidation rates of each sulfide—and thus the kinetics of the reaction—as this factor is based on the acidity production on average and does not refer to a reaction rate. Furthermore, this factor does not consider the influence of minerals between themselves; that is, the interactions between semi-conducting minerals, known as galvanic interactions, which modify (inhibit or activate) the geochemical behavior of sulfide minerals. According to this, Chopard et al. (2017) suggested using an oxidation factor considering the kinetics of reactions of each sulfide for the mineralogical AP calculation to improve AP estimation. Therefore, a new r_s factor replaces the average acidity production. The factor r_s is set as 1 for pure pyrite, and the others are calculated relative to pyrite according to the following equation, where r_s is the relative factor, r_i is the oxidation rate of the mineral i , and r_{pyrite} is the oxidation rate of pyrite.

$$r_s = r_i / r_{pyrite} \quad (2.18)$$

However, since the mineralogical static test involves the mineral characterization of many samples, this can make the procedure complex and expensive due to the number of characterization techniques required to carry out the static test. Furthermore, the detection level of some techniques such as XRD is insufficient to identify low amounts, making the accuracy of AP and NP calculations more difficult.

In this work, the method developed by Elghali et al. (2018) was implemented. ABA testing was corrected by introducing the degree of sulfide and carbonate liberation, which accounts for the initial texture of the minerals. Thus, the AP and NP values were calculated as follows:

$$AP = 31.25 \times S_{sulfides} (\text{wt. \%}) \times L_s \left(\text{kg} \frac{\text{CaCO}_3}{\text{t}} \right) \quad (2.19)$$

$$NP = 83.3 \times TIC (\text{wt. \%}) \times L_c \left(\text{kg} \frac{\text{CaCO}_3}{\text{t}} \right) \quad (2.20)$$

where L_s and L_c denote the liberation degrees of sulfides and carbonates, respectively. Values of L_s and L_c were obtained using QEMSCAN. $S_{sulfides}$ and TIC denote the wt. % of sulfur associated with sulfides and total inorganic carbon, respectively. Finally, despite this method being a good approach to assess AP and NP, a common practice is to complement static testing with kinetic tests when the static test results are in the uncertainty zone.

Kinetic testing allows the assessment of the geochemical behavior of desulfurized material. This is performed using humidity cells to evaluate the long-term acid-generating potential and short-term using weathering cells. The humidity cell test method is based on ASTM D5744-96. The procedure is as follows: a seven-day cycle consisting of two days of exposure to ambient air, followed by leaching on the third day and three days of exposure to air, and finally flushing during the seventh day. The total duration of the experiments is between 15 and 20 weeks. The leachates recovered after each cycle are analyzed for several geochemical parameters to identify WR and tailings reactivity, oxidation kinetics, metal solubility, and the overall leaching behavior of the materials. For each sample, pH, Eh, electrical conductivity, metal concentrations, acidity, and alkalinity are analyzed. These data are compiled as instantaneous and cumulative loads, as well as elemental depletion curves that are based on the volume and composition of the leachates and the initial geochemistry of the solid samples. Additionally, the filtered leachates are acidified with 2% HNO_3

for preservation. The resulting solutions are analyzed using ICP-AES to determine metal and sulfate concentrations (Amar et al., 2021; Cruz et al., 2001; Nadeif et al., 2019)

Weathering cells are also used. The conditions of these tests are slightly more aggressive than those for wet cells but close enough to justify their substitution when the quantities of material are limited. The weathering cells are scaled-down versions of humidity cell tests using less material (about 67 g), leaching twice per week, using 50 mL of deionized water, and allowing the equipment to air-dry between leaching. As in the humidity cells, the leachate is left in contact with the solid for a period of a few hours, before filtering the water using a vacuum pump (Bouzahzah et al., 2014).

2.4.1 Desulfurization of tailings

Several studies have been carried out related to the desulfurization of tailings (Benzaazoua et al., 2017, 2000; Nadeif et al., 2019; Skandrani et al., 2019). For instance, the environmental desulfurization of four samples of Canadian mine tailings using flotation was conducted by Benzaazoua et al. (2000). Non-selective flotation was conducted using PAX as a collector, and the process generated both concentrated sulfide and non-reactive desulfurized material. It was demonstrated that environmental desulfurization is an alternative for the management of acid-generating tailings, and it is economically attractive compared to traditional methods for tailings management. However, the behavior of each tailings sample was distinct because they came from different mineral processes. For instance, one of the tailings samples came from a gold cyanidation process. Thus, the desulfurization of these tailings did not provide good sulfide recoveries because of pyrite depression, even after surface activation and pH decrease. Therefore, these results allow us to determine that despite the desulfurization of tailings seeming to be a good alternative, the fact that the tailings already have some depressed species makes its reprocessing challenging. In other words, desulfurization is complex because the tailings contain a mixture of several reagents that modify the behavior of sulfide minerals. For this reason, in this work we propose conducting desulfurization at an early stage of the process rather than in the final step of the flotation, intending to better control the physical–chemical interactions that occur between sulfide minerals and reagents. This methodology could enable optimization of the amount required for each reagent, as well the order of addition of reagents, allowing better control of the pulp potential and, therefore, developing a flotation process that is more efficient and suitable for cleaner production.

Benzaazoua et al. (2017) conducted the desulfurization of pyrrhotite-rich tailings at Raglan mine. These tailings were classified as potentially acid-generating according to the static test. Desulfurization using the flotation process enabled pyrrhotite recoveries higher than 95%, although a high collector dosage was required (150 g/t), as well as high pH (10.5-11.5) and activators. Thus, the flotation provided high sulfide recoveries, which was an excellent result. However, again, the desulfurization increased reagent consumption and required the use of other reagents such as activators, which can increase the cost.

Skandrani et al. (2019) carried out the desulfurization of old gold-bearing mine tailings. They identified that the abandoned tailings had some issues related to the formation of layers on sulfide minerals. These layers resulted in a poor affinity of sulfide minerals with the collector, reducing the flotation performance. Consequently, the team implemented mechanical treatments such as regrinding, agitation, and attrition to remove the oxidized species formed and activate the sulfide mineral surface. After this procedure, they demonstrated that it is possible to produce a concentrate rich in sulfides and gold. In addition, the desulfurized tailings were non-acid-generating due to their high neutralization potential. However, it was concluded that several pretreatments must be used to remove the oxidized species formed on sulfide mineral surfaces to enhance the desulfurization performance. Therefore, this aspect makes reprocessing challenging because the desulfurization flotation circuit requires another stage of regrinding, increasing energy consumption and operating costs.

Another study was performed related to the desulfurization of old tailings at the Au-Ag-Cu Tiouit mine (Anti-Atlas-Morocco) (Nadeif et al., 2019). Kinetic testing was carried out to study the geochemical behavior of the desulfurized tailings. It was found that desulfurization allows for a good but not complete sulfide recovery. Therefore, the desulfurized tailings produced leachates with a slightly higher pH than the initial tailings. Despite this, desulfurization is a better alternative than mine site mitigation.

Finally, in the context of end-of-pipe technology, we compare current methods used to manage tailings that implement strategies of mitigation rather than prevention. Desulfurization of tailings is the best practice to reduce the environmental impact of mining exploitation. However, cleaner production is the motivation of this work. Thus, we aimed to incorporate the “in-process technology” concept into the flotation process to propose new methodologies.

2.4.2 Desulfurization of waste rock

The environmental desulfurization of tailings has gained significant interest in copper mining because it is an excellent alternative for controlling AMD production by reducing the content of sulfide in tailings. WR desulfurization is a novel approach that can be carried out by applying flotation separation in a conventional flotation cell (Denver cell) (Amar et al., 2021, 2020; Benzaazoua et al., 2000). The valorization and management of WR depend on the accurate study of mineral reactivity. It is well known that materials with fine particle sizes have large surface areas and a larger area available for acidification, promoting AMD (Amar et al., 2021). WR can be separated into two fractions, reactive and nonreactive, by applying the diameter of the physical locking of sulfides (DPLS). This concept was developed to manage WR based on particle size. Usually, a particle fraction below 1000 μm is considered the reactive fraction; this is the fraction that produces AMD (Amar et al., 2021).

Recently, Amar et al. (2021) conducted a combined gravity-flotation procedure for WR desulfurization. They demonstrated that the preliminary particle size separation allows defining the DPLS for WR (2.4mm). It was observed by QEMSCAN that the degree of liberation of sulfide minerals decreases as the particle size increases. Therefore, the fine fraction was rich in sulfide minerals and was classified as potentially acid-generating. Thus, the fine fraction was used for the desulfurization process. In consequence, the combined gravity-flotation procedure enabled high sulfide mineral recoveries (89 wt%), and the ABA test demonstrated that the desulfurized material was non-acid-generating because it had a low sulfur content (0.23 wt%). Finally, kinetic testing showed the geochemical behavior of the desulfurized material. In a long-term prediction study, it was observed that the material was non-acid-generating. A similar study was conducted by Amar et al. (2020), who carried out a detailed characterization of WR from the Canadian Malartic mine in Malartic city (Quebec, Canada), followed by the environmental desulfurization of WR. They used the same concept of DPLS to determine the acid potential generating fraction, and the gravity-flotation process was conducted for the desulfurization process. One particularity of this WR was that before the desulfurization, the lithologies were non-acid-generating because the characterization showed that it contained large amounts of carbonates compared to its sulfide content. Therefore, a desulfurized material with no potential acid generation was obtained, and the desulfurization concentrate contained precious metals, such as gold (3.78 g/t) and silver (4.9 g/t). The extraction of these precious metals can offset costs related to reprocessing. Finally, the sulfur

recovery from the gravity method was better than that from the flotation process. This result could be because the particle size used for the desulfurization process is larger than the limit of the particle size required to conduct the flotation process in a Denver cell.

Indeed, a conventional Denver flotation cell requires a grinding stage, which increases energy consumption. In this case, technology to float coarse particles can be beneficial. To the author's knowledge, there are no studies of coarse particle flotation of WR. Therefore, the technology of fluidized-bed flotation (HydroFloat) could be an excellent alternative to float coarse particles ($\approx 800\mu\text{m}$). This technology reduces energy costs because it is possible to avoid the grinding stage during mineral processing and allows reprocessing of WR. In addition, valuable elements can be recovered to finance the process. Moreover, the valorization of WR can be analyzed from two points of view. The first is related to minerals with economic value identified in WR. In this case, the concentrate obtained after the desulfurization process can be integrated into the conventional concentration process. The second is related to reducing the volumes of WR to be stored. For instance, the use of WR in the manufacture of mine backfill, backfilling of construction sites, and as aggregates for construction are some alternatives to WR.

2.4.2.1 Fine- and coarse-particle flotation

The relationship between floatability and particle size has been studied extensively in the literature (de Gontijo et al., 2007; Jameson, 2010; Kohmuench et al., 2018). The particle size presents a set of different problems during the flotation process. The major issue is related to the decrease in recovery when particle size is increased. This decrease in recovery can be analyzed using the well-known “elephant curve” developed by Lynch et al. (1981); see Figure 2.9. These data were collected from the industrial application using conventional flotation (mechanical cell). The figure displays different particle sizes where the maximum recovery is observed in the particle range between 20 and 120 μm . Then, the recovery diminishes for particle sizes $<10\mu\text{m}$ and $>150\mu\text{m}$, corresponding to ultra-fine particle sizes and coarse particle sizes, respectively.

In the case of ultra-fine particle sizes, the main reason for the recovery decrease is that it is strongly influenced by inertia and viscous drag. Therefore, the streamlines diverge as they approach the bubble. The particles tend to follow these streamlines, and therefore the probability of collision between the particles and bubble reduces (Jameson, 2010). The reduced recovery of coarse particles is related to their inability to remain attached to the bubbles due to the high turbulence

generated in the mechanical cell. In other words, the centrifugal force exceeds the attachment forces of surface tension, and therefore the particle is detached from the bubble. There are some advantages and limitations to using fine particles and coarse particles during the flotation process; Table 2.1 displays the most relevant characteristics.

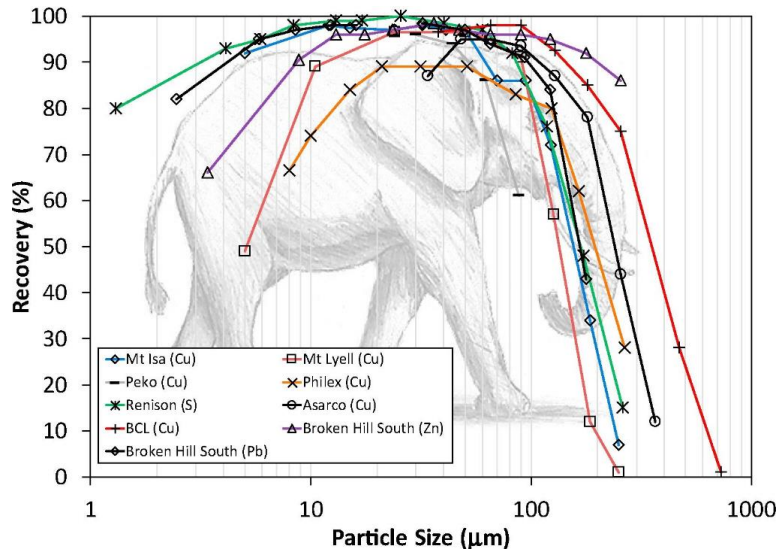


Figure 2.9 Floatability of sulfide minerals using conventional flotation (Lynch et al., 1981).

Jameson et al. (2008) showed that it is possible to calculate the maximum particle size ($d_{p,max}$) that can be floated by a mechanical cell, using the following equation:

$$d_{p,max} = 1.53 \left(\frac{\gamma^6 (1 - \cos\theta)}{\Delta \rho \varepsilon_i^{\frac{4}{5}} \rho_L^{\frac{1}{5}}} \right)^{\frac{1}{2}} \quad (2.21)$$

This equation depends on several factors such as surface tension (γ) and contact angle (θ); $\Delta \rho$ is the difference between the densities of the solid particle and the liquid; ε_i is the specific energy dissipation rate, W/kg; and ρ_L is the liquid density. In addition, the type of mineral plays an important role. It is evident that from this equation, we arrive at the operational limit of the mechanical cell. Therefore, some other alternatives have been developed to improve recovery. In the case of coarse particles, it is possible to keep particles and bubbles in contact in a quiescent environment, which can be reached using the fluidized bed methodology. The fluidized bed enables high recoveries over a wide range of particle sizes. For instance, Jowett (1980) performed a flotation test for galena using conventional flotation and fluidized bed flotation, and Figure 2.10

shows the results. In the mechanical cell, the recovery for the ultrafine particle size is very low, and when the particle size increases to approximately 60 μm , the recovery reaches 97%; for larger sizes, the recovery diminishes drastically. In the fluidized bed cell, the recovery remains between 95 and 100% for particle sizes up to 850 μm ; beyond this size, the recovery gradually declines. These results show that fluidized bed cells can extend the range of particle sizes of galena recovered by flotation more than ten-fold.

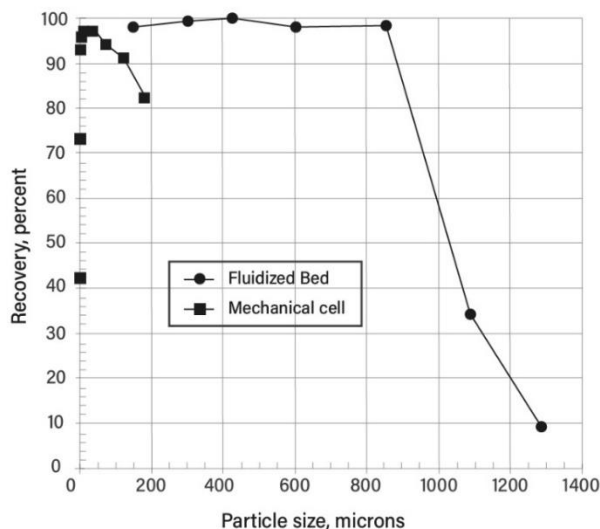


Figure 2.10 Results of mechanical and fluidized bed flotation cells for a sample of galena (Adapted from Jowett, 1980).

One of the technologies implemented in fluidized bed flotation is the HydroFloat®. Initially, the HydroFloat® was developed to provide a solution for the low recovery of coarse phosphate. Using this approach, it is possible to increase recovery from 50% to 90% (Kohmuench, Thanasekaran, 2013). Numerous installations of this technology have been implemented in the industrial mineral sector (more than 50 units installed worldwide). This includes a plant-wide retrofit installation at Mosaic's South Fort Meade Mine (Kohmuench et al., 2007) and PotashCorp's Aurora beneficiation plant (Piegols et al., 2015). In addition, the HydroFloat® has been commercially used to recover vermiculite in the United States, diamonds in Canada, and spodumene in Australia (Awatey et al., 2015, 2013; Fosu et al., 2015). Furthermore, the use of this technology for sulfide and base metal applications has drawn significant attention due to its inherent capacity for energy saving.

Table 2.1 Advantages and limitations of fine- and coarse-particle flotation.

Size of particle	Advantages	Limitations	References
Fine (10-200 μm)	<ul style="list-style-type: none"> In this particle size range, the highest flotation kinetic and grade are obtained. This is the reason why companies operate in this size range. Recoveries approach 100%. Higher liberation of sulfide minerals provides more sites for bubble attachment. Better sulfide mineral hydrophobicity. 	<ul style="list-style-type: none"> Estimates of energy consumption for mining operations show that approximately 75% corresponds to the comminution stage. Energy consumption constitutes a high cost in the mining operation, in some cases approximately 54% of the total cost. The cost of water in mining operations is high, in some cases corresponding to 38% of the total cost. The water loss in tailings is approximately 52% (the management of tailings is challenging in terms of physical and chemical stability). 	(Bulatovic, 2007; Donoso et al., 2013; Fuerstenau; Jameson; Yoon, 2007; Norgate and Haque, 2012, 2010; Wels et al., 2003 al., 2003).
Coarse (200-800 μm)	<ul style="list-style-type: none"> Energy savings, as the particle size is larger and less grinding is required. Water recovery in the thickener and dump is easier. Better management of tailings because less AMD is released as the particle size is larger. Low dust formation. 	<ul style="list-style-type: none"> Low collision between bubble and particle. As the particle size increases, the mass is greater, and therefore gravity affects the floatability. As the particle size increases, the surface area is smaller, and therefore there is less sulfide mineral liberation, affecting the generation of sites for bubble attachment. The bubble-particle aggregate is unstable and tends to separate. In a mechanical flotation cell, the impeller generates excessive turbulence, causing detachment between the bubbles and coarse particles and, therefore, a drop in recovery. 	(Awatey et al., 2015; Devasahayam, 2007; Fuerstenau; Jameson; Yoon, 2007; Kohmuench et al., 2018; Osses et al., 2019)

Finally, the above information suggests that the flotation of coarse particles using fluidized bed flotation may be an excellent alternative for copper sulfide flotation. This technology could have a meaningful impact on the use of strategic resources (water and energy) and diminish the environmental impact because the management of tailings can be improved substantially.

2.4.2.2 Coarse particle flotation using the HydroFloat®

A simplified schematic of the HydroFloat® fluidized-bed separator is shown in Figure 2.11. This technology uses the synergistic combination of flotation and gravity concentration. The principle of operation consists of air bubbles dispersed by a fluidization system; these percolate through the hindered-setting zone and attach to the hydrophobic component, altering its density and rendering it sufficiently buoyant to float and be recovered. A fluidized bed eliminates axial mixing, increases coarse particle residence time, and improves the flotation rate through enhanced bubble–particle interactions. As a result, the recovery rate is high for both fully liberated and semi-liberated particles. The particles may be naturally hydrophobic or made hydrophobic through the addition of flotation collectors. In addition, thanks to the flow of fluidization water, the lighter bubble–particle aggregates rise to the top (overflow) and accumulate due to their lower density, and they are then collected. Hydrophilic particles (non-float fraction) continue to move down through the fluidized bed, settle into the dewatering cone, and are discharged using an underflow control valve (Eriez, 2021; Kohmuench et al., 2018; Mankosa et al., 2021).

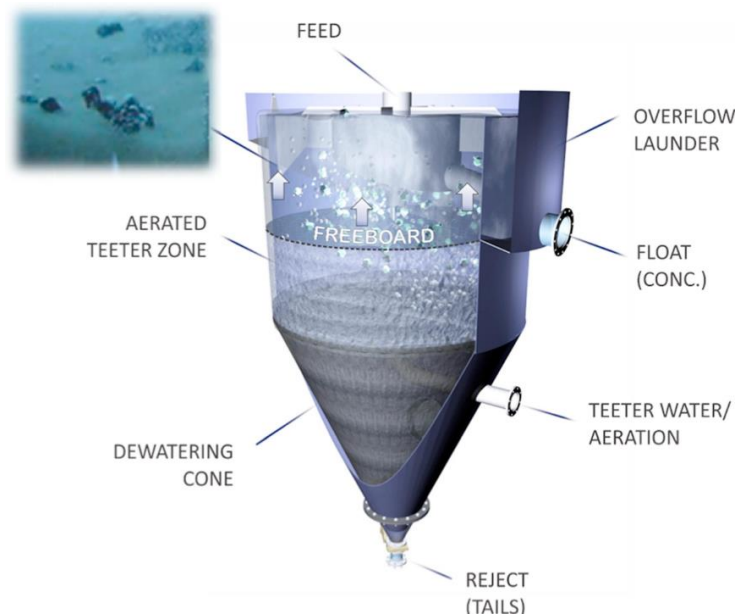


Figure 2.11 Schematic of the HydroFloat® separator with bubble–particle aggregates (Taken from Eriez, 2021).

The HydroFloat® fluidized-bed separator offers several advantages for treating coarse particles: it improves the coarse particles by increasing the bubble–particle collision rates, increasing residence time, decreasing mixing, decreasing turbulence and detachment, and decreasing buoyancy restrictions. These advantages are explained in detail in Table 2.2.

Table 2.2 Fluidized-bed flotation advantages for treating coarse particles.

Characteristics	Advantages	References
Improved attachment	In the fluidized-bed flotation device, the differential velocity between bubbles and particles is significantly reduced. Hence, a decrease in velocity will increase the contact time between bubbles and particles, promoting the probability of attachment and enhancing flotation recovery.	(Kohmuench et al., 2018; Mankosa et al., 2021)
Reduce turbulence	When the flow is changed from turbulent (mechanical cells) to quiescent conditions (fluidized-bed), the optimum conditions for coarse particle flotation are achieved. Here, it is possible to keep the coarse particles dispersed with fluidized water.	(Mankosa et al., 2021; Woodburn et al., 1971)
No buoyancy limitation	The HydroFloat™ operates with a minimal froth layer. This characteristic allows no buoyancy limitation. This fact is essential for very large particles, which could be difficult to recover in conventional flotation machines that operate with froth depths ranging from 100 to 900 mm.	(Kohmuench et al., 2018; Mankosa et al., 2021)
Plug-flow conditions	The low degree of axial mixing allows the uniform distribution of particles across the teeter bed. This fact suggests that the fluidized bed operates under nearly plug-flow conditions. This characteristic ensures that more of the available cell volume is effectively used compared to well-mixed conventional cells.	(Kohmuench et al., 2018; Mankosa et al., 2021, 1992)
Increased retention time	The fluidized water provides a significant increase in the particle retention time. A longer retention time allows good recoveries to be maintained without increasing cell volume.	(Kohmuench et al., 2018; Mankosa et al., 2021).
Reduced maintenance requirements	There is no need for mechanical agitation; therefore, there are no internal moving parts. As a result, equipment maintenance is substantially reduced. Traditional flow meters and valves are also used for the measurement and control of water and air.	(Kohmuench et al., 2018; Mankosa et al., 2021).

The HydroFloat® separator presents some limitations. These are related to operating parameters such as the bed-level, superficial water, and gas rates, which affect the coarse particle floatability and recovery. There are thresholds for each operating parameter, above which recovery starts to decrease. For instance, Awatey et al. (2013) studied the effect of these three parameters on coarse sphalerite recovery. They found that recovery increases when bed-level and fluidization water flow increase. However, there is a threshold below or above which recovery begins to decrease for these parameters. Additionally, the airflow has the smallest effect on the recovery. An optimum value of 0.38cm/s was found, above which no further improvement was observed. This could be an optimum value for practical use. The drop in recovery as the bed level increases may be due to the proximity of the feed system to the top of the teeter bed, which may be inducing localized turbulence or increasing the probability of detachment of coarse particles by injecting feed directly into the teeter bed instead of the quiescent zone above the fluidized zone. In addition, it is noted that as the fluidization flow is increased, the voids between the particles within the teeter bed increase, thereby reducing the effective density of the fluidized zone. As a result, the movement of the bed changes from a hindered-settling environment towards a free-settling one. This has a negative effect on coarse particle recovery, making it necessary to conduct a series of trials to determine the optimum parameters for each mineral that is going to be studied (Awatey et al., 2013).

2.5 Desulfurization of Tailings Using Bulk and Selective Circuit Design Based on Advanced Computational Optimization

Processing sulfide ores using flotation generates large volumes of tailings, which usually contain pyrite and other sulfur ore gangue (Lv et al, 2017). For example, in the production of copper by flotation, the average feed grade is below one percent, and therefore, for every ton of copper produced, more than one hundred tons of tailings are generated. These tailings are considered an environmental problem because of the enormous volume and mineralogical species they contain. One of the contaminants is pyrite, because it is a reactive mineral that can produce acidic water (Qian et al., 2019). This acidic water affects the chemical stability of the tailings by leaching other species such as copper, arsenic, zinc, and lead, which can be present in the tailings. The acidic water, together with the dissolved species, becomes a toxic solution, which is why it is one of the most relevant environmental concerns in the mining industry (Hyon et al., 2020; Qian et al., 2019).

In addition, if the toxic solution is concentrated, e.g., by wind and solar energy, toxic elements can precipitate and generate toxic powder. End-of-pipe technology is usually used to control the acid level in tailings (Jouini et al., 2019). This includes controlling the conditions for pyrite reaction (presence of air, water, or bacteria) or the neutralization control of the tailings. Furthermore, the flotation of pyrite from tailings (desulfurization) has been investigated with recoveries between 69 and 81% with pyrite concentrate grades between 78 and 96% (Santander and Valderrama, 2019). However, tailings flotation requires more consumption of reagents, water, and energy, which results in increased costs and environmental effects. In deep, large quantities of material must be treated because tailings comprise a tremendous amount of material. For example, the industrial flotation circuit proposed by Santander and Valderrama (2019) includes four stages (rougher, scavenger, cleaner, and recleaner), and at least the rougher and scavenger stages must process a large amount of material.

A more assertive approach to avoid acidic water in tailings can involve preventing the presence of pyrite in such waste. This can be considered a cleaner production approach (Fan et al., 2020) because the presence of pyrite is avoided by analyzing the source of such a contaminant. In this sense, developing a procedure that allows designing conceptual flotation circuits that can produce tailings with low pyrite content and assess these types of processes with traditional flotation circuits is one of the objectives of this work. This approach can also be considered a circular economy tactic because a redesign is sought to increase the circularity of the mineral processing sector (Reuter et al., 2019).

The flotation process is a method extensively used in the mining industry. Despite this, there are still some unresolved questions about controlling the operational parameters during the flotation process. The flotation process is a complex system composed of several stages, such as flotation cells, column cells, grinding, thickeners, hydrocyclones, etc., which are part of the flotation circuit. Furthermore, flotation is a physicochemical process. Thus, the pulp's behavior depends on other parameters such as the feed rate, grade mineral, recovery, pH, collectors, depressants, frothers, entrainment, etc. All these aspects make it challenging to develop a model capable of predicting the optimal parameters to be used in a flotation circuit, because the development of a model depends directly on the experimental data and design of the flotation equipment and circuit. For this reason, the design, optimization, and analysis of the flotation process have become a focus of

research since more simplified models have been developed to predict the optimal conditions for plant operation, which helps to reduce the maximum experimentation.

Cisternas et al. (2018) analyzed the advances, challenges, and gaps related to obtaining an optimal flotation design in respect of three elements: superstructure, mathematical model, and optimization algorithms. First, the superstructure represents all the possible alternative flotation circuits from which to search for a suitable process. For instance, a circuit structure can be formed by different stages (rougher, scavenger, cleaner, recleaner) and by introducing different technologies (bank of columns test, grinding, thickeners, etc.). All these possibilities make a combinatorial problem hard to resolve. The generation of superstructures capable of representing all the alternatives is challenging. There are some issues related to the selection of superstructures, such as defining the number and type of stages, eliminating circuit structures that represent nonsensical alternatives, and including several flotation technologies. For instance, Bourke (2002) showed that a flotation process has between four and eight banks, with five or twenty cells per bank. This number of stages and cells results in a vast number of alternatives. For example, Hu et al. (2013) determined 800,000 possible circuits if 5 cells are considered.

Several strategies of superstructure representation have been proposed and have evolved over the years. Mehrotra and Kapur (1974) proposed the first superstructure. They used a superstructure in which concentrate and tail streams can be sent to all equipment, including the same equipment that generates them. The superstructure of Mehrotra and Kapur is a straightforward representation. However, the number of alternatives increases exponentially with the number of flotation stages or cells, limiting their application. Furthermore, some alternatives do not make sense since the tail and the concentrate generated by a unit operation are sent to the same destination. In addition, stream dividers are used, increasing the system's complexity since they introduce bilinear expressions that generate nonconvex models that are challenging to solve. Another superstructure was proposed by Reuter et al. (1988). They used a generic superstructure to represent each stage, and some restrictions were included to reduce the combinatorial problem, such as eliminating structures that did not make sense. However, the number of alternatives was still very high. Schena et al. (1997) used a series of generic superstructures, including mixers and dividers, to represent the streams of interconnection in the circuit. Then, Cisternas et al. (2004) proposed a set of hierarchical superstructures. First, it was considered that a superstructure task was composed of rougher, cleaner, and scavenger tasks. Then, a superstructure flotation bank was utilized for each

task. Next, the division of streams was introduced, using disjunctions to avoid bilinear expressions and replace them with mixed-integer linear expressions. Then, Cisternas et al. (2006) proposed a third level of the superstructure, introducing a regrinding stage to the cell banks and column banks. Again, disjunctions were used to model the selection between equipment alternatives. The approaches of Schena et al. (1997) and Cisternas et al. (2006), did not address the combinatorial problem, and therefore, the problem was difficult to solve. In fact, only a few stages or cells were included in the examples analyzed.

Cisternas et al. (2014) incorporated the concept of the origin-destination matrix for each stream of the concentrate and tail, allowing the designer to select the stream directions, which significantly reduces the alternatives and avoids having streams that do not make sense. Origin-destination matrices for tail and concentrate streams are used to control connections that make no sense. Table 2.3 shows the origin and destination of concentrate (x) and tail (o) streams as an example. The origin-destination matrix identifies all of the concentrate and tail paths that the designer wants to consider in the study. This methodology is used to carry out the third objective of this thesis, i.e., the optimization of flotation circuits. In Table 2.3, the following stages are considered: rougher stage (R), cleaner stage (C), and scavenger stage (S). P and W represent the concentrate and tail, respectively.

Table 2.3 Origin-destination matrix for concentrates (x) and tails (o).

	R	C	S	P	W
R		x	o	x	o
C	o		o	x	
S	x	x			o

The mathematical model is associated with the superstructure, which corresponds to the mass balances in the equipment, stage recovery modeling, and selection of the destination of the streams. Other variables are included as operational conditions (e.g., minimum concentrate grade or total volume of flotation cells). In addition, binary variables are used to represent decisions such as the destination of streams and represent disjunctions (e.g., selection of equipment among a set of alternatives). Another critical aspect of the mathematical model is the objective function, which is

usually an economic expression (e.g., maximization of profits and revenues) (Cisternas et al., 2018).

Therefore, the mathematical model corresponds to a mixed-integer nonlinear programming (MINLP) problem, which is represented as follows:

$$\begin{aligned}
 & \max_{(x,y)} f(x,y) \\
 \text{s. a} \quad & g(x,y) = 0 \\
 & h(x,y) \leq 0 \\
 & x \in \mathcal{R}^n, y \in \{True, False\}^m
 \end{aligned} \tag{2.22}$$

where $f(x,y)$ is the objective function. The vector x corresponds to continuous variables (e.g., mass flow rates), the vector y represents binary variables, $g(x,y) = 0$ corresponds to the mass balances and $h(x,y) \leq 0$ represents decision and logical expressions. This MINLP problem is nonconvex and difficult to solve. Therefore, the algorithm needed to solve this type of problem must be able to solve MINLP problems, where the nonlinear problem is nonconvex, for which algorithms are needed to guarantee the global optimum. Hu et al. (2013) presented two approaches commonly used for flotation circuit design. The first approach describes the flotation kinetics in terms of the first-order rate process. This process predicts the recovery of the floated species from the resident time. The second approach considers the recovery of the floated species as a combination of true flotation and entrainment. These two approaches suggest that a robust model for the recovery is required as a first step for obtaining an optimal circuit design. Nevertheless, the problem is challenging to solve because of the nonconvex expression, such as the bilinear equation. For these reasons, in most examples in the literature, simplifications are included in the case studies; e.g., reducing the number of species to be analyzed (only 2 or 3), reducing the number of stages, reducing the number of cells or banks, avoiding using entrainment and the frothers model, etc. In other words, the algorithm cannot solve real-sized problems (Cisternas et al., 2018).

Other aspects that affect the optimization of the design of flotation circuits are epistemic and stochastic uncertainty. The epistemic uncertainty is associated with the empirical nature of the parameters of the flotation models, and the stochastic uncertainty is associated with the natural variation in the metal price, mineral composition, particle size, etc. Cisternas et al. (2015) argued that using a complex model to predict the behavior of the stages is not necessary for selecting the most appropriate circuits. They represented this epistemic uncertainty using distribution functions

covering a range of recovery values of each species in each stage. They demonstrated that approximate values of stage recovery are sufficient to identify the circuits that are best to treat the specific mineral. Using this approach, the design problem was solved many times for different stage recovery values that were taken from the distribution functions. However, each time the stage recovery was a constant value, which reduced the MINLP to a mixed-integer linear programming (MILP) problem, which is easy to solve for the global optimum.

The MILP problem is represented as follows:

$$\begin{aligned}
 & \max_{(x,y)} z^T x \\
 & \text{s. a} \quad Ax = b \\
 & \quad \forall_{i \in D} \left[Cx + Fy \leq 0 \right] \\
 & x \in \mathcal{R}^n, y \in \{True, False\}^m
 \end{aligned} \tag{2.23}$$

where $z^T x$ is the objective function, the vector x corresponds to continuous variables (e.g., mass flow rates), the vector y represents binary variables, and the vector y corresponds to constants. The equation $Ax = b$ corresponds to the mass balances. The expression $\forall_{i \in D} \left[Cx + Fy \leq 0 \right]$ represents disjunctions for the selection of operational conditions at the flotation stage.

In this work, we use as an objective function the maximization of revenue based on the study by Cisternas et al. (2014), which demonstrated that it is an adequate objective function to solve this type of problem. The revenue is presented by Equation 2.24:

$$\text{Revenue} = CF[p(g - \mu)(q - Rfc) - Trc]H \tag{2.24}$$

where CF is the concentrate mass flow rate, p is the fraction of metal paid, g is the mineral grade of the concentrate, μ is the grade deduction, q is the metal price, Rfc is the refinery charge, and Trc is the treatment charge. H is the number of hours per year of plant operation when the mass flows are in tonne per hour. The formula for calculating revenue incorporates the metallurgical efficiency of the plant, where the recovery and grade are opposite functions.

Figure 2.12 shows the optimal design circuit map for a problem with three flotation stages and two species. The stage recovery of species 1 is represented by a uniform distribution function between 60 and 90% ($U \sim [60,90]$ %). In the same way, the stage recovery of species 2 is represented by

$U \sim [2,20]$ %; this denotes recoveries between 2 and 20%. Hence, species 1 and 2 can represent valuable and gangue material, respectively. The stage recoveries have high epistemic uncertainty, which can be expected in the early stages of circuit design. A sample was taken based on these stage recovery distributions, and the design problem was solved for optimality. The process was repeated 30,000 times, and the solution was plotted using different colors to represent each optimal circuit. Figure 2.12 maps these solutions, showing that only three circuits were obtained (three colors). In Figure 2.12, each color represents the optimal circuits Alt 2, Alt 3, and Alt 4, which are shown in Figure 2.13.

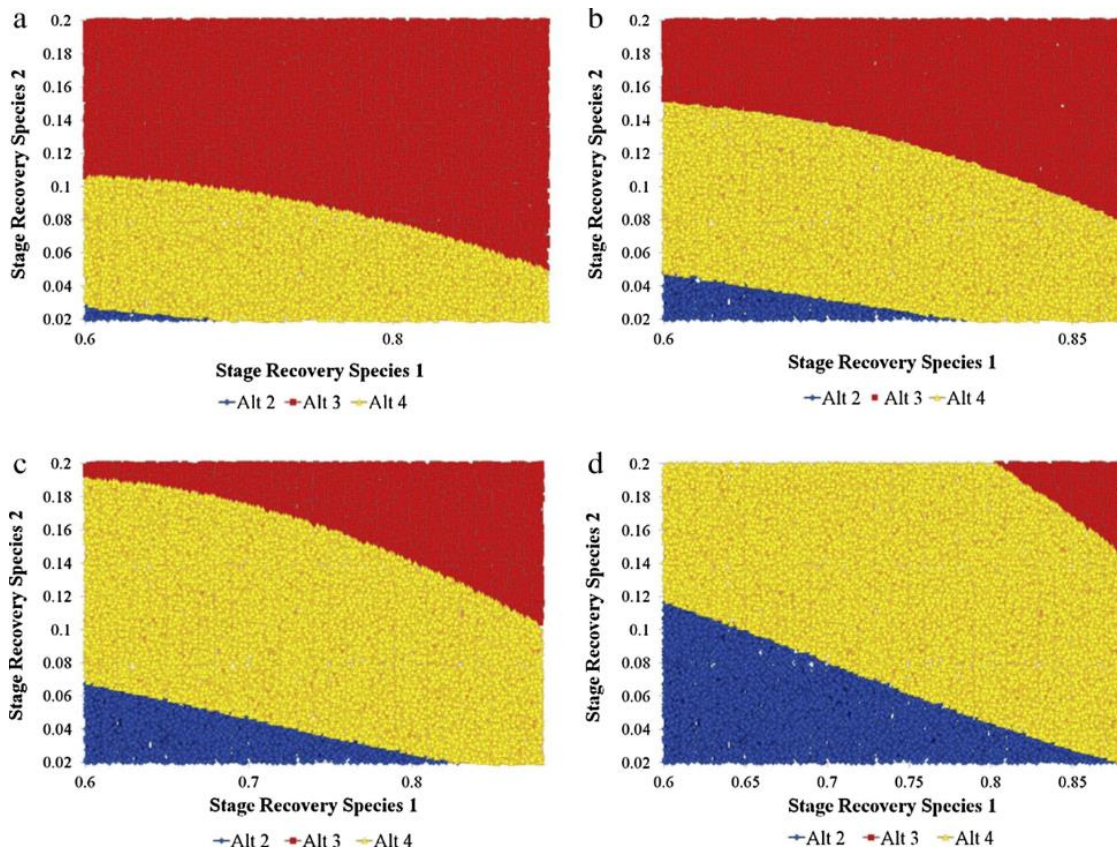


Figure 2.12 Optimal configurations of recovery for species 1 and 2. (a) Low price and low feed grade. (b) Low Price and high feed grade. (c) High price and low feed grade. (d) High price and high feed grade. Flotation plant with three stages (Cisternas et al., 2015).

Figure 2.12 shows that in a wide range of stage recovery values of the species, the optimal structure was always the same (large areas were formed where the optimum was found). Figure 2.12 a, b, c, and d present different values of metal price and feed grade. It is clear from the results that the optimal structure is more sensitive to the stochastic uncertainty of metal price and feed grade (cases

with high/low metal price and high/low feed grade) than the epistemic uncertainty of stage recoveries. In other words, it seems that the optimal structure is more sensitive to the price of the metal and the feed grade rather than the recovery. These findings allow identification of the optimal structures. Therefore, once the structure is selected, the equipment and operational conditions can be designed using models based on experimental tests and optimized using simulations.

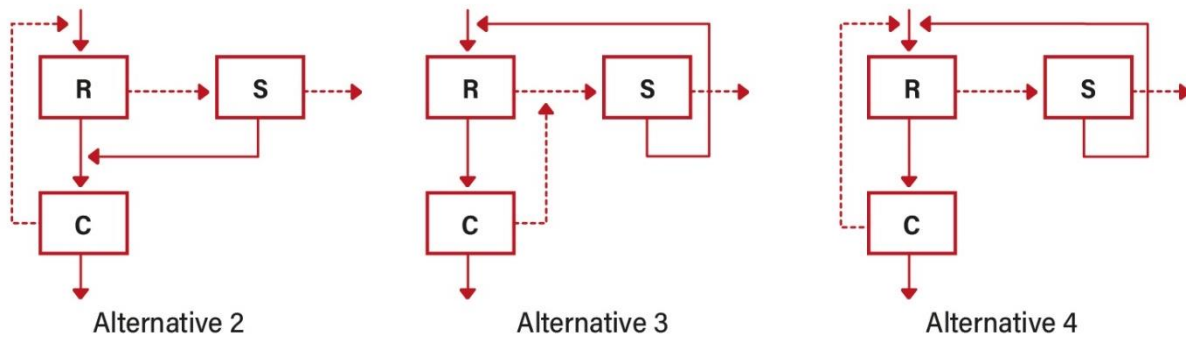


Figure 2.13 Optimal flotation circuits of Figure 2.12 (Cisternas et al., 2015)

Recently, based on Cisternas et al. (2015) findings, design procedures have been developed that can be applied to problems containing several species and separation stages (Acosta-Flores et al., 2018; Calisaya et al., 2016). These procedures are essential advances because they can be applied to real-sized problems. However, all of these design studies consider the production of one concentrate or product from an orebody. In the desulfurization process, several sulfides are expected to be concentrated. Usually, plants concentrate two or more minerals using a circuit for each mineral or produce a bulk concentrate and then perform selective flotation on the bulk concentrate. Based on that, it is possible to apply the circuit design methodology to each circuit to obtain the complete plant design. However, there are no studies on the advantages and disadvantages of using an integrated circuit in the desulfurization process. By integrating the circuit, we will understand a circuit where we do not seek to generate an intermediate product or sequentially separate one product at a time, but rather require simultaneous searching for all products.

Finally, the literature review of this subject allowed us to identify the methodology that implemented in our work, notably the method developed by Cisternas et al. (2015). It also enabled us to identify the gaps that still exist and how we can use this optimization method to study the desulfurization of tailings implementing fractional flotation and integrated flotation circuits.

2.6 Mineral Characterization

The contribution of mineral characterization before, during, and after metallurgical treatment is relevant in mining procedures. Mineralogy is important during all stages of the mining cycle: exploration of the deposit, definition of the deposit, exploitation of the deposit, mineral processing, waste management, and site restoration. Therefore, mineralogy has practical applications in terms of the mineral's valorization. However, it is noted that it is barely used or fully understood in most cases. In the geochemical procedure, minerals undergo several transformations to obtain a concentrate containing valuable elements. In consequence, mineral characterization is essential to evaluate the mineral grade of liberation to be concentrated and diagnose any mineralogical problems. The first and most essential step is the identification of minerals present in the ore. Mineral recovery depends on the nature and abundance of the minerals and their texture, size, and surface properties. Many minerals remain unexploited for many years due to a lack of knowledge of their mineralogical characteristics.

The application of mineralogical studies for mineral recovery has various objectives:

- 1) Identification of the minerals present in the ore.
- 2) Description of the texture and the association with other minerals.
- 3) Measurement of the mineral liberation in the concentrate.
- 4) Qualitative or quantitative determinations such as the relative abundance of minerals, the distribution of valuable minerals in two or more textures, and the mineral grade.
- 5) Determining whether the metallurgical problem (e.g., poor recoveries, low concentrate, low selectivity) comes from the minerals themselves or the treatment (e.g., surface chemistry).
- 6) Highlighting any mineralogical characteristics of the mineral. This could help in the selection of a more convenient procedure for the valorization process and waste management.

Therefore, the characterization of WR and tailings is a relevant aspect in the desulfurization process because it allows determination of the bulk chemical composition of the ore. In this work, several characterization techniques are used to identify species with economic value and species that can cause environmental problems. The characterization is applied to analyze porphyry copper ore and WR derived from porphyry copper ore. The chemical composition is analyzed using ICP-AES,

XRF, and S/C. The mineralogical composition is analyzed using optic microscopy (MO), X-ray diffraction (XRD), scanning electron microscopy (SEM-EDS), and quantitative evaluation of minerals by scanning electron microscopy (QEMSCAN). Finally, the mineral surface is examined using Fourier-transform infrared spectroscopy (FT-IR) and X-ray photoelectron spectroscopy (XPS).

CHAPTER 3 RESEARCH DESIGN AND METHODS

After collecting information from the literature, different methods were designed to examine the issues identified in the previous section. Figure 3.1 shows the general structure of the methodology that was developed around the four different objectives proposed.

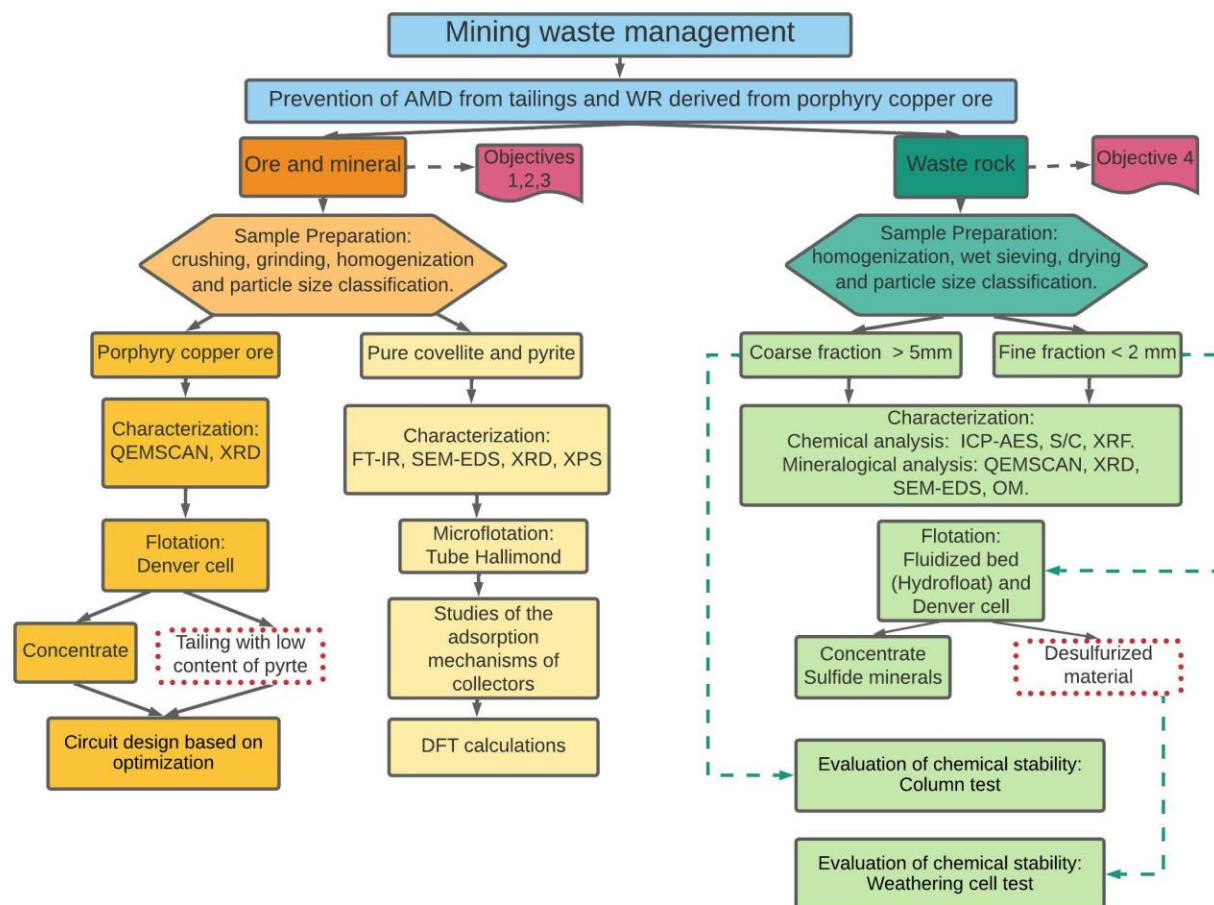


Figure 3.1 The general methodology proposed for the thesis project.

The sample preparation was the first step of the mineral treatment of either a pure mineral, porphyry copper ore, or WR. The porphyry copper ore was provided by Chuqicamata mine located in the north of Chile, around 2 tons of the mineral used in the processing plant was used to run the experiments. The WR was provided by Centinela (north of Chile), around 2.3 tons of WR were separated before to go to the dumps and this WR was used to run the experiments. To fulfill Objective 1, the microflotation of pure mineral covellite and pyrite in a Hallimond tube was conducted. The purity of covellite and pyrite was determined using XRD and SEM-EDS. Based on

data collected from microflotation results, the flotation of porphyry copper ore in a Denver cell was conducted and the recovery results were analyzed to obtain the optimal results based on the concept of bulk and selective flotation. Then, to fulfill Objective 2, pure mineral covellite was further characterized, and the adsorption mechanism of collectors on the mineral surface was assessed using FT-IR, XPS, and DFT calculations.

Moreover, to evaluate the advantages, disadvantages, issues, and costs in the production of tailings with low content of acidifying species, the third objective, whose focus was circuit design based on optimization, proposed two processing strategies framed in the context of desulfurization. The first strategy enabled us to determine whether there are only a few optimal designs for a given problem. In this strategy, two approaches were used; the first approach was to evaluate the desulfurization of tailings that already contain acid species (end-of-pipe technology) using traditional flotation circuits (sequential flotation). The second approach was to carry out desulfurization at an early stage of the flotation process (in-process technology) using sequential and integrated flotation circuits, which produce tailings without the potential generation of AMD. Comparing these approaches allows us to have a more comprehensive view of cleaner production, instead of using traditional methods that are focused on remediation methods. However, the second strategy involved using the flotation data provided by Kevitsa mine for Cu-Ni-PGE ore to determine the optimal design for sequential and integrated flotation circuits for this polymetallic ore. The Kevitsa concentrator employs a copper–nickel sequential flotation circuit. Therefore, the idea was to design sequential flotation and optimize it sequentially. Then, we designed the sequential flotation but optimized the whole process as one. Finally, we designed integrated flotation circuits.

To fulfill Objective 4, after sampling preparation, WR was divided into different particle size fractions, and the geochemical stability of the fraction with a particle size higher than 5mm was evaluated using column testing. Particles smaller than 5mm were chemically and mineralogically characterized with the aim of identifying the DPLS. Once the DPLS was determined, the fractions that would produce AMD were further desulfurized using the flotation process. Fine particle sizes ($< 212\mu\text{m}$) were desulfurized using a Denver cell and coarse particle sizes (-850 to $+212\mu\text{m}$) were desulfurized using HydroFloat® technology. The geochemical stability of desulfurized minerals was assessed using weathering cell tests.

Figure 3.2 shows the methodology proposed to carry out the kinetic tests. One column test was conducted using a particle size > 5 mm. The mineral was further divided into the five fractions F5 (-5 mm to +2.4 mm), F4 (-2.4 mm to +850 μm), F3 (-850 μm to +300 μm), F2 (-300 μm to +53 μm), and F1 (-53 μm). These tests helped to identify the sizes of fractions that are reactive and those in which sulfides are locked and non-reactive. The evolution of the chemical composition of the leachates was used to calculate the long-term acid generation potential and mineral depletion rates. The desulfurized WR obtained from each flotation test was utilized to evaluate geochemical stability in the weathering cell tests following the steps listed in Figure 3.2.

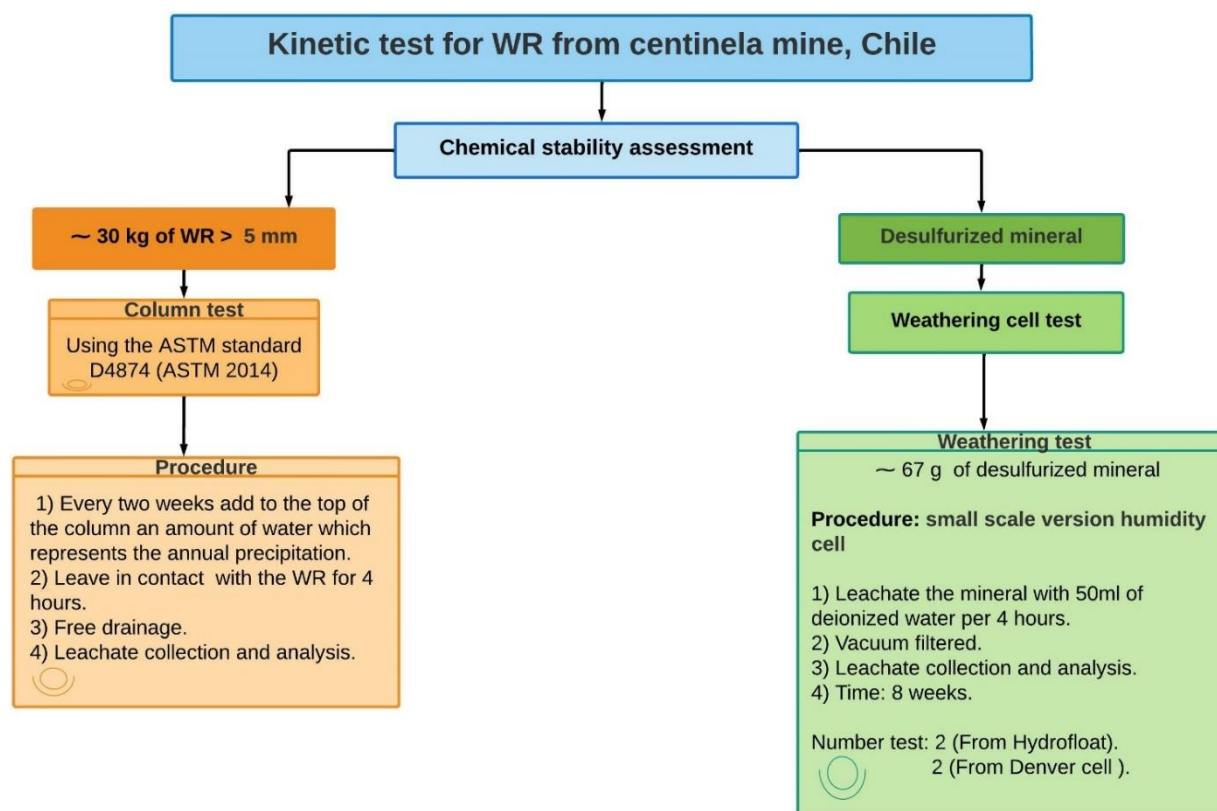


Figure 3.2 Flowsheet proposed for kinetic tests.

Finally, the methodology was performed based on several activities, denoted A1 to A30. Figure 3.3 shows a detailed description of the activities carried out during the development of the thesis and the results expected for each objective proposed.

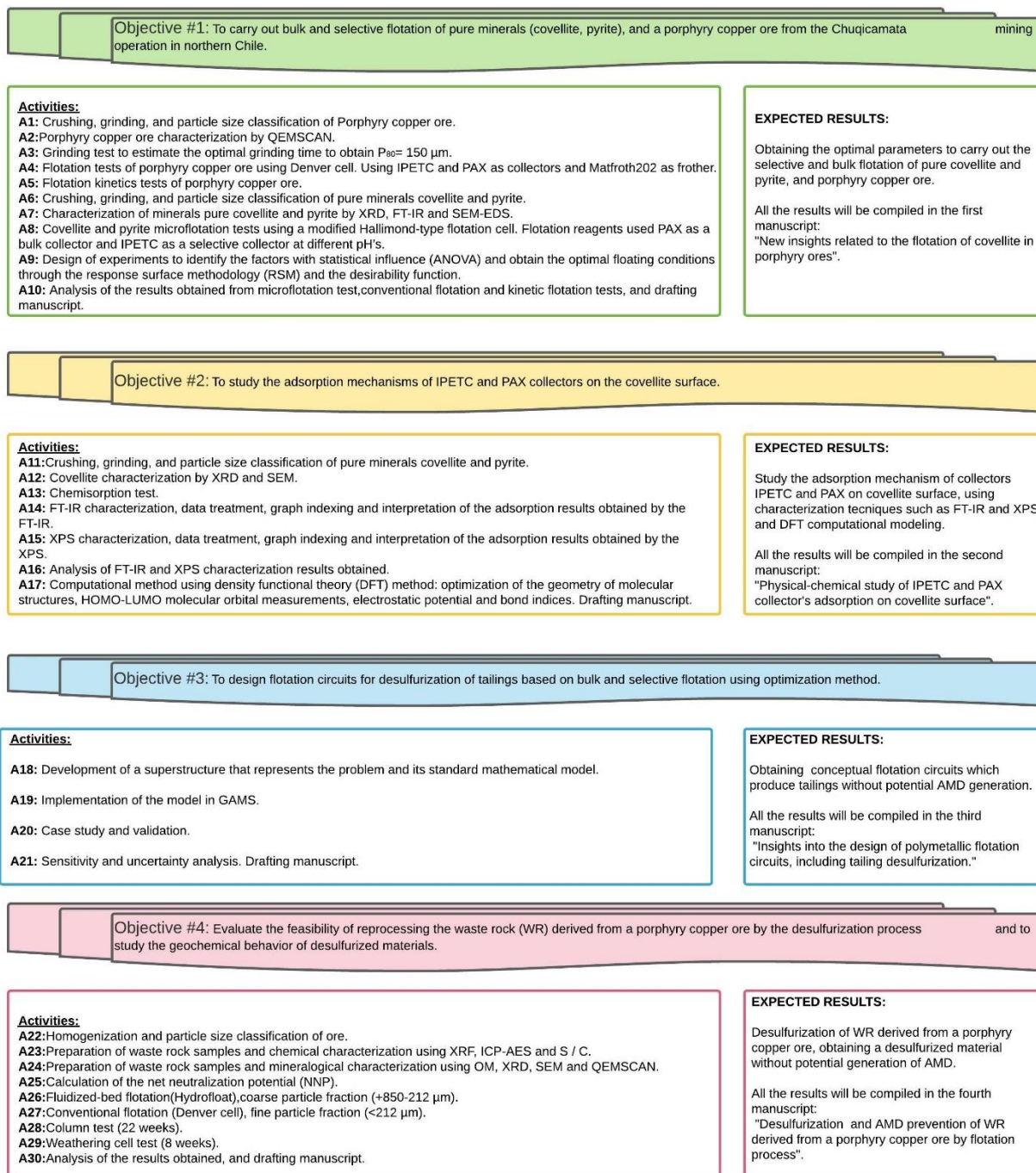


Figure 3.3 Activities conducted to develop each objective proposed in the thesis project.

CHAPTER 4 ARTICLES AND REVIEW OF THE RESULTS

This chapter reviews the objectives, results, and contributions of the articles presented in this dissertation.

4.1 Article I: New Insights Related to the Flotation of Covellite in Porphyry Ores.

Yesica L. Botero, Rodrigo Serna-Guerrero, Alejandro López-Valdivieso, Mostafa Benzaazoua and Luis A. Cisternas.

This article was submitted to Minerals Engineering journal on July 23, 2021.

4.1.1 Overview

The copper ore grade has been decreasing due to over-exploitation. The global average copper ore grade is about 0.49% and is forecast to decrease consistently in the foreseeable future (Northey et al., 2014). This situation demands new strategies to improve the efficiency of concentration plants, including the recovery of copper from other copper sources. The decrease in the ore grade is inevitably associated with increased solid waste production to maintain the same level of copper production. Recent years have seen a growing interest in the processing of WR and tailings, including the recovery of valuable components such as copper sulfide minerals (Araya et al., 2020).

Sulfide copper deposits are mostly composed of chalcopyrite, bornite, molybdenite, chalcocite, and covellite. The vast majority of studies focus on the froth flotation of chalcopyrite, as it currently represents the main source of copper. Voisin (2012) analyzed several samples from different Chilean copper mines, and he found that covellite concentration was between 17 and 0.6 % wt. Therefore, given the decrease in copper ore grade and the need to valorize solid waste and prevent AMD, studies that help to recover covellite from solid waste as a copper source have become necessary. In fact, the copper contribution from covellite to an ore grade might determine whether the ore is processed. Furthermore, the proper recovery of covellite from WR and tailings could help to decrease the cost of waste management and limit the production of AMD (Amar et al., 2021).

Few studies have been conducted related to covellite behavior during the flotation process. The electrochemical behavior and adsorption mechanisms of different reagents such as 1,1,1-butanetriethiol, diethyldithiocarbamate, ethyl xanthate, diethyldithiocarbamate (DTC), and

nimidazoline (1- Hydroxyethyl- 2-Heptadecenyl) have been assessed on the covellite surface, demonstrating that covellite behaves differently depending on the operational conditions used during the flotation process (Porento and Hirva, 2004; Raju and Forsling, 1991; Ackerman et al., 2000; Roos et al., 1990). Therefore, the two collectors that were used to conduct this study (O-isopropyl-N-ethyl thionocarbamate (IPETC) and potassium amyl xanthate (PAX)) have not been yet used in covellite flotation.

4.1.2 Research objective

In this study we aimed to carry out bulk and selective flotation of the pure minerals covellite and pyrite, and porphyry copper ore from the Chuqicamata mining operation in northern Chile. The flotation of pure covellite was the focus of the study, not only because the behavior of covellite is barely studied, but also because the porphyry copper ore used in this work was mineralogically composed of covellite (0.22%), chalcocite (0.21%), chalcopyrite (0.06), and pyrite (0.69%). Therefore, it was necessary to deepen our knowledge of the behavior of covellite during its flotation to reproduce the results obtained for porphyry copper ore. The methods used to accomplish this goal started with mineral characterization, followed by microflotation for pure minerals, and flotation of porphyry copper ore in a Denver cell. Two types of collectors, IPETC and PAX, were used to assess the effect of these collectors in bulk and selective flotation. Furthermore, the response surface methodology was used to optimize the conditions of copper recovery. Figure 4.1 summarizes the methods implemented to fulfill the objectives of this article.

4.1.3 Contributions

We presented a flotation method that enables the bulk and selective flotation of pure minerals and porphyry copper ore. The results show that in the Hallimond tube test, under the conditions studied, covellite has a natural flotation of around 55% and is pH-independent. Pyrite flotation is influenced by the presence of covellite, apparently because covellite is more soluble than other copper sulfide types that activate the pyrite surface. Covellite recovery is influenced by collector type and concentration. Pyrite recovery is influenced by collector type, collector concentration, and pH. Finally, thanks to the high selectivity of the collector IPETC, low collector concentrations are sufficient to float covellite at pH 8 and 11.

Moreover, the results enabled us to determine the optimum parameters to run bulk and selective flotation, providing covellite and pyrite recoveries of 93.4 and 90.2%, respectively, for bulk flotation, and covellite and pyrite recoveries of 80.5 and 20.3%, respectively, for selective flotation. For the porphyry copper ore flotation, the results confirm that IPETC has a better affinity for Cu-bearing minerals, whereas PAX has a better affinity for pyrite. IPETC can be used as a selective or bulk collector, varying only the pH and using low concentrations. After all, it is not necessary to use different collectors for bulk and selective flotation. Furthermore, for porphyry copper ore, bulk flotation is feasible with IPETC at low pH and low collector dosage. This kind of procedure allows the majority of sulfide minerals to float in the rougher stage and produces tailings with low pyrite content. Then, the concentrate can be selectively separated with the same collector (IPETC) by increasing the pH, thus obtaining two concentrates, one of copper and one of iron.

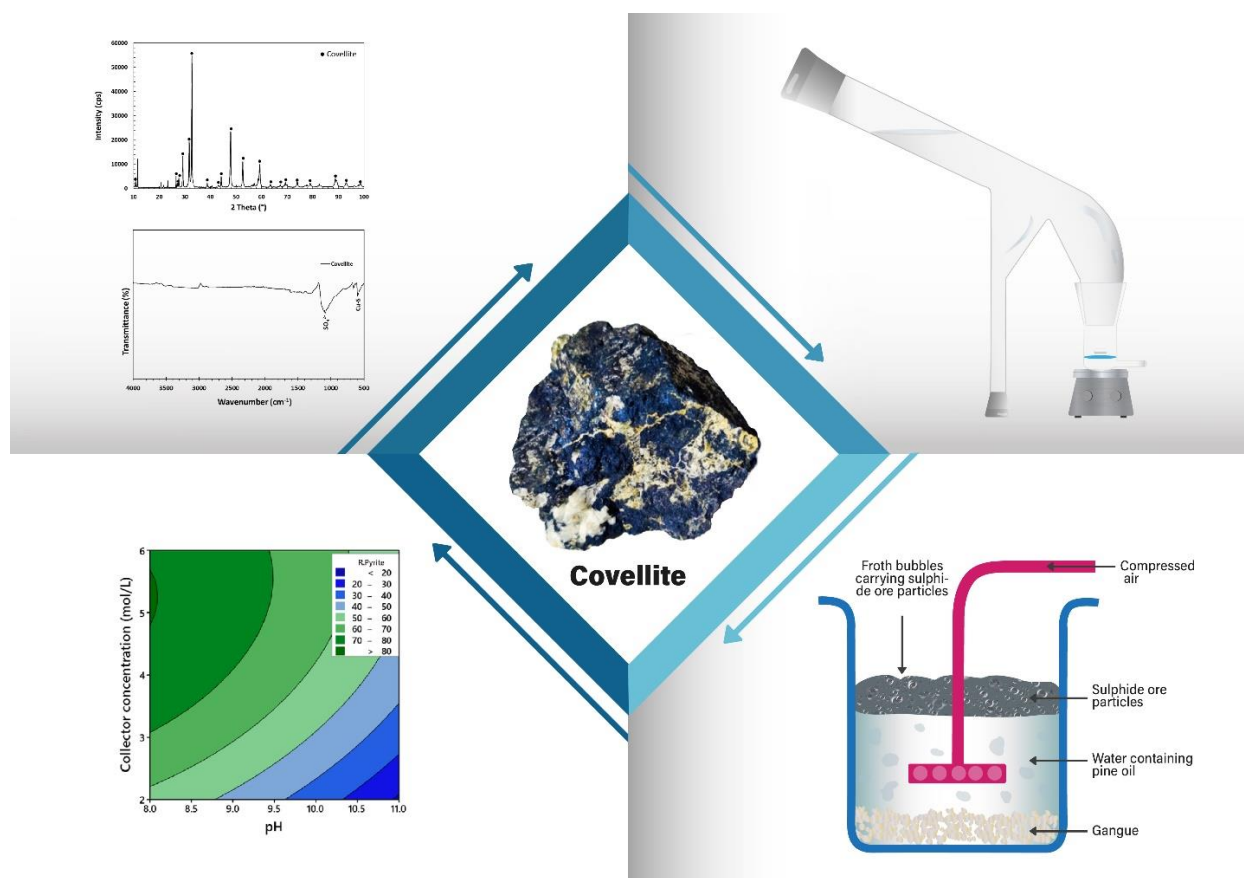


Figure 4.1 Graphical abstract of the methodologies implemented to study the flotation of covellite and porphyry copper ore.

4.2 Article II: Physical–Chemical Study of IPETC and PAX Collector’s Adsorption on Covellite Surface

Yesica. L. Botero, Andrés Canales-Mahuzier, Rodrigo Serna-Guerrero, Alejandro López-Valdivieso, Mostafa Benzaazoua and Luis A. Cisternas

This article was submitted to Applied Surface Science journal on November 24, 2021.

4.2.1 Overview

Considering solid waste valorization, studying covellite is relevant because according to its chemical formula, it has almost double the amount of copper than chalcopyrite. In this sense, even if the solid waste (tailings or WR) has a low level of covellite compared to chalcopyrite, it could provide a significant amount of copper. For instance, Tian et al (2020) reported on a mineral concentrate, wherein the copper-bearing minerals were mainly chalcocite (11 %), chalcopyrite (8 %), bornite (4.3 %), and covellite (1 %). The chalcocite, chalcopyrite, and bornite contributed 45.11 %, 29.6 %, and 15.72 % of the copper, respectively. Although the covellite only comprised 1%, it contributed to 8.6% of the total copper in the concentrate. The relative level of covellite in the concentration allowed us to identify the importance of this mineral as a copper supplier.

Moreover, interesting aspects of covellite properties and their behavior in froth flotation were identified and discussed in the first article. However, there is insufficient information by which to evaluate properly and design feasible operations dedicated to covellite concentration. A dedicated and systematic study on covellite flotation is necessary due to its complex crystal-chemistry, containing both copper (I) and copper (II) ions, as well as sulfide and disulfide ions. Therefore, various reactions can take place between covellite and collectors (Morales-García et al., 2014).

In order to understand the chemical interactions between covellite and collectors, we must discern the chemical properties and structure of covellite and the collectors under study. Therefore, characterization techniques such as Fourier-transform infrared spectroscopy (FT-IR), X-ray photoelectron spectroscopy (XPS), and density functional theory (DFT) calculations are helpful tools by which to study adsorption mechanisms, as well as the electronic structures of molecules and their electron density to understand the adsorption ability of collectors on the mineral surface.

4.2.2 Research objective

The aim of this article was to study the adsorption mechanisms of IPETC and PAX collectors on the covellite surface. To the best of the author's knowledge, no studies have yet been published on the surface interactions between these collectors and covellite. Therefore, this work presents FT-IR and XPS characterization techniques supported by DFT computational modeling to provide detailed information on the behavior of the collector–covellite system, followed by experimental validation. Figure 4.2 summarizes the methods implemented to reach the objectives of this article.

4.2.3 Contributions

This study provides knowledge regarding the physicochemical interactions between the covellite surface and collectors. The relevant findings were as follows.

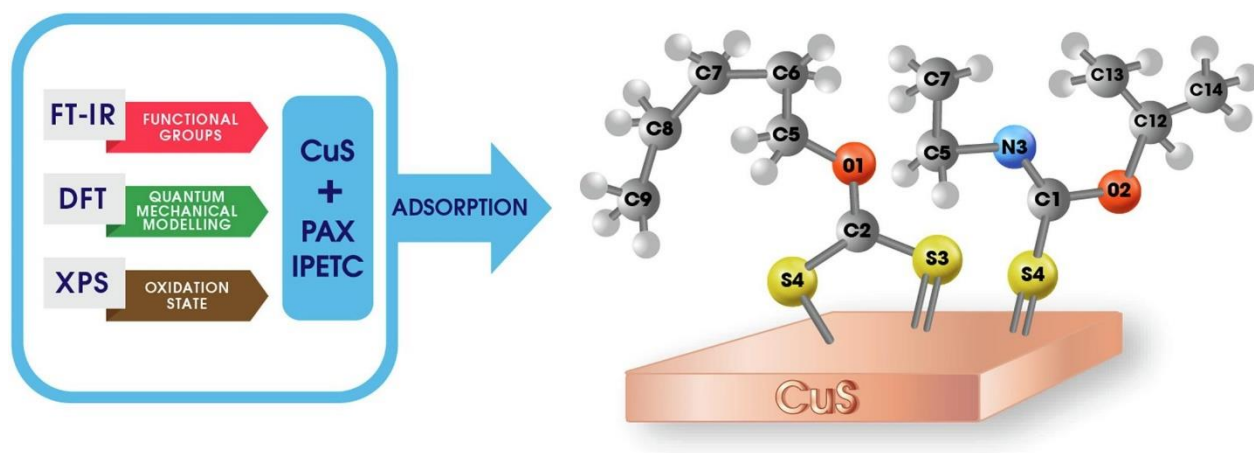


Figure 4.2 Graphical abstract of the methodologies implemented to study the adsorption mechanisms between collectors and the covellite surface.

FT-IR spectra of IPETC indicate that the collector adsorption on the covellite surface is not pH-dependent. The bands related to $-C(=S)-NH$, $-C-H$, NH deformation, CH deformation, and CNC characteristic of IPETC were present in the spectra, demonstrating IPETC adsorption on covellite surface. Besides, the FT-IR spectra of PAX show that collector adsorption on the covellite surface is not pH-dependent. PAX adsorption was identified via the leading functional groups, such as dixantogen $(AX)_2$, and Cu-amylxanthate $(CuAX)$.

Additionally, the high-resolution XPS spectra of the Cu 2p spectrum show that the oxidation state of covellite with PAX is Cu(I). This finding was corroborated by FT-IR by the identification of Cu-amylxanthate $(CuAX)$ and dixantogen $(AX)_2$ on the covellite surface. The adsorption

mechanism of IPETC suggests the binding is facilitated by the S of the collector with Cu atoms on the covellite surface. Moreover, the S 2p spectrum of covellite treated with IPETC displays a principal doublet attributed to S_2^{2-} (C=S functional group), as observed for thiourea. Lastly, the DFT results are in good accordance with the FT-IR and XPS results. The reactive site in the IPETC⁻ collector was the =S element, and bonding with copper only occurred through the C=S group. For PAX⁻, the reactive sites were =S and -S elements. Thus, the bonding with copper occurred through C=S and C-S groups. The global reactivity descriptor calculations demonstrate that PAX⁻ has a powerful collector capacity and, therefore, low stability compared to IPETC⁻. This result agrees with the results obtained from microflotation tests; specifically, the higher recovery with PAX⁻ (93%) than with IPETC⁻ (88%). Additionally, it was demonstrated that copper charge matters when it interacts with the collector. In general, the NBO net atomic charges and the Wiberg bond indices show that Cu(II)'s binding with both collectors has stronger energy than Cu(I). These results enable selection of collectors depending on the type of flotation process that will be conducted, i.e., either bulk or selective.

4.3 Article III: Insights into the Design of Polymetallic Flotation Circuits, Including Tailing Desulfurization.

Yesica L. Botero, Luis A. Cisternas, Isabelle Demers and Mostafa Benzaazoua

This article was submitted to Separation and Purification Technology on February 14, 2023.

4.3.1 Overview

Flotation is the main mineral concentration technology used in the production of coal, copper, zinc, lead, nickel, molybdenum, and other metals. More than two billion tons of various ores are processed by froth flotation annually (Nguyen & Nguyen, 2023). As we look to the future, the use of this process is likely to increase, because the demand for goods that are dependent on metals, such as vehicles, buildings, machinery, and infrastructure is increasing in modern society. As the metal demand increases, lower-grade orebodies will become economically viable. These low-grade ore are more complex, and the processing of higher tonnages will be needed to sustain production. Processing must be environmentally sustainable, and therefore, it is becoming increasingly necessary for mining companies to consider their water use, energy consumption, carbon emissions, and solid waste generation to improve their environmental, social and governance

conditions. Several ore deposits are polymetallic with two, three, or more base metals. Additionally, in the circular economy and environmental regulations, metal valorization and the use of cleaner production technologies are emphasized (Marinina et al, 2022). The need to move from end-of-pipe strategies to clean production necessitates new process designs. On the other hand, the valorization of minerals requires minerals to be viewed as polymetallic resources. Therefore, new process design is a crucial aspect for improving circularity (Cisternas et al, 2021).

Flotation circuits are complex systems composed of several stages, such as a rougher, cleaner, and scavenger, configured in a particular way (Mendez et al, 2009). Usually, flotation circuits have between three and five stages, but some flotation plants have thirteen flotation stages (Sepúlveda et al, 2017). One of the problems associated with circuit design is the large number of feasible flotation circuits, given the combinatorial nature of the problem. If the behavior of each flotation stage is necessary for the design of the flotation circuit, the problem is unsolvable. This is because the behavior of each stage, which depends on physical-chemical aspects and the operational conditions, will depend on the design of the circuit (Hu et al, 2013). Clearly, the behavior of a stage will depend on the feeding characteristics. As the modeling of these systems is still empirical or semi-empirical, it is impossible to conduct experiments under all possible circuit configurations for a given problem. Fortunately, rigorous comprehension of the behavior of a flotation stage is not necessary for the design of these circuits, at least for monometallic circuits.

The flotation circuit for a polymetallic ore usually utilizes fractional flotation with the generation of a bulk concentrate and its subsequent separation, fractional flotation using selective flotation, or a combination of both strategies if three or more concentrates are produced (Frías et al, 2008). Polymetallic ores are usually separated by fractional flotation using selective flotation for each base metal. The methodologies proposed in the literature for the design of flotation circuits consider only one base metal, which was designed for monometallic ores. There is no systematic methodology available for the design of polymetallic circuits. Nevertheless, it is logical to think that the separation sequence will first be selected based on the designer's experience and ore characteristics, and then each flotation circuit will be designed, one at a time, as if it were a design for a monometallic ore. This can include the separation of sulfide ore, which can produce AMD from compounds such as pyrite.

Another issue is the increasing generation of tailing and the consequences of contaminant release through dust, tailings dam seepage, dam wall failure, and potential generators of AMD. Processing higher tonnages of lower-grade ores will increase the risks associated with mine tailings management. Current tailing management includes the use of paste and thickened tailings and the reuse, recycling, and reprocessing of tailings (Araya et al, 2021; Bascetin et al, 2016; Marín et al, 2021). A proactive strategy would be to generate tailings without sulfur species to improve environmental, social, and economic outcomes. There have been several studies on tailing desulfurization; however, these studies have been conducted on abandoned tailings (Nadeif et al, 2019) or end-of-pipe technologies (El-bouazzaoui et al, 2022).

4.3.2 Research objective

Given this background, it is clear that studies on the design of flotation circuits for polymetallic ores, including those using desulfurization, are necessary to meet the future challenges of the mining industry. The aim of this paper is to provide insights into the design of polymetallic flotation circuits, including tailing desulfurization (Figure 4.3). This paper seeks to answer the following questions: Are monometallic mineral flotation circuit design strategies applicable to polymetallic mineral circuit designs? Which separation sequence is the most appropriate for a particular mineral? What are the advantages of designing flotation circuits simultaneously versus one at a time for each metal? Which designs can include desulfurization as part of a flotation circuit? Which challenges exist in terms of conducting physical-chemical studies to improve these circuits?

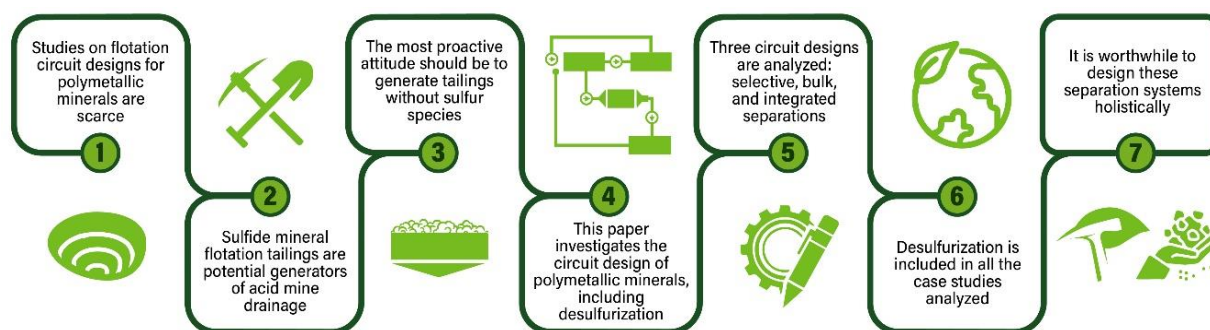


Figure 4.3 Graphical abstract of insights into the design of polymetallic flotation circuits, including tailing desulfurization.

For answering these questions several design and studies are presented based on the application of flotation circuit design optimization. These studies included: 1) the extension of the strategies used

in the design of monometallic mineral to polymetallic mineral processing; 2) an analysis of the types of circuit structures employed which includes fractional flotation with the generation of a bulk concentrate and its subsequent separation, fractional flotation using selective flotation, a new type of flotation circuit here named integrated flotation with combined bulk and selective flotation; 3) designs for the Cu–Ni–PGE Kevitsa mine (Musuku et al, 2016), including the application of different strategies for obtaining the optimal flotation circuit design. The Kevitsa concentrator employs a copper–nickel fractional-selective flotation circuit that includes desulfurization.

4.3.3 Contributions

Based on the results obtained, the following conclusions can be reported. First, the design strategy developed for monometallic minerals using optimization can be applied to polymetallic minerals. Two observations support this statement: a) there are few optimal structures for a given problem despite the uncertainty in the recoveries of each stage and b) few structures accumulate the highest frequencies of occurrence or, in other words, have the greatest chance of being the optimal structure.

Second, the order, from most to least, in terms of the revenue and copper recovery obtained in the circuit design is as follows: integrated disjunctive > integrated > fractional selective > fractional bulk. However, the selective fractional circuit will produce the most significant environmental effects and cost the most. In addition, the fractional selective circuit presented the greatest dispersion in the results and more significant uncertainty in its behavior. The copper grade in the concentrate was similar among the four cases studied; therefore, the results were inconclusive if the standard error bars are considered. The CAPEX and OPEX values were higher for the fractional selective circuits than for the other design cases.

From a desulfurization point of view, all studied circuits comply with the restrictions imposed in the problem definition. To achieve these results, the restrictions included in the model in terms of grade levels and the recovery of species that generate AMD play essential roles. Additionally, the introduction of penalties due to having species in the copper concentrate or small rewards for the recovery of species that create AMD in the objective function is essential.

Third, based on the previously analyzed results, the selective fractional circuit, which is the typical circuit in practice, delivers the worst results, followed by the bulk fractional circuit. The integrated circuit and integrated disjunctive circuit proposed in this manuscript present the best results.

However, they offer the challenge of containing floating minerals that have been depressed and vice versa. Therefore, there is a need for further study to manipulate flotation and depression in different sequences to develop more efficient processes with less environmental impact.

Fourth, based on the Kevitsa concentration case study, it is concluded that the application of optimization can provide designs that can be studied further. The simultaneous design of all circuits for a polymetallic mineral gives better results than a one-at-a-time design. The design of polymetallic mineral flotation circuits as a system where interaction between the circuits is possible can generate an important improvement.

Finally, based on these results, the design of flotation circuits for polymetallic minerals can be carried out in two stages. In the first stage, approximate values of the recoveries at each stage are used to identify a set of optimal solutions. Then, in the second stage, these circuits are studied in depth, including through experimental studies, to select the most suitable design.

4.4 Article IV: Conference Paper: Application of Characterization Techniques for the Prevention of AMD for Waste Rock from a Chilean Porphyry Copper Mine.

Yesica L. Botero, Isabelle Demers, Luis A. Cisternas and Mostafa Benzaazoua.

This article was submitted to Process Mineralogy'22 on June 22, 2022.

The conference paper was presented at the 6th International Symposium on Process Mineralogy, November 2-4, 2022, Sitges, Spain. This paper sets out the first approach of the manuscript “Desulfurization and AMD prevention of WR derived from a porphyry copper ore by flotation process”. The full manuscript is composed of three approaches: first approach, chemical and mineralogical characterization of WR, and ABA test calculation for DPLS determination; second approach, flotation process for desulfurization of reactive fraction of WR; third approach, assessment of the geochemical stability of desulfurized WR using kinetic testing. Experiments related to the second and third approaches were still in progress at the time of this conference. Therefore, the results obtained from these two approaches will be presented in Chapter 5, Section 5.1, “other results”.

4.4.1 Overview

With greater copper demand, the ore grade decreases, and a larger amount of copper mining is necessary to meet the demand, resulting in large quantities of solid waste such as waste rock (WR) and tailings being produced during the extraction of economically valuable minerals. Both types of waste are generally enriched with sulfide minerals such as pyrite, pyrrhotite, and arsenopyrite that have no economic value and can oxidize due to exposure to surrounding water and oxygen, generating AMD. In this work, we focus on WR. Managing this solid waste is challenging for the mining industry; however, not enough attention has been paid to it. The potential generation of AMD depends on the waste's mineralogy and mineral dissolution rates. The geochemical behavior of WR can be highly variable due to its significant heterogeneity (Amos et al., 2015; Wilson et al., 2018). For this reason, the assessment and management of WR is challenging for the mining industry (Blowes et al., 2014; Paktunc and Davé, 2000). The acid generation potential of WR can be determined by predicting the NNP and NPR; several static methods have been developed based on parameters and criteria that differ from one method to another. Static prediction tests attempt to determine the balance between the AP of the material, derived by quantifying the acid-producing components, and the NP, determined by measuring the quantities of acid-consuming components (Lawrence and Scheske, 1997). The NNP and NPR can be interpreted via the acid–base accounting (ABA) diagram criteria to determine the AGP of the ore studied.

Static methods are classified into two categories: chemical and mineralogical tests. One static chemical method is the test of Sobek (1978), which is based on the total sulfur (wt% S) and total carbon (wt% C). However, this method generates some discrepancies in the measurement of AP and NP. First, the AP is calculated based on the total sulfur content instead of only the sulfur associated with sulfides that may produce acid when they oxidize. Second, for NP, the total carbon used in the Sobek test can also include carbon from sources other than carbonates (neutralizing minerals) (Paktunc, 1999). Therefore, the importance of mineralogical characterization in AMD prediction becomes more relevant for identifying all the minerals that can contribute to effective NP and AP calculations (Lawrence and Scheske, 1997). In this sense, static mineralogical methods are used to determine AP and NP based on the mineralogy of the sample. In this work, the method developed by Elghali et al. (2018) was implemented. In this method, the ABA test was corrected by introducing the degree of sulfide and carbonate liberation, which account for the initial texture of minerals.

To classify the WR into reactive and non-reactive fractions, the concept of the diameter of the physical locking of sulfides (DPLS) was used. Introduced by Smith and Huyck (1999), the DPLS refers to the particle size at which the sulfides are locked by non-sulfide gangue and therefore make the mineral non-reactive. In this context, the particle size distribution in WR plays an essential role in AMD assessment. The selection of this value can be difficult since it strongly depends on minerals' textural and mineralogical liberation. Therefore, the chemical and mineralogical characterization of WR is a relevant aspect of AMD assessment and management, since it enables deep analysis of the bulk chemical composition of WR.

4.4.2 Research objective

In this study we investigated the influence of the degree of sulfide liberation and particle size distribution on the geochemical behavior of WR from a Chilean porphyry copper mine. For the static tests, the WR was divided into five fractions to determine the DPLS and predict AMD onset. This type of ore has never been studied using this methodology. Particle sizes smaller than 5mm were selected based on other works (Lapakko, 2003; Smith and Huyck, 1999). This study highlights the benefits and importance of determining the WR mineralogical composition in AMD prediction. Finally, the ABA test and DPLS results will be used in the future work focusing on the desulfurization of WR using the flotation process (HydroFloat–Denver cell) and geochemical stability assessment via kinetic testing. Figure 4.4 summarizes the methods implemented to fulfill the objectives of this article.

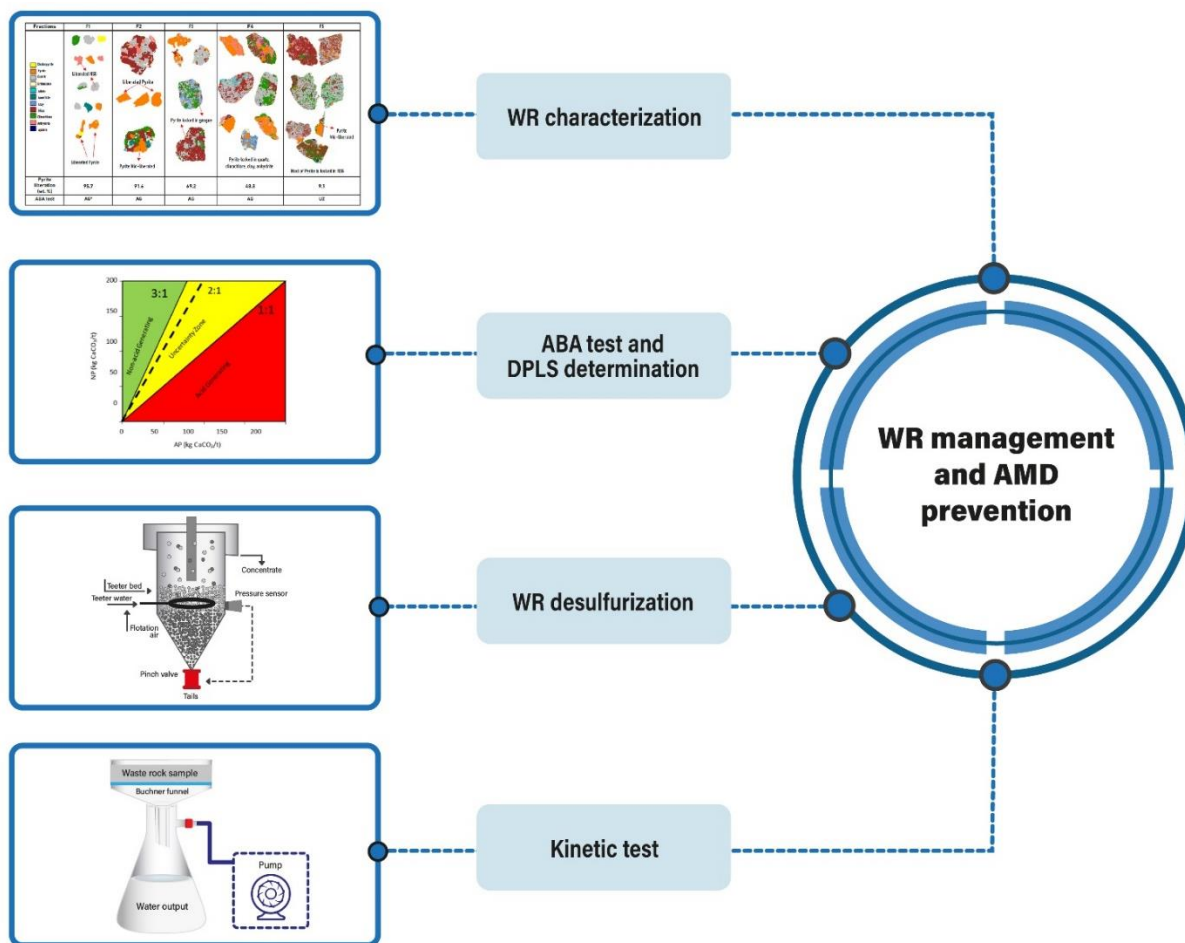


Figure 4.4 Graphical abstract of the methodologies implemented to conduct WR management

4.4.3 Contributions

This article provides valuable information about the mineralogical composition of WR from a porphyry copper ore. This information enables the assessment of the ore before, during, and after metallurgical treatment, since it is possible to determine species that may create environmental problems, allowing us to identify alternative methods of processing. For instance, the desulfurization process in an early stage of the flotation process has been proposed and analyzed in this study. This could help in the selection of a more convenient procedure for the valorization process.

Some relevant results obtained from these experiments include the observation that the DPLS was 2.4 mm. Therefore, particle size fractions lower than this value will produce AMD. Nevertheless, the ABA test demonstrated that particle sizes between 5 mm and 2.4 mm could also be acid-

generating, since they were located in an uncertainty zone. In general, all the fractions assessed displayed high pyrite concentrations of around 6 %, and carbonate concentrations were around 0.3%, suggesting that this type of WR does not have intrinsic neutralizing potential. The gangue mineral of the WR was mostly composed of quartz, anhydrite, muscovite, and clinocllore. Chalcopyrite and rutile were identified with grades around 0.6% for both, demonstrating that this WR could be treated for metal valorization. Finally, the relationship between DPLS and liberation degree was evidenced, since the particle size (-2.4 mm to +850 μm) presented a liberation degree around 50%. The liberation degree for a particle size larger than 2.4 mm was 9.1 %, and particles smaller than this value reached a liberation degree of 96%.

CHAPTER 5 GENERAL DISCUSSION

5.1 Other results

As mentioned previously, Objective 4 focused on evaluating the feasibility of processing WR derived from porphyry copper ore via the desulfurization process and studying the geochemical behavior of desulfurized materials. Therefore, this objective was investigated based on three approaches: chemical and mineralogical characterization of WR, flotation process for desulfurization of the reactive fraction of WR, and assessment of the geochemical stability of desulfurized WR using kinetic testing. The first approach has been presented and assessed in Section 4.4. Thus, in this section we present the results obtained concerning flotation and kinetic tests are presented.

Based on the results obtained during chemical and mineralogical characterization of WR, we determined that the DPLS was 2.4 mm. This enabled us to divide the particle sizes of WR into different fractions and determine the reactive and non-reactive fractions. Therefore, it was found that for the five fractions assessed, F5 (-5 mm to +2.4 mm), F4 (-2.4 mm to +850 μm), F3 (-850 μm to +300 μm), F2 (-300 μm to +53 μm), and F1 (-53 μm), particle sizes higher than F4 will not likely produce AMD, and fractions F3 to F1 will more likely produce AMD.

However, the ABA test results show that F5 was located in an uncertainty zone and F4 was located on the edge of the uncertainty zone and the acid-generating zone. These fractions cannot be desulfurized using the flotation process due to the particle size, which is larger than the particle size that can be floated. Here there are two options to treat these fractions. First, to evaluate the geochemical stability of fractions F5 and F4 using kinetic testing, or second, to implement other desulfurization technique as gravimetry. In our case the use of other technologies for desulfurization was no the focus of the work, so we decided to evaluate the geochemical behavior of F5 and F4 and see according to these results obtained what happens with this fractions.

Then, fractions F3, F2, and F1 were desulfurized using the flotation process and their geochemical stability was further analyzed via kinetic testing. Finally, the geochemical stability of particle sizes higher than 5 mm was also assessed to verify that for this particle size, WR is not AMD-generating.

5.1.1 Desulfurization results (flotation using Denver cell and HydroFloat)

This section presents the results obtained during the flotation in the Denver cell for the fine fraction (<212 μm), and in the HydroFloat for the coarse fraction (-850 μm to +212 μm). For the flotation process, it was necessary to conduct a new particle size classification because in a Denver cell the maximum particle size that can be floated is 200 μm . Likewise, in the HydroFloat cell, the maximum particle size that can be floated is 850 μm . Therefore, the range between -850 μm and +212 μm was used.

5.1.1.1 Denver cell (<212 μm)

Table 5.1 shows the results obtained for flotation in a Denver cell. Three collectors were studied: potassium amyl xanthate (PAX), sodium isobutyl xanthate (SIBX), and sodium dialkyl dithiophosphate (K2044). In addition, two mixtures were prepared at a 25:75 ratio: MIX C3 (SIBX: K2044) and MIX C4 (PAX: K2044). We used copper sulfate (CuSO_4) as the activator. P_{80} was 132 μm .

Table 5.1 Results for Denver cell flotation (particle size < 212 μm).

Code	Head sulfide grade, %	%R _{sulfide}	Enrichment ratio	Tailings sulfide grade, %	Concentrate sulfide grade, %	Collector type	Activator
T1-1	7.00 \pm 0.52	68.2 \pm 4.9	0.10 \pm 0.007	2.50 \pm 1.10	46.21 \pm 3.07	PAX	YES
T1-3	6.74 \pm 0.08	58.2 \pm 1.6	0.09 \pm 0.002	3.1 \pm 0.18	44.44 \pm 2.75		NO
T2-1	7.44 \pm 0.54	77.6 \pm 7.1	0.12 \pm 0.007	1.94 \pm 1.45	46.86 \pm 1.84	SIBX	YES
T2-3	7.27 \pm 0.11	89.9 \pm 2.6	0.14 \pm 0.001	0.86 \pm 0.48	46.78 \pm 0.19		NO
T3-1	7.05 \pm 0.35	75.1 \pm 1.6	0.11 \pm 0.003	1.97 \pm 0.47	47.93 \pm 0.04	MIX C3	YES
T3-3	7.00 \pm 0.81	91.4 \pm 8.9	0.15 \pm 0.005	0.78 \pm 1.63	41.98 \pm 2.11		NO
T4-1	6.97 \pm 0.02	72.9 \pm 0.2	0.11 \pm 0.002	2.12 \pm 0.01	45.47 \pm 0.62	MIX C4	YES
T4-3	6.66 \pm 0.08	93.3 \pm 5.4	0.14 \pm 0.009	0.51 \pm 0.82	43.16 \pm 0.19		NO
T5-1	6.26 \pm 0.03	91.0 \pm 1.0	0.13 \pm 0.002	0.64 \pm 0.49	45.08 \pm 0.90	K2044	YES
T5-2	6.91 \pm 0.60	83.9 \pm 3.2	0.14 \pm 0.007	1.29 \pm 0.51	41.32 \pm 0.89		NO

The results show that the best conditions for desulfurization were MIXC4 without an activator and K2044 with an activator. The best conditions were selected based on the tailings sulfide grade (aim for the lowest %S) and on sulfide recovery in the concentrate (aim for high R%) (see Table 5.1). In MIXC4 without an activator, the recovery of sulfide (% R sulfide) was higher (93.31%), the tailings sulfide grade was 0.51 \pm 0.82 %, and the concentrated sulfide grade was lower (43.16 \pm 0.19%). The last result could be explained by the enrichment ratio, which was higher (0.14 \pm 0.009) than for the K2044. In the second case, using K2044 as a collector, sulfide recovery (% R sulfide)

was lower (91.06%) than for MIXC4; this could be explained by the enrichment ratio being lower (0.13 ± 0.002) than for MIXC4. The tailings sulfide grade was $0.64 \pm 0.49\%$, and the concentrated sulfide grade was $45.08 \pm 0.90\%$, higher than for MIXC4. This could be explained by the head sulfide grade, which was lower ($6.26 \pm 0.03\%$) than for MIXC4 ($6.66 \pm 0.08\%$). The sample T3-3 presents interesting results, but the error in the % R sulfide is too large ($91.46 \pm 8.94\%$), which presents uncertainty in this measure. The S_{sulfide} of the head sample was 7.25 %, and the head grades in Table 5.1 were calculated using concentrate and tailings values. The results show that WR desulfurization was achieved. Therefore, samples T4-3 and T5-1 could be used to assess the geochemical stability by conducting kinetic tests.

The desulfurized samples were also analyzed considering the ABA test (see Figure 5.1), and the results corroborate that samples T4-3 and T5-1 (red points) require kinetic testing to assess their AMD generation potential, since these fractions were located in the uncertainty zone. Four more samples were located in this area. Nevertheless, we selected only T4-3 and T5-1 to analyze the geochemical behavior, because they had a higher sulfide recovery rate according to Table 5.1. It is worth mentioning that the sample T3-3 which has also high sulfide recovery (91.46 %) and was located in y-axis in the ABA test, was not introduced in the kinetic test analysis due to its high standard deviation. This could be explained because there was no reproducibility in the experimental data.

Considering the concentrates, samples C4-3 and C5-1 were mineralogically characterized using XRD. The results are shown in Table 5.2. It can be seen that C5-1 enables more concentration of pyrite than C4-3, since the pyrite recovery was 77% and 64% for C5-1 and C4-3, respectively. This result suggests that the K2044 could be a good collector for pyrite flotation. Concerning chalcopyrite, the recoveries were 77% and 56.6% for C4-3 and C5-1, respectively, demonstrating the influence of the xanthate collector in the copper flotation. The C4-3 sample was treated with a mixture of collectors PAX and K2044 (25:75). These results also show that the copper valorization is viable due to the copper grade in the concentrate, which was around 1.18%, and the enrichment ratio was 6. Typically, the copper grade in porphyry copper ore is around 0.4%. Therefore, this concentrate could be used as the feed in a further process, either through flotation or leaching to separate pyrite from chalcopyrite.

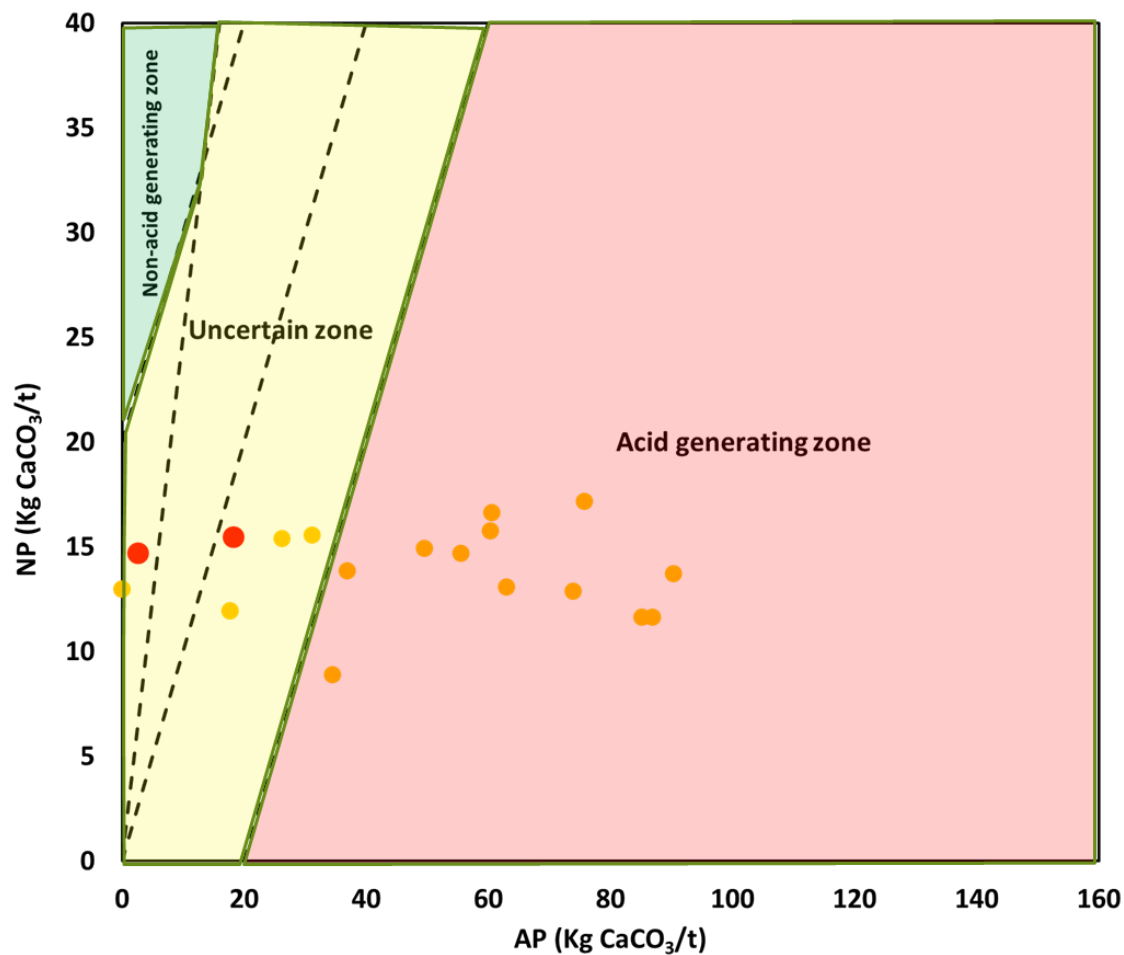


Figure 5.1 Analysis of desulfurized WR via ABA testing.

Table 5.2 Mineralogical composition of concentrates C4-3 and C5-1.

Mineral	Sample	
	C4-3 wt (%)	C5-1 wt (%)
Pyrite	40.8	60.1
Anhydrite	12.9	2.5
Gypsum	8.2	6.9
Muscovite	5.6	2.8
Chalcopyrite	3.4	3.0
Quartz	16.0	11.9
Clinocllore	9.6	12.2
Sphalerite	3.4	0.6

5.1.1.2 HydroFloat cell (-850 μm to +212 μm)

Table 5.3 shows the results obtained from flotation in the HydroFloat® cell. The collectors studied were potassium amyl xanthate (PAX) and diisobutyl dithiophosphate (DDTP). P_{80} was 608 μm . The results show that the best conditions for desulfurization involved using DDTP, since a lower sulfide grade was observed in the tailings and the global sulfide recoveries were higher using this collector than for PAX (except for T4, see Table 5.2). It can be also noted that with a high collector concentration and high water flow, the sulfide recoveries were higher. Therefore, samples T7 and T8 could be used to assess the geochemical stability by conducting kinetic tests. The HydroFloat process has not yet been used for the desulfurization process. Thus, obtaining sulfide recoveries around 89 % with DDTP enables us to identify this technology as a good alternative for coarse particle desulfurization. In addition, identifying that DDTP enables higher recoveries is an excellent result, since this collector is environmentally friendly. This compound is able to decompose very little carbon sulfide (CS_2) because of its hydraulic stability compared to xanthates. Therefore, framed in the context of cleaner production, this result was achieved from a desulfurization perspective as well as from the use of eco-friendly reagents.

Table 5.3 Results for HydroFloat® flotation for desulfurized tailings (-850 μm to + 212 μm).

Sample	S_{total}	S_{sulfate}	S_{sulfide}	% R_{sulfide}	Collector type	Collector concentration (g/ton)	Water flow (L/min)
T1	4.344	2.214	2.130	61.0	PAX	150	7
T2	3.693	1.639	2.053	71.8	PAX	150	8
T3	4.760	1.997	2.763	72.2	PAX	300	7
T4	3.184	1.987	1.197	83.9	PAX	300	8
T5	3.629	1.797	1.832	79.7	DDTP	150	7
T6	3.461	2.167	1.294	82.4	DDTP	150	8
T7	3.005	1.907	1.098	86.8	DDTP	300	7
T8	2.782	1.873	0.909	89.4	DDTP	300	8

The experimental results of the sulfide recoveries were also assessed using ANOVA testing at a 5% significance level. Figure 5.2 shows the Pareto chart, which permits the detection of the factor and interaction effects that are most important to the flotation recovery. The Pareto chart shows that the main factors influencing the sulfide recovery by flotation follow the order collector type > collector concentration > water flow. The linear model that describes the experiment is shown in the following equation:

$$S_{\text{Recovery}} = 78.40 - 6.18 \text{ Collector} + 3.48 \text{ Water flowrate} + 4.67 \text{ Collector concentration} \quad (5.1)$$

R^2 , R_{adj}^2 , and R_{pred}^2 for the sulfide recovery model were 0.92, 0.87, and 0.70, respectively. These values are frequently observed in multiphase systems and flotation modeling (Cisternas et al., 2019; Lucay et al., 2020). Therefore, this model was used to determine the optimal conditions and to analyze the effects of collector type, collector concentration, and water flow in the desulfurization of WR. These results also show that for the conditions studied, chemical factors (collector type, collector concentration) have a greater effect than operational factors (water flow).

The ABA test results for the desulfurized WR using the HydroFloat® process have not yet been obtained since there are still some measurements that must be performed in Canada to obtain NP values. Moreover, characterization by XRD of the concentrate obtained during desulfurization is still in process.

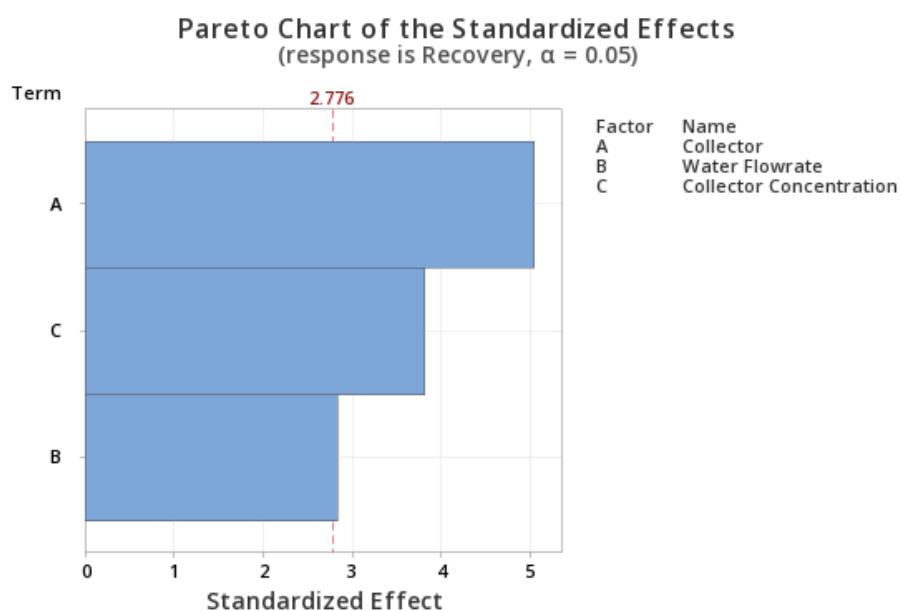


Figure 5.2 Pareto chart of standardized effect on sulfide recoveries.

5.1.2 WR geochemical behavior

5.1.2.1 Column testing

The geochemical behavior of the particle size $> 5\text{mm}$ was assessed by conducting column testing. The pH, Eh, electrical conductivity, acidity-alkalinity, and element cumulative charge were measured over 22 weeks. The results show that the pH values remained near neutral (6.5-7.7) and

the redox potential (Eh) values varied between 353 and 686 mV (Figure 5.3a). There was no important variation in the Eh from the beginning until week 22, showing the leachate stability during this period. The electrical conductivity showed a decreasing trend, explained by a decrease in the leachate chemical loading (Figure 5.3b). The alkalinity shows that the WR had no intrinsic neutralizing potential since the data collected during the 22 weeks do not show a marked variation. Moreover, the acidity and alkalinity show a similar trend of decreasing over time. However, until week 22 the variation is not quite noticeable. Finally, the acidity is lower than the alkalinity but not significantly low, which demonstrates the geochemical stability of the WR (Figure 5.3c). The cumulative charge of elements Fe, Cu, Zn, Pb, Ca, and Mg is presented in Figure 5.3d. Iron was leached in small concentrations with a maximum of 0.1 mg/L (0.04 mg/kg cumulative charge). Zinc was leached with a maximum of 0.25 mg/L (0.28 mg/kg). Copper was leached with a maximum of 0.2 mg/L (0.10 mg/kg), and Pb was leached with a maximum of 0.01 mg/L (0.01mg/kg); these levels were very low during the period of the test. However, it can be seen that calcium was leached in high concentrations between 660 and 742 mg/L (81-870 mg/kg cumulative charge). This could be due to the high presence of anhydrite in the WR, as was demonstrated by the characterization of WR. Furthermore, the high presence of Mg is due to the presence of clinocllore in WR. Therefore, the charge of these elements remains below the regulatory limits set by Directive 019, Québec, Canada.

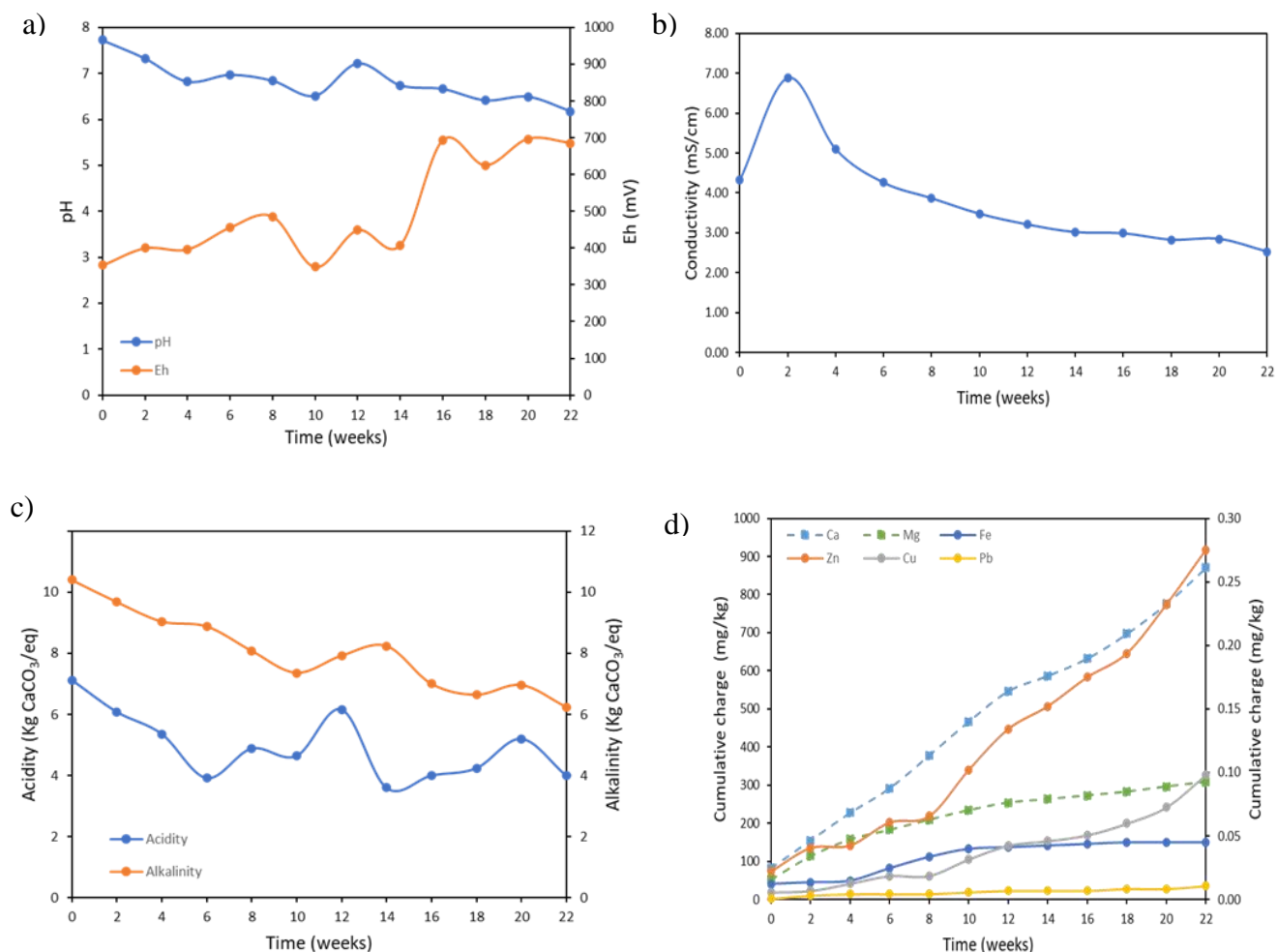


Figure 5.3 Column test results for particle sizes > 5mm. a) pH and Eh evolution, b) conductivity evolution, c) acidity and alkalinity evolution, d) elemental cumulative charge, dashed lines refer to left y-axis while solid lines refer to right y-axis.

5.1.2.2 Weathering test

According to ABA testing, F5 was located in the uncertainty zone, and F4 was located almost on the edge between the uncertainty zone and acid-generating zone. Therefore, the geochemical stability of these two fractions was assessed by weathering cell testing. Moreover, T4-3 and T5-1 were the samples that presented higher sulfide recovery during the desulfurization process using Denver cells. The particle size for these samples was < 212 μm . In addition, for T5-1, the operational conditions comprised the collector K2044 (dithiophosphate) with an activator, and for T4-3 the operational conditions comprised a mixture of collectors KAX-K2044 (25:75) without an activator.

The results show that the pH values remained near neutral (6.2-6.9) for all samples, and the behavior during the 8 weeks seemed to be stable (Figure 5.4a). The redox potential (Eh) values varied between 255 and 319 mV (Figure 5.4b). There is no important variation in the Eh from the beginning until week 8, showing the leachate stability during this period. The electrical conductivity for F4 and F5 showed a decreasing trend, explained by a decrease in the leachate chemical loading (Figure 5.4c). However, for T5-1 and T4-3, it seems that since the beginning of the test, the leachates of those samples were not chemically loaded, suggesting their chemical stability.

The cumulative charge of elements Fe, Cu, Zn, Ca, and Mg, and sulfate is presented in Figure 5.5 a-d. In general, for the four samples (F5, F4, T4-3, and T5-1) the iron was leached in small concentrations with values lower than 0.1 mg/L (0.04 mg/kg cumulative charge). Zinc was leached with a maximum of 0.15 mg/L (0.27 mg/kg). Figure 5.5 a-c show that Zn will continue dissolving; this behavior is expected since it has high solubility and mobility with neutral pH. Copper was leached with a maximum of 0.1 mg/L (0.14 mg/kg), except for F5, which was lower than 0.65mg/L (2.41mg /kg cumulative charge). This behavior was expected since this sample was treated with the activator copper sulfate and residual copper ions could have been released during the test. However, it can be seen that the calcium was leached at a high charge with a maximum of 4088 mg/kg cumulative charge. Furthermore, the sulfate charge was over 2000 mg/L (11,180 mg/kg cumulative charge). These results could be related to the high amount of anhydrite in WR. Therefore, in this research, sulfate cannot be used as an indicator of sulfide oxidation because its presence is explained by anhydrite dissolution. In addition, the presence of Mg is due to the occurrence of clinocllore in WR. Therefore, the concentration of these elements remains below the regulatory limits set by Directive 019, Québec, Canada. According to these results, we conclude that the samples assessed using weathering cell testing are not likely to produce AMD. Therefore, the desulfurization process using a Denver cell for the fine fraction (< 212 μm) was conducted with success.

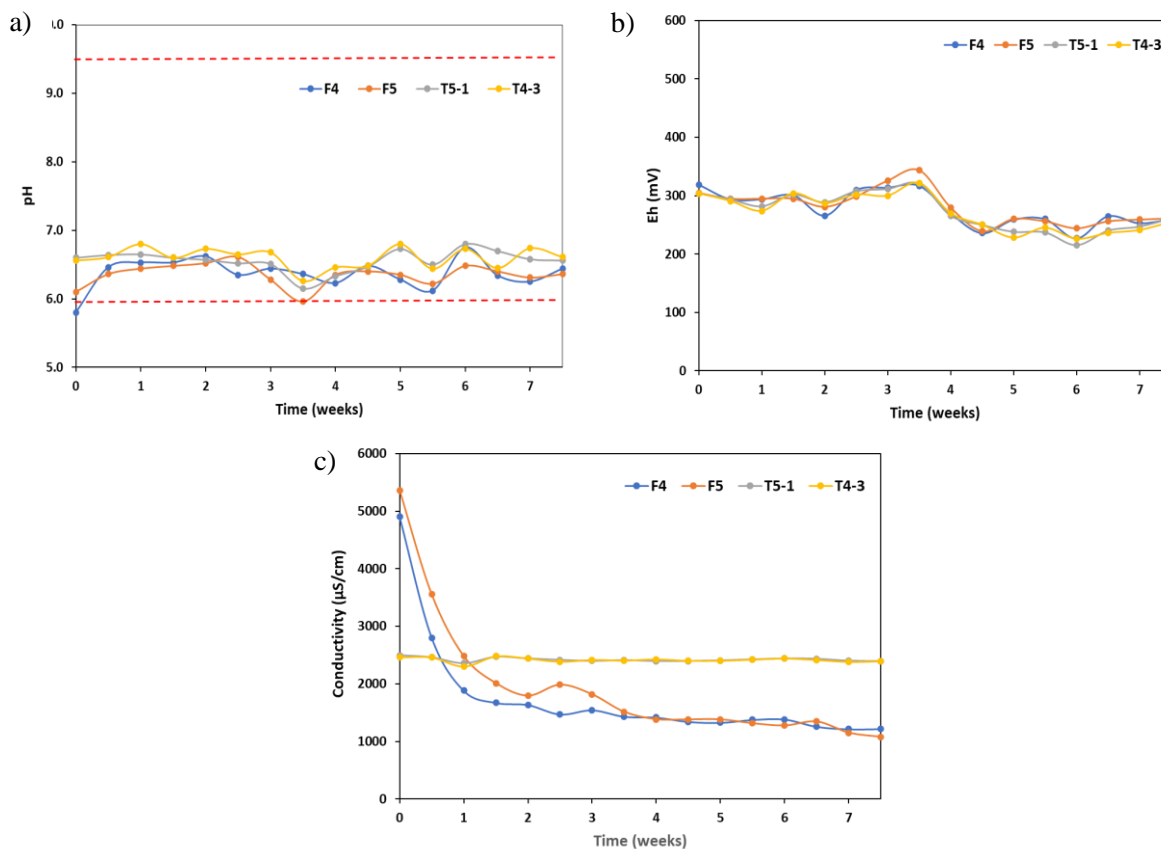


Figure 5.4 a) pH, b) Eh, and c) conductivity results of weathering cells for F4, F5, and desulfurized samples T5-1 and T4-3.

Finally, it is worth mentioning that the weathering test showed that F5 and F4 unlikely produce AMD. Therefore, this finding enables us to refine the DPLS. Before the kinetic test, the DPLS was defined as 2.4 mm, now it could be refined as 850 µm.

5.2 Discussion and contributions of the study

In this research, we used the flotation process as a tool to solve different issues related to solid waste assessment and management for AMD prevention. One issue was associated with tailings management; it was identified that the problem was the use of traditional flotation methods, which enable the creation of acidifying species. Therefore, the solution was to develop and propose new designs of flotation flowsheets that consider the desulfurization process at an early stage of the flotation process. Therefore, the concept of in-process technology was introduced, which refers to AMD prevention more than end-of-pipe technologies, which focus on AMD mitigation.

Another issue identified was related to WR management. It was identified that aspects such as complex mineralogical composition, particle size distribution, and liberation degree make WR assessment challenging. Therefore, a methodology was proposed that enabled the identification of fractions that will produce AMD and those that will not produce AMD. For those fractions that will produce AMD, the desulfurization process was proposed. However, one of the challenges to float WR is that the particle size tends to be coarse. In addition, HydroFloat technology was implemented for the first time for the desulfurization of WR from porphyry copper ore.

Finally, finding alternative sources for copper supply enabled us to identify that porphyry copper ores are composed of other copper sulfides such as covellite. Therefore, from the literature review, it was found that there is a lack of information related to how covellite behaves during the flotation process. We conducted fundamental studies to fill this gap and to find the optimal parameters to be used during the flotation process.

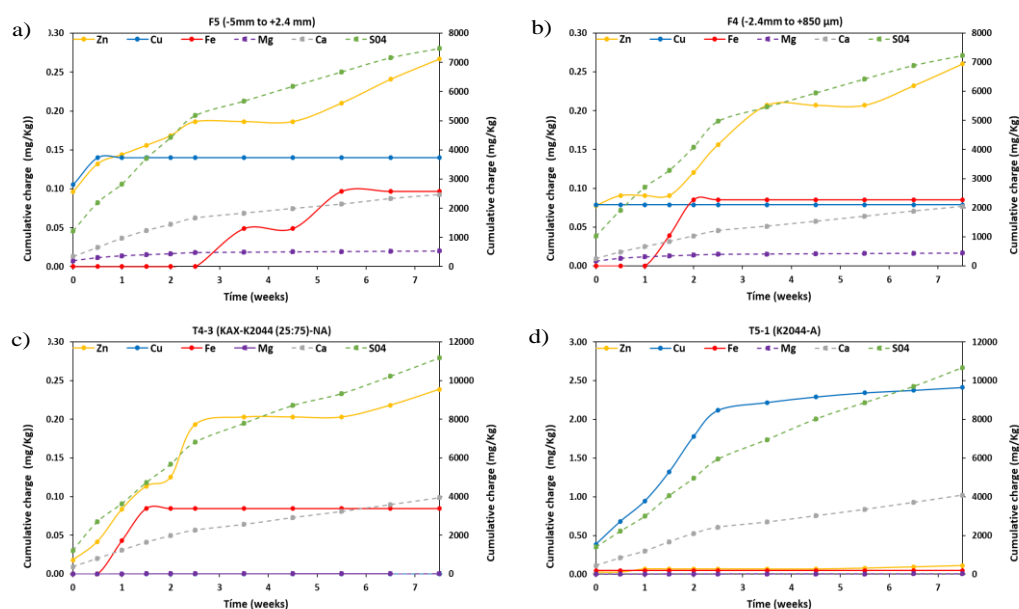


Figure 5.5 Cumulative charge of elements Fe, Cu, Zn, Ca, and Mg, and sulfate of weathering cell results for a) F5, b) F4, and desulfurized samples c) T4-3 and d) T5-1. Dashed lines refer to the right y-axis while solid lines refer to the left y-axis.

5.3 Limitations of the study

When considering WR management, some limitations were identified. The first was related to technologies used for WR desulfurization. In this work, the flotation process was used as a tool for

the desulfurization process. Therefore, one limitation was the particle size, which must be lower than 850 μm (limit particle size flotation). Therefore, for particle sizes larger than 850 μm , and materials that could produce AMD, other types of desulfurization technologies could be implemented; for instance, gravimetric separation or sorting. In this work, particle sizes larger than 850 μm were assessed via kinetic testing, and it was found that these could be non-acid-generating, as discussed in Section 5.2.2. Therefore, as a result of this study, it seems that the flotation process was an appropriate method to conduct the desulfurization process. The second limitation was related to the use of weathering cells instead of humidity cells. Weathering cells were used due to the limited time available to conduct this study. However, as the conditions used in weathering cells are more aggressive, kinetic testing showed that WR is unlikely to produce AMD.

CHAPTER 6 CONCLUSIONS AND RECOMMENDATIONS

6.1 Conclusions

The findings enable us to identify that from the porphyry copper ores it is possible to improve the copper recovery by studying other minor copper minerals, such as covellite. With this purpose, high covellite recoveries were obtained using both bulk and selective flotation. It was demonstrated that the covellite physicochemical behavior is different to chalcopyrite, the main porphyry copper mineral.

The results obtained from article I: New insights related to the flotation of covellite in porphyry ores, show that in the Hallimond tube test, under the conditions studied, covellite has a natural flotation of around 55% and is pH-independent. Covellite recovery is influenced by collector type and concentration, and thanks to the high selectivity of the collector IPETC, low collector concentrations are sufficient to float covellite at pH 8 and 11. The results of the porphyry copper ore flotation confirm that IPETC has a better affinity for copper, whereas PAX has a better affinity for iron. IPETC can be used as a selective or bulk collector, varying only the pH and using low concentrations. After all, it is not necessary to use different collectors for bulk and selective flotation. Furthermore, bulk flotation is feasible with IPETC at low pH and low collector dosage for porphyry copper ore.

The results obtained from article II: Physical–chemical study of IPETC and PAX collector adsorption on covellite surface, show that in the FT-IR the bands related to $-C(=S)-NH$, $-C-H$, NH deformation, CH deformation, and CNC characteristic of IPETC were present in the spectra, demonstrating IPETC adsorption on covellite surface. Moreover, PAX adsorption was identified via the leading functional groups, such as dixantogen $(AX)_2$, and Cu-amylxanthate $(CuAX)$. The XPS shows that the adsorption mechanism of IPETC suggests that the binding is facilitated by the S of the collector with Cu atoms on the covellite surface. Additionally, the high-resolution XPS spectra of the Cu 2p spectrum show that the oxidation state of covellite with PAX is Cu(I). This finding was corroborated by FT-IR by the identification of Cu-amylxanthate $(CuAX)$ and dixantogen $(AX)_2$ on the covellite surface. Lastly, the DFT results are in good accordance with the FT-IR and XPS results.

Likewise, the assessment of the flotation flowsheet, introducing the concept of the desulfurization process, allows us to identify the optimal circuits from a significant number of separation strategies

and flotation circuit alternatives for polymetallic ores. It was demonstrated that a holistic approach allows to obtain better designs and to analyze the advantages, disadvantages, and costs that could entail each flowsheet proposed.

The results obtained from the article III: Insights into the design of polymetallic flotation circuits, including tailing desulfurization, show that the design strategy developed for monometallic minerals using optimization can be applied to polymetallic minerals. Two observations support this statement: a) there are few optimal structures for a given problem despite the uncertainty in the recoveries of each stage, and b) few structures accumulate the highest frequencies of occurrence or, in other words, have the greatest chance of being the optimal structure.

Also, from the different design strategies implemented, integrated disjunctive, integrated, fractional selective, and fractional bulk; the selective fractional circuit will produce the most significant environmental effects and cost the most.

From a desulfurization point of view, the selective fractional circuit, which is the typical circuit in practice, delivers the worst results, followed by the bulk fractional circuit. The integrated circuit and integrated disjunctive circuit proposed in this manuscript present the best results. However, they offer the challenge of containing floating minerals that have been depressed and vice versa. Therefore, there is a need for further study to manipulate flotation and depression in different sequences to develop more efficient processes with less environmental impact.

Based on the Kevitsa concentration case study, it is concluded that applying optimization can provide designs that can be studied further. The simultaneous design of all circuits for a polymetallic mineral gives better results than a one-at-a-time design. The design of polymetallic mineral flotation circuits as a system where interaction between the circuits is possible can generate an important improvement.

Besides, the concept of cleaner production was incorporated since the desulfurization in an early stage of the flotation process was proposed to treat a porphyry copper ore, producing tailings with low content of sulfurous species as well as the desulfurization of the waste rock for acid mine drainage prevention.

The results obtained from the article IV: Application of characterization techniques for preventing AMD for waste rock from a Chilean porphyry copper mine, show that the DPLS was 2.4 mm. Therefore, particle size fractions lower than this value will produce AMD. Nevertheless, the ABA

test demonstrated that particle sizes between 5 mm and 2.4 mm could also be acid-generating, since they were located in an uncertainty zone. All the fractions assessed displayed high pyrite concentrations of around 6 %, and carbonate concentrations were around 0.3%, suggesting that this type of WR does not have intrinsic neutralizing potential. The gangue mineral of the WR was mostly composed of quartz, anhydrite, muscovite, and clinocllore. Chalcopyrite and rutile were identified with grades around 0.6% for both, demonstrating that this WR could be treated for metal valorization. Finally, the relationship between DPLS and liberation degree was evidenced since the particle size (-2.4 mm to +850 μm) presented a liberation degree of around 50%. The liberation degree for a particle size larger than 2.4 mm was 9.1 %, and particles smaller than this value reached a liberation degree of 96%.

Moreover, it was demonstrated that the desulfurization process using a Denver cell for the fine fraction (< 212 μm) was conducted with success, since the kinetic tests show that the elements Fe, Cu, Zn, Ca, and Mg were leached in small concentrations. Therefore, the concentration of these elements remains below the regulatory limits set by Directive 019, Québec, Canada. According to these results, we conclude that the samples assessed using weathering cell testing are not likely to produce AMD.

It is worth noting that all the strategies implemented in this thesis, flotation, mineral characterization, physicochemical interaction between minerals and reagents, flotation flowsheet analysis, and geochemical behavior assessment of ores, contribute to the integrated assessment of the behavior of the ore before, during, and after mineral processing, which is relevant in mining procedures. In deep, the analysis of a WR from a porphyry copper ore demonstrated that all these issues are essential to identify the fraction that can generate AMD and the treatment process.

6.2 Recommendations

This section presents some recommendations related to future work that could be conducted based on the results obtained during the execution of this thesis. It is recommended to study the issue of desulfurization holistically, seeking more efficient solutions from a metallurgical and environmental point of view. In addition, it is suggested that ores composed of different valuable species, such as chalcopyrite and covellite, should be studied with collector formulations because the physicochemical behavior of each mineral could be different. Besides, using greener collectors is an excellent option thinking in cleaner production. Moreover, further studies are necessary to

better understand the interaction between covellite, sulfurous gangue, and non-sulfurous gangue because of the higher solubility of covellite compared with other copper sulfide minerals. Likewise, it is worth mentioning that it is necessary to study the selective flotation of the bulk concentrated, which enables the development of separation strategies based on cleaner production. Finally, the development of methodologies to analyze the AMD potential that includes environmental aspects such as rainfall level and water quality used to assess the potential acid generation from the waste rock and tailings is of huge importance.

Finally, framed in the concept of cleaner production, it is necessary to identify the possible uses of the pyrite concentrate. Some studies have shown the use of pyrite in various fields. For instance, to obtain SO_2 by adding pyrite in a boiling furnace (Song et al., 2019). Pyrite has also been used as a source of lixiviant in the bioleaching of electronic waste (Bryan et al., 2015). In addition, it has been used in agriculture cultivating grass with the pyrite additive, this showed greater availability of certain trace elements and an increase in nutritional parameters (Castelo-Branco et al., 1999). In mining, pyrite has been used to control the redox potential to improve chalcopyrite bioleaching in the presence of *Leptospirillum ferriphilum* (Hong et al., 2021). Finally, analyzing the pyrite concentrate as a residue and how its geochemical behavior would be like if it were to be stored in a landfill, (Grieco et al., 2021), they demonstrated that the waters that interact with traditional flotation tailings (tailings with pyrite) they are slightly more acidic and much higher in total metal content than those that interact with flotation tailings that have been desulfurized. Furthermore, the distribution of metals is different, with the former being highest in sulfide-hosted metals and the second-highest in gangue-hosted metals. Therefore, it is suggested that pyrite separation may play an important role in the sustainable extraction of pyrite-rich ores, either for dumping highly hazardous pyrite concentrates separately or for trading as by-products.

REFERENCES

- Ackerman, P.K., Harris, G.H., Klimpel, R.R., Aplan, F.F., 2000. Use of xanthogen formates as collectors in the flotation of copper sulfides and pyrite. *Int J Miner Process* 58, 1–13. [https://doi.org/10.1016/S0301-7516\(99\)00068-X](https://doi.org/10.1016/S0301-7516(99)00068-X)
- Ackerman, P.K., Harris, G.H., Klimpel, R.R., Aplan, F.F., 1999. Use of chelating agents as collectors in the flotation of copper sulfides and pyrite. *Min Metall Explor* 16, 27–35. <https://doi.org/10.1007/BF03402853>
- Acosta-Flores, R., Lucay, F.A., Cisternas, L.A., Galvez, E.D., 2018. Two-phase optimization methodology for the design of mineral flotation plants, including multispecies and bank or cell models. *Minerals & Metallurgical Processing*. <https://doi.org/10.19150/mmp.8055>
- Agorhom, E.A., Skinner, W., Zanin, M., 2014. Diethylenetriamine depression of Cu-activated pyrite hydrophobised by xanthate. *Miner Eng* 57, 36–42. <https://doi.org/10.1016/j.mineng.2013.12.010>
- Ait-Khouia, Y., Benzaazoua, M., Demers, I., 2021. Environmental desulfurization of mine wastes using various mineral processing techniques: Recent advances and opportunities. *Miner Eng* 174, 107225. <https://doi.org/10.1016/j.mineng.2021.107225>
- Ackerman, P.K., G.H. Harris, R.R. Klimpel, F.F. Aplan, Evaluation of flotation collectors for copper sulfides and pyrite, I. Common sulfhydryl collectors, *International Journal of Mineral Processing*. 21 (1987) 105–127. [https://doi.org/10.1016/0301-7516\(87\)90009-3](https://doi.org/10.1016/0301-7516(87)90009-3).
- Amar, H., Benzaazoua, M., Edahbi, M., Villeneuve, M., Joly, M.-A., Elghali, A., 2021. Reprocessing feasibility of polymetallic waste rock for cleaner and sustainable mining. *J Geochem Explor* 220, 106683. <https://doi.org/10.1016/j.gexplo.2020.106683>
- Amar, H., Benzaazoua, M., Elghali, A., Bussière, B., Duclos, M., 2020. Upstream environmental desulphurisation and valorisation of waste rocks as a sustainable AMD management approach. *J Geochem Explor* 215, 106555. <https://doi.org/10.1016/j.gexplo.2020.106555>
- Amos, R.T., Blowes, D.W., Bailey, B.L., Segó, D.C., Smith, L., Ritchie, A.I.M., 2015. Waste-rock hydrogeology and geochemistry. *Applied Geochemistry* 57, 140–156. <https://doi.org/10.1016/j.apgeochem.2014.06.020>

Araya, N., Kraslawski, A., Cisternas, L.A., 2020. Towards mine tailings valorization: Recovery of critical materials from Chilean mine tailings. *J Clean Prod* 263, 121555. <https://doi.org/10.1016/j.jclepro.2020.121555>

Araya, N., Ramírez, Y., Kraslawski, A., & Cisternas, L. A. (2021). Feasibility of re-processing mine tailings to obtain critical raw materials using real options analysis. *Journal of Environmental Management*, 284, 112060. <https://doi.org/10.1016/j.jenvman.2021.112060>

Awatey, B., Skinner, W., Zanin, M., 2015. Incorporating fluidised-bed flotation into a conventional flotation flowsheet: A focus on energy implications of coarse particle recovery. *Powder Technol* 275, 85–93. <https://doi.org/10.1016/j.powtec.2015.01.065>

Awatey, B., Thanasekaran, H., Kohmuench, J.N., Skinner, W., Zanin, M., 2013. Optimization of operating parameters for coarse sphalerite flotation in the HydroFloat fluidised-bed separator. *Miner Eng* 50–51, 99–105. <https://doi.org/10.1016/j.mineng.2013.06.015>

Ávila-Márquez, D.M., I.A. Reyes-Domínguez, A. Blanco-Flores, H.P. Toledo-Jaldin, G. López-Téllez, J. Aguilar-Carrillo, E.J. Gutiérrez-Castañeda, Study of the Influence of Xanthate Derivative Structures on Copper Sulfide Mineral Adsorption Under Acidic Conditions, *Metallurgical and Materials Transactions B*. 50 (2019) 86–97. <https://doi.org/10.1007/s11663-018-1452-z>.

Bu, Y., Y. Hu, W. Sun, Z. Gao, R. Liu, Fundamental Flotation Behaviors of Chalcopyrite and Galena Using O-Isopropyl-N-Ethyl Thionocarbamate as a Collector, *Minerals*. 8 (2018) 115. <https://doi.org/10.3390/min8030115>.

Biesinger, M.C., L.W.M. Lau, A.R. Gerson, R.S.C. Smart, Resolving surface chemical states in XPS analysis of first row transition metals, oxides and hydroxides: Sc, Ti, V, Cu and Zn, *Applied Surface Science*. 257 (2010) 887–898. <https://doi.org/10.1016/j.apsusc.2010.07.086>.

Bag, B., B. Das, B.K. Mishra, Geometrical optimization of xanthate collectors with copper ions and their response to flotation, *Minerals Engineering*. 24 (2011) 760–765. <https://doi.org/10.1016/j.mineng.2011.01.006>.

Bishop, J.L., M.D. Lane, M.D. Dyar, S.J. King, A.J. Brown, G.A. Swayze, Spectral properties of Ca-sulfates: Gypsum, bassanite, and anhydrite, *American Mineralogist*. 99 (2014) 2105–2115. <https://doi.org/10.2138/am-2014-4756>.

Bascetin A., Tuylu S., Adıguzel D., & Ozdemir O. (2016). New Technologies on Mine Process Tailing Disposal. *Journal of Geological Resource and Engineering*, 4(2). <https://doi.org/10.17265/2328-2193/2016.02.002>

Benzaazoua, M., Bouzahzah, H., Taha, Y., Kormos, L., Kabombo, D., Lessard, F., Bussière, B., Demers, I., Kongolo, M., 2017. Integrated environmental management of pyrrhotite tailings at Raglan Mine: Part 1 challenges of desulphurization process and reactivity prediction. *J Clean Prod* 162, 86–95. <https://doi.org/10.1016/j.jclepro.2017.05.161>

Benzaazoua, M., Bussière, B., Dagenais, A.-M., Archambault, M., 2004. Kinetic tests comparison and interpretation for prediction of the Joutel tailings acid generation potential. *Environmental Geology* 46, 1086–1101. <https://doi.org/10.1007/s00254-004-1113-1>

Benzaazoua, M., Bussière, B., Kongolo, M., McLaughlin, J., Marion, P., 2000. Environmental desulphurization of four Canadian mine tailings using froth flotation. *Int J Miner Process* 60, 57–74. [https://doi.org/10.1016/S0301-7516\(00\)00006-5](https://doi.org/10.1016/S0301-7516(00)00006-5)

Bicak, O., Ekmekci, Z., Bradshaw, D.J., Harris, P.J., 2007. Adsorption of guar gum and CMC on pyrite. *Miner Eng* 20, 996–1002. <https://doi.org/10.1016/j.mineng.2007.03.002>

Blowes, D.W., Ptacek, C.J., Jambor, J.L., Weisener, C.G., Paktunc, D., Gould, W.D., Johnson, D.B., 2014. The Geochemistry of Acid Mine Drainage, in: *Treatise on Geochemistry*. Elsevier, pp. 131–190. <https://doi.org/10.1016/B978-0-08-095975-7.00905-0>

Botero, Y.L., Alves, L.T., Cisternas, L.A., 2021. Gestión del drenaje ácido de minas en relaves, in: Cisternas, L., Gálvez, E., Rivas, M., Valderrama, J. (Eds.), *Economía Circular En Procesos Mineros*. Ril editores, Santiago de Chile, pp. 93–120.

Boulton, A., Fornasiero, D., Ralston, J., 2001. Depression of iron sulphide flotation in zinc roughers. *Miner Eng* 14, 1067–1079. [https://doi.org/10.1016/S0892-6875\(01\)00112-1](https://doi.org/10.1016/S0892-6875(01)00112-1)

Boulton, A., Fornasiero, D., Ralston, J., 2001. Selective depression of pyrite with polyacrylamide polymers. *Int J Miner Process* 61, 13–22. [https://doi.org/10.1016/S0301-7516\(00\)00024-7](https://doi.org/10.1016/S0301-7516(00)00024-7)

Bourke, P., 2002. *Selecting Flotation Cells: How Many and What Size?*

Bouzahzah, H., Benzaazoua, M., Bussière, B., 2013. Acid-generating potential calculation using 515 mineralogical static test: modification of the Paktunc equation., in: World 516 Mining Congress. Montréal, Québec, Canada.

Bouzahzah, H., Benzaazoua, M., Bussiere, B., Plante, B., 2014. Prediction of Acid Mine Drainage: Importance of Mineralogy and the Test Protocols for Static and Kinetic Tests. *Mine Water Environ* 33, 54–65. <https://doi.org/10.1007/s10230-013-0249-1>

Bryan, C. G., Watkin, E. L., McCredden, T. J., Wong, Z. R., Harrison, S. T. L., & Kaksonen, A. H. (2015). The use of pyrite as a source of lixiviant in the bioleaching of electronic waste. *Hydrometallurgy*, 152, 33–43. <https://doi.org/10.1016/j.hydromet.2014.12.004>

Buckley, A.N., Hope, G.A., Lee, K.C., Petrovic, E.A., Woods, R., 2014. Adsorption of O-isopropyl-N-ethyl thionocarbamate on Cu sulfide ore minerals. *Miner Eng* 69, 120–132. <https://doi.org/10.1016/j.mineng.2014.08.002>

Bulatovic, S.M., 2007. Handbook of flotation reagents: chemistry, theory and practice: Volume 1: flotation of sulfide ores. Elsevier.

Bulatovic, S.M., 1999. Use of organic polymers in the flotation of polymetallic ores: A review. *Miner Eng* 12, 341–354. [https://doi.org/10.1016/S0892-6875\(99\)00015-1](https://doi.org/10.1016/S0892-6875(99)00015-1)

Bulut, G., Ceylan, A., Soylu, B., Göktepe, F., 2011. Role of starch and metabisuphite on pure pyrite and pyritic copper ore flotation. *Physicochemical Problems of Mineral Processing* 48, 39–48.

Burrows, D.R., Rennison, M., Burt, D., Davies, R., 2020. The Onto Cu-Au Discovery, Eastern Sumbawa, Indonesia: A Large, Middle Pleistocene Lithocap-Hosted High-Sulfidation Covellite-Pyrite Porphyry Deposit. *Economic Geology* 115, 1385–1412. <https://doi.org/10.5382/econgeo.4766>

Bussière, B., 2007. Hydrogeotechnical properties of hard rock tailings from metal mines and emerging geoenvironmental disposal approaches. *Canadian Geotechnical Journal* 44, 1019–1052.

Calisaya, D.A., López-Valdivieso, A., de la Cruz, M.H., Gálvez, E.E., Cisternas, L.A., 2016. A strategy for the identification of optimal flotation circuits. *Miner Eng* 96–97, 157–167. <https://doi.org/10.1016/j.mineng.2016.06.010>

Camus, F., 1975. Geology of the El Teniente Orebody with Emphasis on Wall-Rock Alteration. *Economic Geology* 70, 1341–1372.

Cabrera-German, D. J.A. García-Valenzuela, M. Martínez-Gil, G. Suárez-Campos, Z. Montiel-González, M. Sotelo-Lerma, M. Cota-Leal, Assessing the chemical state of chemically deposited copper sulfide: A quantitative analysis of the X-ray photoelectron spectra of the amorphous-to-covellite transition phases, *Applied Surface Science*. 481 (2019) 281–295. <https://doi.org/10.1016/j.apsusc.2019.03.054>.

Choudhary, V., A. Bhatt, D. Dash, N. Sharma, DFT calculations on molecular structures, HOMO–LUMO study, reactivity descriptors and spectral analyses of newly synthesized diorganotin(IV) 2-chloridophenylacetohydroxamate complexes, *Journal of Computational Chemistry*. 40 (2019) 2354–2363. <https://doi.org/10.1002/jcc.26012>.

Castelo-Branco, M. A., Santos, J., Moreira, O., Oliveira, A., Pereira Pires, F., Magalhaes, I., Dias, S., Fernandes, L. M., Gama, J., Vieira E Silva, J. M., & Ramalho Ribeiro, J. (1999). Potential use of pyrite as an amendment for calcareous soil. *Journal of Geochemical Exploration*, 66(1–2), 363–367. [https://doi.org/10.1016/S0375-6742\(99\)00026-6](https://doi.org/10.1016/S0375-6742(99)00026-6)

Chandra, A.P., Gerson, A.R., 2009. A review of the fundamental studies of the copper activation mechanisms for selective flotation of the sulfide minerals, sphalerite and pyrite. *Adv Colloid Interface Sci* 145, 97–110. <https://doi.org/10.1016/j.cis.2008.09.001>

Chandra, A.P., Puskar, L., Simpson, D.J., Gerson, A.R., 2012. Copper and xanthate adsorption onto pyrite surfaces: Implications for mineral separation through flotation. *Int J Miner Process* 114–117, 16–26. <https://doi.org/10.1016/j.minpro.2012.08.003>

Chen, J., Li, Y., Chen, Y., 2011. Cu–S flotation separation via the combination of sodium humate and lime in a low pH medium. *Miner Eng* 24, 58–63. <https://doi.org/10.1016/j.mineng.2010.09.021>

Chernyshova, I.V., 2003. An in situ FTIR study of galena and pyrite oxidation in aqueous solution. *Journal of Electroanalytical Chemistry* 558, 83–98. [https://doi.org/10.1016/S0022-0728\(03\)00382-6](https://doi.org/10.1016/S0022-0728(03)00382-6)

Chopard, A., Benzaazoua, M., Bouzahzah, H., Plante, B., Marion, P., 2017. A contribution to improve the calculation of the acid generating potential of mining wastes. *Chemosphere* 175, 97–107. <https://doi.org/10.1016/j.chemosphere.2017.02.036>

Cisternas, L., Lucay, F., Botero, Y., 2019. Trends in Modeling, Design, and Optimization of Multiphase Systems in Minerals Processing. *Minerals* 10, 22. <https://doi.org/10.3390/min10010022>

Cisternas, L. A., Ordóñez, J. I., Jeldres, R. I., & Serna-Guerrero, R. (2021). Toward the Implementation of Circular Economy Strategies: An Overview of the Current Situation in Mineral Processing. *Mineral Processing and Extractive Metallurgy Review*, 1–23. <https://doi.org/10.1080/08827508.2021.1946690>

Cisternas, L.A., Gálvez, E.D., Zavala, M.F., Magna, J., 2004. A MILP model for the design of mineral flotation circuits. *Int J Miner Process* 74, 121–131. <https://doi.org/10.1016/j.minpro.2003.10.001>

Cisternas, L.A., Jamett, N., Gálvez, E.D., 2015. Approximate recovery values for each stage are sufficient to select the concentration circuit structures. *Miner Eng* 83, 175–184. <https://doi.org/10.1016/j.mineng.2015.09.003>

Cisternas, L.A., Lucay, F., Gálvez, E.D., 2014. Effect of the objective function in the design of concentration plants. *Miner Eng* 63, 16–24. <https://doi.org/10.1016/j.mineng.2013.10.007>

Cisternas, L.A., Lucay, F.A., Acosta-Flores, R., Gálvez, E.D., 2018. A quasi-review of conceptual flotation design methods based on computational optimization. *Miner Eng* 117, 24–33. <https://doi.org/10.1016/j.mineng.2017.12.002>

Cisternas, L.A., Méndez, D.A., Gálvez, E.D., Jorquera, R.E., 2006. A MILP model for design of flotation circuits with bank/column and regrind/no regrind selection. *Int J Miner Process* 79, 253–263. <https://doi.org/10.1016/j.minpro.2006.03.005>

Cruz, C., Botero, Yesica.L., Jeldres, R.I., Uribe, L., Cisternas, L.A., 2021. Current Status of the Effect of Seawater Ions on Copper Flotation: Difficulties, Opportunities, and Industrial Experience. *Mineral Processing and Extractive Metallurgy Review* 1–19. <https://doi.org/10.1080/08827508.2021.1900175>

Cruz, R., Bertrand, V., Monroy, M., González, I., 2001. Effect of sulfide impurities on the reactivity of pyrite and pyritic concentrates: a multi-tool approach. *Applied Geochemistry* 16, 803–819. [https://doi.org/10.1016/S0883-2927\(00\)00054-8](https://doi.org/10.1016/S0883-2927(00)00054-8)

Dalm, M., Buxton, M.W.N., van Ruitenbeek, F.J.A., Voncken, J.H.L., 2014. Application of near-infrared spectroscopy to sensor based sorting of a porphyry copper ore. *Miner Eng* 58, 7–16. <https://doi.org/10.1016/j.mineng.2013.12.016>

Das, A., Sarkar, B., 2018. Advanced Gravity Concentration of Fine Particles: A Review. *Mineral Processing and Extractive Metallurgy Review* 39, 359–394. <https://doi.org/10.1080/08827508.2018.1433176>

De Gontijo, C.F., Fornasiero, D., Ralston, J., 2007. The limits of fine and coarse particle flotation. *Canadian Journal of Chemical Engineering* 85, 739–747. <https://doi.org/10.1002/cjce.5450850519>

De Wet, J.R., Pistorius, P.C., Sandenbergh, R.F., 1997. The influence of cyanide on pyrite flotation from gold leach residues with sodium isobutyl xanthate. *Int J Miner Process* 49, 149–169. [https://doi.org/10.1016/S0301-7516\(96\)00031-2](https://doi.org/10.1016/S0301-7516(96)00031-2)

Descostes, M., Vitorge, P., Beaucaire, C., 2004. Pyrite dissolution in acidic media. *Geochim Cosmochim Acta* 68, 4559–4569. <https://doi.org/10.1016/j.gca.2004.04.012>

Devasahayam, S., 2007. Application of particle size distribution analysis in evaluating the weathering in coal mine rejects and tailings. *Fuel Processing Technology* 88, 295–301. <https://doi.org/10.1016/j.fuproc.2006.10.013>

Dennington, R., T.A. Keith, J.M. Millam, GaussView, (2016).

Dong, D., Espinoza, L.A.T., Loibl, A., Pfaff, M., Tukker, A., van der Voet, E., 2020. Scenarios for anthropogenic copper demand and supply in China: implications of a scrap import ban and a circular economy transition. *Resour Conserv Recycl* 161, 104943. <https://doi.org/10.1016/j.resconrec.2020.104943>

Donoso, M., Robles, P.A., Gálvez, E.D., Cisternas, L.A., 2013. Particle Size Effect on the Efficient Use of Water and Energy in Mineral Concentration Processes. *Ind Eng Chem Res* 52, 17686–17690. <https://doi.org/10.1021/ie402099n>

Egiebor, N.O., Oni, B., 2007. Acid rock drainage formation and treatment: a review. *Asia-Pacific Journal of Chemical Engineering* 2, 47–62. <https://doi.org/10.1002/apj.57>

Ekmekçi, Z., Demirel, H., 1997. Effects of galvanic interaction on collectorless flotation behaviour of chalcopyrite and pyrite. *Int J Miner Process* 52, 31–48. [https://doi.org/10.1016/S0301-7516\(97\)00050-1](https://doi.org/10.1016/S0301-7516(97)00050-1)

Elghali, A., Benzaazoua, M., Bouzahzah, H., Bussière, B., Villarraga-Gómez, H., 2018. Determination of the available acid-generating potential of waste rock, part I: Mineralogical approach. *Applied Geochemistry* 99, 31–41. <https://doi.org/10.1016/j.apgeochem.2018.10.021>

Elghali, A., Benzaazoua, M., Bussière, B., Bouzahzah, H., 2019. Determination of the available acid-generating potential of waste rock, part II: Waste management involvement. *Applied Geochemistry* 100, 316–325. <https://doi.org/10.1016/j.apgeochem.2018.12.010>

Elshkaki, A., Graedel, T.E., Ciacci, L., Reck, B.K., 2016. Copper demand, supply, and associated energy use to 2050. *Global Environmental Change* 39, 305–315. <https://doi.org/10.1016/j.gloenvcha.2016.06.006>

El-bouazzaoui, A., Ait-khouia, Y., Demers, I., & Benzaazoua, M. (2022). Alternative flotation collectors for the environmental desulfurization of gersdorffite (NiAsS) bearing mine tailings: Surface chemistry. *Colloids and Surfaces A: Physicochemical and Engineering Aspects*, 647, 128943. <https://doi.org/10.1016/j.colsurfa.2022.128943>

El-bouazzaoui, Abdelilah, Ait-khouia, Y., Chopard, A., Demers, I., & Benzaazoua, M. (2022). Environmental desulfurization of mine tailings using froth flotation: The case of Amaruq Mine (Nunavut, Canada). *Minerals Engineering*, 187, 107762. <https://doi.org/10.1016/j.mineng.2022.107762>

Eriez, 2021. Hydrofloat separator [WWW Document]. URL <https://www.eriezflotation.com/pdfs/FGB-105-Eriez-Hydrofloat-Separator.pdf> (accessed 12.16.21).

Fairthorne, G., Fornasiero, D., Ralston, J., 1996. Solution properties of thionocarbamate collectors. *Int J Miner Process* 46, 137–153. [https://doi.org/10.1016/0301-7516\(95\)00008-9](https://doi.org/10.1016/0301-7516(95)00008-9)

Fala, O., Molson, J., Aubertin*, M., Bussière*, B., 2005. Numerical Modelling of Flow and Capillary Barrier Effects in Unsaturated Waste Rock Piles. *Mine Water Environ* 24, 172–185. <https://doi.org/10.1007/s10230-005-0093-z>

- Fan, Y. Van, Chin, H.H., Klemeš, J.J., Varbanov, P.S., Liu, X., 2020. Optimisation and process design tools for cleaner production. *J Clean Prod* 247, 119181. <https://doi.org/10.1016/j.jclepro.2019.119181>
- Feng, B., Feng, Q., Lu, Y., Gu, Y., 2013. The effect of PAX/CMC addition order on chlorite/pyrite separation. *Miner Eng* 42, 9–12. <https://doi.org/10.1016/j.mineng.2012.10.011>
- Finkelstein, N.P., 1997. The activation of sulphide minerals for flotation: a review. *Int J Miner Process* 52, 81–120. [https://doi.org/10.1016/S0301-7516\(97\)00067-7](https://doi.org/10.1016/S0301-7516(97)00067-7)
- Fukui, K., Role of Frontier Orbitals in Chemical Reactions, *Science* (1979). 218 (1982) 747–754. <https://doi.org/10.1126/science.218.4574.747>.
- Folmer, J.C.W., F. Jellinek, The valence of copper in sulphides and selenides: An X-ray photoelectron spectroscopy study, *Journal of The Less-Common Metals*. 76 (1980) 153–162. [https://doi.org/10.1016/0022-5088\(80\)90019-3](https://doi.org/10.1016/0022-5088(80)90019-3).
- Fornasiero, D., Ralston, J., 1992. Iron hydroxide complexes and their influence on the interaction between ethyl xanthate and pyrite. *J Colloid Interface Sci* 151, 225–235. [https://doi.org/10.1016/0021-9797\(92\)90253-I](https://doi.org/10.1016/0021-9797(92)90253-I)
- Fosu, S., Awatey, B., Skinner, W., Zanin, M., 2015. Flotation of coarse composite particles in mechanical cell vs. the fluidised-bed separator (The HydroFloat™). *Miner Eng* 77, 137–149. <https://doi.org/10.1016/j.mineng.2015.03.011>
- Frías, C., Frades, M., Pecharromán, E., & Díaz, G. (2008). Improving polymetallic ores beneficiation by means of the primalead process. In P. R. Taylor, Y. Choi, & C. G. Anderson (Eds.), *Hydrometallurgy 2008: Proceedings of the Sixth International Symposium*. Society for Mining, Metallurgy, and Exploration.
- Frisch, M.J., G.W. Trucks, H.B. Schlegel, G.E. Scuseria, M.A. Robb, J.R. Cheeseman, G. Scalmani, V. Barone, G.A. Petersson, H. Nakatsuji, X. Li, M. Caricato, A. Marenich, J. Bloino, B.G. Janesko, R. Gomperts, B. Mennucci, H.P. Hratchian, J. v. Ortiz, A.F. Izmaylov, J.L. Sonnenberg, D. Williams-Young, F.L. F. Ding, F. Egidi, J. Goings, B. Peng, A. Petrone, T. Henderson, D. Ranasinghe, V.G. Zakrzewski, J. Gao, N. Rega, G. Zheng, W. Liang, M. Hada, M. Ehara, K. Toyota, R. Fukuda, J. Hasegawa, M. Ishida, T. Nakajima, Y. Honda, O. Kitao, H. Nakai, T. Vreven, K. Throssell, J.A. Montgomery, Jr.J.E. Peralta, F. Ogliaro, M. Bearpark, J.J. Heyd, E.

Brothers, K.N. Kudin, V.N. Staroverov, T. Keith, R. Kobayashi, J. Normand, K. Raghavachari, A. Rendell, J.C. Burant, S.S. Iyengar, J. Tomasi, M. Cossi, M.K. J. M. Millam, C. Adamo, R. Cammi, J.W. Ochterski, R.L. Martin, K. Morokuma, O. Farkas, J.B. Foresman, D.J. Fox, Gaussian 09, (2016).

Fuerstenau, M. C., Miller, J. D., & Kuhn, M.C., n.d. Chemistry of flotation. Society for Mining Metallurgy.

Fuerstenau, M.C.; Jameson, G.J.; Yoon, R.H., 2007. Froth Flotation: A Century of Innovation., Society for Mining, Metallurgy, and Exploration. Littleton, Colo.

Fuerstenau, M.C., Misra, M., Palmer, B.R., 1990a. Xanthate adsorption on selected sulfides in the virtual absence and presence of oxygen, Part 2. *Int J Miner Process* 29, 111–119. [https://doi.org/10.1016/0301-7516\(90\)90009-N](https://doi.org/10.1016/0301-7516(90)90009-N)

Fuerstenau, M.C., Natalie, C.A., Rowe, R.M., 1990b. Xanthate adsorption on selected sulfides in the virtual absence and presence of oxygen, Part 1. *Int J Miner Process* 29, 89–98. [https://doi.org/10.1016/0301-7516\(90\)90007-L](https://doi.org/10.1016/0301-7516(90)90007-L)

Gascón, R., Soto, M.C., Oblasser, A., Al., E., 2015. Guía metodológica para la estabilidad química de faenas e instalaciones mineras.

Ginocchio, R., León-Lobos, P., 2011. Fitoestabilización de Depósitos de Relaves en Chile.

Göktepe, F., 2010. Effect of H₂O₂ and NaSH Addition to Change the Electrochemical Potential in Flotation of Chalcopyrite and Pyrite Minerals. *Mineral Processing and Extractive Metallurgy Review* 32, 24–29. <https://doi.org/10.1080/08827508.2010.509677>

Goh, S.W., A.N. Buckley, R.N. Lamb, Copper(II) sulfide?, *Minerals Engineering*. 19 (2006) 204–208. <https://doi.org/10.1016/j.mineng.2005.09.003>.

Goh, S.W., A.N. Buckley, R.N. Lamb, R.A. Rosenberg, D. Moran, The oxidation states of copper and iron in mineral sulfides, and the oxides formed on initial exposure of chalcopyrite and bornite to air, *Geochimica et Cosmochimica Acta*. 70 (2006) 2210–2228. <https://doi.org/10.1016/j.gca.2006.02.007>.

Gregory, J., Barany, S., 2011. Adsorption and flocculation by polymers and polymer mixtures. *Adv Colloid Interface Sci* 169, 1–12. <https://doi.org/10.1016/j.cis.2011.06.004>

Grieco, G., Sinojmeri, A., Bussolesi, M., Cocomazzi, G., & Cavallo, A. (2021). Environmental impact variability of copper tailing dumps in fushe arrez (Northern albania): The role of pyrite separation during flotation. *Sustainability* (Switzerland), 13(17). <https://doi.org/10.3390/su13179643>

Guo, B., Peng, Y., Espinosa-Gomez, R., 2015. Effects of free cyanide and cuprous cyanide on the flotation of gold and silver bearing pyrite. *Miner Eng* 71, 194–204. <https://doi.org/10.1016/j.mineng.2014.11.016>

Guo, B., Peng, Y., Espinosa-Gomez, R., 2014. Cyanide chemistry and its effect on mineral flotation. *Miner Eng* 66–68, 25–32. <https://doi.org/10.1016/j.mineng.2014.06.010>

Gylienė, O., Servienė, E., Vepškaitė, I., Binkienė, R., Baranauskas, M., Lukša, J., 2015. Correlation between the sorption of dissolved oxygen onto chitosan and its antimicrobial activity against *Esherichia coli*. *Carbohydr Polym* 131, 218–223. <https://doi.org/10.1016/j.carbpol.2015.05.068>

Haldar, S.K., 2018. *Mineral exploration: Principles and applications.*, Second edi. ed. Elsevier.

Hanwell, M.D., D.E. Curtis, D.C. Lonie, T. Vandermeersch, E. Zurek, G.R. Hutchison, Avogadro: an advanced semantic chemical editor, visualization, and analysis platform, *Journal of Cheminformatics*. 4 (2012) 17. <https://doi.org/10.1186/1758-2946-4-17>.

He, S., Fornasiero, D., Skinner, W., 2005. Correlation between copper-activated pyrite flotation and surface species: Effect of pulp oxidation potential. *Miner Eng* 18, 1208–1213. <https://doi.org/10.1016/j.mineng.2005.07.016>

He, S., Skinner, W., Fornasiero, D., 2006. Effect of oxidation potential and zinc sulphate on the separation of chalcopyrite from pyrite. *Int J Miner Process* 80, 169–176. <https://doi.org/10.1016/j.minpro.2006.03.009>

Hicyilmaz, C., Emre Altun, N., Ekmekci, Z., Gokagac, G., 2004. Quantifying hydrophobicity of pyrite after copper activation and DTPI addition under electrochemically controlled conditions. *Miner Eng* 17, 879–890. <https://doi.org/10.1016/j.mineng.2004.02.007>

Houot, R., Duhamet, D., 1990. Importance of oxygenation of pulps in the flotation of sulfide ores. *Int J Miner Process* 29, 77–87. [https://doi.org/10.1016/0301-7516\(90\)90006-K](https://doi.org/10.1016/0301-7516(90)90006-K)

Hong, M., Huang, X., Gan, X., Qiu, G., & Wang, J. (2021). The use of pyrite to control redox potential to enhance chalcopyrite bioleaching in the presence of *Leptospirillum ferriphilum*. *Minerals Engineering*, 172(April), 107145. <https://doi.org/10.1016/j.mineng.2021.107145>

Huzinaga T.H., *Gaussian Basis Sets for Molecular Calculations*, Elsevier Science & Techn., 2012.

Hu, W., Hadler, K., Neethling, S.J., Cilliers, J.J., 2013. Determining flotation circuit layout using genetic algorithms with pulp and froth models. *Chem Eng Sci* 102, 32–41. <https://doi.org/10.1016/j.ces.2013.07.045>

Huang, G., Grano, S., 2006. Galvanic interaction between grinding media and arsenopyrite and its effect on flotation. *Int J Miner Process* 78, 182–197. <https://doi.org/10.1016/j.minpro.2005.10.008>

Huang, P., Cao, M., Liu, Q., 2013. Selective depression of pyrite with chitosan in Pb–Fe sulfide flotation. *Miner Eng* 46–47, 45–51. <https://doi.org/10.1016/j.mineng.2013.03.027>

Huang, P., Wang, L., Liu, Q., 2014. Depressant function of high molecular weight polyacrylamide in the xanthate flotation of chalcopyrite and galena. *Int J Miner Process* 128, 6–15. <https://doi.org/10.1016/j.minpro.2014.02.004>

Hyon, D., Kim, R., Jang, S., Kim, I., 2020. The Influence of Acid Mine Drainage on Distribution Region of Heavy Minerals (Fetio 3 , ZrSiO 4): On Case of DanChon Coast in the Eastern Sea of Korea. *Soil and Sediment Contamination: An International Journal* 29, 133–150. <https://doi.org/10.1080/15320383.2019.1685457>

Hope,G.A., R. Woods, S.E. Boyd, K. Watling, A SERS spectroelectrochemical investigation of the interaction of butylethoxycarbonylthiourea with copper surfaces, *Colloids and Surfaces A: Physicochemical and Engineering Aspects*. 232 (2004) 129–137. <https://doi.org/10.1016/j.colsurfa.2003.10.011>.

Ignatkina, V.A., Selection of selective collectors for flotation of minerals with similar flotation properties, *Russian Journal of Non-Ferrous Metals*. 52 (2011) 1–7. <https://doi.org/10.3103/S1067821211010093>.

Jain, R.K., Domen, J.K., Cui, Zengdi., 2016. Environmental Impact of Mining and Mineral Processing, *Environmental Impact of Mining and Mineral Processing*. Elsevier. <https://doi.org/10.1016/C2014-0-05174-X>

Jameson, G.J., 2010. Advances in fine and coarse particle flotation. *Canadian Metallurgical Quarterly* 49, 328–330. <https://doi.org/10.1179/cmqr.2010.49.4.325>

Jameson, G.J., Nguyen, A.V., Ata, S., 2008. Flotation of Fine and Coarse Particles, in: *Froth Flotation: A Century of Innovation*. USA, pp. 339–372.

Jamieson, H.E., Walker, S.R., Parsons, M.B., 2015. Mineralogical characterization of mine waste. *Applied Geochemistry* 57, 85–105. <https://doi.org/10.1016/j.apgeochem.2014.12.014>

Janetski, N.D., Woodburn, S.I., Woods, R., 1977. An electrochemical investigation of pyrite flotation and depression. *Int J Miner Process* 4, 227–239. [https://doi.org/10.1016/0301-7516\(77\)90004-7](https://doi.org/10.1016/0301-7516(77)90004-7)

Janzen, M.P., Nicholson, R. v, Scharer, J.M., 2000. Pyrrhotite reaction kinetics: reaction rates for oxidation by oxygen, ferric iron, and for nonoxidative dissolution. *Geochim Cosmochim Acta* 64, 1511–1522. [https://doi.org/10.1016/S0016-7037\(99\)00421-4](https://doi.org/10.1016/S0016-7037(99)00421-4)

Jouini, M., Rakotonimaro, T. V., Neculita, C.M., Genty, T., Benzaazoua, M., 2019. Prediction of the environmental behavior of residues from the passive treatment of acid mine drainage. *Applied Geochemistry* 110, 104421. <https://doi.org/10.1016/j.apgeochem.2019.104421>

Jowett, A., 1980. Formation and Disruption of Particle-Bubble Aggregates in Flotation, in: Somasundaran, P. (Ed.), *Fine Particles Processing*. New York, pp. 720–754.

Karikalan, N., Karthik, R., Chen, S.-M., Karuppiyah, C., Elangovan, A., 2017. Sonochemical Synthesis of Sulfur Doped Reduced Graphene Oxide Supported CuS Nanoparticles for the Non-Enzymatic Glucose Sensor Applications. *Sci Rep* 7, 2494. <https://doi.org/10.1038/s41598-017-02479-5>

Kalanur, S.S., H. Seo, Synthesis of Cu x S Thin Films with Tunable Localized Surface Plasmon Resonances, *ChemistrySelect*. 3 (2018) 5920–5926. <https://doi.org/10.1002/slct.201800441>.

Kelm, U., Helle, S., Matthies, R., Morales, A., 2009. Distribution of trace elements in soils surrounding the El Teniente porphyry copper deposit, Chile: the influence of smelter emissions and a tailings deposit. *Environmental Geology* 57, 365–376. [https://doi.org/10.1007/s00254-008-1305-](https://doi.org/10.1007/s00254-008-1305-1)

Kelsall, G.H., Yin, Q., Vaughan, D.J., England, K.E.R., Brandon, N.P., 1999. Electrochemical oxidation of pyrite (FeS₂) in aqueous electrolytes. *Journal of Electroanalytical Chemistry* 471, 116–125. [https://doi.org/10.1016/S0022-0728\(99\)00261-2](https://doi.org/10.1016/S0022-0728(99)00261-2)

Kloprogge, J.T., B.J. Wood, *Handbook of Mineral Spectroscopy*, Elsevier, 2020. <https://doi.org/10.1016/C2015-0-01704-X>.

Kundu, M., T. Hasegawa, K. Terabe, K. Yamamoto, M. Aono, Structural studies of copper sulfide films: Effect of ambient atmosphere, *Science and Technology of Advanced Materials*. 9 (2008). <https://doi.org/10.1088/1468-6996/9/3/035011>.

Khmeleva, T.N., Beattie, D.A., Georgiev, T.V., Skinner, W.M., 2003. Surface study of the effect of sulphite ions on copper-activated pyrite pre-treated with xanthate. *Miner Eng* 16, 601–608. [https://doi.org/10.1016/S0892-6875\(03\)00133-X](https://doi.org/10.1016/S0892-6875(03)00133-X)

Khmeleva, T.N., Skinner, W., Beattie, D.A., Georgiev, T. v, 2002. The effect of sulphite on the xanthate-induced flotation of copper-activated pyrite. *Physicochemical problems of mineral processing* 36, 185–195.

Khoso, S.A., Gao, Z., Sun, W., 2021. Recovery of high-grade copper concentrate from sulfur-rich porphyry ore using tricarbonyl starch micromolecule as pyrite depressant. *Miner Eng* 168, 106916. <https://doi.org/10.1016/j.mineng.2021.106916>

Khoso, S.A., Hu, Y., Lyu, F., Liu, R., Sun, W., 2019. Selective separation of chalcopyrite from pyrite with a novel non-hazardous biodegradable depressant. *J Clean Prod* 232, 888–897. <https://doi.org/10.1016/j.jclepro.2019.06.008>

Kohmuench, J.N., Mankosa, M.J., Kennedy, D.G., Yasalonis, J.L., Taylor, G.B., Luttrell, G.H., 2007. Implementation of the HydroFloat technology at the South Fort Meade Mine. *Min Metall Explor* 24, 264–270. <https://doi.org/10.1007/BF03403375>

Kohmuench, J.N., Mankosa, M.J., Thanasekaran, H., Hobert, A., 2018. Improving coarse particle flotation using the HydroFloat™ (raising the trunk of the elephant curve). *Miner Eng* 121, 137–145. <https://doi.org/10.1016/j.mineng.2018.03.004>

Kohmuench, J.N. Thanasekaran, H., 2013. Fluidized-bed flotation: applications from industrial minerals to sulfides., in: *Flotation 2013*. Cape Town, South Africa.

- Koppalkar, S.K., 2010. Effect of operating variables in Knelson concentrators: A pilot-scale study.
- Kuopanportti, H., Suorsa, T., Dahl, O., Niinimäki, J., 2000. A model of conditioning in the flotation of a mixture of pyrite and chalcopyrite ores. *Int J Miner Process* 59, 327–338. [https://doi.org/10.1016/S0301-7516\(00\)00003-X](https://doi.org/10.1016/S0301-7516(00)00003-X)
- Kuopanportti, H., Suorsa, T., Pöllänen, E., 1997. Effects of oxygen on kinetics of conditioning in sulphide ore flotation. *Miner Eng* 10, 1193–1205. [https://doi.org/10.1016/S0892-6875\(97\)00106-4](https://doi.org/10.1016/S0892-6875(97)00106-4)
- Laajalehto, K., Leppinen, J., Kartio, I., Laiho, T., 1999. XPS and FTIR study of the influence of electrode potential on activation of pyrite by copper or lead. *Colloids Surf A Physicochem Eng Asp* 154, 193–199. [https://doi.org/10.1016/S0927-7757\(98\)00897-8](https://doi.org/10.1016/S0927-7757(98)00897-8)
- Lam, E.J., Zetola, V., Ramírez, Y., Montofré, Í.L., Pereira, F., 2020. Making Paving Stones from Copper Mine Tailings as Aggregates. *Int J Environ Res Public Health* 17, 2448. <https://doi.org/10.3390/ijerph17072448>
- Lapakko, K.A., 2003. Developments in humidity-cell tests and their application. *Environmental Aspects of Mine Wastes: Mineralogical Association of Canada Short Course Series* 147–164.
- Laskowski, J.S., Liu, Q., O'Connor, C.T., 2007. Current understanding of the mechanism of polysaccharide adsorption at the mineral/aqueous solution interface. *Int J Miner Process* 84, 59–68. <https://doi.org/10.1016/j.minpro.2007.03.006>
- Lawrence, R.W., Scheske, M., 1997. A method to calculate the neutralization potential of mining wastes. *Environmental Geology* 32, 100–106. <https://doi.org/10.1007/s002540050198>
- Lebo, S.E., Gargulak, J.D., 2004. *Encyclopedia of Polymer Science and Technology*.
- Leppinen, J.O., 1990. FTIR and flotation investigation of the adsorption of ethyl xanthate on activated and non-activated sulfide minerals. *Int J Miner Process* 30, 245–263. [https://doi.org/10.1016/0301-7516\(90\)90018-T](https://doi.org/10.1016/0301-7516(90)90018-T)
- Li, Y., Chen, J., Kang, D., Guo, J., 2012. Depression of pyrite in alkaline medium and its subsequent activation by copper. *Miner Eng* 26, 64–69. <https://doi.org/10.1016/j.mineng.2011.11.001>

- Liu, C., Bai, R., San Ly, Q., 2008. Selective removal of copper and lead ions by diethylenetriamine-functionalized adsorbent: Behaviors and mechanisms. *Water Res* 42, 1511–1522. <https://doi.org/10.1016/j.watres.2007.10.031>
- Liu, Q., Zhang, Y., Laskowski, J.S., 2000. The adsorption of polysaccharides onto mineral surfaces: an acid/base interaction. *Int J Miner Process* 60, 229–245. [https://doi.org/10.1016/S0301-7516\(00\)00018-1](https://doi.org/10.1016/S0301-7516(00)00018-1)
- Liu, G., X. Yang, H. Zhong, Molecular design of flotation collectors: A recent progress, *Advances in Colloid and Interface Science*. 246 (2017) 181–195. <https://doi.org/10.1016/j.cis.2017.05.008>.
- Liu, G., H. Zhong, T. Dai, L. Xia, Investigation of the effect of N-substituents on performance of thionocarbamates as selective collectors for copper sulfides by ab initio calculations, *Minerals Engineering*. 21 (2008) 1050–1054. <https://doi.org/10.1016/j.mineng.2008.04.017>
- López Valdivieso, A., Celedón Cervantes, T., Song, S., Robledo Cabrera, A., Laskowski, J.S., 2004. Dextrin as a non-toxic depressant for pyrite in flotation with xanthates as collector. *Miner Eng* 17, 1001–1006. <https://doi.org/10.1016/j.mineng.2004.04.003>
- Lopez Valdivieso, A., Sánchez López, A.A., Song, S., García Martínez, H.A., Licón Almada, S., 2007. Dextrin as a Regulator for the Selective Flotation of Chalcopyrite, Galena and Pyrite. *Canadian Metallurgical Quarterly* 46, 301–309. <https://doi.org/10.1179/cmqr.2007.46.3.301>
- López-Valdivieso, A., Sánchez-López, A.A., Padilla-Ortega, E., Robledo-Cabrera, A., Galvez, E., Cisternas, L., 2018. Pyrite depression by dextrin in flotation with xanthates. Adsorption and floatability studies. *Physicochemical Problems of Mineral Processing* 54, 1159–1171. <https://doi.org/10.5277/ppmp18147>
- Lotter, N.O., Bradshaw, D.J., Barnes, A.R., 2016. Classification of the Major Copper Sulphides into semiconductor types, and associated flotation characteristics. *Miner Eng* 96–97, 177–184. <https://doi.org/10.1016/j.mineng.2016.05.016>
- Lottermoser, B.G., 2007. *Mine Wastes Characterization, Treatment, Environmental Impacts*. Springer.
- Lucay, F.A., Sales-Cruz, M., Gálvez, E.D., Cisternas, L.A., 2020. Modeling of the Complex Behavior through an Improved Response Surface Methodology. *Mineral Processing and Extractive Metallurgy Review* 1–27. <https://doi.org/10.1080/08827508.2020.1728265>

Luo, Z., Guo, Y., Liu, J., Qiu, H., Zhao, M., Zou, W., Li, S., 2016. Microbial synthesis of poly- γ -glutamic acid: current progress, challenges, and future perspectives. *Biotechnol Biofuels* 9, 134. <https://doi.org/10.1186/s13068-016-0537-7>

Lv, C.C.; Ding, J.; Liu, Y.; Fu, G.; Qian, P.; Ye, S.F., 2017. Characterization of a Copper Mine Tailing and Comprehensive Recovery of Cu and S from the Tailing. *Journal of Residuals Science & Technology* 14, 125–135.

Lynch, A.J., Johnson, N.W., Manlapig, E.V., Thorne, C.G., 1981. *Mineral and Coal Flotation Circuits: Their Simulation and Control*. Elsevier, Amsterdam.

Leppinen, J.O., C.I. Basilio, R.H. Yoon, FTIR study of thionocarbamate adsorption on sulfide minerals, *Colloids and Surfaces*. 32 (1988) 113–125. [https://doi.org/10.1016/0166-6622\(88\)80008-8](https://doi.org/10.1016/0166-6622(88)80008-8).

Little, L.H., G.W. Poling, J. Leja, INFRARED SPECTRA OF XANTHATE COMPOUNDS: II. ASSIGNMENT OF VIBRATIONAL FREQUENCIES, *Canadian Journal of Chemistry*. 39 (1961) 745–754. <https://doi.org/10.1139/v61-090>.

Mayo, D.W., F.A. Miller, R.W. Hannah, *Course Notes on the Interpretation of Infrared and Raman Spectra*, John Wiley & Sons, Inc., Hoboken, NJ, USA, 2004. <https://doi.org/10.1002/0471690082>.

Marin, O. J. Ordoñez, E. Galvez, L. Cisternas, Pourbaix diagrams for copper ores processing with seawater, *Physicochemical Problems of Mineral Processing*. 56 (2020) 624–640. <https://doi.org/10.37190/ppmp/123407>.

Miar, M., A. Shiroudi, K. Pourshamsian, A.R. Oliaey, F. Hatamjafari, Theoretical investigations on the HOMO–LUMO gap and global reactivity descriptor studies, natural bond orbital, and nucleus-independent chemical shifts analyses of 3-phenylbenzo[*d*]thiazole-2(3*H*)-imine and its para -substituted derivatives: Solvent and, *Journal of Chemical Research*. 45 (2021) 147–158. <https://doi.org/10.1177/1747519820932091>.

Ma, X., Xia, L., Wang, S., Zhong, H., Jia, H., 2017. Structural Modification of Xanthate Collectors To Enhance the Flotation Selectivity of Chalcopyrite. *Ind Eng Chem Res* 56, 6307–6316. <https://doi.org/10.1021/acs.iecr.6b04566>

Mankosa, M.J., Kohmuench, J.N., Eisenmann, M.D., Luttrell, G.H., 2021. Testing of the HydroFloat Separator for Coal Cleaning Applications.

Mankosa, M.J., Luttrell, G.H., Adel, G.T., Yoon, R.H., 1992. A study of axial mixing in column flotation. *Int J Miner Process* 35, 51–64. [https://doi.org/10.1016/0301-7516\(92\)90004-G](https://doi.org/10.1016/0301-7516(92)90004-G)

Marín, O., Valderrama, J. O., Kraslawski, A., & Cisternas, L. A. (2021). Potential of Tailing Deposits in Chile for the Sequestration of Carbon Dioxide Produced by Power Plants Using Ex-Situ Mineral Carbonation. *Minerals*, 11(3), 320. <https://doi.org/10.3390/min11030320>

Marinina, O., Kirsanova, N., & Nevskaya, M. (2022). Circular Economy Models in Industry: Developing a Conceptual Framework. *Energies*, 15(24), 9376. <https://doi.org/10.3390/en15249376>

Martin, C.J., McIvor, R.E., Finch, J.A., Rao, S.R., 1991. Review of the effect of grinding media on flotation of sulphide minerals. *Miner Eng* 4, 121–132. [https://doi.org/10.1016/0892-6875\(91\)90028-T](https://doi.org/10.1016/0892-6875(91)90028-T)

Matinde, E., 2018. Mining and metallurgical wastes: a review of recycling and re-use practices. *J South Afr Inst Min Metall* 118. <https://doi.org/10.17159/2411-9717/2018/v118n8a5>

McKeown, R., Barbour, L., Rowlett, D., Herasymuik, G., 2000. Characterization of the grain-size distribution for waste rock from metal mines: A review of the existing data and an evaluation of the implications for hydrogeologic behavior., in: *The CSCE Annual Conference*. Londn.

Mehrabani, J.V., Mousavi, S.M., Noaparast, M., 2011. Evaluation of the replacement of NaCN with *Acidithiobacillus ferrooxidans* in the flotation of high-pyrite, low-grade lead–zinc ore. *Sep Purif Technol* 80, 202–208. <https://doi.org/10.1016/j.seppur.2011.04.006>

Mehrotra, S.P., Kapur, P.C., 1974. Optimal-Suboptimal Synthesis and Design of Flotation Circuits. *Separation Science* 9, 167–184. <https://doi.org/10.1080/00372367408057055>

MEND, 1998. Design Guide for the Subaqueous Disposal of Reactive Tailings in Constructed Impoundments.

Mendez, D. A., Gálvez, E. D., & Cisternas, L. A. (2009). State of the art in the conceptual design of flotation circuits. *International Journal of Mineral Processing*, 90(1–4), 1–15. <https://doi.org/10.1016/j.minpro.2008.09.009>

Mielczarski, J., Suoninen, E., Johansson, L.-S., Laajalehto, K., 1989. An XPS study of adsorption of methyl and amyl xanthates on copper. *Int J Miner Process* 26, 181–191. [https://doi.org/10.1016/0301-7516\(89\)90028-8](https://doi.org/10.1016/0301-7516(89)90028-8)

Miller, J.D., du Plessis, R., Kotylar, D.G., Zhu, X., Simmons, G.L., 2002. The low-potential hydrophobic state of pyrite in amyl xanthate flotation with nitrogen. *Int J Miner Process* 67, 1–15. [https://doi.org/10.1016/S0301-7516\(02\)00011-X](https://doi.org/10.1016/S0301-7516(02)00011-X)

Miller, S., Jeffery, J., Wong, J., 1991. Use and misuse of the acid base account for “amd” prediction., in: *Proceedings of the 2nd International Conference on the Abatement of Acidic Drainage*. montreal.

MINING-DOT-COM, 2021. Copper price scales \$9,000 after Goldman calls it the new oil [WWW Document]. URL <https://www.mining.com/copper-price-scales-9000-after-goldman-calls-it-the-new-oil/> (accessed 4.13.21).

Morales-García, A., Soares, A.L., dos Santos, E.C., de Abreu, H.A., Duarte, H.A., 2014. First-Principles Calculations and Electron Density Topological Analysis of Covellite (CuS). *J Phys Chem A* 118, 5823–5831. <https://doi.org/10.1021/jp4114706>

Moslemi, H., Gharabaghi, M., 2017. A review on electrochemical behavior of pyrite in the froth flotation process. *Journal of Industrial and Engineering Chemistry* 47, 1–18. <https://doi.org/10.1016/j.jiec.2016.12.012>

Mu, Y., Peng, Y., Lauten, R.A., 2016. The depression of pyrite in selective flotation by different reagent systems – A Literature review. *Miner Eng* 96–97, 143–156. <https://doi.org/10.1016/j.mineng.2016.06.018>

Mu, Y., Peng, Y., Lauten, R.A., 2015. Electrochemistry aspects of pyrite in the presence of potassium amyl xanthate and a lignosulfonate-based biopolymer depressant. *Electrochim Acta* 174, 133–142. <https://doi.org/10.1016/j.electacta.2015.05.150>

Murray, J., Kirschbaum, A., Dold, B., Guimaraes, E., Miner, E., 2014. Jarosite versus Soluble Iron-Sulfate Formation and Their Role in Acid Mine Drainage Formation at the Pan de Azúcar Mine Tailings (Zn-Pb-Ag), NW Argentina. *Minerals* 4, 477–502. <https://doi.org/10.3390/min4020477>

Musuku, B., Muzinda, I., & Lumsden, B. (2016). Cu–Ni processing improvements at First Quantum’s Kevitsa mine. *Minerals Engineering*, 88, 9–17. <https://doi.org/10.1016/j.mineng.2015.08.005>

Nadeif, A., Taha, Y., Bouzahzah, H., Hakkou, R., Benzaazoua, M., 2019. Desulfurization of the Old Tailings at the Au-Ag-Cu Tiouit Mine (Anti-Atlas Morocco). *Minerals* 9, 401. <https://doi.org/10.3390/min9070401>

Naidu, G., Ryu, S., Thiruvengkatachari, R., Choi, Y., Jeong, S., Vigneswaran, S., 2019. A critical review on remediation, reuse, and resource recovery from acid mine drainage. *Environmental Pollution* 247, 1110–1124. <https://doi.org/10.1016/j.envpol.2019.01.085>

Nakai, I., Y. Sugitani, K. Nagashima, Y. Niwa, X-ray photoelectron spectroscopic study of copper minerals, *Journal of Inorganic and Nuclear Chemistry*. 40 (1978) 789–791. [https://doi.org/10.1016/0022-1902\(78\)80152-3](https://doi.org/10.1016/0022-1902(78)80152-3).

NIST X-ray Photoelectron Spectroscopy Database, NIST Standard Reference Database Number 20, (2000). <https://doi.org/10.18434/T4T88K>.

Ndlovu, S., Simate, G.S., Matinde, E., 2017. Waste production and utilization in the metal extraction industry. CRC Press, Boca raton, London.

Nguyen, N. N., Nguyen, C. V., & Nguyen, A. V. (2023). The significant interfacial properties in the flotation separation of (critical) minerals from the Earth's crust. In *Reference Module in Chemistry, Molecular Sciences and Chemical Engineering*. <https://doi.org/10.1016/B978-0-323-85669-0.00080-5>

Norgate, T., Haque, N., 2012. Using life cycle assessment to evaluate some environmental impacts of gold production. *J Clean Prod* 29–30, 53–63. <https://doi.org/10.1016/j.jclepro.2012.01.042>

Norgate, T., Haque, N., 2010. Energy and greenhouse gas impacts of mining and mineral processing operations. *J Clean Prod* 18, 266–274. <https://doi.org/10.1016/j.jclepro.2009.09.020>

Northey, S., Mohr, S., Mudd, G.M., Weng, Z., Giurco, D., 2014. Modelling future copper ore grade decline based on a detailed assessment of copper resources and mining. *Resour Conserv Recycl* 83, 190–201. <https://doi.org/10.1016/j.resconrec.2013.10.005>

Nuorivaara, T., Björkqvist, A., Bacher, J., Serna-Guerrero, R., 2019. Environmental remediation of sulfidic tailings with froth flotation: Reducing the consumption of additional resources by optimization of conditioning parameters and water recycling. *J Environ Manage* 236, 125–133. <https://doi.org/10.1016/j.jenvman.2019.01.107>

Ogawa, Y., Yamaguchi, F., Yuasa, K., Tahara, Y., 1997. Efficient Production of γ -Polyglutamic Acid by *Bacillus subtilis* (natto) in Jar Fermenters. *Biosci Biotechnol Biochem* 61, 1684–1687. <https://doi.org/10.1271/bbb.61.1684>

Osses, R., Pineda, J.A., Ovalle, C., Linero, S., Fityus, S., 2019. Particle size effects on the water retention properties of colluvial sediments. 7th Asia-Pacific Conference on Unsaturated Soils, AP-UNSAT 2019 335–339. <https://doi.org/10.3208/jgssp.v07.054>

Ouyang, X., Qiu, X., Chen, P., 2006. Physicochemical characterization of calcium lignosulfonate—A potentially useful water reducer. *Colloids Surf A Physicochem Eng Asp* 282–283, 489–497. <https://doi.org/10.1016/j.colsurfa.2005.12.020>

Ouyang, X.P., Zhang, P., Tan, C.M., Deng, Y.H., Yang, D.J., Qiu, X.Q., 2010. Isolation of lignosulfonate with low polydispersity index. *Chinese Chemical Letters* 21, 1479–1481. <https://doi.org/10.1016/j.ccl.2010.06.032>

Paktunc, A., Davé, N., 2000. Mineralogy of pyritic waste rock leached by column experiments and prediction of acid mine drainage., in: *In Applied Mineralogy in Research, Economy, Technology, Ecology and Culture, Proceedings of the 6th International Congress on Applied Mineralogy, ICAM*. pp. 621–623.

Paktunc, A.D., 1999. Mineralogical constraints on the determination of neutralization potential and prediction of acid mine drainage. *Environmental Geology* 39, 103–112. <https://doi.org/10.1007/s002540050440>

Pecina-Treviño, E.T., Uribe-Salas, A., Nava-Alonso, F., Pérez-Garibay, R., 2003. On the sodium-diisobutyl dithiophosphinate (Aerophine 3418A) interaction with activated and unactivated galena and pyrite. *Int J Miner Process* 71, 201–217. [https://doi.org/10.1016/S0301-7516\(03\)00059-0](https://doi.org/10.1016/S0301-7516(03)00059-0)

Peng, Y., Grano, S., Fornasiero, D., Ralston, J., 2003a. Control of grinding conditions in the flotation of galena and its separation from pyrite. *Int J Miner Process* 70, 67–82. [https://doi.org/10.1016/S0301-7516\(02\)00153-9](https://doi.org/10.1016/S0301-7516(02)00153-9)

Peng, Y., Grano, S., Fornasiero, D., Ralston, J., 2003b. Control of grinding conditions in the flotation of chalcopyrite and its separation from pyrite. *Int J Miner Process* 69, 87–100. [https://doi.org/10.1016/S0301-7516\(02\)00119-9](https://doi.org/10.1016/S0301-7516(02)00119-9)

Peng, H., D. Wu, M. Abdalla, W. Luo, W. Jiao, X. Bie, Study of the Effect of Sodium Sulfide as a Selective Depressor in the Separation of Chalcopyrite and Molybdenite, *Minerals*. 7 (2017) 51. <https://doi.org/10.3390/min7040051>.

Peregoedova, A., 2012. Étude expérimentale des propriétés hydrogéologiques des roches stériles à une échelle intermédiaire de laboratoire.

Perdew, J.P., Y. Wang, Accurate and simple analytic representation of the electron-gas correlation energy, *Physical Review B*. 45 (1992) 13244–13249. <https://doi.org/10.1103/PhysRevB.45.13244>.

Piegols, G., DePlato, D., Kohmuench, J.N., Yan, E.S., 2015. Application of Classification and Fluidized-Bed Flotation at PCS Aurora., in: *Beneficiation of Phosphates, Proceedings VII, Engineering Foundation Conference on Beneficiation of Phosphates VI*. Melbourne, Australia., p. 14.

Porento, M., P. Hirva, Theoretical studies on the interaction of anionic collectors with Cu^+ , Cu^{2+} , Zn^{2+} and Pb^{2+} ions, *Theoretical Chemistry Accounts: Theory, Computation, and Modeling (Theoretica Chimica Acta)*. 107 (2002) 200–205. <https://doi.org/10.1007/s00214-001-0316-8>.

Porento, M., Hirva, P., 2004. A theoretical study on the interaction of sulfhydryl surfactants with a covellite (001) surface. *Surf Sci* 555, 75–82. <https://doi.org/10.1016/j.susc.2004.02.033>

Prestidge, C.A., Ralston, J., Smart, R.St.C., 1993. The competitive adsorption of cyanide and ethyl xanthate on pyrite and pyrrhotite surfaces. *Int J Miner Process* 38, 205–233. [https://doi.org/10.1016/0301-7516\(93\)90076-M](https://doi.org/10.1016/0301-7516(93)90076-M)

Qian, G., Fan, R., Short, M.D., Schumann, R.C., Pring, A., Gerson, A.R., 2019. The Combined Effects of Galvanic Interaction and Silicate Addition on the Oxidative Dissolution of Pyrite: Implications for Acid and Metalliferous Drainage Control. *Environ Sci Technol* 53, 11922–11931. <https://doi.org/10.1021/acs.est.9b03965>

Raju, G.B., Forsling, W., 1991. Adsorption mechanism of diethyldithiocarbamate on covellite, cuprite and tenorite. *Colloids and Surfaces* 60, 53–69. [https://doi.org/10.1016/0166-6622\(91\)80268-S](https://doi.org/10.1016/0166-6622(91)80268-S)

Rankin, W.J., 2014. Sustainability, in: Seetharaman, S. (Ed.), *Treatise on Process Metallurgy*. Elsevier, pp. 1376–1424. <https://doi.org/10.1016/B978-0-08-096988-6.00033-X>

Rashchi, F., Finch, J.A., Sui, C., 2004. Action of DETA, dextrin and carbonate on lead-contaminated sphalerite. *Colloids Surf A Physicochem Eng Asp* 245, 21–27. <https://doi.org/10.1016/j.colsurfa.2004.05.018>

Rath, R.K., Subramanian, S., 1999. Adsorption, electrokinetic and differential flotation studies on sphalerite and galena using dextrin. *Int J Miner Process* 57, 265–283. [https://doi.org/10.1016/S0301-7516\(99\)00028-9](https://doi.org/10.1016/S0301-7516(99)00028-9)

Rassolov, V.A., J.A. Pople, M.A. Ratner, T.L. Windus, 6-31G * basis set for atoms K through Zn, *The Journal of Chemical Physics*. 109 (1998) 1223–1229. <https://doi.org/10.1063/1.476673>.

Reuter, M.A., van Deventer, J.S.J., Green, J.C.A., Sinclair, M., 1988. Optimal design of mineral separation circuits by use of linear programming. *Chem Eng Sci* 43, 1039–1049. [https://doi.org/10.1016/0009-2509\(88\)85066-8](https://doi.org/10.1016/0009-2509(88)85066-8)

Reuter, M.A., van Schaik, A., Gutzmer, J., Bartie, N., Abadías-Llomas, A., 2019. Challenges of the Circular Economy: A Material, Metallurgical, and Product Design Perspective. *Annu Rev Mater Res* 49, 253–274. <https://doi.org/10.1146/annurev-matsci-070218-010057>

Rezvanipour, H., Mostafavi, A., Ahmadi, A., Karimimobarakabadi, M., Khezri, M., 2018. Desulfurization of Iron Ores: Processes and Challenges. *Steel Res Int* 89, 1700568. <https://doi.org/10.1002/srin.201700568>

Rikers, R.A., Rem, P., Dalmijn, W.L., 1998. Improved method for prediction of heavy metal recoveries from soil using high intensity magnetic separation (HIMS). *Int J Miner Process* 54, 165–182. [https://doi.org/10.1016/S0301-7516\(98\)00017-9](https://doi.org/10.1016/S0301-7516(98)00017-9)

Robben, Wotruba, 2019. Sensor-Based Ore Sorting Technology in Mining—Past, Present and Future. *Minerals* 9, 523. <https://doi.org/10.3390/min9090523>

Roos, J.R., Celis, J.P., Sudarsono, A.S., 1990. Electrochemical control of chalcocite and covellite-xanthate flotation. *Int J Miner Process* 29, 17–30. [https://doi.org/10.1016/0301-7516\(90\)90003-H](https://doi.org/10.1016/0301-7516(90)90003-H)

Rosso, K.M., Hochella, M.F., 1999. A UHV STM/STS and ab initio investigation of covellite {001} surfaces. *Surf Sci* 423, 364–374. [https://doi.org/10.1016/S0039-6028\(98\)00941-8](https://doi.org/10.1016/S0039-6028(98)00941-8)

Rappe, A.K. C.J. Casewit, K.S. Colwell, W.A. Goddard, W.M. Skiff, UFF, a full periodic table force field for molecular mechanics and molecular dynamics simulations, *J Am Chem Soc.* 114 (1992) 10024–10035. <https://doi.org/10.1021/ja00051a040>.

Sizova, O., A.Yu. Sokolov, L. v. Skripnikov, V.I. Baranovski, Quantum chemical study of the bond orders in the ruthenium, diruthenium and dirhodium nitrosyl complexes, *Polyhedron.* 26 (2007) 4680–4690. <https://doi.org/10.1016/j.poly.2007.04.008>.

Schrader, B., *Infrared and Raman Spectroscopy. methods and applications.*, VCH Verlagsgesellschaft mbH, Weinheim, Germany, 1995.

Shankaranarayana, M.L., C.C. Patel, INFRARED SPECTRA AND THE STRUCTURES OF XANTHATES AND DIXANTHOGENS, *Canadian Journal of Chemistry.* 39 (1961) 1633–1637. <https://doi.org/10.1139/v61-209>.

Szczepanik, D.W., J. Mrozek, Ground-state projected covalency index of the chemical bond, *Computational and Theoretical Chemistry.* 1023 (2013) 83–87. <https://doi.org/10.1016/j.comptc.2013.09.008>.

Santander, M., Valderrama, L., 2019. Recovery of pyrite from copper tailings by flotation. *Journal of Materials Research and Technology* 8, 4312–4317. <https://doi.org/10.1016/j.jmrt.2019.07.041>

Sepúlveda, F. D., Lucay, F., González, J. F., Cisternas, L. A., & Gálvez, E. D. (2017). A methodology for the conceptual design of flotation circuits by combining group contribution, local/global sensitivity analysis, and reverse simulation. *International Journal of Mineral Processing*, 164. <https://doi.org/10.1016/j.minpro.2017.05.008>

Schena, G., Zanin, M., Chiarandini, A., 1997. Procedures for the automatic design of flotation networks. *Int J Miner Process* 52, 137–160. [https://doi.org/10.1016/S0301-7516\(97\)00065-3](https://doi.org/10.1016/S0301-7516(97)00065-3)

Shen, W.Z., Fornasiero, D., Ralston, J., 1998. Effect of collectors, conditioning pH and gases in the separation of sphalerite from pyrite. *Miner Eng* 11, 145–158. [https://doi.org/10.1016/S0892-6875\(97\)00147-7](https://doi.org/10.1016/S0892-6875(97)00147-7)

Skandrani, A., Demers, I., Kongolo, M., 2019. Desulfurization of aged gold-bearing mine tailings. *Miner Eng* 138, 195–203. <https://doi.org/10.1016/j.mineng.2019.04.037>

Smith, K., Huyck, H., 1999. The Environmental Geochemistry of Mineral Deposits, Part A. Processes, Techniques, and Health Issues, in: Plumlee, GS; Logsdon, M. (Ed.), . Pacific Section Society of Economic, Littleton, CO.

Smuda, J., Dold, B., Spangenberg, J.E., Friese, K., Kobek, M.R., Bustos, C.A., Pfeifer, H.-R., 2014. Element cycling during the transition from alkaline to acidic environment in an active porphyry copper tailings impoundment, Chuquicamata, Chile. *J Geochem Explor* 140, 23–40. <https://doi.org/10.1016/j.gexplo.2014.01.013>

Soares, A.L., dos Santos, E.C., Morales-García, Á., Duarte, H.A., de Abreu, H.A., 2016. The Stability and Structural, Electronic and Topological Properties of Covellite (001) Surfaces. *ChemistrySelect* 1, 2730–2741. <https://doi.org/10.1002/slct.201600422>

Song, W., Zhou, J., Wang, B., Li, S., & Cheng, R. (2019). Production of SO₂ Gas: New and Efficient Utilization of Flue Gas Desulfurization Gypsum and Pyrite Resources. In *Industrial and Engineering Chemistry Research*. <https://doi.org/10.1021/acs.iecr.9b04403>

Sui, C., Finch, J.A., Xu, Z., 1998. Effect of diethylenetriamine on xanthane interaction with Pb-contaminated pyrite. *Miner Eng* 11, 639–649. [https://doi.org/10.1016/S0892-6875\(98\)00048-X](https://doi.org/10.1016/S0892-6875(98)00048-X)

Sun, W., Wang, D., 2009. *Electrochemistry of Flotation of Sulphide Minerals*.

Tian, X., X. Li, P. Bi, Effect of O-isobutyl-N-ethylthionocarbamates of flotation behavior of porphyry copper ore and its adsorption mechanism, *Appl. Surf. Sci.* 503 (2020),144313, <https://10.1016/j.apsusc.2019.144313>.

Tomasi, J., B. Mennucci, R. Cammi, Quantum Mechanical Continuum Solvation Models, *Chemical Reviews*. 105 (2005) 2999–3094. <https://doi.org/10.1021/cr9904009>.

Thermo scientific XPS simplified, (n.d.). <https://xpssimplified.com/>.

Voigt, S., Szargan, R., Suoninen, E., 1994. Interaction of copper(II) ions with pyrite and its influence on ethyl xanthate adsorption. *Surface and Interface Analysis* 21, 526–536. <https://doi.org/10.1002/sia.740210804>

Voisin, L., 2012. New Strategies for the Treatment of Copper Concentrates with High Arsenic Content in Chile [WWW Document]. URL http://mric.jogmec.go.jp/public/kouenkai/2012-11/briefing_121108_5new.pdf

Wang, X.-H., Eric Forssberg, K.S., 1991. Mechanisms of pyrite flotation with xanthates. *Int J Miner Process* 33, 275–290. [https://doi.org/10.1016/0301-7516\(91\)90058-Q](https://doi.org/10.1016/0301-7516(91)90058-Q)

Wang, X.-H., Forssberg, K.S.E., 1996. The solution electrochemistry of sulfide-xanthate-cyanide systems in sulfide mineral flotation. *Miner Eng* 9, 527–546. [https://doi.org/10.1016/0892-6875\(96\)00041-6](https://doi.org/10.1016/0892-6875(96)00041-6)

Weisener, C., Gerson, A., 2000. An investigation of the Cu (II) adsorption mechanism on pyrite by ARXPS and SIMS. *Miner Eng* 13, 1329–1340. [https://doi.org/10.1016/S0892-6875\(00\)00116-3](https://doi.org/10.1016/S0892-6875(00)00116-3)

Wels, C., Robertson, A., MacG, 2003. Conceptual model for estimating water recovery in tailings impoundments., in: 10th International Conference on Tailings and Mine Waste. Taylor & Francis, Vail Colorado USA, p. 87–94.

Wills, B.A., Finch, J.A., 2016. Froth Flotation, in: *Wills' Mineral Processing Technology*. Elsevier, pp. 265–380. <https://doi.org/10.1016/B978-0-08-097053-0.00012-1>

Wilson, D., Amos, R.T., Blowes, D.W., Langman, J.B., Ptacek, C.J., Smith, L., Segó, D.C., 2018. Diavik waste rock project: A conceptual model for temperature and sulfide-content dependent geochemical evolution of waste rock – Laboratory scale. *Applied Geochemistry* 89, 160–172. <https://doi.org/10.1016/j.apgeochem.2017.12.007>

Woodburn, E.T., King, R.P., Colborn, R.P., 1971. The effect of particle size distribution on the performance of a phosphate flotation process. *Metallurgical and Materials Transactions B* 2, 3163–3174. <https://doi.org/10.1007/BF02814969>

Wiberg, K.B., Application of the pople-santry-segal CNDO method to the cyclopropylcarbiny and cyclobutyl cation and to bicyclobutane, *Tetrahedron*. 24 (1968) 1083–1096. [https://doi.org/10.1016/0040-4020\(68\)88057-3](https://doi.org/10.1016/0040-4020(68)88057-3).

X-ray Photoelectron Spectroscopy (XPS) Reference Pages, (n.d.). <http://www.xpsfitting.com/>.

Yin, W., Yang, B., Fu, Y., Chu, F., Yao, J., Cao, S., Zhu, Z., 2019. Effect of calcium hypochlorite on flotation separation of covellite and pyrite. *Powder Technol* 343, 578–585. <https://doi.org/10.1016/j.powtec.2018.11.048>

Yıldırım Gülsoy, Ö., Gülcan, E., 2019. A new method for gravity separation: Vibrating table gravity concentrator. *Sep Purif Technol* 211, 124–134. <https://doi.org/10.1016/j.seppur.2018.09.074>

Yuan, T., J. Wang, Z. Li, Measurement and modelling of solubility for calcium sulfate dihydrate and calcium hydroxide in NaOH/KOH solutions, *Fluid Phase Equilibria*. 297 (2010) 129–137. <https://doi.org/10.1016/j.fluid.2010.06.012>.

Zhan, C.G., J.A. Nichols, D.A. Dixon, Ionization Potential, Electron Affinity, Electronegativity, Hardness, and Electron Excitation Energy: Molecular Properties from Density Functional Theory Orbital Energies, *The Journal of Physical Chemistry A*. 107 (2003) 4184–4195. <https://doi.org/10.1021/jp0225774>.

Zhao, G., H. Zhong, X. Qiu, S. Wang, Y. Gao, Z. Dai, J. Huang, G. Liu, The DFT study of cyclohexyl hydroxamic acid as a collector in scheelite flotation, *Minerals Engineering*. 49 (2013) 54–60. <https://doi.org/10.1016/j.mineng.2013.04.025>.

Zhang, C., Wu, D., Qiu, X., 2018. Stimulatory effects of amino acids on γ -polyglutamic acid production by *Bacillus subtilis*. *Sci Rep* 8, 17934. <https://doi.org/10.1038/s41598-018-36439-4>

Zhang, X., Wang, X., Li, Y., Han, Y., Gu, X., Wang, S., 2021. Adsorption mechanism of a new depressant on pyrite surfaces and its application to the selective separation of chalcopyrite from pyrite. *Colloids Surf A Physicochem Eng Asp* 625, 126892. <https://doi.org/10.1016/j.colsurfa.2021.126892>

Zhao, G., Peng, J., Zhong, H., Wang, S., Liu, G.Y., 2016. Synthesis of novel ether thionocarbamates and study on their flotation performance for chalcopyrite. *Minerals* 6. <https://doi.org/10.3390/min6030097>

Zhu, X., Tao, Y., Sun, Q., Man, Z., 2017. The low efficiency of lignite separation by an enhanced gravity concentrator. *Energy Sources, Part A: Recovery, Utilization, and Environmental Effects* 39, 835–842. <https://doi.org/10.1080/15567036.2016.1270373>

APPENDIX A ARTICLE 1: NEW INSIGHTS RELATED TO THE FLOTATION OF COVELLITE IN PORPHYRY ORES

Article 1: Yesica L. Botero, Rodrigo Serna-Guerrero, Alejandro López-Valdivieso, Mostafa Benzaazoua and Luis A. Cisternas. New insights related to the flotation of covellite in porphyry ores. *Minerals Engineering*, 2021. (Doi:10.1016/j.mineng.2021.107242).

This article was submitted to *Minerals Engineering* journal on July 23, 2021.

Abstract

Covellite usually occurs accompanying other copper minerals, like chalcopyrite and chalcocite, but there are few studies on covellite flotation. The effect of collectors O-isopropyl-N-ethyl thionocarbamate (IPETC) and potassium amyl xanthate (PAX) and pH on covellite and pyrite flotation was investigated through a Hallimond tube test using pure covellite and pyrite and a Denver cell test using porphyry ore. Pure covellite and pyrite were characterized by X-ray diffraction (XRD), Fourier transform infrared spectroscopy (FT-IR). Moreover, the covellite was characterized using scanning electron microscopy coupled to energy dispersive spectroscopy (SEM-EDS). Porphyry ore was characterized by automated mineralogy using scanning electron microscopy (QEMSCAN®). Design of experiments was utilized to identify the factors with a statistical influence (ANOVA) and obtain the optimal flotation conditions using response surface methodology (RSM) and desirability function. ANOVA test demonstrated that the factors that influence covellite behavior are the collector type and dosage. The results obtained on pure minerals shows that with a high PAX concentration and low pH, it is possible to carry out bulk flotation with recoveries of 93% covellite and 90 % pyrite, and with a low IPETC dosage and high pH, it is possible to get a selective flotation with around 81% covellite and 20% pyrite recoveries. These results were determined using RSM and desirability function, and corroborated with the Hallimond tube test. Then, the flotation results of mixture covellite-pyrite show that selective flotation is

feasible with IPETC at alkaline pH with a low dosage displaying recoveries of 97 % covellite and 53 % pyrite. Also, bulk flotation is feasible with PAX at a pH of 8 and a high collector concentration with recoveries of 96% covellite and 88% pyrite. The results show that covellite recovery is not pH-dependent. The Denver cell test with a porphyry ore shows a selective flotation with IPETC at a pH of 11 with a low collector dosage (5 g/ton), achieving recoveries of 92% covellite and 39% pyrite. Also, recoveries of 85% covellite and 75% pyrite were observed for a bulk flotation with IPETC at pH = 8 at the same collector dosage. Therefore, the IPETC can be used as a selective or bulk collector when varying the pH and collector concentration. These results demonstrate that covellite flotation performances remain constant over a wide range of pH values, which allows a selective separation from other sulfides such as pyrite.

Key words: Covellite, Pyrite, Thionocarbamate, Amyl xanthate, Bulk flotation, Selective flotation, Design of experiment.

A.1 Introduction

The ore copper grade has been decreasing due to exploitation. The global average copper ore grade is about 0.49% and is forecast to decrease consistently in the foreseeable future (Northey et al., 2014). This situation demands new strategies to improve the efficiency of concentration plants, including the recovery of copper in all its mineral forms. Sulfide copper deposits are mostly composed of chalcopyrite, bornite, molybdenite, chalcocite, and covellite. The vast majority of studies focus on froth flotation of chalcopyrite, as it currently represents the main source of copper. The decrease in ore grade is inevitably associated with increased solid waste production to maintain the same level of copper production. There is an additional concern regarding the presence of sulfur minerals, including covellite, in waste rock (WR) and tailings responsible for adverse environmental effects such as acid mine drainage (AMD). Consequently, the last years have seen a growing interest in the processing of WR and tailings, including the recovery of valuable components such as copper sulfide minerals (Araya et al., 2020). For instance, WR collected in the waste dump from Langlois mine at Lebel-sur-Quévillon (Quebec, Canada) has been studied for polymetallic recovery and to prevent AMD (Amar et al., 2021). In other studies, pyrite and other valuable components were recovered by flotation from copper tailings to prevent the generation of

AMD (Nuorivaara et al., 2019; Santander and Valderrama, 2019). Usually, covellite is considered of limited relevance for the industry because of its low grade in ore, tailings, and WR (Camus, 1975; Kelm et al., 2009; Lam et al., 2020; Smuda et al., 2014). However, Voisin (2012) analyzed several samples from different copper Chilean mines, and he found that covellite concentration was between 17 and 0.6 % wt. Nevertheless, given the decrease of copper ore grade and the need to valorize solid waste and prevent AMD, studies that help to recover covellite from these three sources have become necessary. In fact, the copper contribution from covellite to an ore grade might determine whether the ore is processed. Also, the proper recovery of covellite from WR and tailings could help to decrease the cost of waste management and limit the production of AMD (Amar et al., 2021).

Some studies examining covellite behavior in flotation processes have been published. Porento and Hirva (2004) performed theoretical research using *Ab Initio* calculations on the interaction of sulfhydryl surfactants (1,1,1-butanetriethiol, diethyldithiocarbamate and ethyl xanthate) with covellite surfaces. They compiled data about all the possible covellite-collector interactions. They justified that it is more straightforward to study covellite using computational methods than to carry out flotation tests because the flotation process comprises a highly complex behavior. The results showed that 1,1,1-butanetriethiol interacts more strongly than diethyldithiocarbamate or ethyl xanthate, making it a promising collector for covellite flotation. However, this methodology only provided a limited analysis of the specific interaction between the covellite surface and the chosen collectors. In a real flotation process, multiple parameters modify the covellite behavior, including the effect of pH, interactions with other minerals, and the Redox potential (E_{ph}). In this sense, it is better to complement this kind of result with a real flotation test.

Another study was accomplished by Raju and Forsling (1991), who studied the adsorption of diethyldithiocarbamate (DTC) on covellite, cuprite, and tenorite surfaces. In this case, the research was focused only on the adsorption mechanism of each collector with each type of mineral using the UV-visible spectrophotometric technique. They evaluated the effect of different collector concentrations and pH on the adsorption on the mineral surface. They identified various copper-DTC complexes that formed on each mineral surface, but flotation tests were not carried out.

Roos et al. (1990) studied the electrochemical behavior of chalcocite and covellite for flotation purposes. They performed this study in a micro-flotation-electrochemical cell, investigating the effect of electrochemical potential on covellite floatability. They identified the potential range where the hydrophobization of covellite and chalcocite is possible. Reportedly, hydrophobization of covellite is possible between +50 and +200mV.

Two more studies were conducted to examine the effect of xanthogen formates and chelating agents in copper sulfide flotation (Ackerman et al., 2000, 1999). The flotation of pure minerals, including chalcopyrite, chalcocite, covellite, bornite, and pyrite, were studied by varying the alkyl group of xanthogen formates. They found that the xanthogen formates are excellent collectors for most copper sulfides and the chain length of the xanthogen decreases chalcopyrite recovery while remaining constant for the other minerals. For pyrite, the long chain substituents have some effect on the reactive grouping causing a more favorable position to make it a more robust collector for pyrite as well (Ackerman et al., 2000). On the other hand, the use of chelating agents as collectors in the flotation of copper sulfides and pyrite was carried out using fourteen reagents. Their effectiveness in floating was evaluated and the best overall copper sulfide collector was an imidazoline (1-Hydroxyethyl- 2-Heptadecenyl). Nevertheless, it was also proved that it is an excellent collector for pyrite (Ackerman et al., 1999).

Recently, Yin et al. (2019) analyzed covellite and pyrite separation using pure minerals. The work focused on calcium hypochlorite ($\text{Ca}(\text{ClO})_2$) as a pyrite depressant on the flotation separation. The results showed that $\text{Ca}(\text{ClO})_2$ strongly inhibits pyrite flotation, while covellite was unaffected by this depressant. Even though such work provides some valuable insights into covellite flotation, it was focused on enhancing the pyrite depression. For this reason, the infrared spectroscopy (IR) and X-ray photoelectron (XPS) analysis were carried out to characterize the ($\text{Ca}(\text{ClO})_2$) adsorption on the pyrite surface.

Although the above-mentioned works discuss interesting aspects of covellite properties and their behavior in froth flotation, there is insufficient information to evaluate properly and design feasible operations dedicated to covellite concentration. It is worth noting that a dedicated and systematic study on covellite flotation is necessary due to its complex crystal-chemistry containing both copper (I) and copper (II) ions, as well as sulfide and disulfide

ions (Persson, 1994). Therefore, various reactions could take place between covellite and collectors. A further complication stems from potential interactions with other minerals such as chalcocite and pyrite, often associated with covellite.

Pyrite is considered in the copper flotation process as the main sulfide gangue mineral, which decreases the grade and quality of the concentrate. Pyrite flotation is well known to be pH-dependent, which allows its depression and selective separation from sulfidic copper minerals at alkaline pH. The species responsible for pyrite depression are $S_2O_3^{2-}$ and $Fe(OH)_3$, which oxidize the pyrite surface and inhibit its natural floatability. Pyrite is also affected by the oxidation level. López-Valdivieso et al. (2018) studied the surface of pyrite and determined that oxidation improves the formation of ferric oxyhydroxide species on the pyrite surface, which promotes the adsorption of depressors such as dextrin. All these parameters allow pyrite surface modification and separation during the flotation process (Cruz et al., 2021).

It is well known that in a traditional flotation process the pyrite ends up in tailings. However, there is a growing need for cleaner production strategies, with the prevention of AMD as a more sustainable alternative to downstream waste remediation (Benzaazoua et al., 2000). Consequently, the production of tailings with a minimum content of acidifying species such as pyrite should be seriously considered. To that aim, this study explores a two-stage method to separate covellite from pyrite. In the first place, this study evaluates bulk flotation of pyrite-containing ores using collectors with low selectivity to produce tailings with low pyrite content. Potassium amyl xanthate (PAX) was used in this study as a non-selective collector. It is a common collector used in the flotation of sulfide minerals. The PAX adsorption occurs by ion exchange between xanthate ions and the substrate surface (Ejtemaei and Nguyen, 2017; Mielczarski et al., 1989). This kind of collector is commonly used in the scavenger stage in industrial flotation processes because it allows floating of all the sulfide minerals. However, in this study it was adapted in the rougher stage for bulk flotation.

Secondly, the evaluation of selective collectors with copper sulfide for subsequent covellite-pyrite separation will be presented. The selection of an adequate collector is critical for effective mineral separation via froth flotation, and it is defined by the interaction with the mineral surfaces of interest. *O*-isopropyl-*N*-ethyl thionocarbamate (IPETC) was chosen as a

selective collector for copper sulfide ore. Its reportedly high selectivity is due to its behavior as a chelating agent that associates explicitly with copper metal ions. Another interesting characteristic of IPETC is its $P_{K_a} > 12$, which means that the solubility of IPETC does not change at high pH, giving it a robust performance (Fairthorne et al., 1996, 1997).

This paper aims to provide more insights into covellite flotation to decrease the knowledge gap on this topic, and to provide new data. With this aim, the flotation behavior of covellite was investigated by analyzing pure covellite and a porphyry ore from the north of Chile composed of covellite (0.22%), chalcocite (0.21%), chalcopyrite (0.06%), and pyrite (0.69%) under different pH values, collector types, and collector concentrations.

A.2 Materials and methods

A.2.1 Materials and reagents

A pure mineral sample of covellite was obtained from a local Chilean mine. The pure pyrite was purchased from Ward's Science. Porphyry ore was obtained from a mine in Antofagasta region, Chile. The covellite was associated with gypsum and quartz, as will be seen in Section 3.1. The initial samples of covellite were obtained in the form of rocks measuring approximately 12 x 15 cm. Thus, it was necessary to carry out preliminary crushing before use in the experimental campaign. Particle sizes of approximately 1 cm were obtained after crushing. Following further crushing in an agate mortar to liberate the covellite, it was manually sorted from the quartz and gypsum. The covellite was subsequently dry-sieved to obtain different size fractions. The -2 mm to +800 μm fraction was collected for use in the Hallimond tube tests. In preparation for each Hallimond tube test, 1 g of crushed sample was further ground in an automatic agate mortar immediately before the Hallimond tube test to achieve $P_{80} = 100 \mu\text{m}$. This particle size was selected according to reported values of copper recovery from Chuquicamata mine, where the maximum copper recovery was between 90 to 120 μm (Bulatovic, 2007). The same comminution procedure was carried out for pyrite. However, as X-ray diffraction later confirmed that the pyrite was 100% pure, it did not require any sorting.

The porphyry ore was crushed, ground, and sieved according to the ASTM-C117. (1995) procedure. The particle size obtained was $P_{80} = 766 \mu\text{m}$. An additional test was necessary to

estimate the optimum milling time to achieve $P_{80} = 150\mu\text{m}$, which is representative of industrial operations. The grinding test was carried out in duplicate using a Standard ball mill brand HEBRO, made of AISI 316 stainless steel with a capacity of 1.5 kg. The time tested was 5, 10, and 15 min. The porphyry ore was sieved in an automatic sieve shaker (DURA TAP, model #258) for 15 minutes to produce experimental data for granulometric analysis. The optimum time of grinding to achieve $P_{80} = 150\ \mu\text{m}$ was 13 minutes.

IPETC and PAX were supplied by Qingdao Sunrun Chemical Co., Ltd. (China) with a nominal purity of $\geq 95\%$ and $\geq 90\%$, respectively. For the Hallimond tube test, sodium hydroxide (NaOH) 0.1 M was used as a pH regulator. For the porphyry ore, lime was used as a pH regulator and Matfroth-202 as a frother. The frother was provided by Mathiesen S.A.C. (Chile).

A.2.2 Mineral characterization

The mineralogical phases of covellite and pyrite were identified by X-ray diffraction (XRD) in a PANanalytical device, model XPERT PRO MPD Alpha 1, equipped with an X-ray source of Cu, monochromator K-alpha and detector PIXcel1D, 45 kV, 40mA. The analysis was performed in a 2θ range from 10° to 100° including 2θ steps at 0.3s intervals. Also, these minerals were characterized by Fourier transform infrared spectrometer (FT-IR) using a PerkinElmer device, model Spectrum two ATR-IR spectrometer, in a spectral range of $4000 - 400\ \text{cm}^{-1}$.

The morphological surface of covellite was characterized by scanning electron microscopy (SEM) with detector EDS in a Hitachi, model SU5000, Bruker detectors series 6. It was operated at 20kV, taking images at 2500X using backscattered-electron (BSE) imaging. Microanalysis by X-ray dispersive spectroscopy (EDS) was performed to obtain a semiquantitative mineral composition.

The mineral identification and quantification of the porphyry ore were conducted using quantitative evaluation of minerals by scanning electron microscopy (QEMSCAN®) coupled with X-ray energy dispersive spectroscopy, model ZEISS EVO series. Bruker detectors AXS XFlash series 6, software IDiscover 5.3.2.501.

A.2.3 Hallimond tube test and design of experiment (DoE)

Hallimond tube tests were carried out using a modified Hallimond-type flotation cell (see Figure S1). The operational parameters in these experiments were as follows: 150 mL cell volume, 1 g of mineral (pure covellite and/or pyrite) per test, nitrogen flow rate ($N_2 = 33$ mL/min), magnetic stirring between 1000 and 1200 rpm, and a flotation time of 3 minutes. The pH values tested were 8, 9.5, and 11 using 0.1 M NaOH as a pH regulator. Two types of collectors were used: PAX and IPETC at different concentrations (i.e., 2×10^{-5} , 4×10^{-5} and 6×10^{-5} mol/L). Figure 1a shows the flow diagram for the Hallimond tube tests. The Hallimond tube tests of covellite and pyrite were first carried out in the absence of a collector at different pH values (8, 9.5, and 11) to evaluate the natural flotation of the minerals and effect of pH.

For each mineral, the effect of the collector concentration, the type of collector, and the pH on mineral recovery was studied following a 3^2 factorial design of experiments, considering the type of collector as a categorical factor and collector concentration and pH as continuous factors. Therefore, the experimental design consisted of 18 experiments, which were carried out in duplicate, resulting in a total of 36 experiments. Finally, based on the DoE and using the Minitab 19 program, the system was modeled and optimal conditions were determined based on response surface methodology (RSM), desirability function, and ANOVA test to determine the effect of factors. An empirical second-order model, as represented in equation (1), was used to describe the experimental data. In equation A.1, y represents the metal recovery, x_i represents the input variables, and ε is the residual associated to the experiments. The model parameters are a_o , a_i , a_{ii} and a_{ij} that represent the constant term, the coefficients of the linear term, the coefficients of the quadratic term, and the coefficients of the interaction term, respectively. The R-squared (R^2), the adjusted R-squared (R^2_{adj}), and the predicted R-squared (R^2_p) were determined. In this approach, R^2 indicates how well the model fits the data, R^2_{adj} adjusts for the number of terms in the model, and R^2_p indicates the ability of the model to predict responses for new observations.

$$y = a_o + \sum_i a_i x_i + \sum_i a_{ii} x_i^2 + \sum_i \sum_{j \neq i} a_{ij} x_i x_j + \varepsilon \quad (\text{A.1})$$

The desirability function, introduced by Derringer and Suich (1980), is a proven procedure for the simultaneous determination of optimum conditions of input variables that can determine optimum performance levels for one or more responses (see for example Vieceli et al. (2016)). The general approach of the desirability function is first to convert the response y_k into an individual desirability function (d_k) that varies over the range 0 to 1 (lowest desirability to highest desirability). The weight (w_k) of the desirability function for each response defines its shape. The weight for each response is selected to accentuate or diminish the goal. Then, the individual desirability results are combined into a composite desirability function, D , by computing their geometric mean of different d_k values. In this research, the composite desirability function was determined based on two individual desirability function that represents the covellite (d_1) and pyrite (d_2) recovery, as follows:

$$D = (d_1^{w_1} d_2^{w_2})^{\frac{1}{(w_1+w_2)}} \quad (\text{A.2})$$

Minitab 19 was used to optimize the response parameters.

A.2.4 Denver cell test and flotation kinetic test of porphyry ore

The Denver cell test and flotation kinetic test were performed in a Denver cell using the following operational parameters: 3.3 L cell volume, solid percentages (36% v/v), airflow (6 L/min), and impeller speed 1200 rpm. Two methodologies were implemented during rougher flotation step to achieve the bulk and selective flotation. The first one considered IPETC as a selective collector. The process started with grinding for 13 minutes with the lime with the objective to facilitate the depression of pyrite; after this time, the pulp was placed in the Denver cell and the collector IPETC was added and conditioned for 3 minutes, followed by the frother. The second methodology considered PAX as a bulk collector. In this case, the grinding was carried out with the PAX collector with the aim to float both covellite and pyrite; then, the lime was added in the Denver cell, followed by the frother. These two methodologies were implemented with the kinetic test, as well.

The flotation experiments were carried out at three pH values and four collector concentrations. The collector concentrations were 5, 10, 20, and 30 g/ton; the frother used was Matfroth-202 with 20 g/ton of dosage, the flotation time was 12 minutes, and the lime

was used as a pH regulator at pH values of 8, 9.5, and 11. The flotation time was selected based on industrial experience. The flotation kinetic test was performed with 5 g/ton collector dosage, frother dosage 20 g/ton, and two pH values (8 and 11). The total flotation time was 20 minutes, with samples collected at 0.5, 1, 3, 5, 8, 10, 12, 15, and 20 minutes. The collector dosage and pH were selected based on the results of flotation tests, as will be discussed later. The froth was collected every 15 seconds for both flotation and kinetic tests. Figure 1b shows the flowsheet for the flotation and kinetic test.

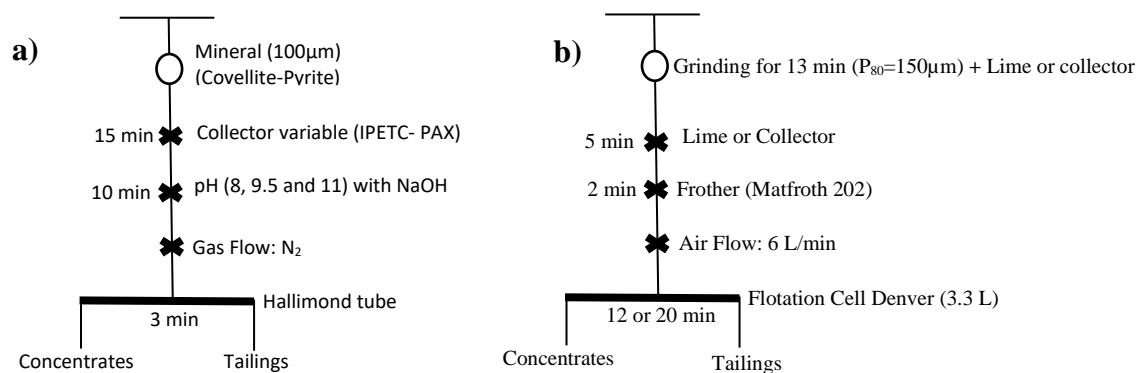


Figure. A.1. Flowsheet a) Hallimond tube test and b) Denver cell test and flotation kinetic tests of porphyry ore.

A.3 Results and discussion

A.3.1 Pure mineral characterization

The X-ray diffraction (XRD) spectrum of the covellite sample used in this work is shown in Figure 2a. As seen, the mineral exhibits the characteristic peaks of covellite (peaks indexed in the graph), while the presence of gypsum was also identified with its characteristic peak at $2\theta = 12^\circ$ (non-indexed peak in the graph). The estimated composition from this mineral is 83% covellite and 17% gypsum. Figure 2b shows a photograph of the covellite sample used in this study for the Hallimond tube test. Covellite and quartz occur as crystals, while gypsum is present mainly in the form of veins. The XRD analysis and semi-quantification show that the pyrite sample contains 99.8% pyrite.

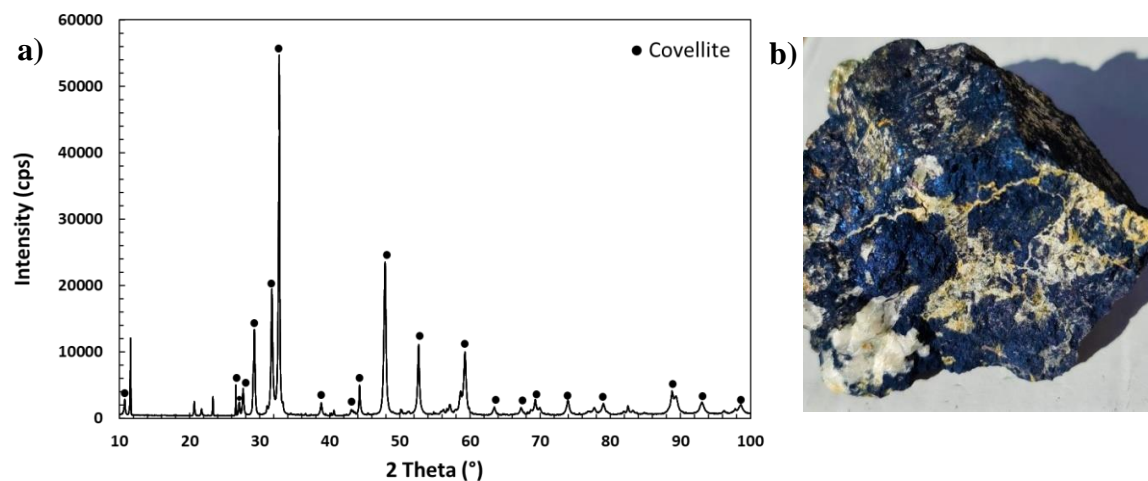


Figure A.2. a) X-ray diffraction pattern corresponding to covellite b) Image covellite mineral.

The FT-IR spectra of covellite (Figure A.3a) show a band at 618.3 cm^{-1} corresponding to the stretching vibrations of Cu-S (Karikalan et al., 2017). Moreover, the FT-IR analysis corroborated the presence of gypsum ($\text{CaSO}_4 \cdot 2\text{H}_2\text{O}$) identified by XRD. A strong band was observed at 1100 cm^{-1} and a small band at 696 cm^{-1} , which corresponds to the tetrahedral group SO_4^{2-} of gypsum vibrations (Bishop et al., 2014; Marvin, 1955). It is worth mentioning that copper sulfate can also contribute to the SO_4^{2-} band. Figure 3b displays the spectra obtained with pyrite. Compared with the characteristic spectrum of pyrite available from the data bank (“RRUFF,” 2020), this sample presents the same bands between $550\text{--}900\text{ cm}^{-1}$ and 1100 cm^{-1} , but at a lower intensity.

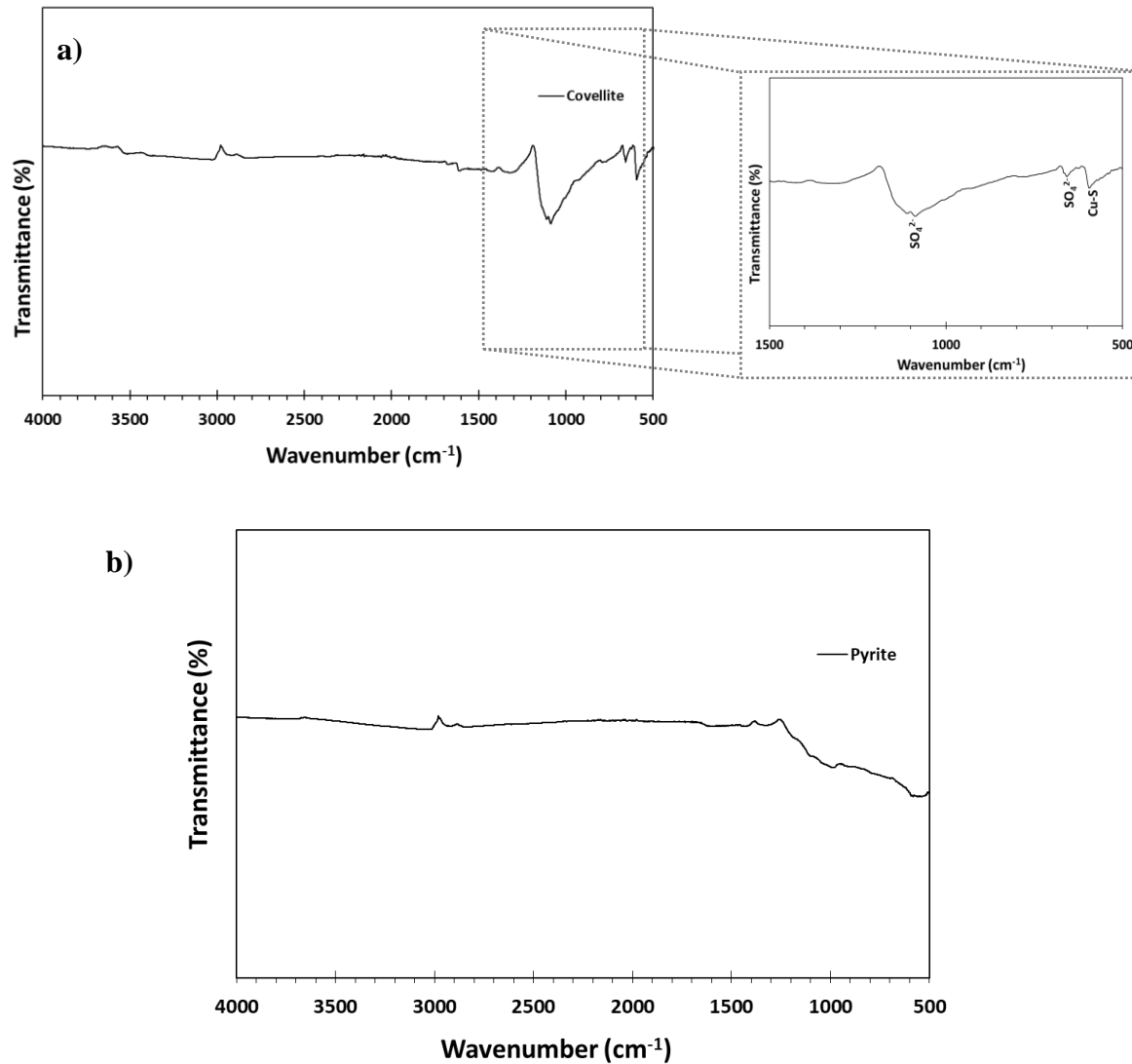


Figure A.3. FT-IR spectra corresponding to a) covellite and b) pyrite.

Figures A.4a and A.4b show a mineral enriched with Cu element. EDS results show that covellite has some impurities, Si and Ca, indicating that covellite is associated with quartz and gypsum. The analysis of elemental composition (Figure A.4b) shows the Cu content is 31.9 %, Si 16.5%, Ca 6.5%, S 18.8%, and O 26.3%. Therefore, different components need to be dissociated to achieve covellite flotation. Figures 4c-g show the elemental mapping, which provides insight into how the elements Cu, Si, Ca, S, and O are distributed. This analysis allows the determination that, despite the previous mineral preparation described in section 2.1, the covellite used for Hallimond tube test still had some impurities.

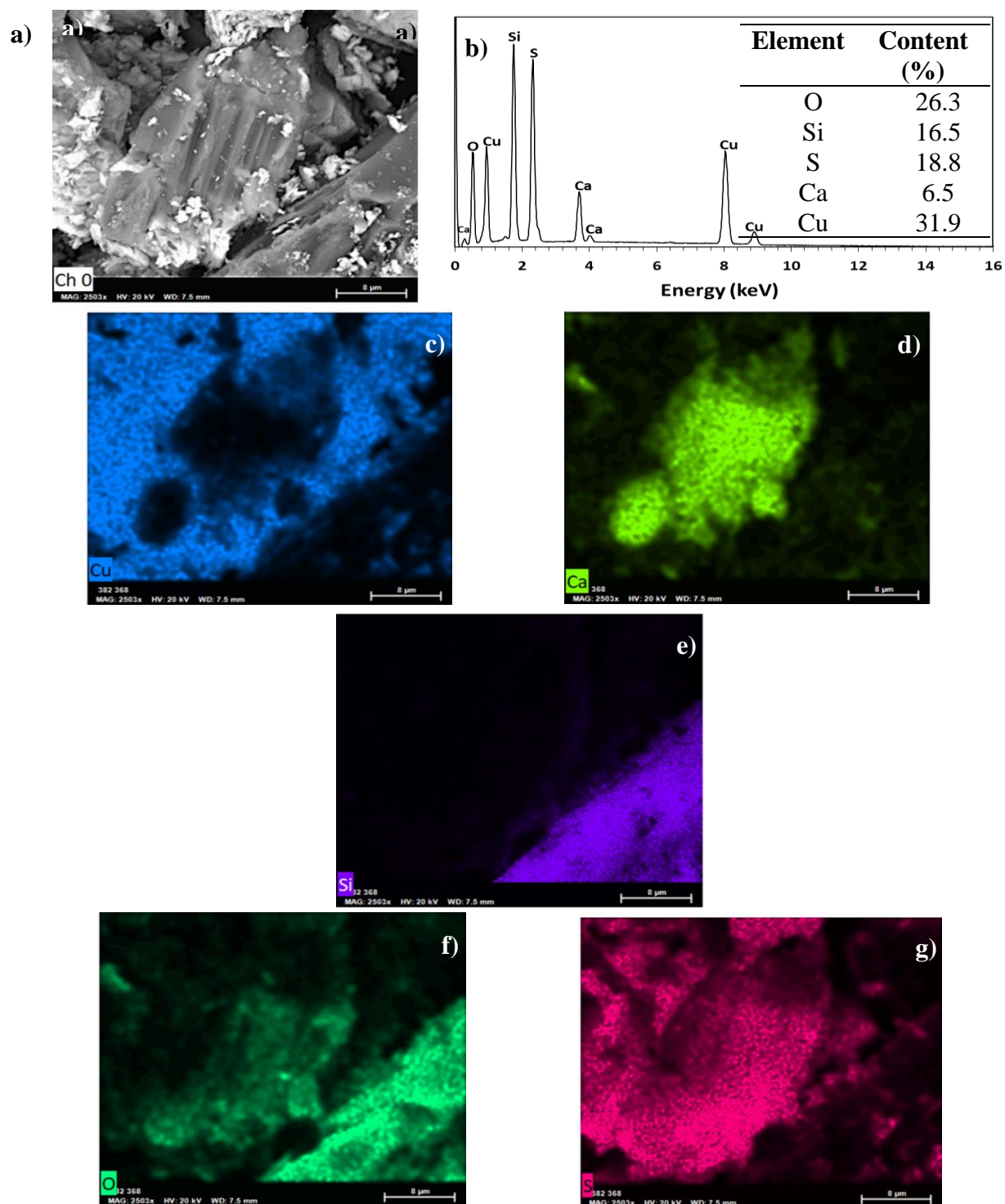


Figure A.4. SEM-EDS images of covellite a) BSE covellite image, b) elemental composition of covellite from c) to g) element mapping.

The modal mineralogy of the porphyry ore as determined by QEMSCAN® is presented in Figure A.5. The QEMSCAN® mineralogy for the porphyry ore was mostly composed of feldspars (61.15%), quartz (19.55%), and chlorite/bornite (12.96%). Pyrite (0.69%), copper minerals (0.43%), and molybdenite (0.01 %) were minor components.

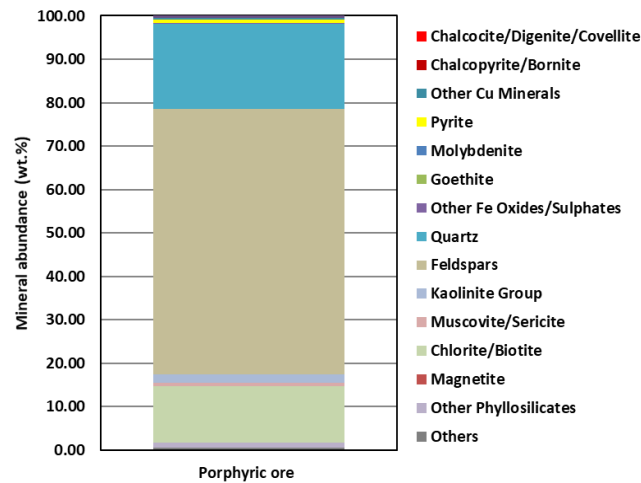


Figure A.5. Porphyry copper ore modal composition (wt.%)

The copper grade contribution of the copper minerals to the porphyry ore is shown in Table A.1. As seen, this is a low-grade copper ore (0.38 wt%) with the major copper grade contribution from chalcocite (0.16 wt%) and covellite (0.15 wt%), and a low contribution of chalcopyrite (0.02 wt%). In conventional operations, this mineral could be considered as waste rock, having a copper grade comparable with historical tailings. However, economic factors may favor the processing of such ore and it is thus important to highlight the need to study copper sources where the presence of chalcopyrite is negligible. In fact, some mining companies in Chile operate with a cut-off grade of 0.35% copper. The iron grade contribution is displayed in Table A.1. It has been identified that the major iron sources are pyrite (0.32%), biotite (0.18 %), and magnetite/hematite (0.15%). Taking into consideration the significant presence of phyllosilicates and oxides in the ore (see Figure A.5), a complex pulp behavior can be expected as the reagents used in the flotation of pyrite could affect the phyllosilicates and oxides differently, impacting the expected performance of reagents as will be discussed

in section 3.3. Finally, the sulfur distribution is shown in Table A.1. Pyrite (0.37%), covellite (0.08%), and chalcocite (0.04 %) are the major sources of S. The most problematic of those sulfides in terms of AMD generation is the pyrite, which due to its oxidation from Fe^{2+} to Fe^{3+} could generate acidity.

Table A.1 Copper, iron, and sulfur grade contribution in ore

Copper grade contribution		Iron grade contribution		Sulfur grade contribution	
Mineral	Wt %	Mineral	Wt %	Mineral	Wt %
Chalcocite/Digenite	0.16	Chalcopyrite/Bornite	0.02	Chalcocite	0.04
Covellite	0.15	Other Cu Minerals	0.01	Covellite	0.08
Chalcopyrite	0.02	Magnetite/Hematite	0.15	Chalcopyrite	0.02
Bornite	0.01	Goethite	0.01	Bornite	<0.01
Cu-bearing Phyllosilicates	0.01	Other Fe Oxides/Hydroxides	0.02	Pyrite	0.37
Cu-bearing Wad	0.03	Pyrite/Pyrrhotite	0.32	Molybdenite	<0.01
		Chlorite	0.18		
		Group/Biotite			
		Others	0.01		
Total	0.38	Total	0.72	Total	0.52

A.3.2 Hallimond tube test and DoE with pure minerals

The results of collectorless micro-flotation of covellite and pyrite at pH values 8, 9.5, and 11 are shown in Figure A.6. The covellite flotation does not appear to be pH-dependent, with a natural recovery of approximately 55%. The natural hydrophobization of covellite could be a result of two phenomena: i) copper (I) dissolution from the covellite surface, and ii) the covellite surface being rich in sulfide (S^{2-}) and disulfide (S_2^{2-}) groups. Covellite flotation may not depend on pH because covellite has no hydrolyzable ions (e.g., Fe (II)) and thus it does not form hydroxides at alkaline pH (Goh et al., 2006; Persson, 1994). In the case of pyrite, the behavior is different; the pyrite has 10% natural floatability at pH 8 and 9.5. However, when the pH increases to 11 the pyrite is depressed, decreasing its floatability to 2%. The pH-dependence of pyrite flotation is well documented (Ackerman et al., 2000; Evangelou and Zhang, 1995; López-Valdivieso et al., 2018; Mu et al., 2016; Paredes et al., 2019), as corroborated in this study.

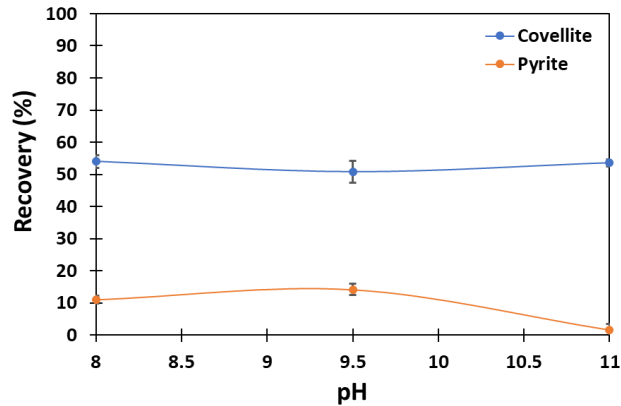


Figure A.6. Natural floatability of covellite and pyrite ($P_{80}=100\mu\text{m}$).

The micro-flotation results for covellite-IPETC and covellite-PAX are shown in Figures A.7a and A.7b, respectively. The collector has a marked effect on the covellite flotation, as the recovery increases up to 90-95%. Covellite flotation in the presence of a collector remains independent with respect to pH within the range hereby studied. As seen in Figure 7a, covellite recovery increases with collector concentration. At 6×10^{-5} mol/L of IPETC recovery increases by 10%, and for PAX (Figure A.7b) recovery increases by 20%. Therefore, covellite flotation is enhanced with both collectors.

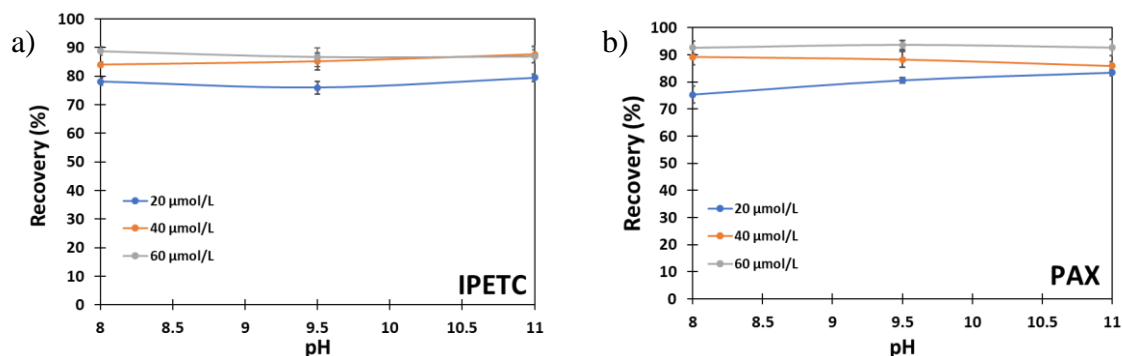


Figure A.7. Micro-flotation pure mineral a) Covellite-IPETC, b) Covellite-PAX ($P_{80}=100\mu\text{m}$).

The micro-flotation results for pyrite-IPETC and pyrite-PAX are shown in Figures A.8a and A.8b, respectively. As seen, pyrite flotation is affected by pH, collector type, and collector concentration. The minimum pyrite recovery was obtained at a lower collector concentration and higher pH with both collectors.; the pyrite recovery was 17% and 32% for IPETC and PAX, respectively. The low pyrite recovery with IPETC corroborated the possibility of using

this collector in a selective flotation separation from the covellite. The maximum pyrite recovery was obtained at higher collector concentrations and lower pH with both collectors; the pyrite recovery was 79% and 90 % for IPETC and PAX, respectively, which shows that PAX is an alternative to be used in the bulk flotation.

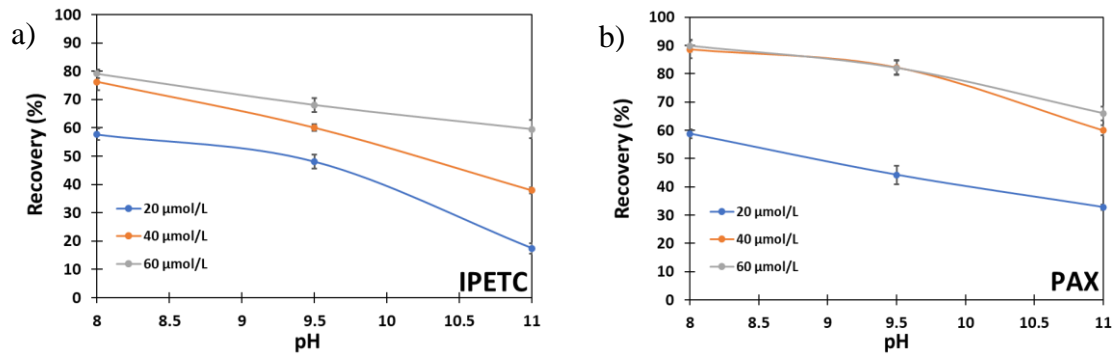


Figure A.8. Micro-flotation pure mineral a) Pyrite-IPETC, b) Pyrite-PAX ($P_{80}=100\mu\text{m}$).

The experimental results of the pure mineral recoveries were analyzed using the ANOVA test at 5% significance level. The Pareto chart permits the detection of the factor and interaction effects that are most important to the flotation recovery. Figure A.9 shows the Pareto chart of standardized effects and draws a reference line that separates the potentially important effect from the non-important ones at the significance level. The Pareto charts in Figure A.9a revealed that the main factors influencing the recovery of covellite by flotation follow the order: collector concentration > collector type > square collector concentration > pH \times collector concentration, where the two first factors are statistically significant. In the case of pyrite recovery (Figure A.9b), the order is: collector concentration > pH > collector type > square collector concentration. Note that the square interaction means a quadratic behavior, and therefore, a minimum and maximum could exist.

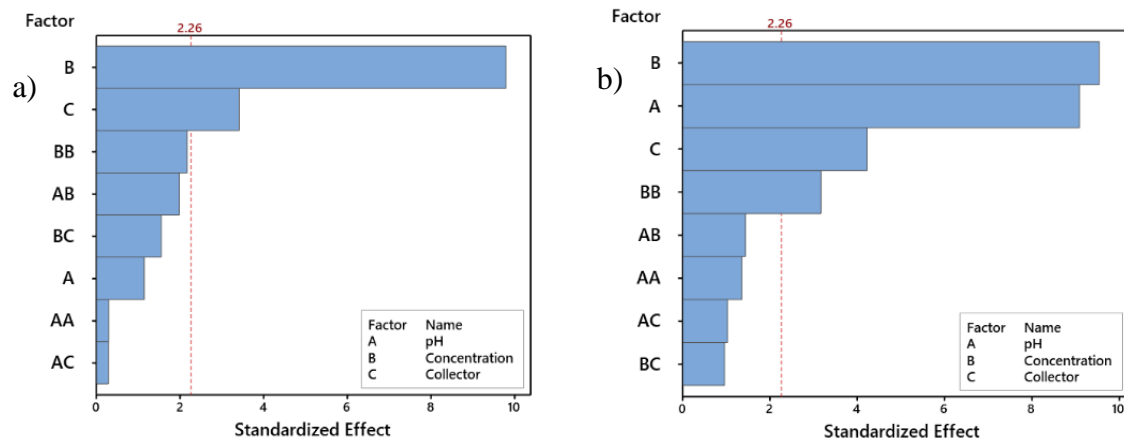


Figure A.9. Pareto chart of standardized effect. a) covellite recovery and b) pyrite recovery

Second-order polynomial equations were used to assess the empirical relationship between independent variables (pH, collector concentration) and mineral recovery, as shown in Table A.2. The R^2 , R^2_{adj} , and R^2_p for the pyrite recovery models were 0.96, 0.92, and 0.83, respectively. For covellite recovery, the R^2 , R^2_{adj} , and R^2_p values were 0.93, 0.87, and 0.70, respectively. These values are frequently observed in multiphase systems and flotation modeling (Cisternas et al., 2019; Lucay et al., 2020). Therefore, these models were used to determine optimal conditions and to analyze the effect of both pH and collector concentration.

Table A.2. Regression models for mineral recovery (c : collector concentration in $\mu\text{mol/L}$).

Collector	Mineral	Model
IPETC	Covellite	$57.3 - 0.26 pH + 1.122 c + 0.130 pH^2 - 0.0055 c^2 - 0.0470 pH c$
PAX	Covellite	$54.9 - 0.05 pH + 1.212 c + 0.130 pH^2 - 0.0055 c^2 - 0.047 pH c$
IPETC	Pyrite	$-12 + 17.4 pH + 1.570 c - 1.69 pH^2 - 0.0222 c^2 - 0.095 pH c$
PAX	Pyrite	$-28 + 19.6 pH + 1.726 c - 1.69 pH^2 - 0.0222 c^2 - 0.095 pH c$

The contour plots for recoveries of covellite and pyrite are exhibited in Figure A.10. It is clear that pH has a prominent impact on pyrite recovery, whereas the effect is low in covellite recovery. Also, it is clear that collector concentration plays an influential role in both pyrite and covellite recovery. Finally, the effect of collector type is more critical in pyrite recovery than covellite recovery. This behavior can be identified in Figure A.10c and A.10d, where

the pyrite recovery decrease by 16% when the IPETC collector is used, suggesting this collector can be utilized as a selective collector. In comparison, the covellite (Figure A.10a and 10b) does not present a significant difference in copper recovery when the collector is changed.

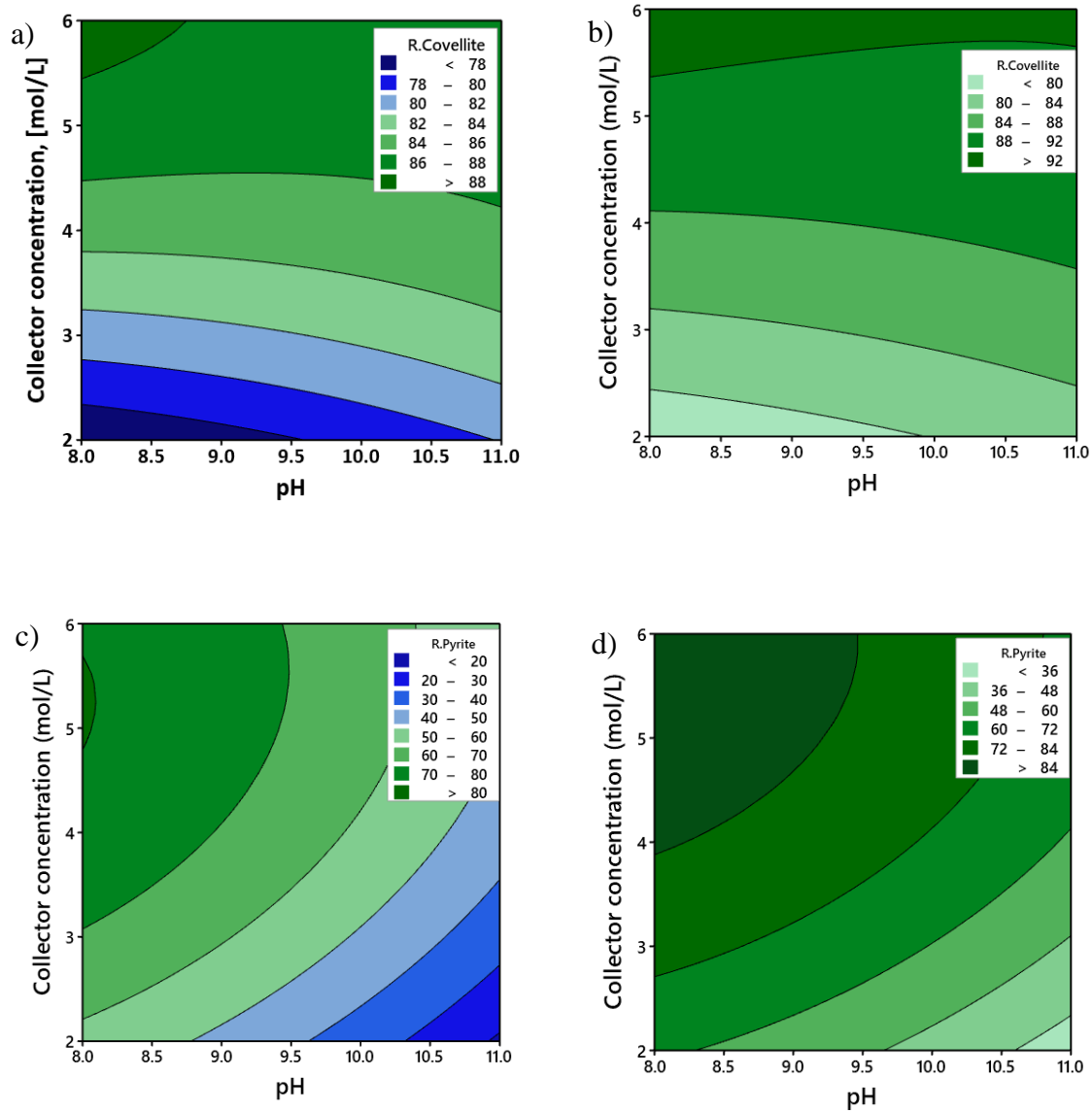


Figure A.10. Contour plot for covellite a) IPETC, b) PAX and pyrite c) IPETC, d) PAX recoveries. Collector concentration [mol/L] 10^{-5}

Two multi-objective optimization problems were analyzed using desirability functions. In the first, it was sought to optimize the recoveries of covellite and pyrite; that is, bulk flotation

(both maximum recoveries have a desirability of 1). In the second, the objectives were to maximize the recovery of covellite and minimize the recovery of pyrite; that is, selective flotation (maximum covellite recovery has desirability of 1 and minimum pyrite recovery has desirability of 1). The fitted models from Table A.2 were used to solve both problems. For the first problem, the optimal conditions correspond to pH 8 and a PAX concentration of 6×10^{-5} mol/L, with covellite and pyrite recoveries of 93.4% and 90.2%, respectively. Figure A.11a shows that the values of both individual desirability functions are close to 1 and both use PAX as collector. Therefore, the individual desirability for each response was weighted, giving equal importance to the covellite and pyrite recoveries, which resulted in a composite desirability of 0.99. For the second problem, the optimal conditions are pH 11 and an IPETC concentration of 2×10^{-5} mol/L, with covellite and pyrite recoveries of 80.5% and 20.3%, respectively. Figure A.11b shows that it is not possible to obtain individual desirability values close to 1 because collector concentration and collector type have the opposite effect on the desirability of covellite and pyrite recovery. Therefore, it was necessary to balance both desirability functions. Pyrite recovery is more affected by the concentration and type of collector than the covellite; accordingly, pyrite recovery was weighted as three times the desirability of covellite recovery to obtain a composite desirability close to 0.5. Under these conditions, the desirability for pyrite and covellite recoveries were 0.88 and 0.28, respectively.

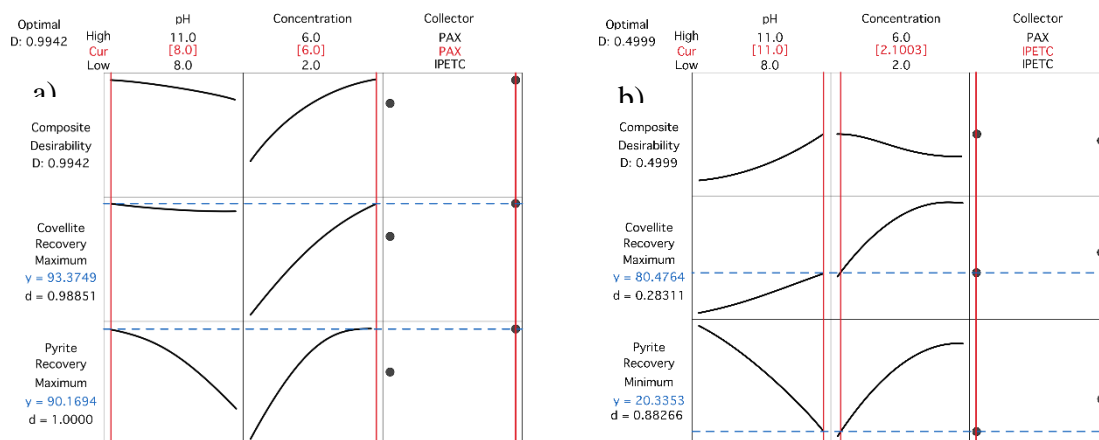


Figure A.11. Optimization plots for a) bulk flotation and b) selective flotation

The optimal conditions determined correspond to the exact conditions utilized in the experimental test. Therefore, there is no need to repeat the experimental test for verification of optimal conditions. According to the optimization and the results obtained after the Hallimond tube test for covellite and pyrite, the parameters required to carry out bulk flotation are PAX with a concentration of 6×10^{-5} mol/L and $\text{pH} = 8$. The expected recoveries are 90% for pyrite and 95% for covellite. On the other hand, the optimal parameters for successful selective flotation are IPETC with a concentration of 2×10^{-5} mol/L at $\text{pH} = 11$, with expected recoveries of 17% for pyrite and 80% for covellite.

Finally, two Hallimond tube tests were carried out with a covellite/pyrite mixture (50:50) using the parameters identified as optimal for bulk and selective flotation. Table A.3 shows the results of the experiments. For the selective flotation, covellite and pyrite recoveries were 97% and 53%, respectively, showing some degree of selectivity under these conditions. However, the recovery of pyrite was higher than predicted (i.e., 17%). A possible explanation is that surface activation of pyrite occurs as a result of copper dissolved in the solution, an effect reported in previous studies with chalcopyrite and CuSO_4 solutions (Chandra and Gerson, 2009). Also, the covellite recovery in the covellite/pyrite mixture is higher than the pure covellite recovery. This can be explained by a greater relative amount of collector available for the covellite because it has a higher affinity for the collector than does pyrite. On the other hand, for the bulk flotation, covellite and pyrite recoveries were 96% and 88%, respectively, a behavior corresponding to bulk flotation. These results are similar to the experiments performed with pure minerals (covellite 95% and pyrite 90%).

It is worth mentioning that the present work was not focused on the mechanism of collector adsorption on mineral surfaces. Nevertheless, some studies examining copper sulfides collector's adsorption have been published that can help us to have an approximation of how the system collector – copper sulfide behaves. For instance, Fairthorne et al. (1996) shown that chalcopyrite treated with IPETC is independent of pH (as was identified in our work for covellite), and the possible bond formed between IPETC and chalcopyrite surface could be through Cu-S bond. Thus, there are no studies about IPETC-covellite interactions, but it could be suggested that covellite could present similar behavior. On the other hand, Roos et al. (1990) studied the adsorption mechanism of potassium ethyl xanthate (KEtX) on the covellite surface. They found that copper-xanthate species (Cu-EtX and $\text{Cu}(\text{EtX})_2$) and dixanthogen

(EtX)₂ were the species responsible for covellite hydrophobization. These results suggest that covellite-PAX interaction could behave similarly. Nevertheless, future work is necessary to examine the physical-chemical interactions of pure covellite with reagents more deeply. There are still some unresolved questions about covellite behavior.

Table A.3. The micro-flotation results for covellite/pyrite mixture (50:50)

Type Flotation	pH	Collector concentration	Type Collector	CuS grade (%)		Recovery (%)	
				Concentrate	Tailing	CuS	FeS ₂
Selective	11	2×10^{-5}	IPETC	75.9	10.2	97	53
Bulk	8	6×10^{-5}	PAX	68.7	38.8	96	88

A.3.3 Denver cell test with porphyry ore

The flotation results for porphyry ore are shown in Figures A.12a and A.12b, respectively. Once again, the results corroborate that copper recovery is not pH-dependent, while iron recovery does depend on pH. WC refers to covellite without a collector. For the condition IPETC-pH11 with 5 g/ton of collector dose, the recoveries were 92% Cu and 26% Fe, showing selective flotation. The same behavior was found for PAX-pH11 with a dosage of 5 g/ton, with recoveries of 82% Cu and 20% Fe. Bulk flotation was achieved with the IPETC-pH8 with 5 g/ton of collector dose; the recovery was 85% Cu and 50% Fe. Nevertheless, a proper analysis of the recovery of iron in a porphyry ore must include the contribution from the various mineral species. Therefore, the concentrate obtained after each flotation was analyzed by XRD. The results show that floated iron comes from chalcopyrite, pyrite, and hematite, respectively representing 18%, 67%, and 16 % of the total Fe recovery. Considering the previous values, the pyrite recovery was 75%. The same analysis was carried out for the results obtained in selective flotation with 26% and 20% of Fe recovery for IPETC and PAX, respectively, which corresponds to 39% and 30% of pyrite recovery for IPETC and PAX. In general, with a collector dosage greater than 10 g/ton the flotation with the collectors IPETC and PAX can be considered as bulk flotation, except for PAX-pH8. Additionally, with IPETC it is possible to achieve either selective or bulk flotation through variations in pH and concentration.

It is worth mentioning that 5 g/ton corresponds approximately to 2.5×10^{-5} and 3.4×10^{-5} mol/L of PAX and IPETC, respectively. Consistently, the flotation behavior of porphyry ore can be considered comparable with the flotation behavior of pure minerals, except for tests with PAX at pH 8. The same qualitative consistency was observed for the tests at 10 g/ton that correspond approximately to 4.9×10^{-5} and 6.8×10^{-5} mol/L of PAX and IPETC, respectively. Flotation tests were performed at 3 g/ton of collector to observe the behavior at lower concentrations. Note that 3 g/ton corresponds approximately to 1.5×10^{-5} and 2.0×10^{-5} mol/L of PAX and IPETC, respectively. The observed results were similar to those obtained at a dose of 5 g/ton. The recoveries achieved are: 1) IPETC-pH 8, 81% Cu and 55% Fe; 2) IPETC-pH 11, 92% Cu and 32% Fe; 3) PAX-pH 8, 42% Cu and 9% Fe; and 4) PAX-pH 11, 87% Cu and 27% Fe.

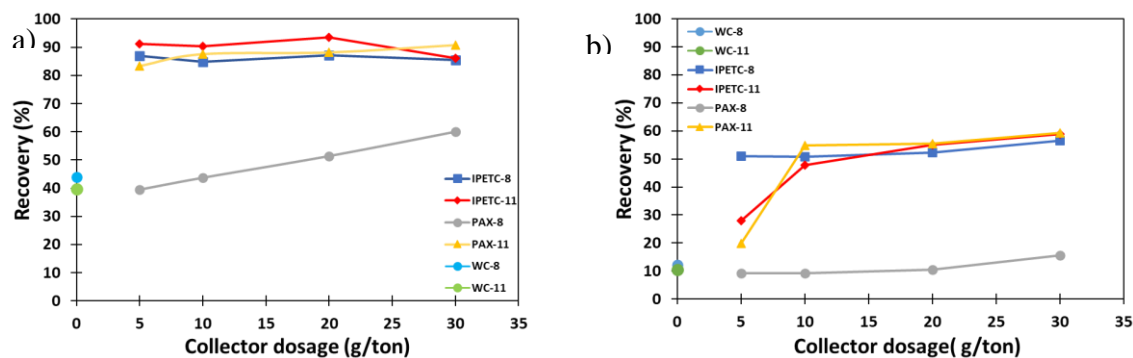


Figure A.12. Denver cell test results for porphyry ore a) Copper recovery, b) Iron recovery ($P_{80}=150\mu\text{m}$).

It is worth mentioning that the experiment with PAX-pH8 results in low copper and iron recoveries. The recoveries at a high collector dosage (30 g/ton) were 60 % for copper and 15% for iron. This behavior could be due to the complex mineralogical composition of the ore. According to the QEMSCAN® results, the porphyry ore is composed of feldspars (61%), quartz (19%), chlorite/biotite (13%), and kaolinite (2%). It has been documented that these minerals could adversely affect the floatability of copper because these minerals report to the concentrate. For instance, Malysiak et al. (2002) studied the feldspar interaction and its effect on the flotation using zeta potential. The initial zeta potential of feldspar is negative in the range of pH 4 to 10 and remains the same when the xanthate is introduced. However, when feldspar is in contact with CuSO_4 the zeta potential becomes positive in a range of pH 4 to 8,

which demonstrates a copper activation of the feldspar surface. Then, with a subsequent introduction of xanthate ions, the zeta potential returns negative, indicating the adsorption of xanthate ions onto the copper-activated feldspar. All these changes in potential demonstrated that at $\text{pH} \leq 8$ it is possible to float feldspar, which indeed decreases the amount of collector available. This decreased amount of collector might limit the copper recovery. Also, at pH 10 it was demonstrated that under all conditions the zeta potential remains negative. This last behavior could explain the high copper recovery at pH 11 with PAX. Fornasiero and Ralston (2005) demonstrated a similar behavior with quartz, showing a copper activation of quartz. The zeta potential of quartz was negative from pH 3 to 10 and became positive with the addition of a solution of copper chloride in a pH range of 7 to 10, which demonstrated copper activation on the quartz surface. With the subsequent introduction of xanthate ions, the zeta potential returned negative in the range of 3 to 10, indicating the adsorption of xanthate ions onto the copper-activated quartz. Thus, it is possible to float quartz in a pH range of 7 to 10; they found that the flotation with PAX at pH 8 was detrimental for copper recovery. This study showed the same behavior for chlorite activated with copper (II) and floated with PAX. In the case of kaolinite, there is a significant effect of kaolinite in the copper flotation only with percentages greater than 10 % (Jeldres et al., 2019). Another reason that covellite does not float well with PAX at pH8 could be that the zeta potential of covellite at pH8 is positive (Acar and Somasundaran, 1992; Fullston et al., 1999), whereas the feldspar at the same pH is negative, as was mentioned before. Therefore, as those zeta potentials are opposite, it could generate the heterocoagulation between the covellite surface and feldspar, affecting its floatability.

Moreover, it could be that the zeta potential of covellite treated with PAX remains positive and, therefore, after the interaction with feldspar, keeps the same behavior of heterocoagulation. On the other hand, covellite treated with PAX at pH11 shows that it floats very well; that could be due to at pH 11 the zeta potential of covellite became negative. Therefore feldspar does not affect the covellite flotation. Finally, the covellite treated with IPETC at pH 8 shows that pH does not affect its flotation. This behavior could be due to the zeta potential of covellite became negative as the feldspar, therefore

the formation of this aggregate on the covellite surface is avoided (Acar and Somasundaran, 1992; Fullston et al., 1999). Given this unexpected behavior, tests were carried out with PAX

at pH 9.5, resulting in copper and iron recoveries between the values observed at pH 8 and 11. The copper recoveries were 57, 77, and 82% for PAX at doses of 10, 20, and 30 g/ton, respectively. For iron, the recoveries were 12, 20, and 25% for PAX at doses of 10, 20, and 30 g/ton, respectively. These results confirmed the behavior of the porphyric mineral at pH < 11 with PAX.

According to results obtained from porphyry ore flotation, the optimum parameters to get bulk and selective flotation were a collector dosage of 5 g/ton with both collectors at pH 8 and 11, respectively. Thus, the flotation kinetic tests were carried out using these parameters. The results are shown in Figures A.13a and A.13b. In general, the kinetic test shows the same recoveries as the Denver cell test, including the low copper and iron recoveries with PAX at pH 8. Note that the maximum recovery in most of these tests was obtained after 5 minutes.

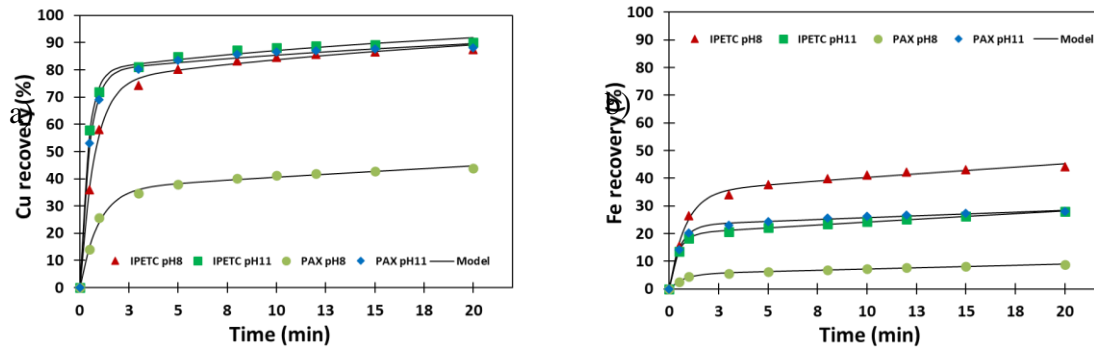


Figure A.13. Experimental values and fast/slow model for a) Copper recovery and b) Iron recovery

For the kinetics quantification, the two most popular models were used to model the kinetics test: fast/slow and Klimpel models (Braga et al., 2020; Kelly and Carlson, 1991; Saleh, 2010). The fast/slow model considers that the components can be classified as fast-floating and slow-floating, and the recovery can be represented by:

$$R = 100 [F_f(1 - e^{-k_f t}) + (1 - F_f)(1 - e^{-k_s t})] \quad (\text{A.3})$$

where F_f is the fast-floating fraction, k_f and k_s are the rate kinetics coefficient of fast- and slow- floating fractions. The second model, known as the Klimpel model, assumes a rectangular distribution of rate constant, and it is given by:

$$R = R_{\infty} \left[1 - \frac{1}{k_R t} (1 - e^{-k_R t}) \right] \quad (\text{A.4})$$

where k_R is the rectangular kinetic coefficient and R_{∞} is the recovery after a long flotation time. The experimental values were adjusted to these models using the mean-square-deviation as the objective function. All the parameters were fixed using the solve option in Microsoft Excel, and the root-mean-square-deviation was determined as:

$$RMSD = \sqrt{\sum (R^{exp} - R^{cal})^2 / N} \quad (\text{A.5})$$

The results are given in Table A.4.

Table A.4. Kinetic parameters and root-mean-square-deviation.

	Copper				Iron			
	IPETC-pH8	IPETC-pH11	PAX-pH8	PAX-pH11	IPETC-pH8	IPETC-pH11	PAX-pH8	PAX-pH11
Fast/slow model								
k_f	1.3310	2.4689	1.0724	2.1039	1.2263	2.2214	1.3758	1.8944
k_s	0.0408	0.0457	0.0072	0.0346	0.0087	0.0055	0.0019	0.0036
F_f	0.7539	0.7961	0.3609	0.7947	0.3496	0.1989	0.0536	0.2310
$RMSD$	1.3	1.1	0.8	1.0	0.9	0.2	0.1	0.4
Klimpel model								
R_{∞}	88.29	89.51	43.79	88.27	43.55	25.49	8.05	27.11
k_R	2.46	5.12	1.83	4.46	1.97	3.22	1.45	3.42
$RMSD$	1.3	1.1	1.0	0.7	1.3	1.4	0.5	0.8

Both models provide similar $RMSD$ values for copper, whereas the fast/slow model provides better results for iron. Based on the kinetics parameters, the kinetics follow the following order: IPETC-pH11 > PAX-pH11 > IPETC-pH8 > PAX-pH8 for copper, and PAX-pH11 > IPETC-pH11 > IPETC-pH8 > PAX-pH8 for iron. The kinetic behavior is closely related to induction time, which is a function of the particle surface properties, chemical conditions, and hydrodynamics of the system (Albijanic et al., 2012; Yoon and Yordan, 1991). Therefore, it is evident that the kinetic responses for copper and iron must be different. For each mineral, the collector type and pH have an important effect on the kinetics. The results confirm that IPETC has a better affinity for copper, whereas PAX has a better affinity for iron. The $RMSD$ values indicate that a good agreement is obtained in both models (see Figure A.13).

A.4 Conclusions

In the Hallimond tube test, under the conditions studied, covellite has a natural flotation of around 55% and is pH-independent. The pyrite flotation is influenced by the presence of covellite, apparently, because covellite is more soluble than other copper sulfide types that activate the pyrite surface. The covellite recovery is influenced by collector type and concentration. Pyrite recovery is influenced by collector type, collector concentration, and pH. Finally, thanks to the high selectivity of the collector IPETC, low collector concentrations are sufficient to float the covellite at pH 8 and 11.

The bulk flotation was optimized; the optimum parameters were pH 8 with a PAX concentration of 6×10^{-5} mol/L, providing covellite and pyrite recoveries of 93.4 and 90.2%, respectively. The desirability obtained was close to 1, which indicates that is possible to realize bulk flotation obtaining maximum covellite and pyrite recoveries. In the case of selective flotation optimization, the optimal conditions were pH 11 with an IPETC concentration of 2×10^{-5} mol/L, providing covellite and pyrite recoveries of 80.5 and 20.3%, respectively. However, the desirability obtained was close to 0.5 because collector concentration and collector type have the opposite effect on the desirability of the covellite and pyrite recovery, which means that increase covellite recovery and decrease pyrite recovery have opposite behavior.

In the porphyry ore flotation, the kinetics follow the following order: IPET-pH11 > PAX-pH11 > IPET-pH8 > PAX-pH8 for copper, and PAX-pH11 > IPET-pH11 > IPET-pH8 > PAX-pH8 for iron. The results confirm that IPETC has a better affinity for copper, whereas PAX has a better affinity for iron. Nevertheless, the IPETC can be used as a selective or bulk collector varying only the pH and using low concentrations. After all, it is not necessary to use different collectors for bulk and selective flotation. In porphyry ore, the bulk flotation is feasible with IPETC at pH 8 and 5 g/ton collector dosage. This kind of procedure allows the majority of sulfide minerals to float in the rougher stage and produces a tailing with low pyrite content. Then, the concentrate could be selectively separated with the same collector (IPETC) by increasing the pH, thus obtaining two concentrates, one of copper and one of iron. The last concentrate, due to its high degree, could be used as a raw material in other applications (e.g., siderurgy industry).

Experimental results with the porphyry ore show that clay minerals may have a marked effect on the covellite floatability. The activation of the feldspar surface with copper and subsequent interaction with xanthates could decrease copper recovery, which can be explained by the floatability of feldspars. Nevertheless, the IPETC did not have these issues. This could be because the solubility of IPETC did not change as the pH increased, indicating high chemical stability. Nevertheless, these issues need further studies. Finally, future work is necessary to more deeply examine the physical-chemical interactions of pure covellite with reagents. There are still some unresolved questions about covellite behavior.

Authors & Contributions

Yesica. L. Botero. Conceptualization, methodology, experimental test, formal analysis, writing original draft preparation, corresponding and first author.

Rodrigo Serna-Guerrero. Writing-review and editing, conceptualization, supervision, funding acquisition.

Alejandro López-Valdivieso. Conceptualization, methodology, supervision.

Mostafa Benzaazoua. Writing-review and editing, formal analysis, funding acquisition.

Luis Cisternas. Writing-review and editing, Conceptualization, methodology, formal analysis, supervision, project administration, funding acquisition.

APPENDIX B ARTICLE 2: PHYSICAL-CHEMICAL STUDY OF IPETC AND PAX COLLECTOR'S ADSORPTION ON COVELLITE SURFACE

Article 2: Yesica. L. Botero, Andrés Canales-Mahuzier, Rodrigo Serna-Guerrero, Alejandro López-Valdivieso, Mostafa Benzaazoua and Luis A. Cisternas. Physical-chemical study of IPETC and PAX collector's adsorption on covellite surface. *Applied Surface Science*, 2022. (Doi:10.1016/j.apsusc.2022.154232).

This article was submitted to *Applied Surface Science* journal on November 24, 2021.

Highlights

- Collectors IPETC and PAX have a marked effect on the covellite flotation.
- XPS shows that the covellite surface has two oxidation states, Cu(I) and Cu(II).
- IPETC adsorption on covellite is realized through S of the collector with Cu atoms.
- PAX adsorption on CuS is realized through =S and –S of the collector with Cu atoms.

Abstract

The adsorption mechanisms of the collectors O-isopropyl-N-ethyl thionocarbamate (IPETC) and potassium amyl xanthate (PAX) on a covellite surface were studied through microflotation tests, Fourier-transform infrared spectroscopy (FT-IR), X-ray photoelectron spectroscopy (XPS), and density functional theory (DFT) calculations. The microflotation test demonstrated that the collectors have a marked effect on the covellite flotation and that covellite flotation is not pH-dependent. The FT-IR spectra for covellite treated with IPETC and PAX collectors at pH 8 and 11 does not differ significantly. For IPETC, the leading adsorption –C(=S)–NH group vibration was identified, and the NH stretching band is absent from both spectra. The spectra show the frequencies for the PAX, Cu-amylxanthate (CuAX), and (AX)₂ dixantogen that formed. The XPS spectra showed that the adsorption mechanism

of PAX on the covellite surface is principally through C 1s and S 2p. The adsorption mechanism of IPETC on the covellite surface suggests that the bond is enabled through the =S element of the collector with Cu atoms in the covellite surface. Finally, the DFT calculations predict that for IPETC the bond with copper only occurred through the C=S group. For PAX, the bond with copper occurred through the C=S and C–S groups.

Key words: covellite; collector adsorption; thionocarbamate; amyl xanthate; density functional theory.

B.1 Introduction

Copper is mainly derived from primary sources. This is a significant issue in the mining sector because the global reserves of copper are expected to decrease dramatically by 2050, with a corresponding ore grade decline to approximately 0.1 %. Thus, as the copper demand increases, the ore grade decreases (Elshkaki et al., 2016). The high demand for copper is associated with the growth in global population and economic development, increasing the consumption of this metal in several economic sectors, notably wiring, plumbing, and electricity (Cisternas et al., 2021). This has been further exasperated by the global targets to reduce greenhouse gas emissions, which include a transition towards electric vehicles that use four times as much copper as petroleum-fueled cars (MINING-DOT-COM, 2021). This shift also requires investments in infrastructure to provide sufficient charging stations (MINING-DOT-COM, 2021).

For this reason, increasing copper extraction efficiency is mandatory. Currently, chalcopyrite is the leading mineral from which copper is extracted. Nevertheless, a possible way to enhance copper supply is to exploit other minerals, such as covellite. Covellite can be found in ore, waste rock, and tailing deposits. For instance, Burrows et al. (2020) reported a copper–gold deposit in Eastern Sumbawa, Indonesia, where copper occurs exclusively as covellite associated with pyrite (with 0.6% Cu). Lam et al. (2020) reported a copper tailings site with 0.21 % chalcopyrite, 0.09 % chalcocite, and 0.10 % covellite. Thus, historical tailings sites can be used as a source of copper extraction if mineral species other than chalcopyrite are targeted. According to its chemical formula, it is worth mentioning that covellite has almost double the amount of copper that chalcopyrite. In this sense, even if the ore has a low level of covellite compared to chalcopyrite, it could provide a significant

amount of copper. For instance, Tian et al. (2020) reported on a mineral concentrate, wherein the copper-bearing minerals were mainly chalcocite (11 %), chalcopyrite (8 %), bornite (4.3 %), and covellite (1 %). The chalcocite, chalcopyrite, and bornite contributed 45.11 %, 29.6 %, and 15.72 % of the copper, respectively. Although the covellite only comprised 1%, it contributed 8.6% of the total copper in the concentrate. The relative level of covellite in the concentration allows us to identify the importance of this mineral as a copper supplier.

Interest in covellite has increased because it is utilized in optics—thanks to its excellent semiconductor properties—and as a cathode material, but this latter is usually synthetic covellite (Lotter et al., 2016; Yin et al., 2019). In spite of this, only a few studies have been dedicated to covellite flotation (Yin et al., 2019; Roos et al., 1990; Raju and Forsling 1991; Porento and Hirva, 2004). These works have taken different focuses: the electrochemical behavior of covellite when interacting with collectors, adsorption behavior when using adsorption density measurements, the effect of calcium hypochlorite ($\text{Ca}(\text{ClO})_2$) as a depressor on the flotation separation of covellite–pyrite, and a theoretical study of the interaction of surfactants on the covellite surface. Thus, there is a dearth of information about covellite flotation and the interaction mechanism between covellite and reagents (particularly collectors and pH modifiers). Consequently, the present work is focused on an adsorption study of collectors O-isopropyl-N-ethyl thionocarbamate (IPETC) and potassium amyl xanthate (PAX) at different pH levels on a covellite surface, using FT-IR, XPS characterization techniques, and computational modeling via the DFT method.

To understand the chemical interactions between covellite and collectors, we must discern the chemical properties and structure of covellite and the collectors under study. Several works have studied covellite's topological and electrochemical properties using modeling methods (Soares et al., 2016; Karikalan et al., 2017; Rosso and Hochella 1999; Kalanur and Seo 2018). Covellite has a complex structure with hexagonal symmetry, described as tetrahedral (CuS_4) and trigonal (CuS_3) (see Figure B.1) (Morales-garcia et al., 2014). The arrangements of atoms are generally analyzed along the (001) direction, where the trigonal planar arrangement is attributed to Cu(1)-S(1) bonding, and tetrahedral arrangement is attributed to Cu(2)-S(2) bondings, which relate to the following the sequence: (Cu(2)-S(2)₄)-(Cu(1)-S(1)₃)-(Cu(2)-S(2)₄). The Cu(1), Cu(2), S(1), and S(2) correspond to Cu(I), Cu(II), S^{2-} and S_2^{2-} , respectively. The disulfide bond (S(2)-S(2)) is covalent and Cu-S is ionic. The

cleave energy has a value between 0.1 and 1 J m⁻², and is used to identify the favored cleavage plane of a bulk surface. Smaller values are associated with the cleavage plane. This energy was calculated for the bulk surface of covellite along the (001) direction. The Cu(2)-S(1) bond has lower energy ($\gamma = 0.30 \text{ J m}^{-2}$). Then, the Cu(2) acquires a trigonal planar geometry (Cu(1)-S(1)₃); this could be why the oxidation state of covellite is defined as Cu(I) (Soares et al., 2016; Karikalan et al., 2017; Rosso and Hochella 1999).

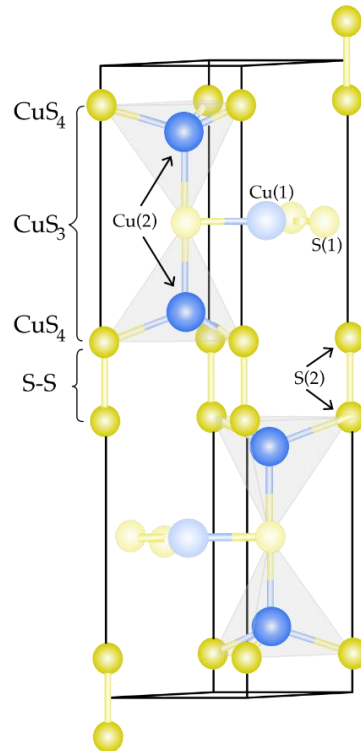


Figure B.1. Crystal structure of covellite. Spheres represent S(2) (dark yellow), S(1) (light yellow), Cu(2) (dark blue) and Cu(1) (light blue). (Adapted from Morales-Garcia et al., 2014).

Xanthate and thionocarbamate collector types are widely employed in copper mining. The IPETC is considered a selective collector, offering a higher selectivity against iron sulfides such as pyrite, and high chemical stability in a wide range of pH due to its $\text{pK}_a \geq 12$ (Fairthorne et al., 1996). The high selectivity is because the thionocarbamates do not form complexes with Fe^{2+} or Fe^{3+} in dilute aqueous solutions at pH 4.0 and 7.0. This is due to the low affinity of Fe^{3+} for ligands containing aliphatic nitrogen. As a result, this reagent gives excellent pyrite rejection (Ackerman et al., 1987). Also, the low affinity of iron ions with thionocarbamates could be linked to the band gap of the copper and iron atoms. For instance,

chalcopyrite has a narrow band gap making the back donation covalent bond stronger, while the pyrite has a broad band gap making the opposite manner (Porento and Hirva, 2002).

Furthermore, the IPETC contains N and S functional groups for chelation, making it an effective collector in terms of copper recovery (Buckley et al., 2014). Another characteristic of IPETC is that the O-alkyl group present in its composition influences the hydrophobicity of the collector, while the N-alkyl group controls the degree of reactivity towards the copper surface, which is affected by steric accessibility (Zhao et al., 2016; Ma et al., 2017). The electron-withdrawing substituents in N-alkyl groupings reduce the electrostatic effect and normal covalent bond, thereby reducing the reactive strength between sulfide minerals and collectors and improving the selectivity of collectors against iron sulfide minerals (Porento and Hirva, 2002).

PAX belongs to the xanthate family, commonly utilized as a bulk collector due to its comparatively lower selectivity. It is usually used in the flotation process in the scavenger stage. PAX is prepared by reacting n-amyl alcohol, carbon disulfide, and potassium hydroxide. The carbon disulfide promotes the hydrophobicity of the collector, and the long alkyl chain increases its collecting power (Ma et al., 2017; Mielczarski et al., 1989). Even though IPETC and PAX have been commonly employed in mineral processing, some unresolved questions exist concerning the type of species adsorbed, its adsorption mechanism, and the relationship between species adsorbed and floatability.

Recently, some computational methods have been explored to study the interaction between collector molecules and mineral surfaces (Porento and Hirva, 2002; Liu et al., 2017). DFT is a helpful tool utilized to study the electronic structures of molecules and their electron density in order to understand the adsorption ability of the collectors on the mineral surface (Liu et al., 2017). DFT has thus been used to study the adsorption mechanisms of different collectors on chalcopyrite. For instance, Liu et al. (2008) studied the collecting efficiency of two ether thionocarbamates, O-butoxy isopropyl-N-ethoxycarbonyl (BIPECTC) and O-(2-butoxy-1-methylethoxy) isopropyl-N-ethoxycarbonyl thionocarbamate (BMIPECTC), on chalcopyrite flotation. Using DFT, they performed frontier molecular orbital analysis, binding model simulation with copper ions, and molecular hydrophobicity analysis of each thionocarbamate. DFT calculations revealed that BMIPECTC has a higher reactivity and

interacts strongly with copper compared to BIPECTC. Additionally, Ma et al. (2017) studied the collector S-benzoyl O-isobutyl Xanthate (BIBX) in the selective flotation of chalcopyrite. They determined the chemical reactivity of the BIBX molecule using the concept of frontier orbitals (HOMO-LUMO), and found that the negative electrostatic potential is located on the C=S and C=O groups. Thus, the HOMO orbitals in BIBX were associated with sulfur atoms and the electron donor center of the BIBX (reactive sites in the molecule), and the presence of C=O in the BIBX increased the contribution of the LUMO orbital, thus increasing the scope for accepting electrons from copper. In another study by Liu et al. (2008) the frontier molecular orbitals and the atomic charges were calculated to study the reactivity of thionocarbamates containing different N-substituent groups. The collectors studied were O-isobutyl-N-ethyl-thionocarbamate (IBETC), O-isobutyl-N-allyl-thionocarbamate (IBALTC), O-isobutyl-N-acetyl-thionocarbamate (IBACTC) and O-isobutyl-N-ethoxycarbonyl-thionocarbamate (IBECTC). The HOMO orbitals suggested that the order of electron-donating capacity was IBETC > IBALTC > IBACTC > IBECTC, and the LUMO orbital suggested that the order of electron-accepting capacity was IBACTC \approx IBECTC > IBALTC > IBETC. This result implies that IBACTC and IBECTC react with copper through a normal covalent bond and a π -backdonation covalent bond. They concluded that such behavior is a result of the ability of copper to form a stable six-membered complex with these collectors, making the IBECTC and IBACTC more efficient collectors of copper sulfide minerals than IBETC and IBALTC. These results show the relevance and significant contribution of the DFT when used as a complementary tool to study collector–mineral systems.

To the best of the author's knowledge, no studies have yet been published on the surface interactions between collectors and covellite, particularly with IPETC and PAX collectors. Therefore, this work presents FT-IR and XPS characterization techniques supported by DFT computational modeling to provide detailed information on the behavior of the collector–covellite system, followed by experimental validation.

B.2 Materials and methods

B.2.1 Materials

The mineral sample of covellite was obtained from a local Chilean mine. The covellite was associated with gypsum and quartz, as will be shown later (Section 3.1) via X-ray diffraction (XRD) characterization. The initial covellite samples were approximately 12 x 15 cm in size. The samples were crushed using a jaw crusher (BB 250XL) with a jaw width of 120 x 90 mm and a gap width of setting 0-30 mm, until particles reached sizes below 1 cm. The covellite samples were further crushed by hand in an agate mortar for liberation, and were manually separated from the quartz and gypsum. The hand-picked covellite was dry-sieved to obtain different-size fractions. A coarse fraction (-2 mm +800 μm) was stored for use in the flotation test. Prior to each microflotation test, the necessary quantity of this fraction was grounded in an automatic agate mortar to obtain $P_{80} = 100 \mu\text{m}$.

The reagent employed for the microflotation and adsorption experiments was ultra-pure water (UPW), obtained using a MilliQ water purifier at a resistance of 18.2 M Ω . Sodium hydroxide (NaOH) of analytical grade was purchased from Ward's science and used to prepare an aqueous solution (0.01 M) as the pH regulator. IPETC and PAX were supplied by Qingdao Sunrun Chemical Co., Ltd. (China) at a nominal purity of $\geq 95 \%$ and $\geq 90 \%$, respectively. Finally, as mentioned, covellite was associated with gypsum. Therefore, to conduct the FT-IR and XPS characterization, it was necessary to wash the covellite to dissolve the gypsum present. Then, for each experiment, 1 g of covellite was placed in a beaker with 150 ml of ultra-pure water, stirred at 1000 rpm for 30 minutes, and filtered (this process was repeated twice). Then, the filtered mineral was dried at 40 °C in a vacuum oven for 24 hours.

B.2.2 Methods

B.2.2.1 Covellite characterization

The mineralogical phase of covellite was identified by X-ray diffraction (XRD) in a PANalytical device, model XPERT PRO MPD Alpha 1, equipped with an X-ray source (Cu), monochromator (K-alpha) and detector (PIXcel1D, 45 kV, 40 mA). The analysis was performed in a 2θ range from 10° to 100° degrees. The morphological surface of covellite was characterized by scanning electron microscopy (SEM) with an EDS detector in a Hitachi Bruker detector, model SU5000, series 6. It was operated at 20 kV, taking images at 2500X using back-scattered electron (BSE) imaging. Microanalysis by X-ray dispersive

spectroscopy (EDS) was performed to obtain the semiquantitative chemical composition. The adsorption was studied by FT-IR on a JASCO model FT-IR-4600, with a resolution of 0.7cm^{-1} , and ATR-IR accessory, in a spectral range of $4000\text{--}400\text{ cm}^{-1}$ using a germanium crystal for opaque minerals. XPS was used for the adsorption analysis in a Kratos Axos Ultra, with monochromatic Al $K\alpha$ radiation and 20 eV pass energy. The binding energies were calibrated based on the C 1s peak (284.8 eV). Accurate curve-fitting analyses of the high-resolution Cu 2p, S 2p, O 1s, and C 1s were performed using CasaXPS software.

B.2.2.2 Microflotation test

Microflotation tests were carried out using a modified Hallimond-type flotation cell manufactured in-house. The operational parameters were as follows: 150 mL cell volume, 1 g of covellite previously grounded with a size fraction of $-74 +38\ \mu\text{m}$ were used per test, $\text{N}_2 = 33\ \text{mL}/\text{min}$ nitrogen flow rate, and magnetic stirring between 1000 and 1200 rpm. The conditioning time was performed into a 200 ml beaker to ensure proper mixing. The conditioning time of 15 min was used for the collectors and 10 min for pH control. Afterward, the treated mineral was transferred into the Hallimond tube for flotation. The flotation time was 3 minutes. The pH values tested were 8, 9.5, and 11, controlled using a 0.01 M NaOH solution as the pH regulator. These pH values were selected because this pH range is typical in copper flotation operation. Three different collector concentrations were employed: 2×10^{-5} , 4×10^{-5} , and $6 \times 10^{-5}\ \text{mol}/\text{L}$. The tests were performed in duplicate. Figure B.2 shows the flowsheet for the microflotation tests.

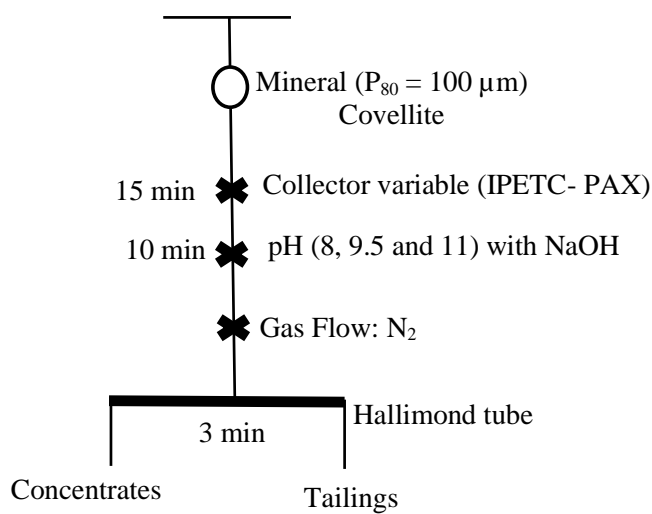


Figure B.2. Flowsheet of microflotation test using a modified Hallimond-type flotation cell.

B.2.2.3 Adsorption tests

Adsorption tests were carried out to study the chemical interaction between the covellite surface and each collector species. For the XPS analysis, 1 g of fine-fraction covellite (-53 μm) was added in ultrapure water and mixed with the collectors (IPETC and PAX) at a concentration of 1×10^{-3} mol/L at pH 8 and 11. After 30 minutes of stirring, the mineral slurry was washed once with ultrapure water, filtered, and dried at 40 °C in a vacuum oven for 24 h. The powder thus obtained was analyzed by XPS. The same adsorption procedure was employed for the FT-IR analysis, although in this case, the covellite particles were grounded in an automatic agate mortar to a particle size of $\leq 10 \mu\text{m}$.

B.2.2.4 Computational methods

The geometries of collectors IPETC and PAX and their corresponding complexes with Cu(I) and Cu(II) cations were optimized using the DFT method (Ma et al., 2017; Mielczarski et al., 1989), with the hybrid exchange–correlation functional B3PW91[26] and the basis set 6-31g(d) (Perdew and Wang, 1999; Rassolov et al., 1998), using Gaussian 09 computational chemistry software (Huzinaga 2012; Frisch et al., 2016). The Polarizable Continuum Model using the integral equation formalism variant (Dennington et al., 2016) was adopted to calculate the properties of molecules in an aqueous solution. The binding model and molecular energy were calculated with the same basis set. The Avogadro package (Tomasi et al., 2005) was employed for drawing, and we pre-optimized the initial molecular structures through molecular mechanics using the Universal Force Field (UFF) (Hanwell et al., 2012).

B.3 Results and discussion

B.3.1 Covellite characterization

The XRD spectrum of the covellite sample is shown in Figure B.3. It shows crystalline covellite with the most intense peaks at (006), (103), (102), (110), (108), (116), (100), and (101). It showed an amorphous structure, with the peaks indexed in the graph with rhombus symbols (Rappe et al., 1992). The presence of gypsum was identified via the high peak position of $2\theta = 12^\circ$ and some less intense peaks between 20 and 25 degrees (circles). The composition of this mineral is 83% covellite and 17% gypsum.

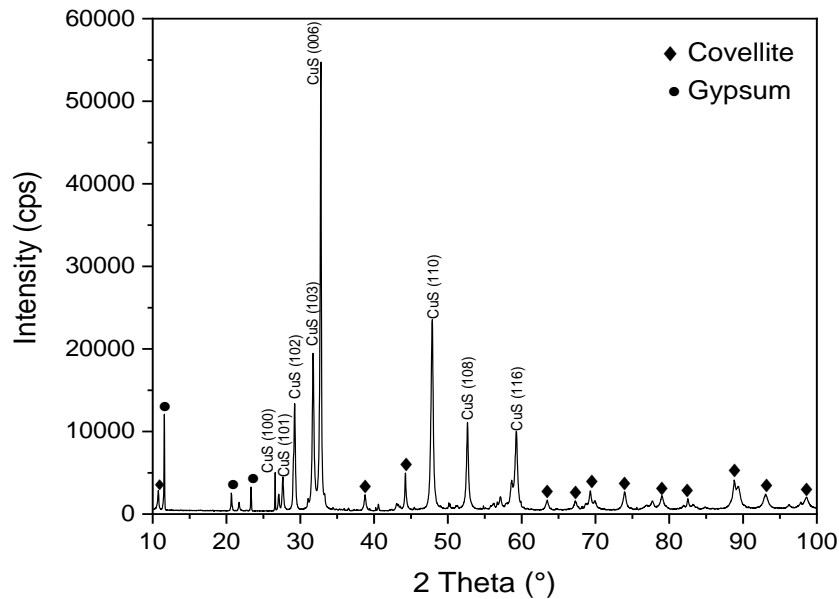


Figure B.3 X-ray diffraction pattern corresponding to covellite.

The morphology and different mineralogical phases are shown in Figure B.4a-g. Figure B.4a presents the EDS analysis of the covellite; the elements present were Cu (50.3%), Ca (4.3%), S(28.7%), Si(3.7%), and O (13%). Other mineral phases associated with covellite, such as $\text{CaSO}_4 \cdot 2\text{H}_2\text{O}$ and SiO_2 , were also identified. These results corroborate the XRD findings, although SiO_2 was not recognized by the latter. This is perhaps due to the low SiO_2 concentration, below the limit of detection in XRD. Additionally, Figure B.4c-g depict elemental mapping, differentiating how the elements Cu, Ca, S, Si, and O are distributed. This analysis shows that even after the mineral preparation described in Section 2.1, the covellite used for microflotation testing had Ca- and Si-containing impurities.

B.3.2 Microflotation test

First, covellite microflotation tests were carried out without a collector at pH 8, 9.5, and 11. The results indicate that the natural floatability of covellite is not pH-dependent in this range, with an average recovery of approximately 53 ± 2 %. Then, microflotation tests using collectors were performed at the same pH values and collector concentrations of 2×10^{-5} , 4×10^{-5} , and 6×10^{-5} mol/L. The collector had a marked effect on the covellite flotation, as the recovery increased to 88-93%. Additionally, covellite flotation was not pH-dependent. As seen in Table B.1, the covellite recovery increased significantly with higher collector

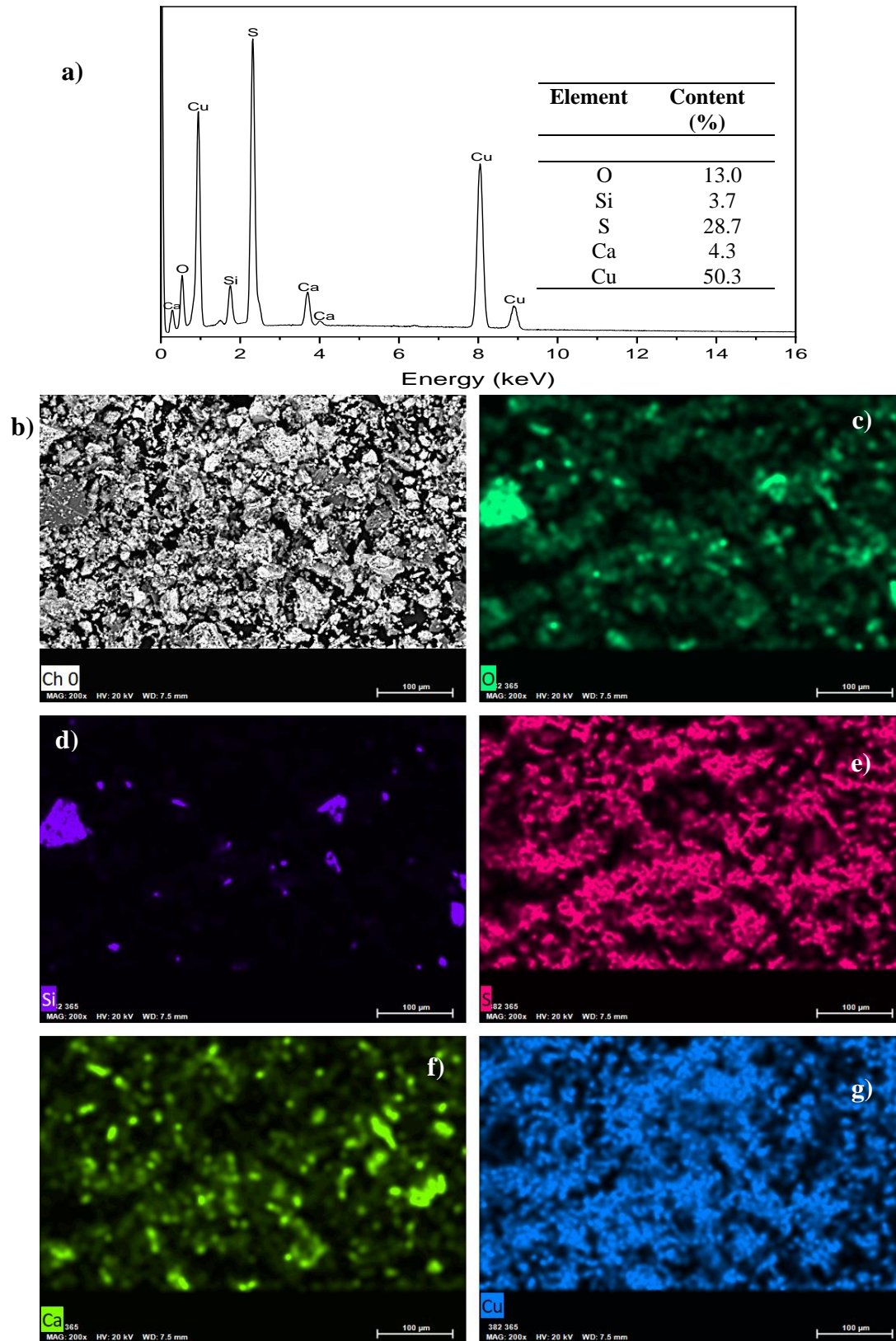


Figure B.4. SEM images of covellite: a) EDS elemental analysis; b) BSE covellite image; from c) to g) elemental mapping.

concentrations. At 6×10^{-5} mol/L of IPETC, for example, the recovery increased by 10% compared with 2×10^{-5} mol/L, while the difference in recovery using PAX was 13%.

B.3.2 Microflotation test

First, covellite microflotation tests were carried out without a collector at pH 8, 9.5, and 11. The results indicate that the natural floatability of covellite is not pH-dependent in this range, with an average recovery of approximately 53 ± 2 %. Then, microflotation tests using collectors were performed at the same pH values and collector concentrations of 2×10^{-5} , 4×10^{-5} , and 6×10^{-5} mol/L. The collector had a marked effect on the covellite flotation, as the recovery increased to 88-93%. Additionally, covellite flotation was not pH-dependent. As seen in Table B.1, the covellite recovery increased significantly with higher collector concentrations. At 6×10^{-5} mol/L of IPETC, for example, the recovery increased by 10% compared with 2×10^{-5} mol/L, while the difference in recovery using PAX was 13%.

Table B.1. Covellite recovery (mean values and standard error) in microflotation tests without collector, covellite–IPETC, and covellite–PAX.

Collector concentration (mol/L)	Covellite recovery (%)			
	pH			
	8	9.5	11	Average
Non-collector	54 ± 2	51 ± 3	54 ± 1	53 ± 2
IPETC				
2×10^{-5}	78 ± 1	76 ± 2	79 ± 1	78 ± 2
4×10^{-5}	84 ± 1	85 ± 3	88 ± 3	86 ± 3
6×10^{-5}	89 ± 2	87 ± 3	87 ± 2	88 ± 2
PAX				
2×10^{-5}	75 ± 3	81 ± 1	83 ± 2	80 ± 4
4×10^{-5}	89 ± 3	88 ± 3	86 ± 1	88 ± 2
6×10^{-5}	93 ± 2	94 ± 2	93 ± 3	93 ± 2

These results show a clear interaction between the PAX and IPETC collectors and covellite surfaces. To better understand the nature of such interactions, FT-IR and XPS characterization supported by DFT computational modeling are presented in the following sections.

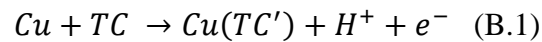
B.3.3 FT-IR characterization

Figure B.5 shows the FT-IR spectra for IPETC, covellite, washed covellite, covellite with IPETC at pH 8 (covellite+IPETC-8), and covellite with IPETC at pH 11 (covellite+IPETC-11), respectively. The IPETC spectrum shows a high frequency, resulting from the NH stretching vibration at 3278 cm^{-1} . Then, in the region 3000 to 2800 cm^{-1} , the bands correspond to the -C-H group (CH_3 at 2984 cm^{-1} , CH_2 at 2937 cm^{-1} , and CH_3 at 2875 cm^{-1}) (Cabrera-German et al., 2019). The broad bands between 1700 and 1600 cm^{-1} correspond to the C=C group. The intense band at $\sim 1520\text{ cm}^{-1}$ is due to -C(=S)-NH group vibration (Fairthorne et al., 1996; Cabrera-German et al., 2019). The bands at 1360 - 1300 cm^{-1} are attributable to CN stretching, NH deformation, and CH deformation. The peaks at 1176 and 1142 cm^{-1} correspond to COC and CNC asymmetric stretching, respectively (Cabrera-German et al., 2019). Bands at 1230 - 1210 cm^{-1} are also present in the spectrum, corresponding to O-C=S asymmetric vibration, and 1110 cm^{-1} is attributed to O-C=S symmetric vibration (Fairthorne et al., 1996). The CN, C=S , and CH vibrations are represented by the 1100 - 1090 cm^{-1} bands. Finally, the C=S group is shown at 1050 cm^{-1} , and the C-S groups at 1050 and 725 - 590 cm^{-1} (Hope et al., 2004; Leppinen et al., 1988; Bu et al., 2018; Mayo et al., 2004).

The covellite spectrum shows a band at 618.3 cm^{-1} corresponding to the stretching vibrations of Cu-S (Karikalán et al., 2017). The presence of gypsum ($\text{CaSO}_4 \cdot 2\text{H}_2\text{O}$) on the surface of covellite sample was again corroborated. Strong bands were observed at 1100 cm^{-1} and 696 cm^{-1} , associated with the tetrahedral group SO_4^{2-} of gypsum vibrations (Schrader, 1995; Bishop et al., 2014). The washed covellite reveals a spectrum without the interference of gypsum. Here, the bands at 1100 cm^{-1} and 696 cm^{-1} disappear. These results could be explained based on the study executed by Yuan et al. (2010), where the solubility of calcium sulfate dihydrate ($\text{CaSO}_4 \cdot 2\text{H}_2\text{O}$) and the effect of NaOH solution was studied. At room temperature ($20\text{ }^\circ\text{C}$), gypsum's solubility is 2.1 g/L . Since in our work 1 g of covellite (including ca. 17% gypsum) was used for the adsorption test, the total solubilization of gypsum would require 81 mL of water—a considerably lower volume than that used in the test (i.e., 150 mL). Another important aspect is the effect of NaOH on gypsum solubility. Yuan et al. (2010) demonstrated that NaOH, in the concentration range utilized in our work, further increases the solubility of gypsum. Therefore, the formation of Ca(OH)_2 precipitate

in the slurry is unlikely. This analysis suggests that the gypsum does not interfere with the adsorption of the collectors on the covellite surface.

As seen in Figure B.5, both the covellite+IPETC-8 and covellite+IPETC-11 spectra reflect IPETC adsorption on the covellite surface. Additionally, according to the Pourbaix diagram of covellite, in the pH range of 8-11, solid species Cu_2O and $\text{Cu}(\text{OH})_2$ could be formed at potentials higher than zero (positive potentials) (Marin et al., 2020). Nevertheless, the FT-IR shows no bands between 3650 and 3200 cm^{-1} corresponding to the OH group in both spectra. Therefore, the pulp potential could occur below this value, which is why the collector-adsorbed species on the covellite surface do not appear to be pH-dependent. A similar interaction between collector and covellite at this pH range would explain the results obtained in the microflotation tests (Section 3.2). The band at $\sim 1590 \text{ cm}^{-1}$ present in both spectra is due to the adsorption of $-\text{C}(=\text{S})-\text{NH}$ group vibration. The peaks at 3000 to 2800 cm^{-1} are bands of the $-\text{C}-\text{H}$ group corresponding to the collector adsorbed onto covellite. The bands between 1360 and 1300 cm^{-1} are due to NH and CH deformation, the 1176 cm^{-1} band is due to COC, and 1142 cm^{-1} is related to the CNC of the adsorbed collector. Nevertheless, the characteristic NH stretching band (3278 cm^{-1}) of IPETC is absent from both spectra. The absence of this band could be due to the formation of $\text{Cu}(\text{IPETC}')$ as a result of an anodic oxidation process involving the release of H^+ from the NH group (see Eq. 1). In Eq. 1, TC is a thionocarbamate, and TC' is a molecule without the hydrogen removed from the nitrogen atom (Ackerman et al., 1987; Cabrera-German et al., 2019). Table B.2 summarizes all the peaks indexed in the spectra.



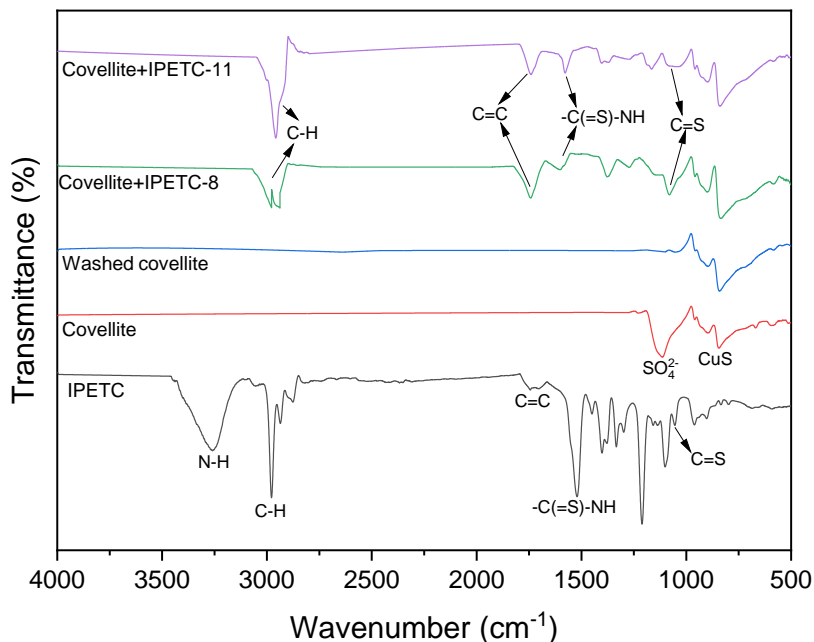


Figure B.5. Infrared spectra of covellite before and after treatment with IPETC at pH 8 and 11.

Figure B.6 exhibits the FT-IR spectra for PAX, covellite, washed covellite, covellite with PAX at pH 8 (covellite+PAX-8), and covellite with PAX at pH 11 (covellite+PAX-11), respectively. The PAX spectrum is in the region between 3000 and 2800 cm^{-1} , with bands corresponding to the $-\text{C}-\text{H}$ group (CH_3 at 2984 cm^{-1} , CH_2 at 2937 cm^{-1} , and CH_3 at 2875 cm^{-1}) (Cabrera-German et al., 2019; Mayo et al., 2004). The band at 1750 cm^{-1} corresponds to $\text{C}=\text{O}$ binding (bind type ketone/ aldehyde; this bind is characteristic of PAX because one of the reagents used to prepare the PAX is n-amyl alcohol). The bands at 1490-1000 cm^{-1} and the intense band at 1070 cm^{-1} correspond to $\text{C}=\text{S}$ vibration (carbon disulfide) (Marin et al., 2020; Little et al., 1961). The covellite and washed covellite spectra show the same gypsum solubilization behavior as was aforementioned.

The covellite+PAX-8 and covellite+PAX-11 spectra show PAX adsorption on the covellite surface. Additionally, the collector adsorption on the covellite surface is not pH-dependent for both spectra, as was explained before for the IPETC. This confirms the result obtained in the microflotation test, and the same behavior is shown for IPETC. The region between 3000 and 2800 cm^{-1} present in both spectra is related to the adsorption of $-\text{C}-\text{H}$ group vibration, while 1750 cm^{-1} corresponds to $\text{C}=\text{O}$ adsorption. The region between 1400 and 1000 cm^{-1} refers to several interactions between covellite and PAX. To better identify these bands, the

right side of Figure B.6 shows a closer view of this region so as to show the species formed more clearly. The enhanced area presents the frequencies for the PAX, Cu-amylxanthate (CuAX) and dixantogen (AX)₂ formed. Under COC stretching vibration, (AX)₂ was identified in the bands at 1367-1290 cm⁻¹, 1242-1239 cm⁻¹, 1150 cm⁻¹, and 1109-1108 cm⁻¹. CuAX was identified at 1190-1189 cm⁻¹ and 1125 cm⁻¹. PAX appeared at 1173 cm⁻¹ and 1100 cm⁻¹. Under C=S stretching vibration, the (AX)₂ was identified at 1025 cm⁻¹ and the PAX was identified at 1052-1049 cm⁻¹ (Shankaranarayana and Patel, 1961; Chandra and Gerson 2009). Table B.2 summarizes all the peaks indexed in the spectra.

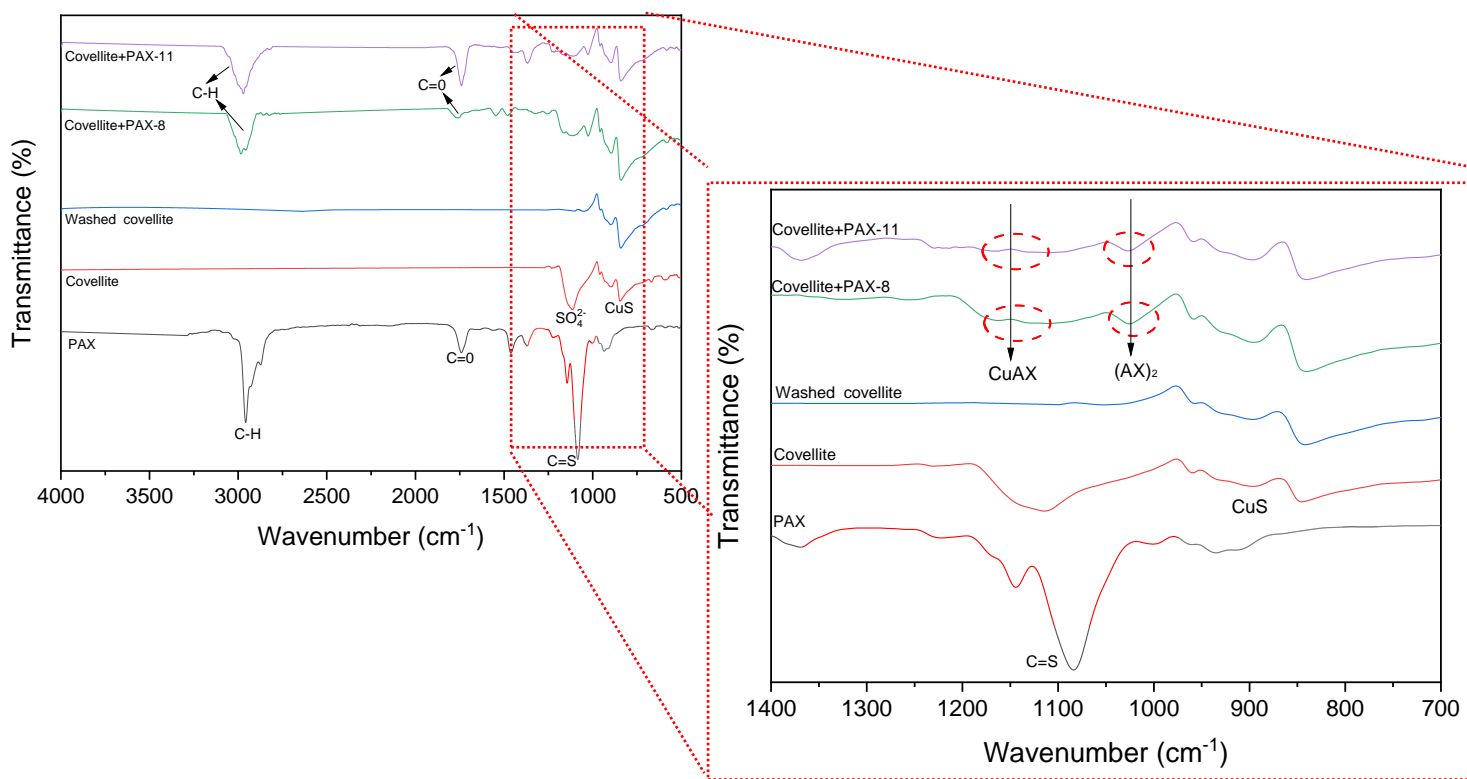


Figure B.6. Infrared spectra of covellite before and after treatment with PAX at pH 8 and 11. Enhanced image shows Cu-amylxanthate (CuAX) and dixantogen (AX)₂.

Therefore, the active hydrophobic species on the covellite surface responsible for covellite flotation are the metal xanthate (MX) and the dixantogen (X₂). The formation of these two species could be due to the solubility of the covellite, which at pH 5.3 is 4×10^{-3} mol/L. This solubility is high compared to the solubility of other copper sulfides such as chalcopyrite (3.3×10^{-4} mol/L.) and chalcocite (2.6×10^{-5} mol/L). Thus, these solubilized ions can cause the rapid oxidation of xanthate to dixanthogen. So, large quantities of X₂ from the PAX in the

Table B.2. The peak position of FT-IR obtained for covellite, washed covellite, covellite – IPETC, and covellite–PAX

	Functional group	Initial peak position (cm ⁻¹)	Final peak position (cm ⁻¹)	Reference
Covellite	Cu–S	618.3		a
	SO ₄ ²⁻	1100 and 696		b,c
Washed covellite	Cu–S	618.3		a
	SO ₄ ²⁻	absent		
IPETC	NH	3270		d
	CH ₃	2984		
	CH ₂	2937		
	CH ₃	2875		
	C=C	1700-1600		e ,d
	–C(=S)–NH	~ 1520		
	CN, NH and CH	1360-1300		
	COC (asym)	1176		
	CNC (asym)	1142		
	O–C=S (asym)	1230-1210		
	O–C=S (sym)	1110		
	CN, C=S and CH	1100-1090		
	C=S	1050		f, g
Covellite+IPETC-8 and Covellite+IPETC-11	–C(=S)–NH		~1590	h,d
	–CH		3000-2000	
	NH, CH		1360-1300	
	COC		1176	
	CNC		1142	
PAX	NH		absent	
	CH ₃	2984		d,g
	CH ₂	2937		
	CH ₃	2875		
	C=O	1750		
	C=S	1490-1000, 1070		i,j
Covellite+PAX-8 and Covellite+PAX-11	–CH		3000-2800	k,l
	C=O		1750	
	(Vibrational mode COC):			
	(AX) ₂		1367-1290, 1242-1239, 1150	
	CuAX		1190-1189, 1125	
	PAX		1173-1100	
	(Vibrational mode C=S):			
	(AX) ₂		1025	
	PAX		1052-1049	

a: Karikalan et al., 2017; b: Bishop et al., 2014; c: Marvin 1955 ; d : Hope et al., 2004 ; e : Fairthorne et al., 1996 ; f :Leppinen et al., 1988 ; g :Schrader 1995 ; h : Buckley et al., 2014 ; i : Marin et al., 2020 ; j : Little et al., 1961 ; k : Chandra and Gerson, 2009 ; l : Peng et al. 2017.

solution are formed, which could then co-adsorb with the MX on the covellite surface and reinforce collection. The adsorption mechanism could be through the electron-donating (reducing reaction) of PAX and chemisorption onto covellite surface. Therefore, the PAX is a reducing agent (Lotter et al., 2016; Ackerman et al., 1987).

B.3.4 XPS characterization

XPS measurements were performed to determine the surface composition of the covellite and its oxidation state, as well as to investigate the adsorption mechanism of the collectors IPETC and PAX on the covellite surface. According to the XRD and FT-IR results detailed in sections 3.1 and 3.3, the covellite samples have traces of gypsum. Therefore, two samples were analyzed—covellite and washed covellite—to see if the gypsum was solubilized or if this specie influences covellite's behavior when interacting with collectors.

Figure B.7 presents the high-resolution XPS spectra of Cu 2p, S 2p, O 1s, and C 1s in covellite and washed covellite. The Cu 2p spectrum shows the leading peaks of covellite. A single sharp peak at 932.14 eV could be due to CuS(I). The binding energy position at 933.12 eV may be related to the CuS(II). This signal is accompanied of characteristics satellites that are located in the energy range of 944-941 eV, these are the signature of Cu(II) (Cabrera-German et al., 2019; Folmer and Jellinek, 1980). Also, the peak located at 934.65 eV may be attributed to the Cu(OH)₂. The lower intense peak at 936.04 could be associated with CuSO₄ (Peng et al., 2017; Folmer and Jellinek, 1980; Klopogge and Wood, 2020). These results demonstrate that although Cu(I) has been typically considered the main oxidation state of covellite, the covellite remains with the oxidation state of Cu(II) (Cabrera-German, 2019; Goh et al. 2006). Nevertheless, once the covellite was washed, its spectrum was shifted to the right at a lower binding energy (see Cu 2p spectrum). The shift at lower binding energy may be related to the change of the local environment of Cu(I) atoms upon crystallization of the copper sulfide (Cabrera-German et al., 2019; Thermo scientific; NIST X-Ray, 2000; X-rayPhotoelectron). Finally, these results suggest that covellite is comprised of copper ions with mixed-valence states of +1 and +2 (Kalanur and Seo 2018; Cabrera-German, 2019; Goh et al., 2006).

The S 2p spectrum of covellite presents two main doublets. The minor doublet could be fitted at 161.28 eV, related to sulfide (S^{2-}), and a predominant doublet at a binding energy of 162.18 eV associated with disulfide (S_2^{2-}). A third doublet located at 163.3 eV may be related

to nonstoichiometric sulfides (S_x^{2-}) or elemental sulfur (S^0) (Nakai et al., 1978), while the peak located at 169.6 eV may be related to sulfides derived from gypsum (SO_4^{2-}) (Kloprogge and Wood, 2018; Kalanur and Seo, 2020; Kundu et al., 2008). The washed covellite spectrum present the peaks associated with sulfide (S^{2-}) at 161.27 eV and disulfide (S_2^{2-}) at 162.23 eV both of them characteristic of the covellite structure (Cabrera-German, 2019; Thermo scientific; Goh et al., 2006). Here, it is corroborated that the gypsum was solubilized because the peak around 169.6 eV disappeared.

The O 1s spectrum of covellite shows a peak at 531.54, which may be related to metal(OH)_x (Cu(OH)₂). Additionally, the intense peak located at 532.54 may be related to SO_4^{2-} . This species could be due to the covellite oxidation or the gypsum present in the covellite. The signal between 533 and 534 eV may be due to the adsorbed H₂O at the surface. The washed covellite spectrum shows a peak related to copper oxide at 529.68 associated with CuO. Also, the intensity of peaks related to the water in washed covellite are higher than covellite (Cabrera-German, 2019; Kloprogge and Wood, 2020; Goh et al., 2006; X-ray photoelectron; Biesinger et al., 2010).

The C 1s spectra show that the covellite and washed covellite have the same peaks, and both of them have been exposed to the atmosphere, as we detected adventitious carbon contamination at 284.7 eV. Also, the C-H was identified at 282.30 related to the carbide (X-ray photoelectron; NIST X-ray; X-ray photoelectron). Table B.3 displays the binding energies of each species formed.

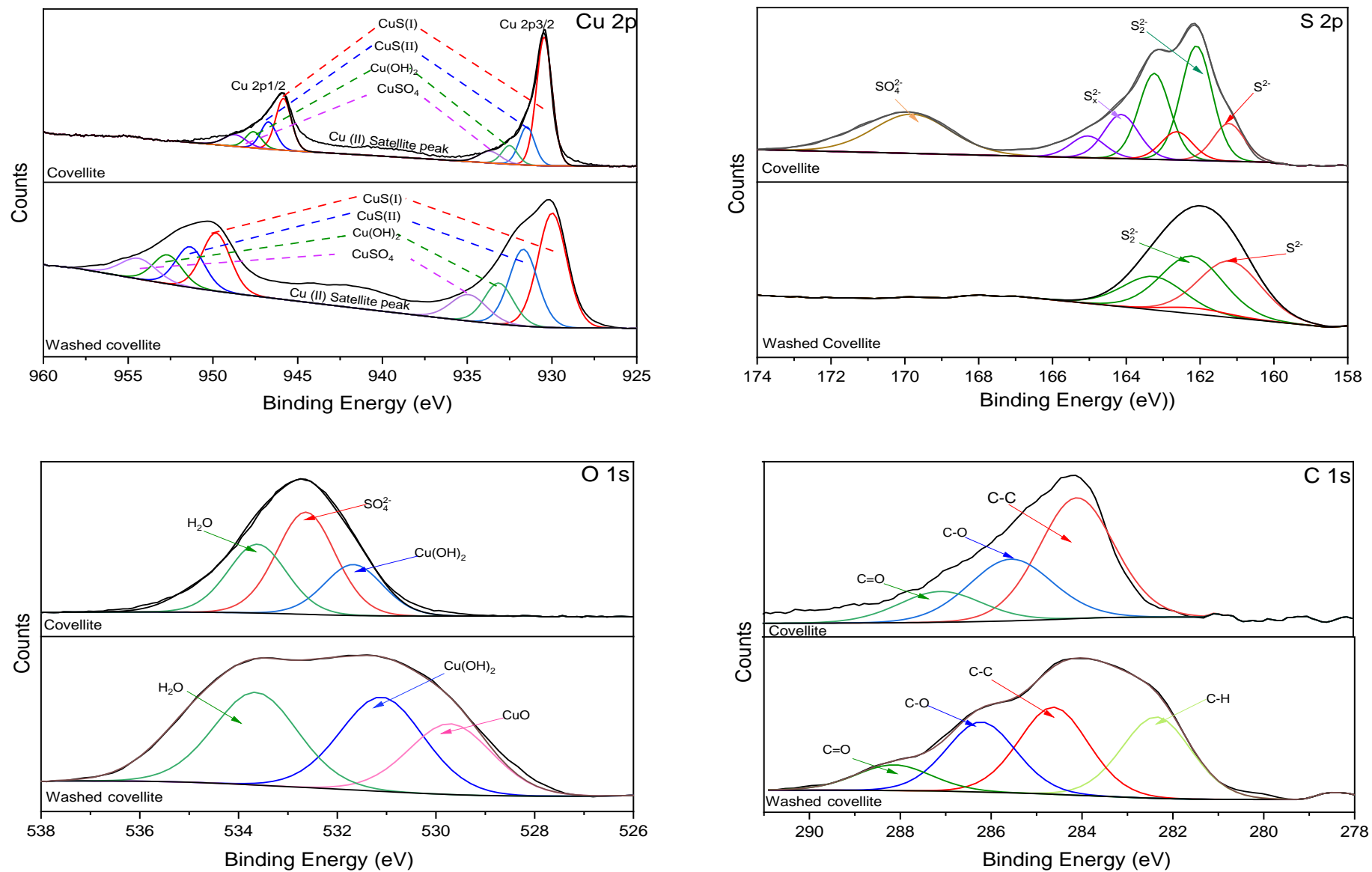


Figure B.7. Cu 2p, S 2p, O 1s, and C 1s XPS spectra recorded on the surface of covellite and washed covellite.

Figure B.8 presents the high-resolution XPS spectra of Cu 2p, S 2p, O 1s, and C 1s of washed covellite, covellite treated with PAX (PAX-11), and covellite treated with IPETC (IPETC-11). A collector adsorption test was performed with each collector at pH 8 and 11. The results show no relevant difference between the behaviors of covellite with PAX at pH 8 and pH 11. This could be because the intensity of metal-hydroxide ($\text{Cu}(\text{OH})_2$) and CuO are not relevant in the spectrum O 1s at 531.40 and 529.68 eV, respectively. It is worth mentioning that the scale of this spectrum was maximized to enlarge the spectrum and better identify the species. The same behavior was observed for IPETC. Therefore, XPS analysis was carried out with PAX and IPETC at pH 11. The spectrum of washed covellite was used to analyze the adsorption mechanism of each collector on the covellite surface. The atomic concentrations of Cu 2p, S 2p, O 1s, and C 1s of washed covellite, covellite treated with PAX, and covellite treated with IPETC. The S to Cu atomic concentration ratio was 1.0, according to the stoichiometry of covellite. The increase in the atomic concentrations of C 1s and S 2p confirms the adsorption of PAX on the covellite's surface. The increase in the atomic concentrations of Cu 2p, S 2p, and C 1s confirms the adsorption of IPETC on the covellite's surface. Additionally, these results show that most of the calcium belonging to gypsum was solubilized.

The mechanism of adsorption of PAX on the covellite surface is principally through Cu 2p, C 1s, and S 2p. The Cu 2p spectrum shows a single sharp peak at 932.2 eV, this signal may be related to the CuS(I) and a minor peak at 933.6 eV may be related to Cu(II). Besides, the absence of the satellites peaks of Cu(II) corroborated that the oxidation state of covellite with PAX is Cu(I). These results confirm that the xanthates are reducing agents because the Cu(II) was reduced to Cu(I) (Acketman et al., 1987). This finding was corroborated by FT-IR by the identification of Cu-amyloxanthate (CuAX) and dixantogen $(\text{AX})_2$ on the covellite surface. The C 1s of washed covellite has an atomic concentration of 15.52%. Then, after treatment with PAX, the atomic concentration of C 1s is 48.6%. These results reveal that Cu atoms can be bonded to the -C site through C-S and C=S groups. Additionally, the S 2p spectrum shows a well-defined doublet at 162.0 eV related to S_2^{2-} . This result suggests that the interaction between PAX with covellite surface is stronger through the disulfide rather than monosulfide. Also, it was corroborated that the gypsum was solubilized because the peak around 169 eV disappeared. Thus, this species does not interfere with the collector adsorption.

The adsorption mechanism of IPETC on the covellite surface could be explained via the atomic concentrations of Cu 2p and S 2p, which increase once the covellite is treated with IPETC. This suggests the bind is facilitated by the S of the collector with Cu atoms on the covellite surface. Moreover, the S 2p spectrum of covellite treated with IPETC displays a principal doublet at 162.18 eV attributed to S_2^{2-} (C=S functional group), as observed for thiourea. Then, at 161.28 eV, we find the peak characteristic of covellite, which is S^{2-} , and the minor doublet at 164.18 eV could be attributed related to elemental sulfur (S^0) or nonstoichiometric sulfides (S_x^{2-}). The peak at 169.46 eV is attributed to SO_4^{2-} , which could be related to the gypsum. The Cu 2p spectrum shows a single sharp peak at 932.3 eV related to the CuS(I), also a peak at 933.50 eV attributed to the CuS(II), this signal is accompanied by the characteristic satellites that are located in the range 944-941 eV, signature of the Cu(II). Also, the peak at 934.50 related to Cu(OH₂) was identify (Biesinger et al., 2010). The NH functional group was not identified by XPS characterization (the N 1s spectrum did not show any signal). Finally, we see slight adsorption of IPETC by O 1s and C 1s (the scale of this spectrum was maximized to enlarge the spectrum and better identify the species), which could be negligible. Table B.3 summarizes all the binding energies peaks indexed in the spectra.

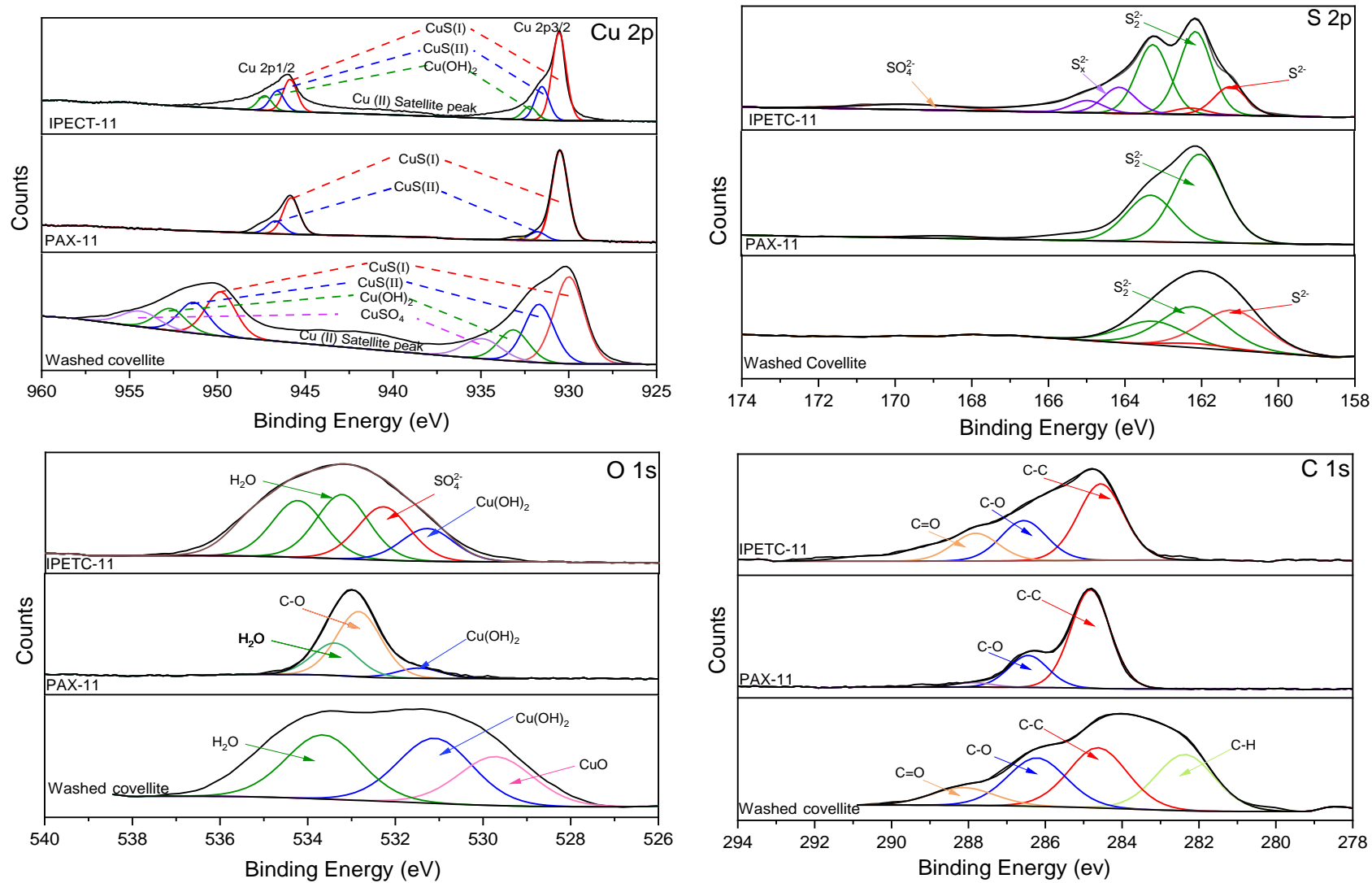


Figure B.8. Cu 2p, S 2p, O 1s and C 1s XPS spectra recorded on the surface of washed covellite, covellite treated with PAX and IPETC at pH 11.

Table B.3. Binding energies (BE) position of the leading peaks in the Cu 2p, S2p, O1s and C1s high resolution spectra obtained for covellite, washed covellite, IPETC-11 and PAX-11

Sample	Cu 2p (eV)		S 2p (eV)		O 1s (eV)		C 1s (eV)	
	Specie	Peak position	Specie	Peak position	Specie	Peak position	Specie	Peak position
Covellite	CuS(I)	932.14	S ²⁻	161.28	Cu(OH) ₂	531.54	C-C	284.70
	CuS(II)	933.12	S ₂ ²⁻	162.18	SO ₄ ²⁻	532.54	C-O	286.00
	Cu(OH) ₂	934.65	S _x ²⁻	163.30	H ₂ O	533.64	C=O	287.60
	CuSO ₄	936.04	SO ₄ ²⁻	169.60				
	Cu(II) satellite	941-944						
Washed covellite	CuS(I)	930.65	S ²⁻	161.27	CuO	529.68	C-H	282.50
	CuS(II)	931.70	S ₂ ²⁻	162.23	Cu(OH) ₂	531.40	C-C	284.80
	Cu ₂ O	933.17	S _x ²⁻	absent	H ₂ O	533.70	C-O	286.29
	CuO/CuSO ₄	935.00	SO ₄ ²⁻	absent			C=O	288.20
	Cu(II) satellite	941-944						
IPETC-11	CuS(I)	932.30	S ²⁻	161.28	Cu(OH) ₂	531.38	C-C	284.70
	CuS(II)	933.50	S ₂ ²⁻	162.18	SO ₄ ²⁻	532.28	C-O	287.80
	Cu(OH) ₂	934.50	S _x ²⁻	164.18	H ₂ O	533.29	C=O	286.60
			SO ₄ ²⁻	169.46	H ₂ O	534.32		
PAX-11	CuS(I)	932.20	S ₂ ²⁻	162.00	Cu(OH) ₂	531.5	C-C	284.80
	CuS(I)	933.6			C-O	533.0	C-O	286.60
					H ₂ O	533.5		

B.3.5 Molecular modeling

It is possible to identify points of activity in the collectors' structures that optimize their molecular geometry and calculate the molecular electrostatic potential to predict the reactive sites of collectors (positive, negative, or neutral electrostatic potential). Moreover, the frontier molecular orbital (FMO) can be determined via the highest occupied molecular orbital (HOMO) and lowest unoccupied molecular orbital (LUMO), which reflect the donor and receptor capacity of the collector, respectively. HOMO is the electron donor, and LUMO is the electron acceptor. The smallest energy gap between HOMO and LUMO ($\Delta E_{HOMO-LUMO}$) means that the chemical reactivity here is strongest (less stable), which increases the ability of the collector to interact with the mineral surface. Additionally, the HOMO–LUMO orbitals allow for calculating the global reactivity descriptors using DFT calculations. The global reactivity descriptors are electrophilicity (ω), which determines the system's chemical reactivity, and electrochemical potential (μ), which describes the charge transfer within a system. Compounds with greater μ are more reactive than those with a low

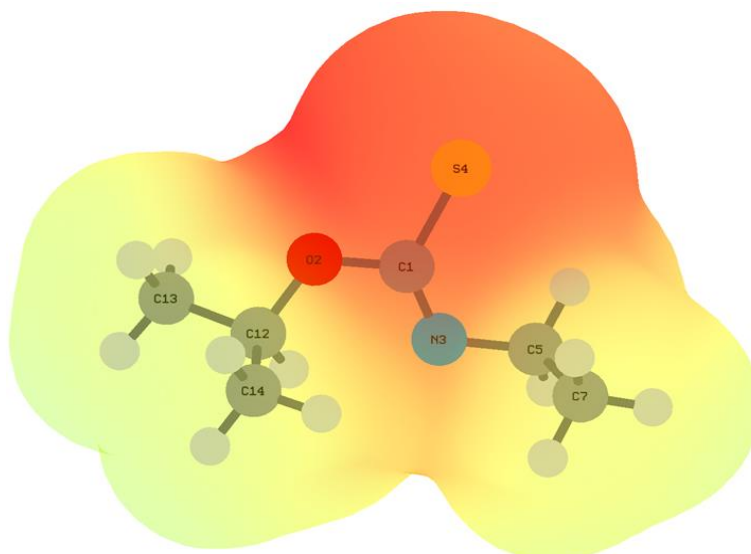
μ . The hardness (η) and softness (S) are related to the HOMO–LUMO energy gap. When the HOMO–LUMO energy gap is high, the molecule is more stable and chemically harder than molecules with a small HOMO–LUMO energy gap. The last descriptor is electronegativity (χ), which measures the molecule's ability to attract electrons to itself (Kundu et al., 2008; Ávila-Márquez et al., 2019). Additionally, the binding model predicts the bonds formed between the active sites of the collector and mineral surface. This analysis can be performed using the Wiberg bond index, which is extensively used as a bond analyzer. This binding model serves to compare the binding ability of collectors and copper ions. Finally, the atomic charges can be calculated using natural bond orbital (NBO) analysis, which describes the reactivity of the molecules.

B.3.5.1 Molecular electrostatic potential and NBO analysis

The optimized molecular geometries of IPETC⁻ and PAX⁻ in water are shown in Figure B.9a and 9b, respectively. The leading elements of the IPETC⁻ structure are labeled C1, N3, O2, and S4, and those of PAX⁻ are C2, O1, S3, and S4, the last of which corresponds to =S (see Figure B.9 a and 9b). Table B.4 presents the NBO atomic charges. Here, it can be seen that when IPETC is ionized, the NBO net charge of S4 increases from -0.37 (IPETC) to -0.65 (IPETC⁻), showing that the S4 in IPETC⁻ has greater electronegativity, and, therefore, a greater ability to attract electrons. For C1, N3, and O2, there was no significant change in electronegativity. This result confirms the hypothesis mentioned in Section 3.3 that IPETC interacts via an anodic oxidation process. Additionally, in Figure B.9a, the molecular electrostatic potential (MEP) describes the electron density of the IPETC⁻ molecule. The red coloration marks the most negative region (electrophile) and yellow the most positive region (nucleophile). Therefore, the MEP and NBO charges predict that the reactive site in the IPETC⁻ is in the S4 element (C=S group). When PAX is ionized to PAX⁻, there is no significant change in electronegativity (see Table B.4). O1, S3, and S4 are the electronegative sites of PAX⁻. The MEP of PAX⁻ shows that the most negative region is between S3 and S4, predicting that S3 (C–S group) and S4 (C=S group) are the reactive sites in the PAX⁻ molecule (see Figure B.9b). For C2 and O2, there was no significant change in electronegativity. These results agree with those obtained via XPS analysis. The XPS result for IPETC⁻ suggests the binding is enabled by the S of the collector with Cu atoms in the

covellite surface. In the case of PAX^- , it was also determined that the principle mechanism of adsorption of PAX^- on the covellite surface is through C 1s and S 2p (see Figure B.8).

a)



b)

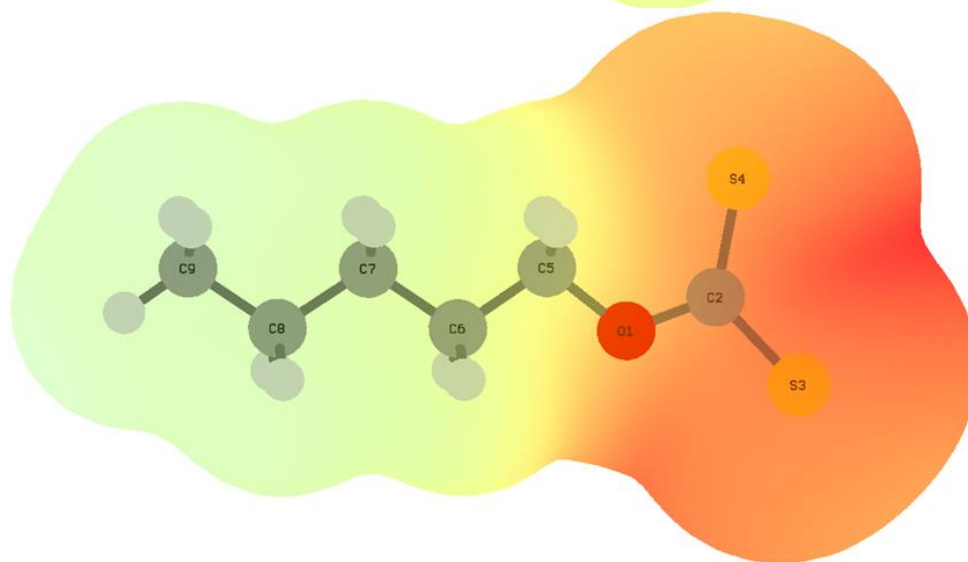


Figure B.9. Molecular electrostatic potential of a) IPETC^- and b) PAX^-

Table B.4. NBO net atomic charges of IPETC and PAX molecules

Element	IPETC	IPETC ⁻	Element	PAX	PAX ⁻
C1	+0.44	+0.41	C2	+0.02	+0.00
O2	-0.53	-0.58	O1	-0.52	-0.53
N3	-0.62	-0.64	S3	-0.42	-0.42
S4	-0.37	-0.65	S4	-0.39	-0.39

B.3.5.2 Frontier molecular orbitals analysis

The global reactivity descriptors are widely employed to explain the electronic properties of compounds, and Table B.5 presents the values for IPETC⁻ and PAX⁻. A high hardness (η) and low electrophilicity (ω) give a low reactivity. Therefore, the IPETC⁻ has lower reactivity than PAX⁻ (see Table B.5). Another descriptor is the electronic chemical potential (μ) associated with molecular stability. When μ is higher, the molecule is more reactive. Therefore, the absolute value of μ shows that IPETC⁻ is more stable (less reactive) than PAX⁻. The same behavior was identified in the HOMO–LUMO energy gap. A higher energy gap means a lower reactivity and, therefore high stability, demonstrating that IPETC⁻ is less reactive. The PAX⁻ has greater electronegativity (χ) and a high charge flow, showing its higher reactivity. Finally, the softness (s) is the inverse of hardness and corroborates this behavior (Miar et al., 2021; Fukui, 1979; Choudhary et al., 2019; Zhan et al., 2003; Ignatkina, 2011).

In conclusion, it is well known that the PAX⁻ is a type of xanthate collector, and xanthates have a powerful collector ability. This fact could explain the low stability of PAX⁻. Nevertheless, these collectors have disadvantages, including ease of decomposition and poor selectivity. The latter is a disadvantage if selective separation is required in the first stage of the flotation process. Finally, the IPETC⁻ calculations demonstrate that it has the highest stability, and, for this reason, it is generally a less potent collector than xanthates. Nevertheless, the advantage of using IPETC⁻ is its solution stability due to having a $pK_a \geq 12$. The pK_a of a collector influences the mechanism of collector adsorption on the mineral surface, and can be a critical factor in determining optimum flotation conditions. Finally, these results support using PAX⁻ as a bulk collector and IPETC⁻ as a selective collector in the flotation process.

Table B.5. Global reactivity descriptors calculated for IPETC⁻ and PAX⁻

	HOMO (eV)	LUMO (eV)	ΔE (eV)	μ (eV)	η (eV)	s (1/eV)	χ (eV)	ω (eV)
(IPETC ⁻)	-0.1854	0.0555	6.5536	-1.7674	3.2768	0.1526	1.7674	0.4766
(PAX ⁻)	-0.1878	-0.0209	4.5405	-2.8398	2.2703	0.2202	2.8398	1.7761

B.3.5.3 Binding model

The binding model between the collector IPETC⁻ and PAX⁻ with covellite was simulated. The structural geometries of the collector were optimized using two copper cations, Cu(I) and Cu(II). The two oxidation states of copper were used because they are shared by the covellite structure, and they could interact differently with the collectors. Nevertheless, the optimized structures of IPETC⁻ with Cu(I) and Cu(II) cations do not exhibit any difference related to copper's binding with IPETC⁻. In both cases, Cu(I) and Cu(II) were bonded with the S4 element (see Figure B.10a). However, the NBO net charges of the elements O2, N3, and S4 of the collector change when the copper ion changes from Cu(I) to Cu(II), demonstrating significant differences between the interactions of these cations with IPETC⁻. The PAX⁻ presents the same behavior. There is no difference between Cu(I) and Cu(II) binding with PAX⁻; in both cases, the copper ions Cu(I) and Cu(II) bond with S3 and S4 of the PAX⁻ molecule (see Figure B.10b). Finally, similar to IPETC⁻, the NBO net charges of the O1, S3, and S4 elements of PAX⁻ are different.

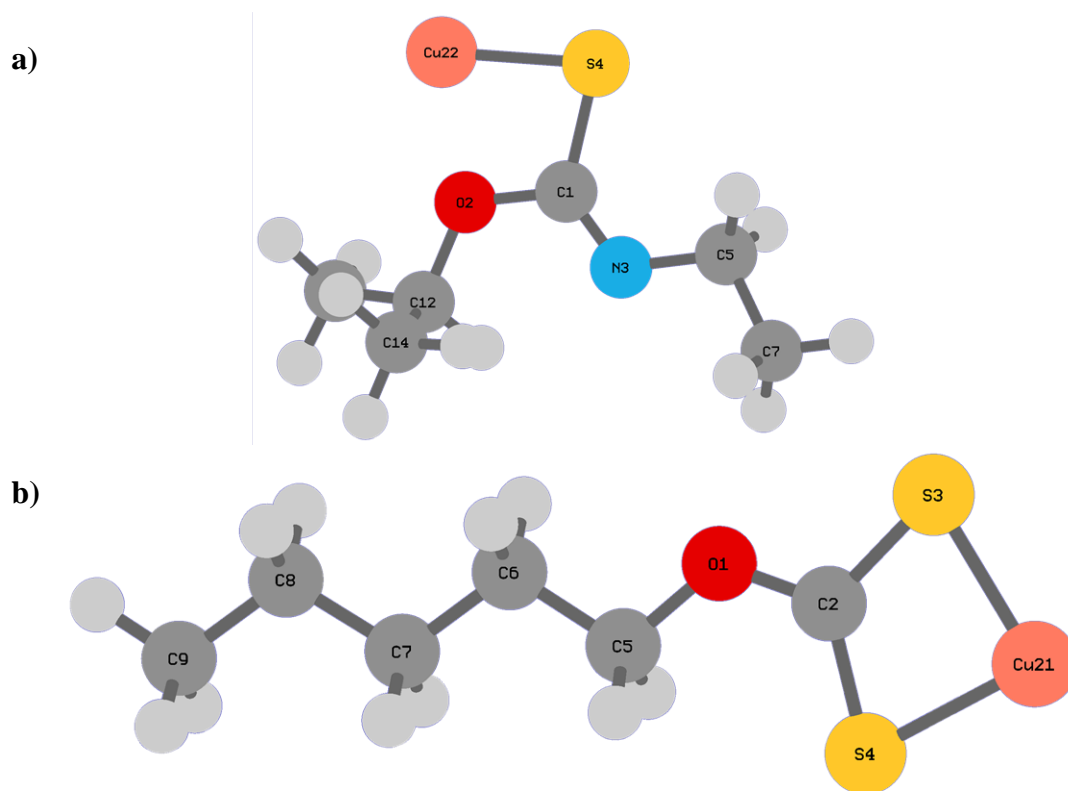


Figure B.10. Optimized geometries of the binding models of a) copper-IPETC⁻ and b) copper-PAX⁻

Besides, the DFT calculations verified that it is less probable to form a stable bond Cu-O. Indeed, as was shown in Figure B.9, section 3.5.1, in the molecular electrostatic potential maps, the negative charges were mainly located on the C=S group, and the most negative atom charge is on S atom (-0.65) compared with O atom (-0.58). Also, the results showed in Figure B.11 suggest that IPETC- Homo orbitals are centered at the C=S group, which indicated that C=S group might be the electron-donating site in the interaction. The same behavior was observed for Homo orbitals in the PAX- with terminals on S atoms. Similar behavior was demonstrated by Zhao et al. (2016) calculating the binding model between copper ion (II) and IPETC using DFT. They demonstrated that the bond only occurs through the C=S group, while the C=S and C=O groups are both involved in other kinds of thionocarbamates, which contain different N-alkyl and O-alkyl groups such as IBECT, BIPECTC, and BMIPECTC.

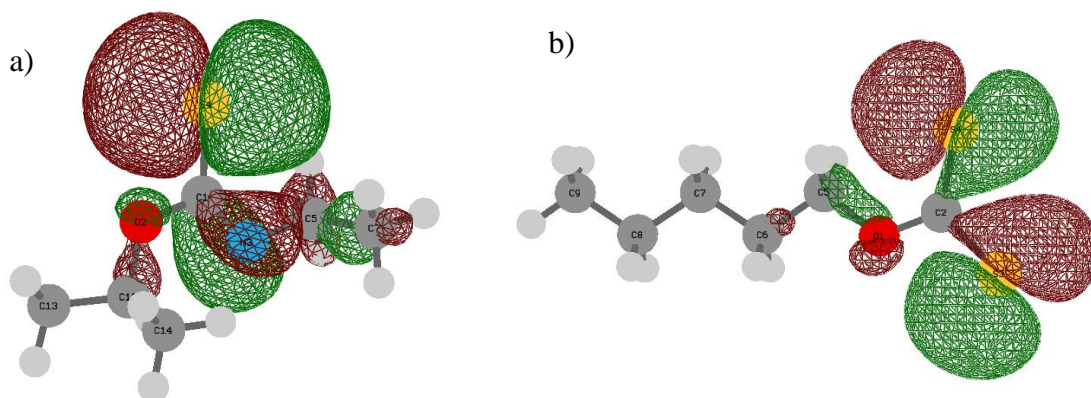


Figure B.11. Homo orbitals for collectors (a) IPETC-, (b) PAX-. Red and green mean positive and negative values of the wavefunction, respectively.

It is worth mentioning that we decided to conduct the DFT calculations using the metal ions rather than periodic mineral crystal planes because the collector reactivity with a metal ion has been extensively studied, demonstrating that the collecting ability of collector on metal ions could be analyzed using this method. For instance, Bag et al. (2011) studied the predictive capacity for geometrical optimization of xanthates with copper ions. Also, they carried out a flotation test to support their findings. The DFT calculations showed the interaction between various alkali-xanthates and copper ions. The results indicate that amyl-

xanthate is most effective compared to ethyl, propyl-, iso-propyl, butyl- and iso-butyl xanthate. Then, from the flotation using the batch flotation technique, the experimental results show that better values of copper recovery were obtained with amyl-xanthate rather than other xanthates, supporting DFT calculations. Another work was conducted by Zhao et al. (2013). They studied the binding model of two hydroxamic acids (BHA and CHA) with Ca(II) ion through DFT calculations. They demonstrated that in alkaline solutions, the dianion of CHA exhibited higher atomic charge value and HOMO energy, bigger dipole moment, and binding energy with Ca(II), and hence stronger collecting ability for scheelite (CaWO_4) than those of BHA. These results agreed with experimental results obtained from the flotation tests, zeta potential, and the determination of adsorption quantity.

Yekeler and Yekeler (2004) conduct the DFT calculations to model the interactions between thiol collectors with Ag (I) ion, and optimize the geometries of collector–Ag complexes formed. The results showed that the optimized geometries agree with the experimental data reported. Also, the calculations showed that HOMO energies could be used as a reactivity descriptor for the selection of collectors, which allows understanding the role of collectors in the initial adsorption step of the flotation processes for acanthite (Ag_2S).

Consequently, these studies demonstrated that molecular modeling using metal ions to represent mineral surface could be used in our work to analyze qualitatively the collector's interaction (PAX and IPETC) with the copper ions (Cu(I) and Cu(II)) contained on the covellite surface. Also, a flotation test could be used to support the findings obtained by DFT calculations. Nevertheless, a disadvantage of using metal ions in molecular modeling is that it does not explore the adsorption mechanism. Several interactions such as chemisorption, physisorption, formation, and precipitation of a metal collector salt, and others may occur between the mineral surface and collectors. Therefore, the phenomena are very complex and involve high computation costs, and the results frequently are not accurate enough. Then, one way to model this system is to overestimate or simplify some of them due to the difficulties in modeling the system—for instance, the complexity of the covellite structure as was done in the present work.

Despite this, the theoretical calculations allow us to understand the role of these collector molecules in the initial adsorption step of the flotation process. Therefore, the results in this

study can be extended in future research, which may be focused on the adsorption mechanisms of PAX and IPETC with the two most stable covellite cleavage surfaces in a periodic crystal plane simulation that contains the copper ions Cu(I) and Cu(II) and comparing these results to explore the adsorption mechanism deeply.

The NBO net charge of these binding models is shown in Table B.7. As regards the IPETC⁻, the net atomic charge in S4 drops when the complexes IPETC⁻Cu(I) and IPETC⁻Cu(II) are formed, suggesting an interaction between collectors and both copper ions. The reduction in Cu(I) and Cu(II) net charges demonstrate adsorption as well. The same behavior is identified for PAX⁻ and the complexes PAX⁻Cu(I) and PAX⁻Cu(II). The net atomic charges in S3 and S4 decrease after their interaction. In general, it can be seen that collectors interact with both copper ions. Nevertheless, there is a stronger interaction between Cu(II) and collectors, which is evident from its oxidation state. Additionally, these results clarify that copper's interaction with IPETC⁻ occurs strongly via S4–Cu binding and that with PAX⁻ occurs via S3–Cu and S4–Cu binding, confirming the XPS results.

Table B.7. NBO net atomic charges of IPETC⁻ and PAX⁻ and the corresponding complexes

Element	IPETC ⁻	IPETC ⁻ Cu(I)	IPETC ⁻ Cu(II)	Element	PAX ⁻	PAX ⁻ Cu(I)	PAX ⁻ Cu(II)
C1	+0.41	+0.40	+0.41	C2	+0.00	+0.02	+0.05
O2	-0.58	-0.63	-0.64	O1	-0.53	-0.50	-0.46
N3	-0.64	-0.58	-0.49	S3	-0.42	-0.29	-0.09
S4	-0.65	-0.49	-0.21	S4	-0.39	-0.28	-0.11
Cu		+0.74	+1.28	Cu		+0.67	+1.18

More evidence of complex formation between IPETC⁻ and PAX⁻ collectors and copper ions was adopted to discuss the bond order variation. The bond order is the number of chemical bonds between a pair of atoms. This method gives the stability and strength of the bond between a pair of atoms. There are many different quantum-chemical definitions of the bond order because it is not a quantum-mechanical observable, and this term is not semantically precise (Wiberg, 1968; Szczepanik and Mrozek, 2013; Sizova et al., 2007). The Wiberg bond index is useful and extensively utilized as a binding analyzer and allows us to calculate the bond strength associated with the main atoms of the molecules and the complexes formed and is provided by the Gaussian package. Table B.8 displays the Wiberg bond indices for IPETC⁻ and PAX⁻, and the complexes formed with copper. As regards IPETC⁻, the Wiberg bond of the C1–S4 became smaller as a result of the electron transfer to copper ions.

Additionally, the C1–N3 bond increased, perhaps due to the N atom offering its electron to compensate for the vacant position in the C=S group. The Cu–S4's Wiberg indexes are approximately 0.53 for Cu(I) and 0.64 for Cu(II), indicating new bonds were formed between copper and IPETC⁻. The Wiberg bond indexes for Cu–O2, Cu–N3, and Cu–C1 are negligible.

As regards PAX⁻, the Wiberg bonds for the C2–S3 and C2–S4 became smaller as a result of the electron transfer to copper ions. The Cu–S3's Wiberg bond is approximately 0.44 for Cu(I) and 0.49 for Cu(II). The Cu–S4's Wiberg bond index is around 0.40 for Cu(I) and 0.46 for Cu(II), indicating new bonds formed between copper ions and PAX⁻. The Cu–O2 and Cu–C2 Wiberg bonds are negligible. In summary, binding occurs through the C=S group of IPETC⁻ and through the C=S and C–S groups of PAX⁻. This is evident in the binding model shown in Figure B.10a and 10b. The Wiberg bond results agree with the XPS and FT-IR results, demonstrating that DFT calculations are an excellent alternative when studying adsorption mechanisms between minerals and collectors.

Table B.8. Wiberg bond indices for IPETC⁻ and PAX⁻, and the complexes formed with copper.

Species	C1–S4	C1–O2	C1–N3	Cu–S4	Cu–O2	Cu–N3	Cu–C1
(IPETC) ⁻	1.1976	0.9696	1.6671	-	-	-	-
(IPETC)(Cu) ⁺	1.1158	0.9185	1.7570	0.5291	0.1323	0.0331	0.0611
(IPETC)(Cu) ⁺⁺	1.0649	0.9427	1.7945	0.6433	0.1205	0.0495	0.0304
Species	C2–S3	C2–S4	C2–O1	Cu–S3	Cu–S4	Cu–O2	Cu–C2
(PAX) ⁻	1.4018	1.4462	1.0466	-	-	-	-
(PAX)(Cu) ⁺	1.3307	1.3649	1.1202	0.4393	0.4074	0.0486	0.1074
(PAX)(Cu) ⁺⁺	1.3129	1.3399	1.1959	0.4922	0.4629	0.0309	0.0515

Finally, this work demonstrated that covellite flotation is not pH-dependent in the range employed. Thus, pH could be used for the selective flotation of covellite against pyrite. FT-IR identified the presence of gypsum on the covellite's surface, and XPS shows that gypsum modifies the covellite oxidation state. Nevertheless, it was demonstrated that the gypsum was dissolved, and the collectors were adsorbed on the covellite surface, improving its floatability. Therefore, it is expected that the gypsum does not affect the floatability of the covellite if its quantity is below the solubility level (~2.1 g/L.). As regards the effect of the collector, the covellite floats very well with both collectors, but covellite recovery increases

as a result of increasing the collector concentration until it becomes constant. Consequently, there are optimal concentrations that must be determined for specific ores. Nevertheless, higher recoveries were achieved using PAX. Therefore, all these findings could be used in the selective flotation of covellite against pyrite, allowing us to find the optimal conditions for collector type, collector concentration, and pH to be implemented for covellite flotation.

B.4 Conclusions

Covellite flotation is not pH-dependent, and its recovery increases significantly with collector concentration. The FT-IR spectra of IPETC indicate that the collector adsorption on the covellite surface is not pH-dependent. The bands related to $-C(=S)-NH$, $-C-H$, NH deformation and CH deformation and CNC characteristic of IPETC were present in the spectra demonstrating IPETC adsorption on covellite surface. Nevertheless, the NH stretching band was absent. On the other hand, the FT-IR spectra of PAX show that collector adsorption on the covellite surface is not pH-dependent. PAX adsorption was identified via the leading functional groups, such as dixantogen $(AX)_2$, which formed via vibrational mode $C=S$, and the Cu-amylxanthate $(CuAX)$.

Additionally, the high-resolution XPS spectra of the Cu 2p spectrum shows that the oxidation state of covellite with PAX is Cu(I). This finding was corroborated by FT-IR by the identification of Cu-amylxanthate $(CuAX)$ and dixantogen $(AX)_2$ on the covellite surface. The adsorption mechanism of IPETC suggests the bind is facilitated by the S of the collector with Cu atoms on the covellite surface. Moreover, the S 2p spectrum of covellite treated with IPETC displays a principal doublet attributed to S_2^{2-} ($C=S$ functional group), as observed for thiourea. Also, the Cu 2p spectrum shows a single sharp peak attributed to the CuS(I) and a minor peak attributed to the CuS(II). The peak related to CuO demonstrated that the covellite was oxidized. Additionally, it was found that the NH was not adsorbed onto covellite surface.

Lastly, the DFT results are in good accordance with the FT-IR and XPS results. The reactive site in the $IPETC^-$ collector was the $=S$ element, and bond with copper only occurred through the $C=S$ group. For PAX^- , the reactive sites were $=S$ and $-S$ elements. Thus, the bond with copper occurred through $C=S$ and $C-S$ groups. The global reactivity descriptor calculations demonstrate that PAX^- has a powerful collector capacity and, therefore, low stability compared to $IPETC^-$. This result agrees with the results obtained from microflotation tests;

specifically, the higher recovery with PAX^- (93%) than with IPETC^- (88%). Additionally, it was demonstrated that copper charge matters when it interacts with the collector. In general, the NBO net atomic charges and the Wiberg bond indices show that Cu(II) 's binding with both collectors has stronger energy than Cu(I) . This result could be helpful when selecting collectors.

Authors and Contributions

Yesica L. Botero. Conceptualization, methodology, experimental test, formal analysis, writing—original draft, review, and editing.

Andres Canales. Molecular modeling methodology and formal analysis.

Rodrigo Serna-Guerrero. Writing—review and editing, supervision, funding acquisition.

Alejandro López-Valdivieso. Conceptualization, supervision, formal analysis.

Mostafa Benzaazoua. Supervision.

Luis Cisternas. Writing—review and editing, conceptualization, methodology, formal analysis, supervision, project administration, funding acquisition.

APPENDIX C ARTICLE 3: INSIGHTS INTO THE DESIGN OF POLYMETALLIC FLOTATION CIRCUITS, INCLUDING TAILING DESULFURIZATION

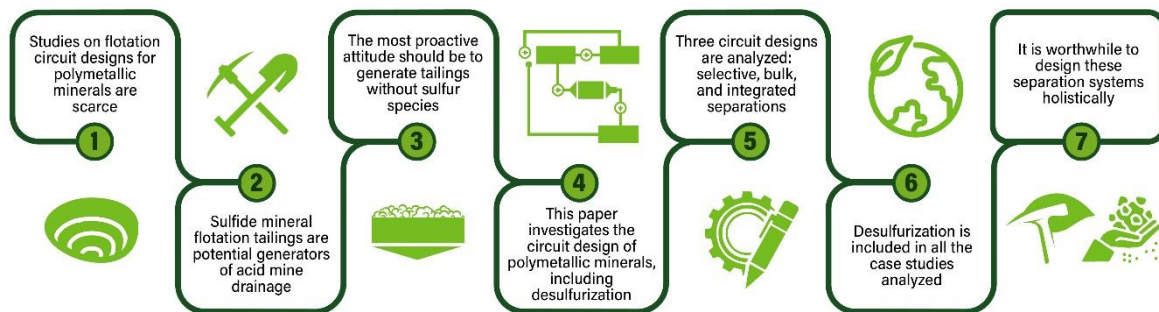
Article 3: Yesica L. Botero, Luis A. Cisternas, Isabelle Demers and Mostafa Benzaazoua. Insights into the design of polymetallic flotation circuits, including tailing desulfurization. *Separation and Purification Technology*, 2023. (Submitted, Doi: 10.2139/ssrn.4366523).

This article was submitted to *Separation and Purification Technology* journal on February 14, 2023.

Abstract

Flotation is a main mineral concentration technology, which is why the design of flotation circuits has been extensively studied in the literature. However, studies on flotation circuit designs for polymetallic minerals have rarely been conducted. On the other hand, sulfide mineral flotation tailings are potential generators of acid mine drainage (AMD), which is one of their main environmental drawbacks. Although there are several strategies to prevent and control AMD, the most proactive attitude is to generate tailings without sulfur species. This paper investigates the circuit design of polymetallic minerals, including desulfurization within the flotation process. Three types of circuit designs are analyzed: fractional flotation with the generation of a bulk concentrate and its subsequent separation, fractional flotation using selective flotation, and integrated flotation with combined bulk and selective flotation. Various aspects are analyzed, such as the effect of stage recovery uncertainty on the design; the impact of the design type on costs, energy use, and environmental effects; and the influence of the design strategy applied. Additionally, the design of a Cu–Ni plant that includes desulfurization is employed to deepen the research. The results show that it is useful to design these separation systems holistically to obtain more efficient designs. It is also concluded that the most traditional way of processing polymetallic minerals consumes more energy, water, and materials, resulting in a more significant environmental impact. Finally, based on these results, a methodology for designing these complex systems is outlined.

Keywords: flotation circuit design, polymetallic ore, desulfurization, acid mine drainage.



Graphic Abstract

C.1 Introduction

Flotation is the main mineral concentration technology used in the production of coal, copper, zinc, lead, nickel, molybdenum, and other metals. It is estimated that it is used for 85% of ores mined. This means that more than two billion tons of various ores are processed by froth flotation annually (Nguyen et al., 2023). As we look to the future, the use of this process is likely to increase, because the demand for goods that are dependent on metals, such as vehicles, buildings, machinery, and infrastructure is increasing in modern society. Watari et al. (2021) predicted an increase in the global demand for metals such as copper, zinc, lead, and nickel of 2–6 fold, depending on the metal, during the 21st century. As the metal demand increases, lower-grade orebodies will become economically viable. These low-grade ore are more complex, and the processing of higher tonnages will be needed to sustain production. Processing must be environmentally sustainable, and therefore, it is becoming increasingly necessary for mining companies to consider their water use, energy consumption, carbon emissions, and solid waste generation to improve their environmental, social and governance conditions. Several ore deposits are polymetallic with two, three, or more base metals. Additionally, in the circular economy and environmental regulations, metal valorization and the use of cleaner production technologies are emphasized (Cisternas et al., 2021; Marinina et al., 2022). The need to move from end-of-pipe strategies to clean production necessitates new process designs. On the other hand, the valorization of minerals requires minerals to be viewed as polymetallic resources. Therefore, new process design is a crucial aspect for improving circularity (Cisternas et al., 2021; De los Rios and Charnley, 2017).

As indicated above, the flotation process is a method that is used extensively in the mining industry. Despite this, there are still some unresolved questions at all levels: from molecular behavior to operation planning (Cisternas et al., 2019; Lai et al., 2021). Usually, the main variables that affect flotation are classified into operation aspects (e.g., particle size, feed rate, mineralogy, pulp density), chemical aspects (e.g., collectors, frother, activators, depressant), and equipment components (e.g., bubble generation, cell design, agitation) (Klimpel, 2003). A quick review of the Web of Science database shows that most studies have focused on physical-chemical aspects such as depressants, collectors, activators, and foaming agents. Secondly, studies have focused on aspects at the equipment level, such as new devices including sensors (Leiva et al., 2022) or cell analysis (Yianatos and Vallejos, 2022). However, fewer studies have been done on flotation circuit design processes. Successful flotation separation is dependent on the design employed. With a sub-optimal design, it is difficult to achieve the results obtained with the optimal design, even if operational conditions, such as the particle size, residence time, or flotation chemistry, are changed.

Flotation circuits are complex systems composed of several stages, such as a rougher, cleaner, and scavenger, configured in a particular way (Mendez et al., 2009). Usually, flotation circuits have between three and five stages, but some flotation plants have thirteen flotation stages (Sepúlveda et al., 2017). One of the problems associated with circuit design is the large number of feasible flotation circuits, given the combinatorial nature of the problem. If the behavior of each flotation stage is necessary for the design of the flotation circuit, the problem is unsolvable. This is because the behavior of each stage, which depends on physical-chemical aspects and the operational conditions, will depend on the design of the circuit (Hu et al., 2013; Leiva et al., 2022). Clearly, the behavior of a stage will depend on the feeding characteristics. As the modeling of these systems is still empirical or semi-empirical, it is impossible to conduct experiments under all possible circuit configurations for a given problem. Fortunately, and as will be seen later, rigorous comprehension of the behavior of a flotation stage is not necessary for the design of these circuits, at least for monometallic circuits.

The flotation circuit for a polymetallic ore usually utilizes fractional flotation with the generation of a bulk concentrate and its subsequent separation, fractional flotation using selective flotation, or a combination of both strategies if three or more concentrates are produced (Frías et al., 2008). For example, several flotation flowsheets that are used in practice for polymetallic ores contain copper, including copper–zinc, lead–zinc, copper–lead–zinc, nickel–copper, and copper–molybdenum (Fuerstenau, M.C.; Jameson, G.; Yoon, 2007). Different structures have been used, as indicated previously, based on the characteristics of the ore. However, polymetallic ores are usually separated by fractional flotation using selective flotation for each base metal. The methodologies proposed in the literature for the design of flotation circuits consider only one base metal, which was designed for monometallic ores. To the best of the current author's knowledge, there is no systematic methodology available for the design of polymetallic circuits. Nevertheless, it is logical to think that the separation sequence will first be selected based on the designer's experience and ore characteristics, and then each flotation circuit will be designed, one at a time, as if it were a design for a monometallic ore. This can include the separation of sulfide ore, which can produce acid mine drainage (AMD) of compounds such as pyrite (Blowes et al., 2003).

Another issue is the increasing generation of tailing and the consequences of contaminant release through dust, tailings dam seepage, dam wall failure, and potential generators of AMD. Processing higher tonnages of lower-grade ores will increase the risks associated with mine tailings management (Edraki et al., 2014). Current tailing management includes the use of paste and thickened tailings and the reuse, recycling, and reprocessing of tailings (Araya et al., 2021, 2020; Bascetin A. et al., 2016; Marín et al., 2021). A proactive strategy would be to generate tailings without sulfur species to improve environmental, social, and economic outcomes. There have been several studies on tailing desulfurization; however, these studies have been on abandoned tailings (Nadeif et al., 2019; Skandrani et al., 2019) or end-of-pipe technologies (A. El-bouazzaoui et al., 2022; Abdelilah El-bouazzaoui et al., 2022).

Given this background, it is clear that studies on the design of flotation circuits for polymetallic ores, including those using desulfurization, are necessary to meet the future challenges of the mining industry. This paper seeks to answer the following questions: Are monometallic mineral flotation circuit design strategies applicable to polymetallic mineral

circuit designs? Which separation sequence is the most appropriate for a particular mineral? What are the advantages of designing flotation circuits simultaneously versus one at a time for each metal? Which designs can include desulfurization as part of a flotation circuit? Which challenges exist in terms of conducting physical-chemical studies to improve these circuits? The manuscript is organized as follows: Firstly, the introduction provides the motivation, gaps, and objectives of this research. Section 2 presents the methodology, which is based on the application of flotation circuit design optimization. Section 3 is related to the strategies used in the design of flotation circuits, including an extension of the strategies used in the design of monometallic mineral to polymetallic mineral processing and an analysis of the types of circuit structures employed. In addition to fractional flotation with the generation of a bulk concentrate and its subsequent separation and fractional flotation using selective flotation, a new flotation circuit is introduced: integrated flotation with combined bulk and selective flotation. Section 4 presents designs for the Cu–Ni–PGE Kevitsa mine (Musuku et al., 2016), including the application of different strategies for obtaining the optimal flotation circuit design. The Kevitsa concentrator employs a copper–nickel fractional-selective flotation circuit that includes desulfurization. Therefore, the idea was to compare the one-at-a-time process design with the as-a-whole process design. The conclusions are delivered at the end of the manuscript (Section 5).

C.2 Design methodology

The methodologies available for the design of monometallic mineral flotation circuits can be classified as those based on heuristics, those based on optimization, and hybrids (Mendez et al., 2009). When selecting a methodology for the design of polymetallic flotation circuits, the methodology must satisfy at least three requirements. First, the methodology must be capable of delivering correct results, as it is not possible to compare results if the methodology does not always give accurate results. Second, it must be possible for the methodology to be applied to systems with many stages, because circuits for polymetallic ores usually have more flotation stages than circuits for monometallic ores. Third, the methodology must be capable of handling several species, because polymetallic ores generally have more minerals.

Methodologies based on heuristics usually give feasible flowsheets but do not guarantee the best solution. In addition, no heuristics are available for the design of polymetallic minerals. Several methods combine heuristics or insights with first principles to obtain a circuit design; these are called hybrid methods (Amini and Noble, 2017; Sepúlveda et al., 2014). Of these methods, linear circuit analysis is the most accepted methodology, because it provides fundamental insights regarding how unit operations interact and respond when arranged in multistage processing circuits (Noble et al., 2019). One advantage of linear circuit analysis is its simplicity; regrettably, several limitations to this technique that can introduce errors and result in incomplete analysis have been identified (Cisternas, L.A.; Acosta-Flores, R.; Gálvez, 2019). In addition, the potential application of this method to polymetallic minerals is complex, since analyzing circuits with many flotation stages and several species is complicated, given the many possible alternatives that must be scrutinized. The application of optimization methodologies appears to be a good option. However, it is necessary to ensure that the application of such methodologies to systems with many stages and species is viable, a situation that limits their application. In fact, it has been observed that most application examples of methodologies based on optimization have used systems with few stages or species (Acosta-Flores et al., 2018). This is because the optimization problem is a nonconvex, mixed-integer, nonlinear programming problem:

$$\begin{aligned}
 & \text{Min } Z = f(x, y) \\
 & \text{s. t. } g(x, y) \leq 0 \\
 & x \in \mathcal{R}^n \quad y \in \{0,1\}^m
 \end{aligned} \tag{C.1}$$

This optimization problem is challenging to solve because bilinear expressions make the model shown in Eq(1) nonconvex. These bilinear expressions represent recovery in the flotation stages. The finding by Cisternas et al. (2015) that the structure of the flotation circuit is not very sensitive to the quality of the flotation model (or to the uncertainty of the recovery in each stage) allowed the application of optimization methodologies to circuits with greater quantities of species and flotation stages (Calisaya et al., 2016). This observation needs to be validated for polymetallic minerals.

In this work, optimization was used to design flotation circuits for polymetallic minerals. Three aspects are essential for the application of optimization for flotation circuit design: the

superstructure, which represents the set of feasible flotation circuits from which the optimal solution is obtained; the mathematical model that represents the superstructure; and the algorithm utilized to solve the mathematical model. A review of these aspects is outside the scope of this manuscript, but a review is available in the literature (Cisternas et al., 2018). Here, a brief discussion is given to justify the methodology utilized.

Several superstructure representation strategies have been proposed and have evolved over the years (Cisternas et al., 2004; Mehrotra and Kapur, 1974; Reuter et al., 1988; Schena et al., 1997). However, most of these show that the number of alternatives increases exponentially with the number of flotation stages or cells; therefore, the problem has high computational costs. Since polymetallic flotation circuits have more stages and species than the processing of monometallic minerals, these superstructure representations have limited application for polymetallic minerals. Cisternas et al. (2014) proposed a superstructure that incorporates the concept of the origin-destination matrix for each concentrate and tail stream, allowing the designer to select the stream directions, which significantly reduces the number of alternatives and avoids the presence of streams without sense (see Figure C.1). Origin-destination matrices for tail and concentrate streams are used to control connections that make no sense and to reduce the number of alternatives. The origin-destination matrix also identifies all concentrate and tail paths that the designer wants to consider in the study. In addition, the matrix makes it necessary to define each flotation stage's task in the flotation circuit.

The strategy uses a flotation stage superstructure that represents alternative flotation circuit configurations. This representation is similar to that used by Cisternas et al. (2014), but several products are allowed in the circuit. In addition, as is discussed later, each flotation stage can operate with different objectives, e.g., to concentrate one mineral or to concentrate a bulk. The superstructure is based on the generic representation of a stage that is used to represent all stages that are to be included in the design (see the left diagram in Figure C.1). In the superstructure, discrete variables represent different alternatives for the circuit configuration, and continuous variables represent design and operational variables. The formulation is complemented with requirements such as the grade for the concentrates and the tail.

The left diagram in Figure C.1 shows a structure representing a flotation stage. The M triangle represents a feed mixer and enables streams from other stages to be fed to stage i . The D triangles in the output streams represent splitters and allow concentrate and tail streams from stage i to be sent to other stages. The table on the right of Figure C.1 illustrates the origin and destination of the concentrate (c) and tail (t) streams.

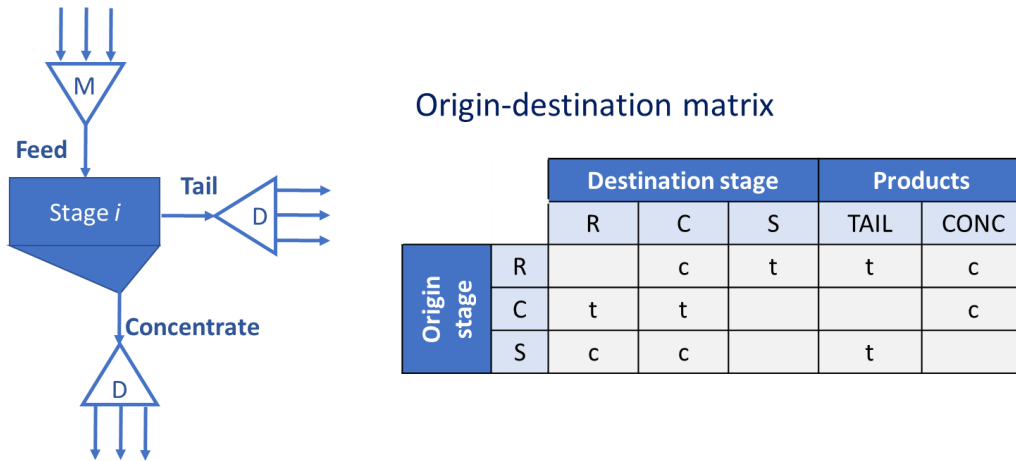


Figure C.1. Superstructure for the flotation circuit design and origin-destination matrix [Rougher stage(R), cleaner stage(C), scavenger stage(S), tail stream(t), concentrate stream(c)].

The mathematical model is associated with the superstructure, which corresponds to the mass balances in the M and D triangles, the stage recovery modeling, and the selection of the destinations of the streams. Other variables, such as the operational conditions (e.g., the minimum concentrate grade or minimum recovery), are included. Additionally, binary variables represent decisions, such as the stream destination or disjunctions (e.g., the selection of a destination among a set of alternatives described in the origin-destination matrix).

Another critical aspect of the mathematical model is the objective function, which is usually an economic expression (e.g., maximization of profits or revenues). In this work, the revenue maximization is utilized as the objective function based on previous studies that demonstrated that it is an adequate objective function for solving this type of problem (Cisternas et al., 2014). The revenue is represented by Equation C.2:

$$Revenue = CF [f_p (g - \mu)(q - Rfc) - Trc - p]H \quad (C.2)$$

where CF is the concentrate mass flow rate in ton/h, f_p is the fraction of metal paid, g is the mineral grade of the concentrate, μ is the grade deduction, q is the metal price in USD/metal tonne, Rfc is the refinery charge in USD/metal tonne, Trc is the treatment charge in USD/concentrate tonne, and H is the number of hours per year of plant operation. In equation (C.2), p is the penalty for the presence of deleterious impurity elements in copper concentrates. The formula for calculating revenue incorporates the metallurgical efficiency of the plant, where the recovery and grade are opposing functions. In this work, it is assumed that the flotation stage recoveries are known, an assumption that will be justified later in the text. In this case, and if the objective function of equation (C.2) is utilized, the design problem of equation (C.1) has the following form:

$$\begin{aligned} & \max_{(x,y)} z^T x \\ & s. t. \quad A_{eq} x = b_{eq} \\ & \quad Ax + By \leq b \\ & \quad x \in \mathcal{R}^n \quad y \in \{0,1\}^m \end{aligned} \quad (C.3)$$

where $z^T x$ is the objective function, the vector x corresponds to continuous variables (e.g., mass flow rates), and the vector y represents binary variables (e.g., the stream direction). A , A_{eq} , and B are matrices, and z , b_{eq} , and b correspond to vectors. The equations correspond to mass balance and flotation stage modeling, whereas inequations represent the stream selection and operational limits. The model presented in equation (3) corresponds to a mixed-integer linear programming (MILP) problem, which can be solved to global optimum using commercial software.

In summary, the methodology to be used corresponds to the superstructure shown in Figure C.1 together with the origin-destination matrix, the mathematical model in equation (C.3), and an algorithm that is capable of solving a MILP problem. In our case, CPLEX 12.9.0.0 was used within the GAMS platform.

C.3 Strategy of flotation circuit design

In this section, a strategy for the design of a flotation circuit for polymetallic minerals is developed. First, it is important to remember that it is impossible to estimate the recovery in each flotation stage without defining the circuit to be analyzed, because the recoveries are a function of the structure of the circuit. Additionally, it should be considered that if the recovery in each stage is a variable, the design problem corresponds to a nonconvex MINLP that is difficult to solve. The first thing to prove is that the optimal structure is not a strong function of the recovery of each stage. If this hypothesis is fulfilled, approximate values for the recovery in each stage can be used and considered as parameters, making the problem to be solved an MILP, which is easy to solve. Second, we aim to take advantage of these analyses to answer some of our questions: Are monometallic mineral flotation circuit design strategies applicable to polymetallic mineral circuit designs? Which separation sequence is most appropriate for a particular mineral?

C.3.1 Approach

Through this strategy, we aim to demonstrate that identification of the circuits to best treat polymetallic flotation circuits can be done using approximate stage recovery values. This hypothesis was tested using two methods of proof: proof by construction and proof by exhaustion. Using the proof by construction method, three types of flotation circuit were elaborated: fractional flotation with the generation of a bulk concentrate and its subsequent separation (henceforth fractional bulk), fractional flotation using selective flotation (henceforth fractional selective), and integrated flotation with combined bulk and selective flotation. In the third type, two representations were utilized: flotation stages defined a priori as bulk or selective (henceforth integrated), and flotation stages that can function as bulk or selective indistinctly (henceforth integrated disjunctive). Then, using the proof by exhaustion method, a total of 30,000 cases were analyzed for each circuit proposed through random data generated from uniform distribution functions for the stage recovery values (Cisternas et al., 2015).

The general structures proposed for the fractional bulk, fractional selective, and integrated flotation circuits are shown in Figure C.2. The fractional selective circuit starts with a selective copper circuit that produces a copper concentrate and an intermediate tail. Then, the

intermediate tail is further introduced into a bulk desulfurization circuit that produces a sulfurous gangue (SG) concentrate and a non-sulfurous gangue (NSG) tail (see Figure C.2a). The fractional bulk starts with a bulk circuit that produces a bulk concentrate and tail known as the NSG. Then, the bulk concentrate is further introduced in a selective flotation circuit. Two products are obtained: a copper concentrate and a tail known as the SG (see Figure C.2b). Finally, the integrated circuit seeks to generate products simultaneously. Therefore, three products are obtained: a concentrate rich in copper sulfides, another rich in iron and arsenic sulfides (SG), and a tailing with a low sulfide content (NSG) (see Figure C.2c).

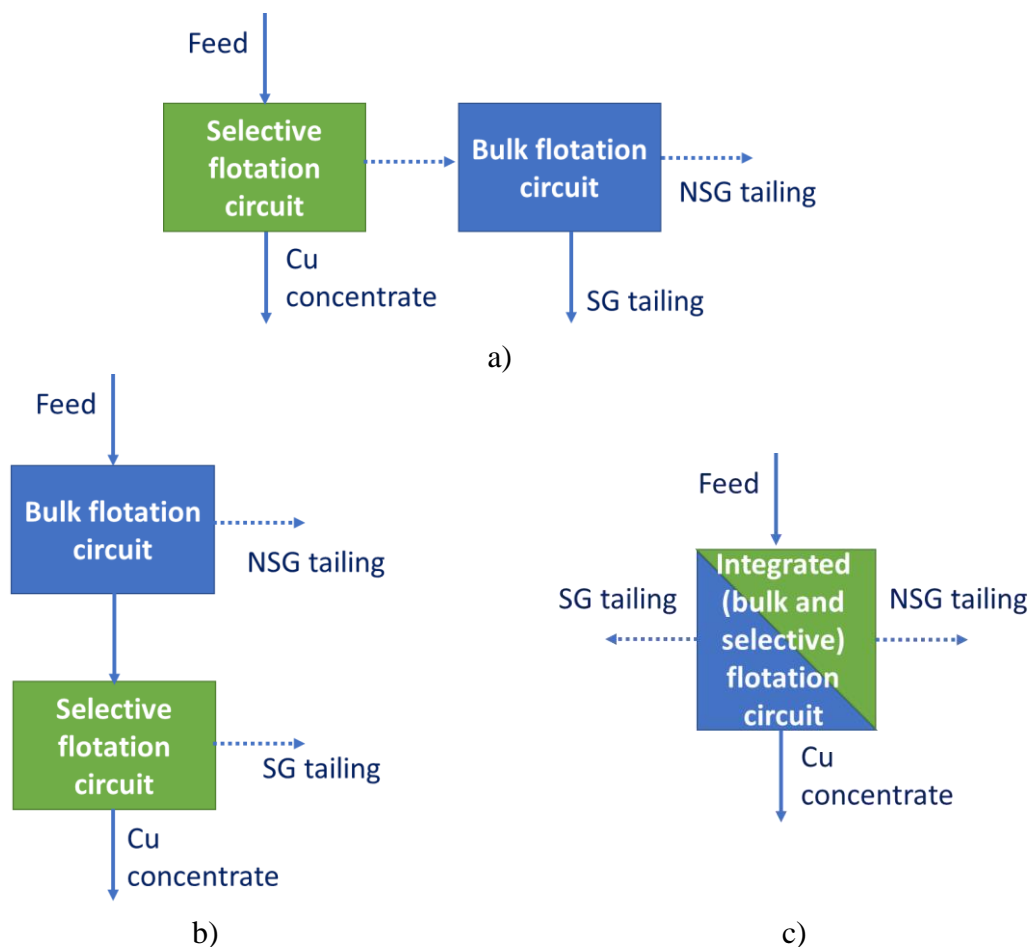


Figure C.2. The general structures proposed for a) fractional selective, b) fractional bulk, and c) integrated flotation circuits.

In all cases analyzed, the feed was composed of 5 tonne/h of chalcopyrite fast (copper grade 35%), 3 tonne/h of chalcopyrite slow (copper grade 28%), 20 tonne/h of pyrite, 1 tonne/h of

arsenopyrite, and 300 tonne/h of NSG. The feed had copper, arsenic, and sulfur grades of 0.84%, 0.14%, and 4.10%, respectively. For the objective function (Equation 2), the following values were considered: $q = 8400$ USD/tonne Cu, $f_p=0.975$, $\mu=0.015$, $Rfc= 200$ USD/tonne Cu, $Trc = 80$ USD/tonne concentrate, $H=7200$ h/year, and $p=2.5$ USD/tonne per extra 0.1% with a no charge maximum of 0.2 % w/w. In addition, the following conditions were included: the NSG had to have an S grade of <1% (to ensure desulfurization), the copper concentrated had to have an As grade of <1.4%, the copper concentrate had to have a Cu grade of >20%, and the NSG had to recover at least 80% of the NSG feed.

To generate the 30,000 cases, uniform distribution functions were used to represent the stage recovery of each species. The bounds of these distribution functions, which are the minimum and maximum values, are given in Table C.1.

Table C.1. Flotation stage recovery bounds (%) for bulk and selective flotation.

	Bulk		Selective	
	Min	Max	Min	Max
Chalcopyrite fast	75	85	70	85
Chalcopyrite slow	0.8–0.9 of Chalcopyrite fast recovery			
Pyrite	70	80	15	30
Arsenopyrite	70	80	15	30
NSG	2	10	2	10

For all cases, eight flotation stages were considered. The number of flotation circuit alternatives given for these origin-destination matrices are 15,552 and 31,104 for the fractional bulk and fractional selective cases, respectively. For the integrated case, two cases were considered: flotation stages defined a priori as bulk or selective (integrated), and flotation stages that can function as bulk or selective indistinctly (integrated disjunctive). For the first case, 2,799,360 flotation circuits were found to be feasible, whereas for the second case, there were 78,382,080.

The superstructure proposed for the fractional selective circuit (Figure 2a) starts with a selective circuit composed of four stages: the rougher (RS), scavenger (SS), and two cleaner (CS1 and CS2) stages. The products of this selective circuit are the final product (P) and the intermediate tail. The circuit is followed by a bulk circuit that is composed of four stages: the rougher (RB), two scavenger (SB1 and SB2), and cleaner (CB) stages. The products of this circuit are the SG, the concentrate, and NSG—the tail. It should be noted that the intermediate

tail is the only union between the selective and bulk circuits. Based on the origin-destination matrices, there are 144 feasible structures for the selective circuit and 216 for the bulk circuit. Thus, the total number of feasible structures for the fractional selective problem is 31,104 alternatives.

The superstructure proposed for the fractional bulk design (Figure 2b) consists of two circuits. The circuit starts with a bulk circuit composed of four flotation stages: the rougher-bulk (RB), two scavenger-bulk (SB1 and SB2), and cleaner-bulk (CB) stages. The products of this bulk circuit are the bulk concentrate (PB) and the NSG. The selective circuit is composed of four flotation stages: the rougher-selective (RS), scavenger-selective (SS), and two cleaner-selective stages (CS1 and CS2). The final concentrate (P) and the SG are the products. The tail and concentrate origin-destination matrices were used to identify the feasible paths for the tail and concentrate streams. For example, for the bulk circuit within the fractional bulk circuit, the concentrate streams of the RB could be sent to the CB or PB, and the tailing streams of the CB could be sent to the RB, SB1, or SB2. Similar alternatives were considered for the selective circuit within the fractional bulk circuit. It is important to note that the only union between the bulk and the selective circuit is the bulk concentrate (PB). Based on the origin-destination matrices, there are 72 feasible structures for the bulk circuit and 216 for the selective circuit. Thus, the total number of possible structures for the fractional bulk problem is 15,552 alternatives.

The superstructure proposed for the integrated circuit (Figure C.2c) comprises four bulk and selective stages. The origin-destination matrix is shown in Table C.2. The bulk stages are the rougher (RB), scavenger 1 and 2 (SB1 and SB2), and cleaner (CB) stages. The selective stages are the rougher (RS), scavenger (SS), and cleaner 1 and 2 (CS1 and CS2) stages. The products are the final concentrate (P), SG, and NSG. Unlike the previous cases, in this origin-destination matrix, and therefore the superstructure, several streams are allowed between the bulk and selective circuits (shown with a blue background in the table). Those streams are identified with capital letters: C for concentrate and T for tail. Those streams indicate the integration between the bulk and selective circuits. Using the origin-destination matrix, 1,944 and 1,440 concentrate and tail paths were identified, respectively. A total of 2,799,360 alternatives were considered in this design problem. Observe that in the matrix shown in Table

C.2, the flotation stages are assigned to a task a priori: bulk or selective. A second option is to consider that each flotation stage does not have a given task. In this case, the recovery of each stage has two options: bulk or selective. This type of problem is represented by disjunctions (henceforth integrated disjunctive). Under these new conditions, the superstructure in Table C.2 represents 78,382,080 feasible options.

Table C.2: Origin-destination matrices for integrated circuits (c and C represent concentrate streams in normal and integrated circuits, respectively; t and T represent tail streams in normal and integrated circuits, respectively)

		Destination stages								Products		
		RB	SB1	SB2	CB	RS	SS	CS1	CS2	P	NSG	SG
Origin stages	RB		t		c	c		C				
	SB1	c		t	c	C				t		
	SB2	t,c	t,c		c					t		
	CB	t	t	t		c,T		C	C			T
	RS				T		t	c	c	c		T
	SS				C	c		c	c			T
	CS1	T			T	t	t		c	c		
	CS2				T	t	t	t		c		

C.3.2 Results

C.3.2.1 Fractional bulk circuit:

A flotation superstructure with eight stages in the bulk circuit was analyzed. This included 15,552 feasible circuit structures. After running the optimization problem 30,000 times with random stage recovery values, only five structures were identified. The random values were obtained using a uniform distribution function with the bound indicated in Table C.1. Of these five circuits, one was obtained in 27,670 (92.2%) cases. The others circuits were observed in 6.2, 1.2, 0.3, and 0.1% of the cases. Thus, the circuits found in 92.2 % and 6.2% of the cases can be considered feasible structures for further analysis. Figure C.3 shows the circuit with the highest probability (92.2%). For the bulk circuit (blue stages), the concentrate streams were distributed as follows: R and C to the selective R, first S to C, and second S to first S.

For the tailings, there was recirculation of C to R, R to first S, first S to second S, and second S to NSG. For the selective circuit (green stages), the concentrate streams were from R to second C, S to first C, and first C to second C. For the tailings, there was recirculation of first C to R, second C to first C, R to S, and S to SG. Finally, the only difference between the circuit with a frequency of 92.2% and the one with a frequency of 6.2% was that, in the latter circuit, the concentrate stream from RS went to CS1.

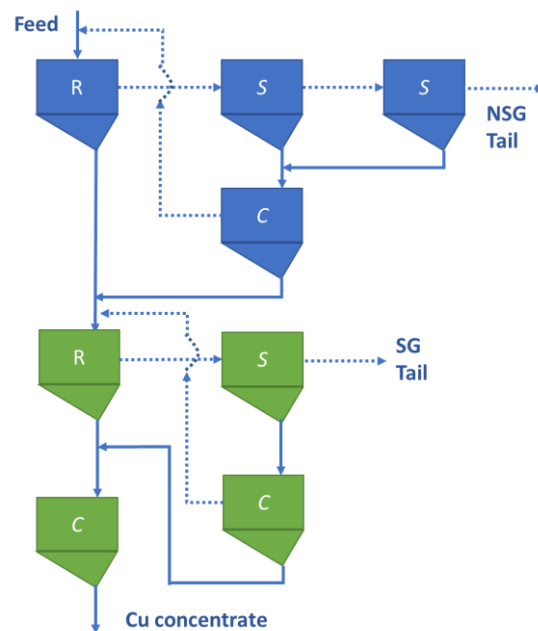


Figure C.3. Optimal fractional bulk flotation circuit. Bulk stages are presented in blue, and selective stages are presented in green.

The three products, NSG tailings, SG tailings, and copper concentrate, were assessed from economic and metallurgical points of view (average revenue, recovery, and grade obtained for each product). The average revenue was 117.6 million dollars. For the copper concentrate, the average grade was 24.9%, and the recovery was 88.1%, showing that most of the copper was concentrated. The copper grade in the SG and NSG was 0.7 and 0.016%, respectively. Thus, the optimal flotation circuit obtained a high copper recovery rate and grade. On the other hand, the grade values for the SG product were higher for iron, arsenic, and sulfur than those obtained with the copper concentrate. In general, the recovery rate of these species was higher than 73%. These results demonstrate that sulfide concentration was achieved. In the

NSG tail, the average copper, iron, arsenic, and sulfur species grades were lower than 0.08%. The NSG grades in copper concentrate, SG, and NSG were 6.3%, 51.8%, and 99.8%, respectively, demonstrating that the desulfurization of polymetallic ore was achieved.

C.3.2.2 Fractional selective circuit

For this case, the superstructure included 31,104 feasible structures. After running the optimization problem 30,000 times, only nine flotation circuits were obtained. The frequency distributions for these nine circuits were 60.5, 15.0, 12.0, 5.1, 3.6, 2.2, 1.1, 0.5, and 0.03%. Thus, only three to four circuits needed to be studied further to select the best option. It is noteworthy that the circuit with the highest frequency, 60.5 %, had the highest probability of being the best circuit, because it was shown to work the best for a high number of stage recovery combinations. Figure C.4 shows the results for the circuit with the highest frequency. The only difference between the circuit with the highest frequency and that with the second highest frequency is the direction of the concentrate stream from the rougher selective circuit. In the second circuit, the rougher concentrate is sent to the second cleaner stage. Thus, the first cleaner stage works as a cleaner of the scavenger stage.

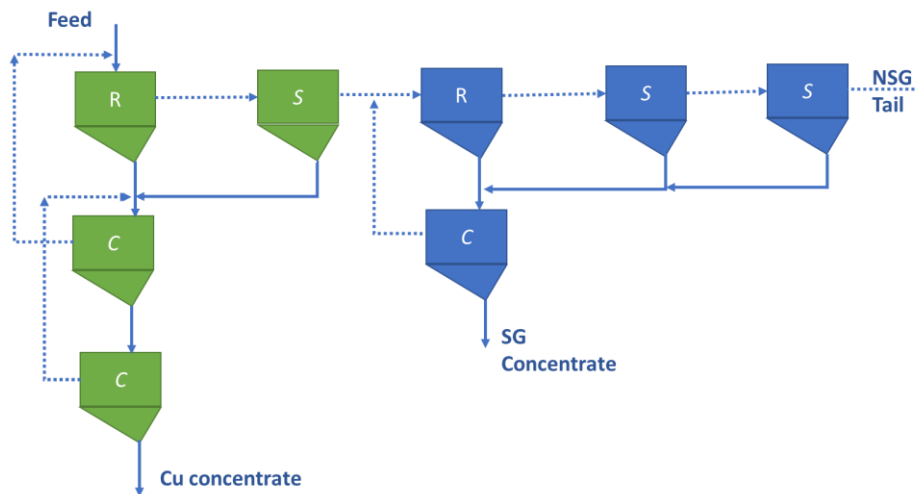


Figure C.4. Optimal sequential flotation circuit. Bulk stages are presented in blue, and selective stages are presented in green.

The three products, NSG tailings, SG tailings, and copper concentrate, were assessed from economic and metallurgical points of view. For the fractional selective circuit, the objective

function was modified by including a reward for the presence of pyrite and arsenopyrite in the desulfurized concentrate and a penalty for the total amount of desulfurized concentrate, similar to the objective function for copper but with a low value compared to that of copper. If this modification was not included, the program would provide many alternatives, because there is nothing in the objective function that represents the design problem of the desulfurization circuit. The average revenue was found to be 121.4 million dollars (without including the reward and penalty associated with the pyrite and arsenopyrite). This result was expected since, in the first selective circuit, four stages were used to get the copper concentrated. For the copper concentrate, the average grade was 27.5%, and the average recovery rate was 89.8%, showing that most of the copper was concentrated. On the other hand, the average recovery rates of the Fe, As, and S species were higher than 77% in the SG tail. For the NSG product, the average sulfur grade was 0.074 %, demonstrating that the desulfurization of polymetallic ore was achieved. The average copper recovery in the SG was 9.9 %, indicating that selective separation occurred.

C.3.2.3 Integrated circuits

For this case, the superstructure included 2,799,360 feasible structures. After running the optimization problem 30,000 times, fifteen circuits were obtained. However, nine had low frequencies of less than 1%. On the other hand, the three circuits with the highest frequencies represented 56.3, 20.4, and 13.5% of the solutions. The circuit with the fourth highest frequency had a value of 2.2%. Thus, three circuits accounted for 90.2% of all cases, and these are worth analyzing if one wishes to select one for the final design. Figure C.5 presents the two circuits with the greatest frequencies. Note that the circuit on the left is not an integrated circuit, because the bulk circuit generates a concentrate that is fed to the second selective circuit. However, the second circuit, presented on the right in Figure C.5, is an integrated circuit. Here, two concentrates are produced in the bulk circuit: one is fed to the rougher stage and the other to the cleaner stage of the selective circuit. In addition, the tail of the rougher stage of the selective circuit is sent to a bulk stage.

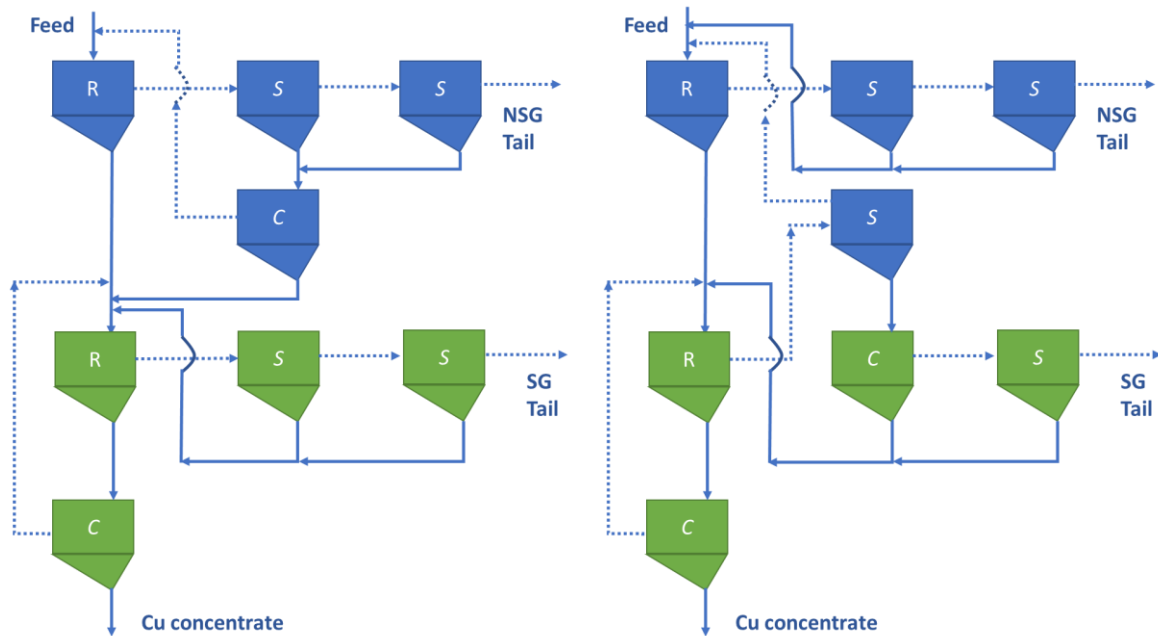


Figure C.5. Optimal integrated flotation circuits (left with a frequency of 56.3, right with a frequency of 20.4). Bulk stages are presented in blue, and selective stages are presented in green.

The average revenue was 124.8 million dollars. In the copper concentrate, the average grade was 24.3%, and the average recovery was 93.8 %, showing that most of the copper was concentrated. The average copper grade was 0.4 and 0.018% in the SG and NSG, respectively. Thus, the proposed flotation circuit enables a high copper concentration to be reached. Additionally, the average sulfur grade in the NSG was 0.095%, demonstrating that the desulfurization process was achieved.

For the integrated disjunctive, the flotation stages can operate as bulk or selective. In other words, the origin-destination matrix of Table C.2 includes flotation stages that can have different recovery values depending on whether they act as bulk or selective. The optimization problem will select the best condition based on the objective function. For this case, the superstructure included 78,382,080 feasible structures. After running the optimization problem 30,000 times, twenty-three circuits were obtained. However, nine had low frequencies of less than 1%, and another eight had frequencies of between 1% and 6%. On the other hand, the four circuits with the highest frequencies had values of 39.9, 10.6, 9.0, and 6.3%. Thus, there were four circuits that are worth analyzing to select the final design. Figure C.6 presents the circuit with the highest frequency. Note that the selective circuit has one

concentrate and two tails. The first tail is sent to the bulk circuit where the sulfur species are recovered and then sent to the selective circuit again. In other words, the SG is depressed, floated, and depressed again. Additionally, a stream from the selective circuit is sent to the bulk circuit and vice versa.

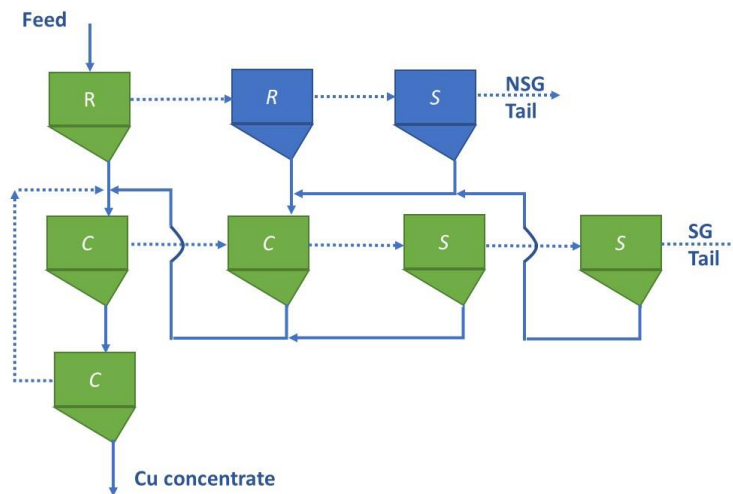


Figure C.6. Optimal integrated flotation circuit with disjunction. Bulk stages are presented in blue, and selective stages are presented in green.

The average revenue was 129.3 million dollars. In the copper concentrate, the average grade was 27.3% and the average recovery rate was 95.7%, showing the best copper recovery and grade. The average copper grade was 0.1 and 0.020% in the SG and NSG, respectively. Thus, the proposed flotation circuit enables a high copper concentration to be reached. Additionally, the average sulfur grade in the NSG was 0.35%, demonstrating that the desulfurization process was achieved.

C.3.3 General discussion

The first question that is analyzed was whether monometallic mineral flotation circuit design strategies are applicable to polymetallic mineral circuit designs. The methodology applied to monometallic minerals using optimization consists of identifying a set of optimal circuits for a given problem. Once these circuits have been identified, one or more are selected for further study. These studies may include simulations, process control design, and laboratory and pilot plant tests, among other methods (Acosta-Flores et al., 2018; Calisaya et al., 2016). The first step is critical because it identifies the few circuits that are optimal for achieving a set of

possible recoveries in each flotation stage. In our case, each of the possible circuit types was solved for 30,000 sets of recovery values for each flotation stage. For the recoveries of chalcopyrite, pyrite, and arsenopyrite, the difference between the maximum and minimum values was 10 to 15%, while for NSG, it was 8% (see Table C.1). The fractional bulk, fractional selective, integrated, and integrated disjunctive superstructures included 15,552, 31,104, 2,799,360, and 78,382,080 alternatives, respectively. After running the problem 30,000 times, 5, 9, 15, and 23 optimal circuit structures were obtained for the fractional bulk, fractional selective, integrated, and integrated disjunctive superstructures, respectively. Thus, the number of optimal circuits per hundred thousand feasible solutions was 32.15, 29.94, 0.54, and 0.03 for the fractional bulk, fractional selective, integrated, and integrated disjunctive superstructures, respectively (see Figure C.7). Therefore, it can be said that there are few optimal structures for a given problem despite the uncertainty in the recovery of each stage.

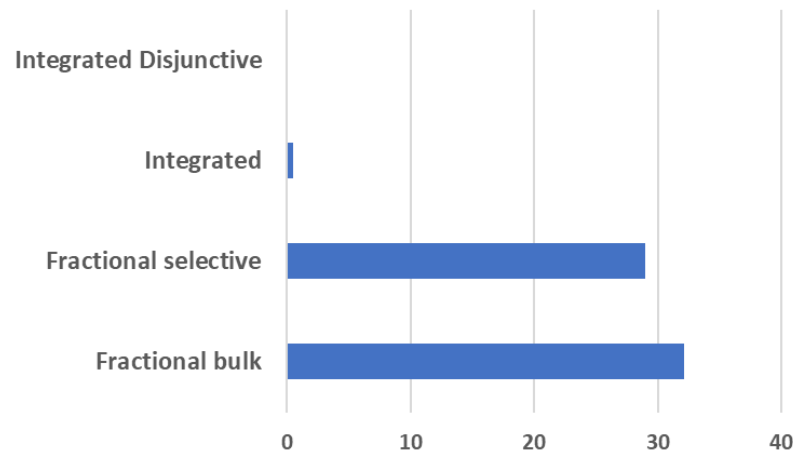


Figure C.7 Number of optimal circuits per hundred thousand feasible solutions.

Additionally, it can be said that a few structures accumulate the highest frequencies of occurrence. In other words, they have the greatest chance of being the optimal structure. This can be observed in Figure C.8, where two to five circuit structures represent over 90% of all cases. Thus, it can be said that the design strategy applied to monometallic ores can be applied to polymetallic minerals. It is also worth noting that the objective of applying optimization is to deliver a set of circuits for further study. The final decision will depend on other factors, such as previous experience with these circuits, process control, and costs, among others.

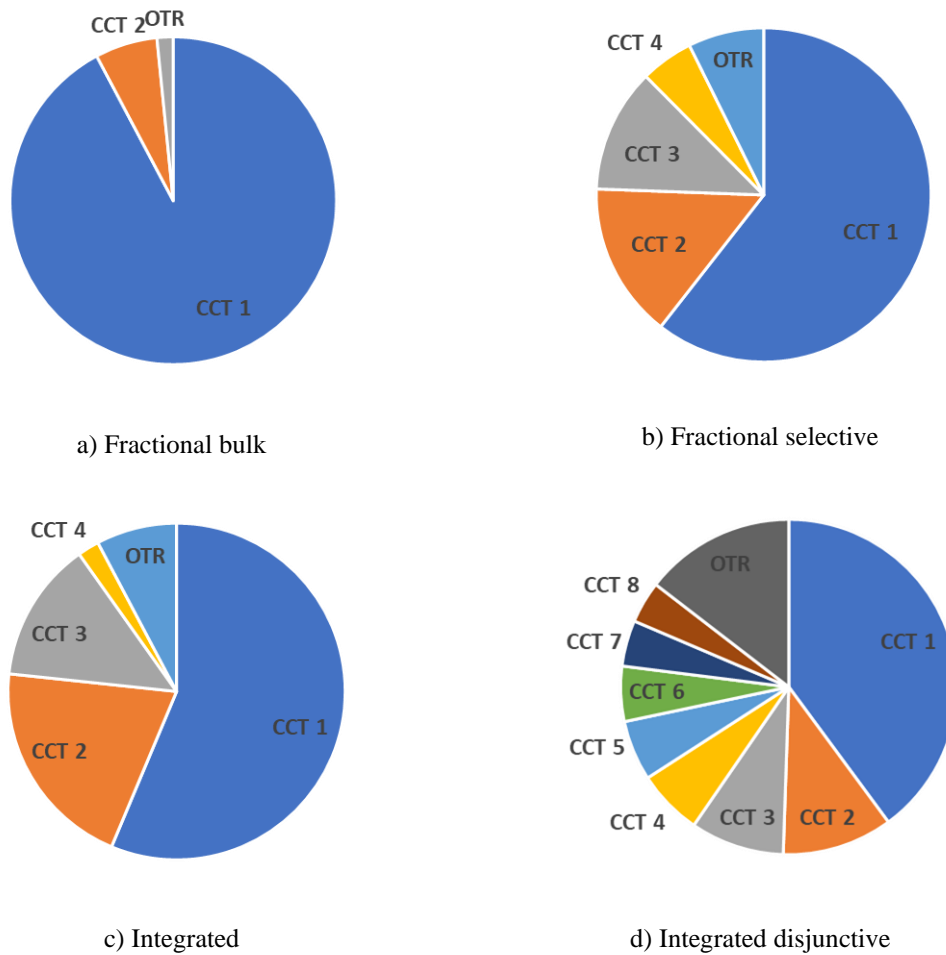


Figure C.8 Pie chart representation of the frequencies of circuit solutions. CCT stands for circuit, and OTR stands for other circuits. Here, CCT1 is the most frequently observed CCT, CCT2 is the second most frequently observed CCT, and so on.

Other research questions were analyzed: Which separation sequence is the most appropriate for a mineral? Which designs can include desulfurization as part of the flotation circuits? Which challenges exist in terms of physical-chemical studies focused on improving these circuits? This is a specific example, but its analysis can give us some insights. The first thing that can be observed is the mass flows within each circuit. Figure C.9 shows the average sum of the mass flows that feed into the flotation stages. It can be considered that with a higher mass flow, there will be more energy and water consumption, larger equipment will be required, and more reagents will be consumed, resulting in a process with more significant environmental impacts and a higher cost. If this is true, the selective fractional circuit will

produce the most significant environmental effects and cost the most. This is because the NSG, which is the species with the greatest quantity, has to be processed more times in the flotation circuit. The difference between the other design strategies is insignificant, and considering that these values correspond to the average mass flows of the 30,000 solutions, conclusions cannot be made for the other design strategies.

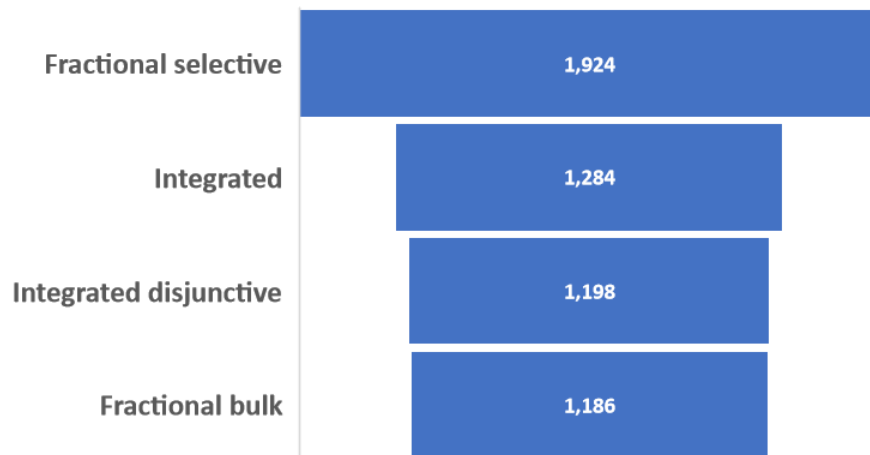
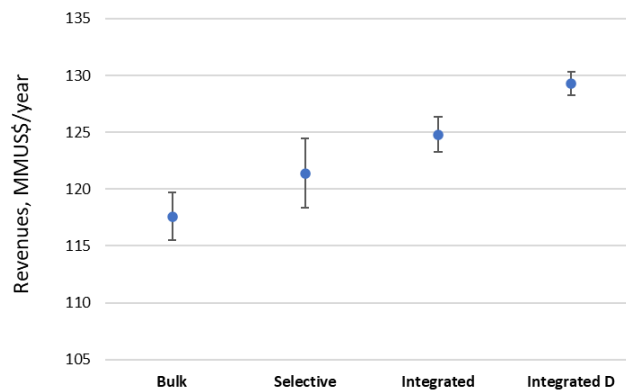
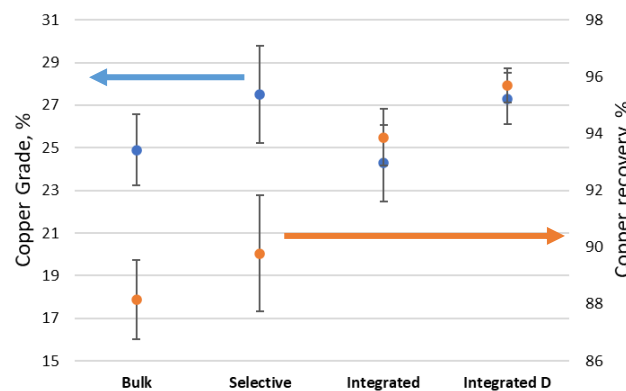


Figure C.9 Average total mass flow rate in tonne/h

Figure C.10 compares the revenue (objective function), the copper grade in the concentrate, and the copper recovery obtained from the four flotation circuits proposed: fractional bulk, fractional selective, integrated, and integrated disjunctive. A higher average recovery and revenue were obtained from the integrated-disjunctive circuit (95.7% and 129.3 million dollars per year, respectively). The order, from least to most, in terms of revenue and copper recovery is fractional bulk < fractional selective < integrated < integrated disjunctive. However, the fractional selective circuit presents the greatest dispersion in the results, meaning that there is more significant uncertainty in its behavior. The copper grade in the concentrate was similar for the four cases studied; therefore, the results are inconclusive if the standard error bars are considered.



a)



b)

Figure C.10. Average values for a) revenue in millions of US dollar per year and b) copper grade and recovery, including standard error bars.

The method proposed by Arfania et al. (2017) to estimate the CAPEX and OPEX was used. Because there were 30,000 results for each design strategy, the average mass flow feed to each flotation stage was used in the calculations. The CAPEX and OPEX results for the fractional selective circuits were found to be higher than those of other cases, as presented in Figure C.11. In the other circuit types, a significant difference between the CAPEX and OPEX values was not observed, and therefore, the results are not conclusive.

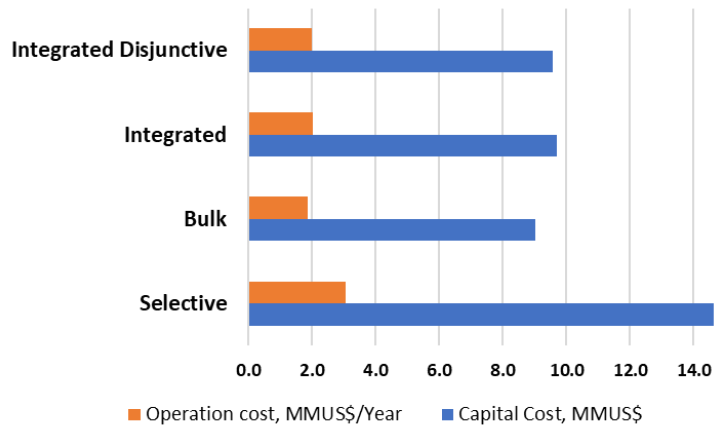


Figure C.11. Average operational and capital costs

From a desulfurization point of view, all circuits comply with the restrictions imposed in the problem definition. For example, the average S grade in the NSG is well below the maximum value allowed (1%). In fact, the circuit that gave the worst results was the integrated disjunctive, with an average S grade of 0.35%. This is because the S grade in the NSG tail was not an objective but a constraint, and this type of design can be better accommodated to achieve the restriction. The average NSG grade in the NSG tailing was 99.8% for the fractional bulk, fractional selective, and integrated circuits and 99.3 % for the integrated disjunctive circuit. To achieve these results, the restrictions included in the model in terms of the grade levels and recovery of species that generate AMD play essential roles. Additionally, the introduction of penalties by species in the copper concentrate or small rewards for the recovery of species that create AMD in the objective function plays an essential role in the process.

Based on the previously analyzed results, the selective fractional circuit delivers the worst results followed by the bulk fractional circuit. However, in practice, the most commonly used circuit is the fractional selective circuit, followed by the fractional bulk circuit (Klimpel, 2003; Xu et al., 2022). The reason for this is that selective fractional separation is the easiest to perform from a physicochemical behavior point of view. The integrated circuit and integrated disjunctive circuit proposed in this manuscript present advantages such as those indicated above. However, they present the challenge of containing floating minerals that have been depressed and vice versa. Although there have been many studies on separating

chalcopyrite from pyrite, the vast majority have focused on pyrite depression as a separation strategy (Castellón et al., 2022; Ran et al., 2023). New collectors or depressants with this separation strategy are a frequent research topic in the literature today (Botero et al., 2022; Mu et al., 2016; Saim and Darteh, 2022). However, this strategy is not suitable from an environmental point of view because it generates AMD or consumes more energy and material resources if the tail is desulfurized. Additionally, strategies to reduce the environmental impact include the use of green reagents (Fan and Hobert, 2022; Liu et al., 2022; Yuan et al., 2022); however, reducing the material to be treated reduces the reagent consumption, a fact that has received little attention. Therefore, there is a need to study other strategies, such as the depression of activated pyrite (San Martín et al., 2021) or the conditions for bulk and selective flotation (Botero et al., 2021). While difficult, it is possible to depress pyrite once it has floated. A study showed that after obtaining a pyrite recovery of greater than 95% by flotation using xanthates, it was possible to reduce the recovery using diethylenetriamine (Ahmadi et al., 2018). Understanding how to manipulate flotation and depression in different sequences is essential to develop more efficient processes with less environmental impact.

C.4 Kevitsa mine (Cu-Ni-PGE) flotation circuit case study

C.4.1 Problem presentation

This section presents the design and analysis of the copper and nickel concentration process and the subsequent tail desulfurization of the Boliden Kevitsa mine. The Geological Survey of Finland discovered Kevitsa's multimetal deposit in 1987. The Canadian mining and metals company First Quantum Mineral decided to build a mining facility in Sodankylä in 2008. Construction of the mine began in the summer of 2010, and production began two years later in 2012. Since June 2016, the Kevitsa mine has been part of the Boliden Group, a Swedish multinational metals, mining, and smelting company ("Boliden," n.d.). In 2016, a manuscript was published in *Minerals Engineering* outlining the process improvements from 2012 to 2016 (Musuku et al., 2016), including circuit configuration, that have enhanced process profitability. This is one of the few cases of polymetallic design available in the literature and is therefore included in this section for further study.

Kevitsa is a low-grade deposit. Pyrrhotite, chalcopyrite, and pentlandite are the main sulfide minerals, and the pyroxene group is the major NSG. Although there is variability in feed grades, the values presented in Table C.3 were used in this research paper. The stage recoveries presented in Table C.3 were determined by using the mass balances reported by Musuku et al. (2016), and results similar to those reported were obtained. The Kevitsa concentrator employs a Cu–Ni fractional selective flotation circuit with a desulfurization circuit at the end of the process. The original flotation circuit is a typical conventional polymetallic flotation (See Figure C.12) where copper is concentrated in the first circuit, and this is followed by a nickel flotation circuit. Two flotation stages are utilized at the end to desulfurize the tailings.

Table C.3. Major minerals and stage recoveries in the Kevitsa concentrator utilized in this study.

Identification	Name	Chalcopyrite	Pentlandite	Pyrrhotite	Nonsulfur gangue
	Formula	CuFeS ₂	(Fe,Ni) ₉ S ₈	Fe _{1-x} S	-
	Symbol	Cp	Pn	Po	NSG
Feed	tonne/h	8.07	5.44	14.73	903.84
	Composition (%)	0.87	0.58	1.58	96.97
Stages recoveries					
Copper Circuit	Rougher	0.543	0.112	0.085	0.013
	Cleaner	0.790	0.459	0.530	0.362
	Scavenger	0.401	0.116	0.086	0.028
Nickel Circuit	Rougher	0.253	0.350	0.272	0.044
	Scavenger	0.773	0.844	0.861	0.203
	Cleaner	0.174	0.697	0.552	0.385
Sulfur Circuit	Rougher	0.293	0.395	0.444	0.013
	Cleaner	0.575	0.553	0.523	0.052

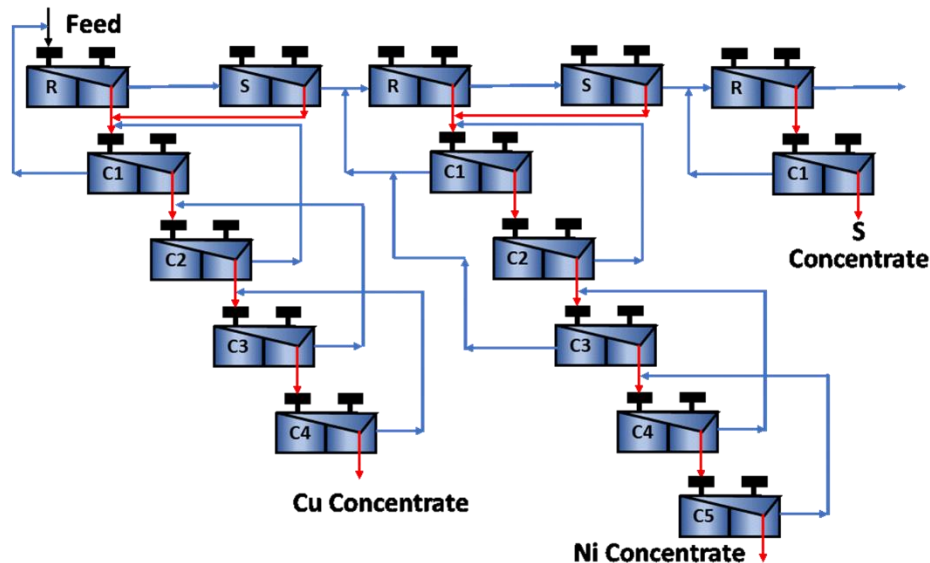


Figure C.12 Original Kevitsa flotation circuit design (Modified from (Musuku et al., 2016))

Three strategies were utilized to improve the Kevitsa concentration. In all cases, desulfurization was not included, but it is discussed at the end. The first strategy consists of a one-at-a-time circuit design. The copper circuit is designed first, and the tailing from this circuit is considered to be the feed for the nickel circuit. The nickel circuit is designed next. In the second strategy, both circuits are designed simultaneously. The tails from the rougher, scavenger, and cleaner stages from the copper circuit can be sent to the rougher stage in the nickel circuit. These two approaches consider fractional selective separation without any integration between the Cu and Ni circuits, other than the tailing from the copper circuit that is fed to the nickel circuit. Additionally, the first case is a sequential local optimization approach where the decision is made initially by the downstream circuit and then by the upstream circuit. The second case is a global optimization approach where the decision is made jointly by all circuits. In the third strategy, integration between these circuits is allowed. Here, several stream connections are allowed. The concentrate from the scavenger in the nickel circuit can be sent to the rougher and cleaner 1 stages of the copper circuit. The tail stream from the rougher, cleaner 1, cleaner 2, and cleaner 3 stages from the copper circuit can be directed to the rougher stage from the nickel circuit. Tail from the copper scavenger stage can be fed to the nickel rougher and scavenger stages. Tail from the copper cleaner 1

stage can be fed to the nickel scavenger stage. Finally, the tail from the nickel cleaner 1 and cleaner 2 stages can be delivered to copper rougher stage.

In all cases, the stage recoveries presented in Table C.3 were utilized. It was assumed, based on Section 3, that the optimal circuit structure would not be sensitive to changes in stage recoveries if they remained within a reasonable range. Therefore, it was assumed that the recoveries presented in Table C.3 may change from one design to another, but not significantly. The objective function utilized was the revenue or net smelter return (Equation 3) for both the copper and nickel concentrates. Therefore, the gains increased as the recovery of the valuable species increased, and it decreased as the worthless species reached the final concentration.

There are 103,680 and 14,515,200 possible alternatives for the copper and nickel circuits, respectively. Although these numbers are large, if the origin-destination matrix is not used, there are more than 2 and 678 million possibilities for the copper and nickel circuits. For the simultaneous solution of both circuits, there are 1,504,936 million viable circuits.

C.4.2 Results and Discussion

Figures C.13, C.14, and C.15 illustrate the optimal circuit designs for the first, second, and third design strategies. The first strategy, the one-at-a-time circuit design, provides the closest design to the improvements applied to the original Kevitsa design (see Figure C.2 in (Musuku et al., 2016)). It introduces cleaner stages for the scavenger stages of both the copper and nickel circuits. The improvements reported by Musuku et al. also included the combination of the cleaner 1 tails with the scavenger tails in the copper and nickel circuits. These modifications were not obtained in any optimized design; therefore, they are suboptimal modifications, at least in terms of the recovery and economic value aspects considered in this study. It is important to note that the integrated circuit (Figure C.15) only includes one integration stream. The tail of cleaner stage 1 of the nickel circuit is sent to the rougher stage of the copper circuit.

The performance levels of the original design and the optimized designs are summarized in Table C.4. The revenues are 314.9, 282.9, 280.6, and 261.9 million dollars per year for the integrated, simultaneous, one-at-a-time, and original designs. It is clear that there are

improvements in copper and nickel recovery and grades in the optimized designs. The simultaneous circuit design generates a slight improvement compared to the one-at-a-time design. Although small, it is worth considering the simultaneous design, which allows conditions that add to the overall gain rather than the individual gain of each circuit to be considered. The integrated design presents significant improvements over the other two designs. These improvements are in terms of revenue, recovery, and grades, as can be observed in Table C.4. As indicated above, only one integration stream is included, which produces significant changes in the process. However, it introduces a greater challenge when incorporating streams that present different operating conditions or where it is necessary to change the surface characteristics of the mineral. This means that some action on this integration stream will be necessary, the study of which is outside the scope of this work. The results show that it is necessary to look at the design problem as a whole and not by the concentration stages of individual minerals. Additionally, it is important to highlight the need to carry out studies that allow the depression of minerals that have been floated and vice versa. These studies can favor flotation systems where all the minerals are sought to be recovered simultaneously. These results and the analysis allow some insight into the question of the advantages of designing flotation circuits simultaneously versus one-at-a-time for each metal.

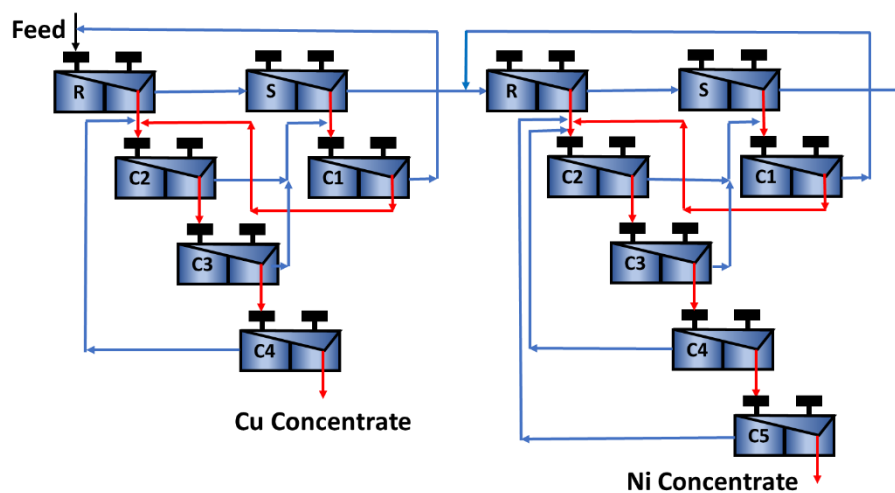


Figure C.13 Optimal Kevitsa flotation circuit design for the first strategy: one-at-a-time circuit design

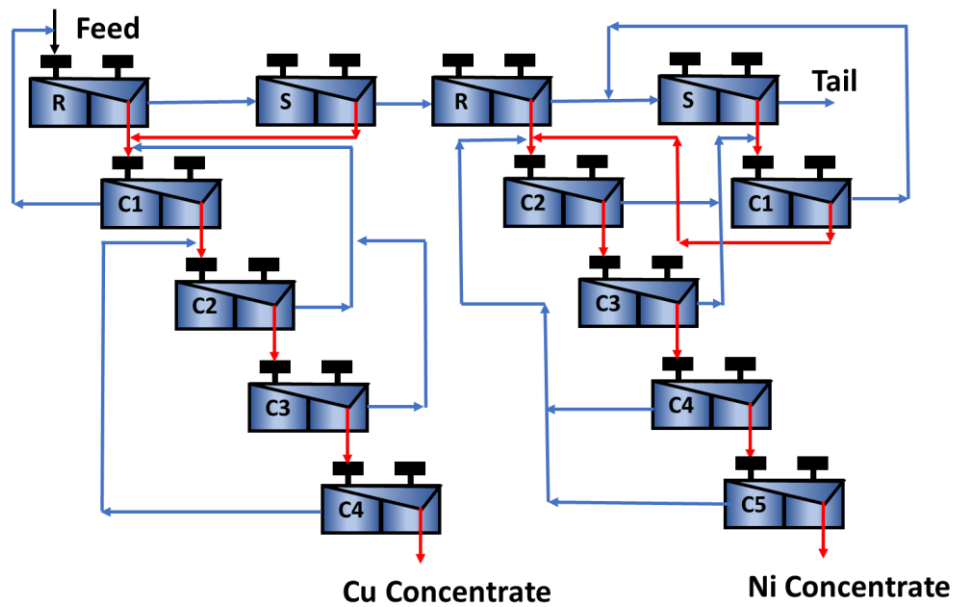


Figure C.14 Optimal Kevitsa flotation circuit design for the second strategy: simultaneous circuit design

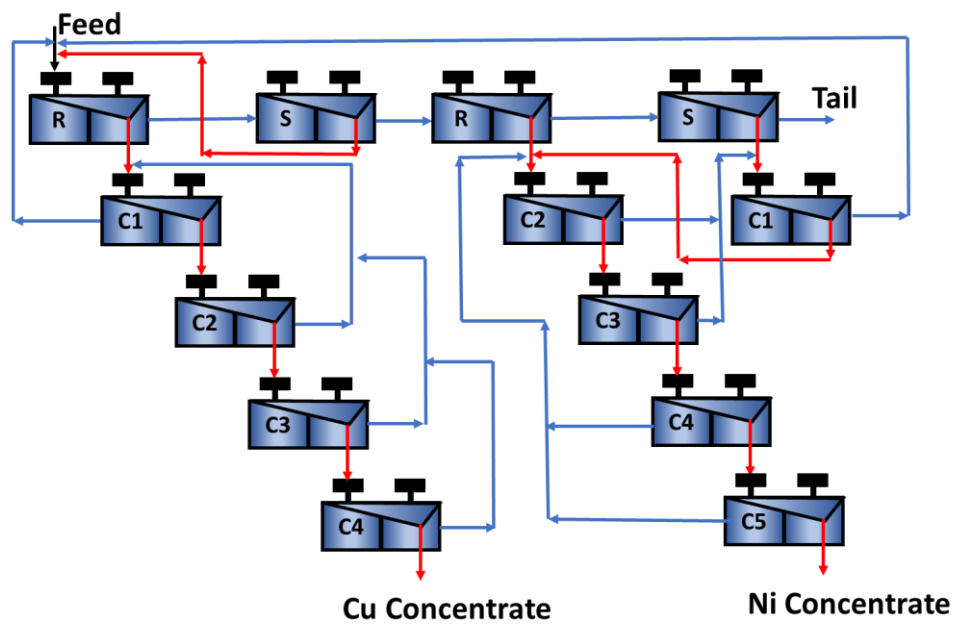


Figure C.15 Optimal Kevitsa flotation circuit design for the third strategy: integrated design.

Table C.4. Summary of the performance of the original design and new design.

Circuit	Revenue	Recoveries				Concentrate grade		
	MMUSD/year	Cp	Pn	Po	NSG	Cu	Ni	Po
Original design								
Cu	72.3	66.06	3.4	4.68	0.20	22.98	0.85	8.53
Ni	189.6	0.13	75.67	54.28	0.64	0.01	7.76	43.9
Total	261.9							
One at a time circuit design								
Cu	75.7	68.37	3.61	4.43	0.19	23.69	0.83	8.05
Ni	204.9	0.23	80.88	58.18	0.62	0.01	8.03	45.56
Total	280.6							
Simultaneous circuit design								
Cu		64.8	2.27	3.08	0.21	26.22	0.61	6.58
Ni		0.08	79.05	56.39	0.61	0.01	8.06	45.75
Total	282.9							
Integrated design								
Cu		88.18	1.95	5.66	0.05	29.09	0.42	9.79
Ni		0.03	79.31	54.89	0.61	0.00	8.18	45.05
Total	314.9							

Desulfurization was not included in the design problem. There are two reasons for this: First, only two flotation stages were considered (see Figure C.12), so there were not many options to be generated or the problem could be analyzed for all possibilities. Even so, the presence of these few options would increase the total number of possible circuits significantly in the simultaneous or integrated designs because of the combinatorial nature of the mathematical problem. Second, desulfurization at the end of the process does not seem to be a novel idea. The studies presented in Section C.3 show that the possibility of generating a pyrrhotite bulk with chalcopyrite or pentlandite could have been interesting to address. Unfortunately, no data or information on its feasibility are available. In any case, the original circuit (with rougher and cleaner) may produce the concentrate with the best grade of pyrrhotite but not the highest recovery, as is known for this type of circuit. For the circuits presented in Figure C.16, from left to right, the recovery rate goes from high to low. In fact, the rougher-scavenger circuit recovers more than twice as much S as the rougher-cleaner circuit.

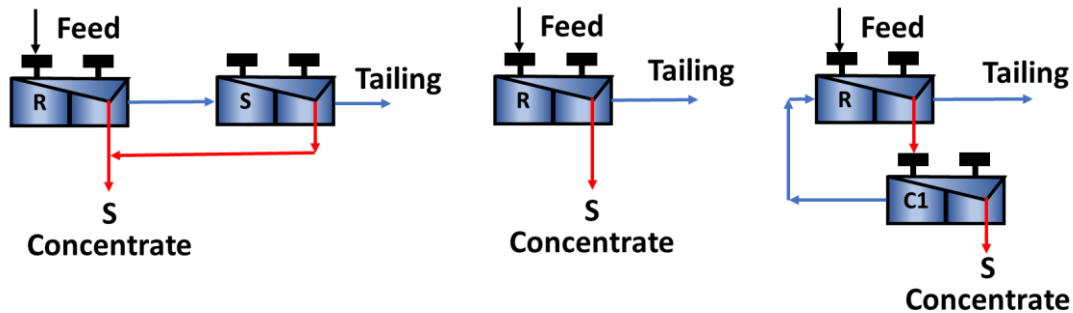


Figure C.16. Desulfurization options for the Kevitsa concentration.

In this example, the possibility of bulk flotation was not considered, since there are no data available to study this possibility. The separation sequence used, fractional selective, proved to be the least efficient in the study presented in Section 3.

C.5 Conclusions

Let's remember that this paper aims provide some insights into the design of polymetallic flotation circuits, including tailing desulfurization by answering questions such as Are monometallic mineral flotation circuit design strategies applicable to polymetallic mineral circuit designs? Which separation sequence is the most appropriate for a particular mineral? What are the advantages of designing flotation circuits simultaneously versus one at a time for each metal? Which designs can include desulfurization as part of a flotation circuit? Which challenges exist in terms of conducting physical-chemical studies to improve these circuits?

Based on the results obtained, the following conclusions can be reported. First, the design strategy developed for monometallic minerals using optimization can be applied to polymetallic minerals. Two observations support this statement: a) there are few optimal structures for a given problem despite the uncertainty in the recoveries of each stage and b) few structures accumulate the highest frequencies of occurrence or, in other words, have the greatest chance of being the optimal structure.

Second, the order, from most to least, in terms of the revenue and copper recovery obtained in the circuit design is as follows: integrated disjunctive > integrated > fractional selective > fractional bulk. However, the selective fractional circuit will produce the most significant environmental effects and cost the most. In addition, the fractional selective circuit presented

the greatest dispersion in the results and more significant uncertainty in its behavior. The copper grade in the concentrate was similar among the four cases studied; therefore, the results were inconclusive if the standard error bars are considered. The CAPEX and OPEX values were higher for the fractional selective circuits than for the other design cases.

From a desulfurization point of view, all studied circuits comply with the restrictions imposed in the problem definition. To achieve these results, the restrictions included in the model in terms of grade levels and the recovery of species that generate AMD play essential roles. Additionally, the introduction of penalties due to having species in the copper concentrate or small rewards for the recovery of species that create AMD in the objective function is essential.

Third, based on the previously analyzed results, the selective fractional circuit delivers the worst results, followed by the bulk fractional circuit. The integrated circuit and integrated disjunctive circuit proposed in this manuscript present the best results. However, they offer the challenge of containing floating minerals that have been depressed and vice versa. Therefore, there is a need for further study to manipulate flotation and depression in different sequences to develop more efficient processes with less environmental impact.

Fourth, based on the Kevitsa concentration case study, it is concluded that the application of optimization can provide designs that can be studied further. The simultaneous design of all circuits for a polymetallic mineral gives better results than a one-at-a-time design. The design of polymetallic mineral flotation circuits as a system where interaction between the circuits is possible can generate an important improvement.

Finally, based on these results, the design of flotation circuits for polymetallic minerals can be carried out in two stages. In the first stage, approximate values of the recoveries at each stage are used to identify a set of optimal solutions. Then, in the second stage, these circuits are studied in depth, including through experimental studies, to select the most suitable design.

Authors & Contributions

Yesica L. Botero. Conceptualization, methodology, formal analysis, writing original draft—review and editing.

Luis Cisternas. writing—review and editing, conceptualization, methodology, formal analysis, supervision, project administration, funding acquisition.

Isabelle Demers. Formal analysis, writing—review and editing, supervision.

Mostafa Benzaazoua. writing—review and editing, supervision.

APPENDIX D ARTICLE 4: APPLICATION OF CHARACTERIZATION TECHNIQUES FOR THE PREVENTION OF AMD FOR WASTE ROCK FROM A CHILEAN PORPHYRY COPPER MINE

Article 4: Yesica L. Botero, Isabelle Demers, Luis A. Cisternas and Mostafa Benzaazoua. Application of characterization techniques for the prevention of AMD for waste rock from a Chilean porphyry copper mine. Conference paper, presented in the 6th International Symposium on Process Mineralogy (Process Mineralogy '22), Sitges, Spain, 2022.

This article was submitted to Process Mineralogy'22 on June 22, 2022.

Abstract

Based on the concept of cleaner production, In-Process technology is an interesting alternative to identify the source of acid generation; this includes adopting actions before stockpiling the waste rock (WR) to know the potential contaminants and predict the method that is more convenient to be implemented for AMD prevention. In our work, various characterization techniques (ICP-MS, S/C, Sulfate, XRD, XRF, and QEMSCAN) were used to quantify WR's net acid generating potential by incorporating the degree of liberation of sulfides and neutralizing minerals. Around 1 tonne of WR < 5mm sampled from the stockpile was separated into five fractions: F5 (-5 mm to +2.4mm), F4 (-2.4mm to +850 μ m), F3 (-850 μ m to +300 μ m), F2 (-300 μ m to +53 μ m) and F1 (-53 μ m). The chemical and mineralogical results show that the WR is mainly composed of pyrite. The pyrite mass percentage for F2 and F3 was 7.9 %, and for F1, F4 and F5 was, on average, 5.4%. The calcium deportment was mostly anhydrite and anorthite. The carbonate content, mainly calcite, was low (<0.3 wt %) for all fractions. The sulfides were liberated from F1 to F4 (97-50%), and F5 was 9% liberated. The WR fractions were submitted to the static test (acid-base accounting (ABA)) to evaluate their acid-generating potential. The acid potential (AP) was measured considering the liberation degree of sulfides. The neutralization potential (NP) was quantified using the method proposed by Lawrence et Wang (1997). The liberation degree of carbonates was not considered due to the low overall amount in the WR. Besides, it was defined the diameter of

the physical locking of sulfides (DPLS) to classify the WR into reactive and non-reactive fractions, based on the particle size of the selected fractions and sulfides liberation degree.

Keywords: waste rock, Acid-Base Accounting static test, DPLS, liberation degree, acid mine drainage.

D.1 Introduction

Copper is mainly supplied from primary sources, which is a significant issue in the mining industry because the global reserves of copper are expected to decrease dramatically by 2050, with a corresponding ore grade decline to approximately 0.1%. Thus, as copper demand increases, the ore grade decreases (Elshkaki et al., 2016). The high demand for copper is correlated to the growth of the global population and economic development, which increases the consumption of this metal in several economic sectors, notably plumbing, wiring, and electricity. The last two are largely related to the global desire for greener economies and the expansion of electric vehicle sales, which use four times as much copper as petroleum-fueled cars. This growth requires greater infrastructure to be able to have adequate charging stations (MINING-DOT-COM, 2021). Thus, with a greater copper demand and ore grade decreases, a larger amount of copper mining is necessary to be able to supply the demand, resulting in large quantities of solid wastes such as waste rock (WR) and tailings being produced during the extraction of economically valuable minerals. Both wastes are generally enriched with sulfide minerals such as pyrite, pyrrhotite, and arsenopyrite that have no economic value and can oxidize due to exposure to surrounding water and oxygen, generating acid mine drainage (AMD).

In this work, we will focus on the WR. Managing this solid waste is challenging for the mining industry; however, not enough attention has been paid to it. WR is removed during development and production as a means to gain access to the ore. That is why the WR usually has a low concentration of valuable minerals. Besides, WR has a heterogeneous mineralogical and chemical composition and physical characteristics due to the deposition of the wastes from different mine sources (Amar et al., 2021; Amos et al., 2015; Elghali et al., 2019, 2018; Jamieson et al., 2015; Matinde, 2018). WR is generally coarse material but could have a wide range of sizes, from huge particle sizes to dust-size particles. The size and shape

of the material depend on the characteristics of the rock (e.g., hardness) and extraction methods (ripping, drilling, and blasting) (Elghali et al., 2019; Fala et al., 2005). The particle size distribution of WR has been studied from various mining sites. It was demonstrated that the WR corresponds to a relatively coarse material. The D_{10} of WR was found to be between 0.2 to 3 mm, and the D_{60} was between 1 to 80 mm (McKeown et al., 2000; Peregoedova, 2012). Its uniformity coefficient ($C_U = D_{60}/D_{10}$) can reach 30 or more. High values of this coefficient indicate well-graded soil.

The potential generation of AMD depends on the waste's mineralogy and the minerals' dissolution rates. The geochemical behavior of WR can be highly variable due to its significant heterogeneity (Amos et al., 2015; Wilson et al., 2018). That is why the assessment and management of WR is challenging for the mining industry (Blowes et al., 2014; Paktunc and Davé, 2000). The acid generation potential of WR can be determined by predicting the Net Neutralizing Potential (NNP) and Neutralizing Potential Ratio (NPR); several static methods have been developed based on parameters and criteria that differ from one method to another. The static prediction tests attempt to determine the balance between the acid potential (AP) of the material, derived by quantifying the acid-producing components, and the neutralization potential (NP), determined by measuring the quantities of acid-consuming components (Lawrence and Scheske, 1997). The NNP and NPR can be interpreted via the Acid-Base Accounting (ABA) diagram criteria to know the Acid generation potential (AGP) of the ore studied. The NNP is calculated by subtracting the AP from the NP ($NNP = NP - AP$). If the NNP value is lower than 20 kg $CaCO_3/t$ the sample is classified as acid-generating. An uncertainty zone is characterized by NNP values between - 20 and 20 kg $CaCO_3/t$ (Miller, S., Jeffery, J., Wong, J., 1991). Neutralization potential ratio ($NPR = NP/AP$) constitutes another index to evaluate AMD production potential. Characteristically, a sample is considered acid-generating if $NPR < 1$, uncertain if $1 < NPR < 2.5$, and non-acid generating if $NPR > 2.5$ (Benzaazoua et al., 2017, 2004; Elghali et al., 2018).

The static methods are classified into two categories: chemical and mineralogical tests. The static chemical method is the test of Sobek (1978) which is based on the total sulfur (wt% S) and total carbon (wt% C). Nevertheless, this method generates some discrepancies in the measurement of AP and NP. First, the AP is calculated based on the total sulfur content

instead of only the sulfur associated with sulfides that may produce acid when they oxidize. Second, for NP, the total carbon used in the Sobek test can also include carbon from sources other than carbonates (neutralizing minerals) (Paktunc, 1999). Therefore, the importance of mineralogical characterization in AMD prediction becomes more relevant for identifying all the minerals that can contribute to effective NP and AP calculations (Lawrence and Scheske, 1997). In this sense, the static mineralogical method is used to determine AP and NP based on the mineralogy of the sample (Lawrence and Scheske, 1997; Paktunc, 1999). Lawrence and Scheske (1997) proposed that NP calculations could be carried out using each neutralizing mineral stoichiometry. The Paktunc (1999) method presented calculations based on the sum of the individual contribution of each mineral in the production of acidity and its neutralization. This method improves the AP and NP predictions by considering other sulfides than pyrite and other carbonate minerals. Nevertheless, some studies recommended reviewing the reactivity factor for AP determination. This was implemented later by Bouzahzah et al. (2013) based on Paktunc's equation. They suggested a modified equation to attempt to include the reaction kinetics of each sulfide for AP calculations. A relative acidity production factor was determined experimentally by calculating the average of the total acidity produced by each sulfide in the leachates of the kinetic tests. Nevertheless, this factor does not consider the oxidation rates of each sulfide - and thus the kinetics of the reaction- as this factor is based on the acidity production in average and does not refer to a reaction rate. Besides, this factor does not consider the interaction between semi-conducting minerals, known as galvanic interactions, which modify (inhibit or activate) the geochemical behavior of sulfide minerals. According to this, Chopard et al. (2017) suggested using an oxidation factor that considers the kinetics of reactions of each sulfide for the mineralogical AP calculation to improve the AP estimation. Therefore, a new factor replaces the average acidity production.

However, since the mineralogical static test involves the mineral characterization of many samples, this can make the procedure tricky and expensive due to the number of characterization techniques required to obtain sufficient data. Furthermore, the detection level of some techniques, such as XRD, is insufficient to identify low amounts, making the accuracy of AP and NP calculations more difficult. In this work, the method developed by Elghali et al. (2018) was implemented. In this method, the ABA test was corrected by

introducing the degree of sulfide and carbonate liberation, which account for the initial texture of minerals. Thus, the AP and NP values were calculated as follows:

$$AP = 31.25 \times S_{\text{sulfides}} (\text{wt.}\%) \times L_s (\text{kg CaCO}_3/\text{t}) \quad (\text{D.1})$$

$$NP = 83.3 \times \text{TIC} (\text{wt.}\%) \times L_c (\text{kg CaCO}_3/\text{t}) \quad (\text{D.2})$$

Where: L_s and L_c are the liberation degree of sulfides and carbonates, respectively. Values of L_s and L_c were obtained using QEMSCAN. S_{sulfides} and TIC are the wt. % of sulfur associated with sulfides and total inorganic carbon, respectively. Nevertheless, it is worth mentioning that it was not possible to calculate the NP using this method because the porphyry copper ore used in this work does not have a significant enough amount of carbonates to be considered in the calculation. Therefore, the method proposed by Lawrence and Wang (1997), which modified that proposed by Sobek et al. (1978), was used. This method proposes longer duration digestion (at room temperature, for one week) to take into account the more or less slow dissolution kinetics of the carbonates and silicates. The authors noted that a prolonged digestion time allowed a lower NP overestimation.

Another relevant aspect to be studied in this work is the diameter of the physical locking of sulfides (DPLS) to classify the WR into reactive and non-reactive fractions. Introduced by Smith and Huyck (1999), the DPLS refers to the particle size in which the sulfides are locked by non-sulfide gangue and therefore make the mineral non-reactive. In this context, the particle size distribution in a WR plays an essential role in the AMD assessment. It was also suggested that the particle size from which the WR could be available for reactions and therefore generate AMD is less than 4mm. Some other studies proposed less than 6.3mm or less than 2mm (Lapakko, 2003; Smith and Huyck, 1999). The selection of this value could be tricky since it strongly depends on minerals' textural and mineralogical liberation. In this sense, the chemical and mineralogical characterization of the WR is a relevant aspect of the AMD assessment and management since it enables a deep analysis of the bulk chemical composition of the WR.

This study investigated the influence of the sulfide's degree of liberation and particle size distribution on the geochemical behavior of a WR from a Chilean porphyry copper mine. For the static tests, the WR was divided into five fractions to determine the DPLS and predict AMD onset. It is worth mentioning that this type of ore has never been studied using this

methodology. Particle sizes less than 5mm were selected based on the works mentioned above (Lapakko, 2003; Smith and Huyck, 1999). This study highlights the benefits and importance of knowing the WR mineralogical composition in AMD prediction. Finally, the ABA test and DPLS results will be used in the future work that will be focused on the desulfurization of WR using the flotation process (Hydrofloat - Denver cell).

D.2 Materials and methods

D.2.1 Sample preparation

Figure D.1 shows the general structure of the methodology that was developed to conduct the sampling preparation, WR characterization, ABA test, and DPLS determination. The methodology was based on developing several steps. The procedure starts with the sample preparation of WR. Firstly, around 2.3 t of WR was taken from a stockpile in a dump; it was homogenized, sieved, and classified into five initial fractions: sieves >2", >1 1/2", >3/4", -3/4" to +5mm, and <5mm. Then, the particle sizes <5mm, were selected to conduct the textural and mineralogical analysis of the WR. Around 1 t of WR <5mm was wet sieved and divided in five fractions as follows: F5 (-5 mm to +2.4mm), F4 (-2.4mm to +850 μ m), F3 (-850 μ m to +300 μ m), F2 (-300 μ m to +53 μ m) and F1 (-53 μ m). Each fraction was characterized by neutralizing potential ((NP) acid-base titration), ICP-MS, XRF, S/C, Ssulfate (chemical analysis), and by XRD and QEMSCAN (mineralogical analysis). The NP was measured using the method proposed by Lawrence, R. W., & Wang, 1997, the liberation of sulfides (Lsulfides) was determined by QEMSCAN, and the AP was calculated using the method proposed by Elghali et al., 2018 (eq.1). Based on the data available, the mineralogical reconciliation was conducted, and the ABA test was determined per fraction. These results allowed us to determine the DPLS of the WR.

D.2.2 WR geological setting

The Centinela mine is located in the Atacama Desert (northern Chile). The Atacama Desert is known worldwide for hosting numerous world-class porphyry Cu deposits. The Centinela mine exposes several porphyry Cu deposits affected by supergene mineralization. These are open pit mines: mirador, penacho blanco, polo, esperanza, south esperanza, and encuentro. The last three are sulfurous pits (Riquelme et al., 2018). The main production is copper

concentrate and cathodes. The WR dumps are located next to each mine, as shown in Figure D.2.

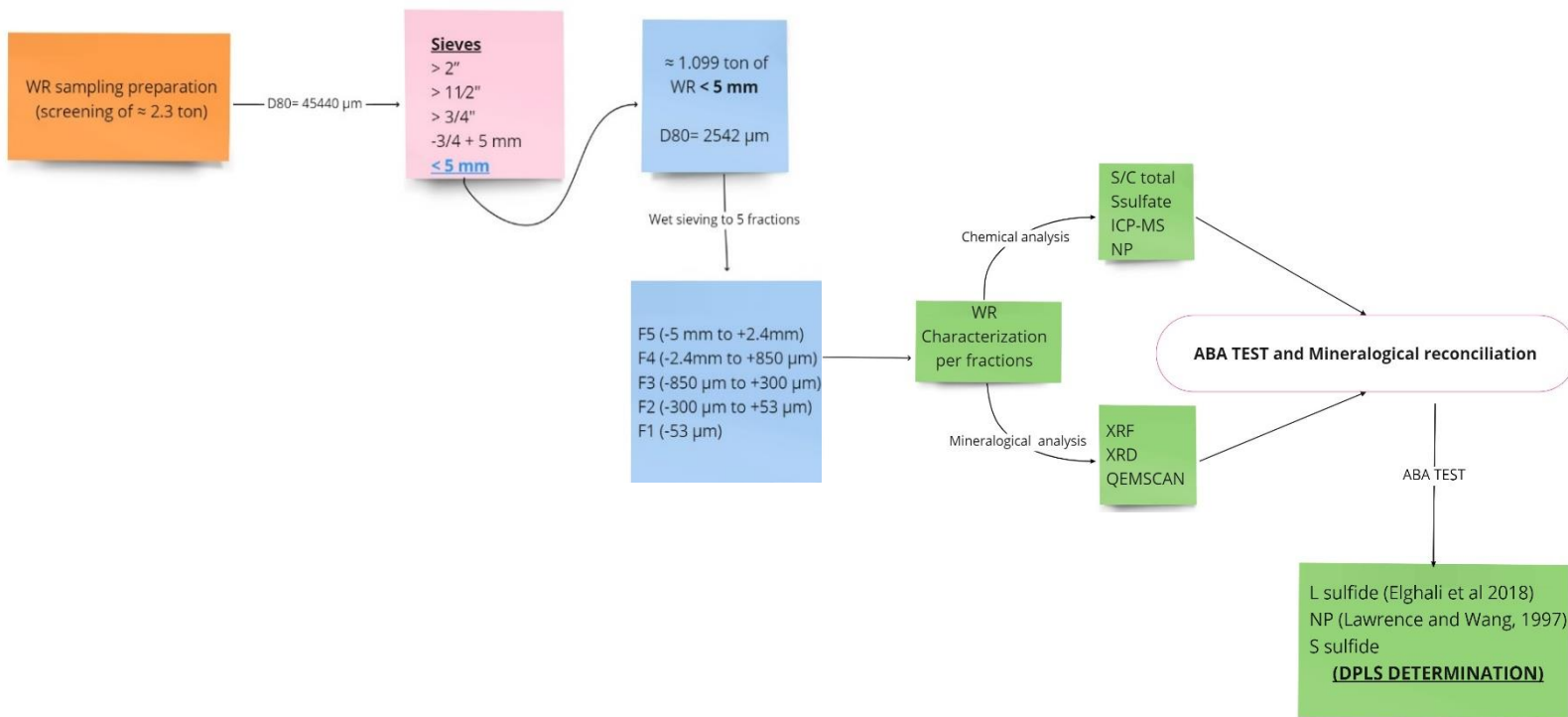


Figure D.1. The methodology implemented for WR sampling preparation and DPLS determination.

D.2.2 WR geological setting

The Centinela mine is located in the Atacama Desert (northern Chile). The Atacama Desert is known worldwide for hosting numerous world-class porphyry Cu deposits. The Centinela mine exposes several porphyry Cu deposits affected by supergene mineralization. These are open pit mines: mirador, penacho blanco, polo, esperanza, south esperanza, and encuentro. The last three are sulfurous pits (Riquelme et al., 2018). The main production is copper concentrate and cathodes. The WR dumps are located next to each mine, as shown in Figure D.2.

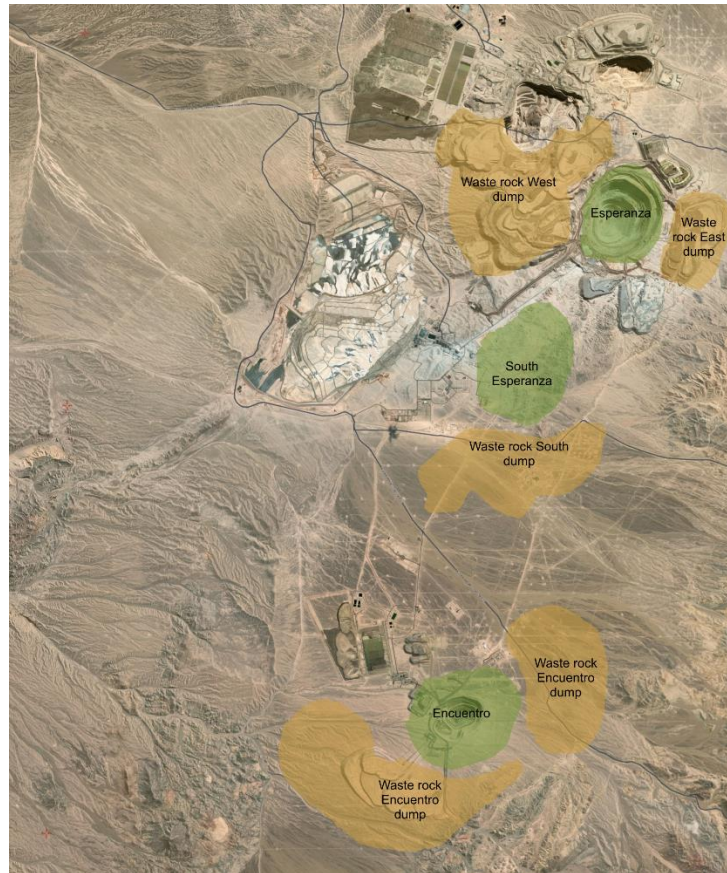


Figure D.2. Distribution of WR dumps in Centinela mine.

D.2.3 WR characterization

D.2.3.1 Physical and chemical analyses

The specific gravity (Gs) of the head sample (>5mm) was performed using helium pycnometry, with micromeritics Accupyc 1330 in URSTM-IRME UQAT laboratory in Quebec, Canada. The particle size distribution of the head sample was determined by sieving using civil series and the fine fraction was measured with a laser particle sizer, using a Malvern Mastersizer S. The WR <5mm was homogenized, wet sieved, and divided into five fractions (F1 to F5) as mentioned in section 2. Then, representative samples were taken from each fraction, followed by pulverization prior to performing all the chemical analyses. The bulk composition of each fraction was determined by ICP-MS (Perkin Elmer optima 3100 RL). The procedure was conducted using four-acid digest package (HCl/HClO₄/HF/HNO₃). The S/C_{total} content were analyzed by induction furnace (ELTRA CS-2000), with a detection

limit of 0.05 and 0.009 wt % for C_{total} and S_{total} , respectively. In the case of S_{total} , it was necessary to measure the S_{sulfate} deportment due to the high content of sulfates in the WR. Therefore, the S_{sulfate} was calculated using the ICP-AES chemical analyzes of sulfates following extraction with 40% HCl (detection limit 0.001%). NP was measured using the method proposed by Lawrence, R. W., & Wang, 1997, HCl 25% and NaOH 0.2 N were used as reagents for the digestion. Finally, the X-ray fluorescence (XRF) (thermo scientific NITON 2008 at SGS laboratory in Ontario, Canada), detection limit 0.01 wt %, was used to determine the major and minor elements as well as some trace elements in the WR.

D.2.3.2 Mineralogical analyses

The mineralogical composition of WR (F1 To F5) was determined by X-ray diffraction (XRD) using a Bruker AXS D8 equipped with a copper anticathode. The peaks were identified by EVA software, and the quantification of the abundance of all identified species was conducted using TOPAS software (Rietveld refinement). The scanning range (2θ) was from 0° to 100° . Mineralogical characterization was carried out using a combination of the field image, particle mineral analysis (PMA), and specific mineral search (SMS) methods of the Quantitative Evaluation of Materials by Scanning Electron Microscope (QEMSCAN 650F instrument). The particle size dictated the employment of the different methods. For samples F1 and F2, the particle size was adequate to be characterized by PMA for Modal Mineralogy, and SMS for liberation analyses. The particle size in the F3 sample required a combination of PMA and field image methods, whereas the F4 and F5 particle sizes only permitted the use of the field image method. The PMA measurements were run at a pixel step size (resolution) of 2 μm and field size of 1000 μm , the SMS measurements were run at a resolution of 3 μm and 1000 μm field size, and field images were run at a resolution of 7 μm with a corresponding field size of 1500 μm . This analysis enables to determine the modal mineralogy, degree of liberation of sulfides and carbonates, elemental deportment, mineral association and mineral textures, per fraction. Finally, the mineralogical reconciliation was conducted using all the chemical and mineralogical analysis data.

D.3 Results and discussion

D.3.1 Physical and chemical characterization

The physical properties of the head sample are presented in Table D.1. The particle size distribution of the head sample, considering 50mm as the maximum particle size, was $D_{90} = 46847 \mu\text{m}$. The specific gravity (Gs) was 2.67 g/cm^3 , typical Gs of a porphyry copper ore. The Chemical assays of the WR per fraction are shown in Table D.1. The dominant elements were Si, Al, Ca, Cu, Fe, K, Mg, Na, P, and Ti, which are related to NSG minerals. The average concentration of five fractions were: Si (18 wt %), K (2.19 wt %), Mg (1.53 wt %), Al (6.18 wt %), Ca (5.13 wt %), and Ti (0.86 wt %). Cu and P in all samples did not exceed 0.2 and 0.24 wt %, respectively. The average concentration of Fe was 5.6 wt %, where F2, F3, and F4 were enriched in Fe. Concentrations of As, Pb, Ni, and Mo were very low, considered negligible.

The total S and C contents show that the WR has a low carbon content. The carbon content did not exceed 0.2 wt % in all fractions. On the other hand, the analysis of the S_{total} was higher than expected due to the high presence of sulfates in this WR (see Table D.1). Thus, it was necessary to measure the S_{sulfate} , which enabled us to know the proportion related to S_{sulfide} (see Table 1). Then, the subtraction of S_{total} from S_{sulfate} permitted to get the S_{sulfide} . The S_{sulfide} is relatively high in all fractions, and it was enriched for F2 (5.46 wt %) and F3 (6.92 wt %). These results are in accordance with the ICP- MS analysis, where iron content was significant, and it could be associated with the sulfide. The copper could contribute to this high sulfide content as well.

In general, the chemical analyses suggest that the neutralizing potential (NP) of this WR could be negligible due to the low content of carbon. Besides, the high amount of Fe and sulfide in all fractions suggest that this WR could have high acid generation potential (AP). Comparing these results with the mineralogical characterization will be necessary to see the relationship between the high Fe and sulfide content with the mineral degree of liberation and mineral association.

Table D.1. Physical, chemical, and mineralogical results of waste rock

Physical properties (Head sample -50mm to +5mm)	Diameter (μm)	D ₉₀	D ₆₀	D ₃₀	D ₁₀	
			46847	14458	3318	246
	Specific gravity (GS) (g/cm ³)	2.67				
Sample <5mm	Fractions					
Chemical analysis (ICP-MS) (wt %)	Element	F1	F2	F3	F4	F5
	Al	6.0	4.7	5.9	6.8	7.5
	Ba	0.01	0.02	0.01	0.02	0.02
	Ca	8.5	10.8	6.0	5.2	4.1
	Cu	0.2	0.2	0.2	0.2	0.2
	Fe	3.8	5.6	7.5	5.7	5.2
	K	2.1	1.6	2.1	2.5	2.7
	Mg	1.7	1.3	1.4	1.6	1.7
	Mn	0.09	0.08	0.09	0.09	0.09
	Na	0.5	0.2	0.3	0.3	0.4
	P	0.1	0.08	0.08	0.1	0.1
	Sr	0.06	0.05	0.04	0.04	0.03
	Ti	0.1	0.1	0.1	0.2	0.2
	V	0.01	0.009	0.01	0.01	0.02
	Zn	0.04	0.05	0.05	0.07	0.05
	As	0.0005	0.0006	0.0006	0.0005	0.0003
	Mo	0.0059	0.0054	0.0044	0.0059	0.0030
	Ni	0.0010	0.0018	0.0068	0.0103	0.0021
	Pb	0.0152	0.0182	0.0162	0.0164	0.0135
	Si	15.4	13.0	17.7	20.7	23.2
S/C analysis (wt %)		F1	F2	F3	F4	F5
	C _{total}	0.19	0.20	0.20	0.18	0.15
	S _{total}	8.90	13.99	11.58	7.76	6.07
	S _{sulfate}	6.73	8.53	4.66	3.87	2.94
	S _{sulfide}	2.17	5.46	6.92	3.89	3.13
XRF (wt %)	Oxides	F1	F2	F3	F4	F5
	Al ₂ O ₃	11.25	8.83	11.33	12.78	13.9
	CaO	12.30	16.22	9.06	7.64	6.04
	Cr ₂ O ₃	<0.01	<0.01	0.02	0.03	<0.01
	Fe ₂ O ₃	5.94	8.81	11.91	8.89	7.94
	K ₂ O	2.38	1.74	2.44	2.80	3.07
	MgO	2.89	2.2	2.56	2.78	2.94
	MnO	0.13	0.10	0.12	0.12	0.13
	Na ₂ O	0.60	0.29	0.40	0.48	0.55
	P ₂ O ₅	0.22	0.18	0.20	0.21	0.23
	SiO ₂	32.89	27.73	37.77	44.21	49.62
	TiO ₂	0.70	0.66	0.77	0.87	0.96
	V ₂ O ₅	0.03	0.02	0.03	0.03	0.04
	LOI	14.67	14.20	16.31	13.53	11.68
XRD (wt %)	Mineral	F1	F2	F3	F4	F5
	Quartz	16.0	15.65	22.55	26.15	29.95
	Clinocllore	13.0	8.6	11.45	13.7	14.5
	Muscovite	20.8	14.0	20.8	24.0	26.7
	Albite	2.5	1.1	1.6	2.0	2.2
	Anorthite	1.4	3.9	2.75	3.8	3.8
	Orthoclase	2.0	1.0	0.2	0.2	0.2
	Rutile	0.47	0.44	0.52	0.6	0.67
	Chalcopyrite	0.51	0.67	0.54	0.48	0.5
	Pyrite	3.67	9.78	12.6	7.0	5.55
	Anhydrite	36.3	45.78	25.0	20.66	15.75

D.3.2 Mineralogical characterization

D.3.2.1 Bulk mineralogy

The XRF results (see Table D.1) show that the five fractions have significant elements reported in oxide form. These results agreed with those obtained from ICP-MS. The average concentration of five fractions was: silicon (SiO_2) with 38.4 wt %, calcium (CaO) with 10.25 wt %, aluminum (Al_2O_3) with 11.61 wt %, and iron (Fe_2O_3) with 8.7 wt %. Other elements, such as potassium (K_2O) and magnesium (MgO) did not exceed 3 wt %. Other elements with remarkable proportions were titanium (TiO_2) with 1 wt %, phosphorus (P_2O_5), and sodium (Na_2O) with 0.3 and 0.6 wt %, respectively. The XRD results for the five fractions (F1 to F5) are shown in Table D.1. The WR was mainly composed of quartz, muscovite, chlorites (clinochlore), feldspaths (albite, anorthite, orthoclase), oxides (rutile), sulfates (anhydrite), and sulfide minerals, notably pyrite (enriched in all fractions) and chalcopyrite. The mineralogical reconciliation was conducted using the chemical analysis (S/C_{total} , S_{sulfate} , S_{sulfide} , ICP-MS, XRF) and the mineralogical analyses (XRD). The XRD was complemented with the modal composition given by QEMSCAN. Due to the detection limit of the XRD (1-5%), some minerals were not identified by XRD but by QEMSCAN (see Table D.1 and Figure D.3).

The QEMSCAN results show that the modal mineral assemblage in all five samples is defined by quartz, muscovite, and anhydrite, on average exceeding 20 wt %. Clinochlore and pyrite exceed 5 wt % on average, orthoclase and anorthite exceed 3 wt % on average, albite does not exceed 3.6 wt % on average, and kaolinite exceed 1 wt % on average. The minerals apatite, rutile, chalcopyrite, magnetite, and sphalerite are present but do not exceed 1 wt %. Stibnite, covellite, other minerals (unclassified Si-bearing phases), pyrrhotite, chalcocite, amphibole, galena, and bornite are present in trace quantities, not exceeding 0.1 wt % (Figure D.3). The sulfide mineralogy is dominated by pyrite, chalcopyrite, sphalerite, stibnite, covellite, pyrrhotite, chalcocite, galena, and bornite in decreasing abundance. Pyrite is the only sulfide that exceeds 1 wt %. Chalcopyrite, sphalerite, and covellite exceed 0.1 wt %, whereas pyrrhotite, chalcocite, galena, and bornite do not exceed 0.1 wt % (Figure D.3). The carbonates do not exceed 0.3 wt % on average. The total of carbonate minerals was expected to be low (dolomite, calcite, and magnesite). Ca sulfate phases measured were all interpreted

to be anhydrite based on totals acquired. These results are in accordance with the ICP-MS analysis since the Al, Ca, Fe, K, Mg, and Si contents of the five fractions explain well the abundance of anhydrite quartz, muscovite, pyrite, and clinocllore minerals. The elemental department of the minerals Fe, Ca, Cu, and S was calculated and will be further explained.

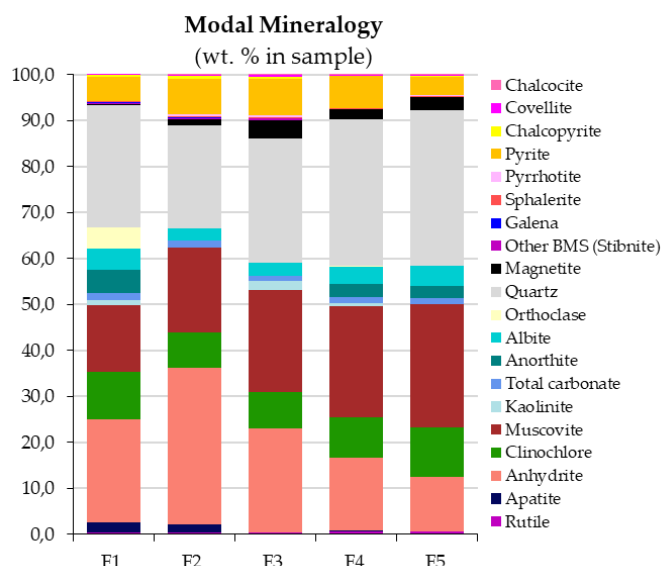


Figure D.3. Reconciled modal composition of WR per fractions.

According to the modal mineralogy, anhydrite is the main S carrier in the samples representing a total S mass % department of 48.7 to 62.5 %. This corresponds to grades of 3.5 to 9.4 % S. Additionally, pyrite is the second major S carrier representing 29.7 to 47.7 % of total S mass at grades of 2.2 to 6.6 wt % S. This mineral may represent an environmental challenge. It is expected that the ABA result will classify the WR as potentially acid generating due to the high content of pyrite. As a function of total S grade, chalcopyrite, sphalerite, covellite, stibnite, pyrrhotite, chalcocite, galena, carbonate, bornite, apatite, and anhydrite carry important amounts of S (Figure D.4). The pyrite sulfide department by fractions were: F1 (2.18 wt %), F2 (5.47 wt %), F3(6.91 wt %), F4 (3.89 wt %), and F5(3.13 wt %) (Figure D.4). In all cases, there is a high sulfide content, but F2 and F3 were enriched, suggesting these two fractions as the particle sizes where the AMD generation could be higher.

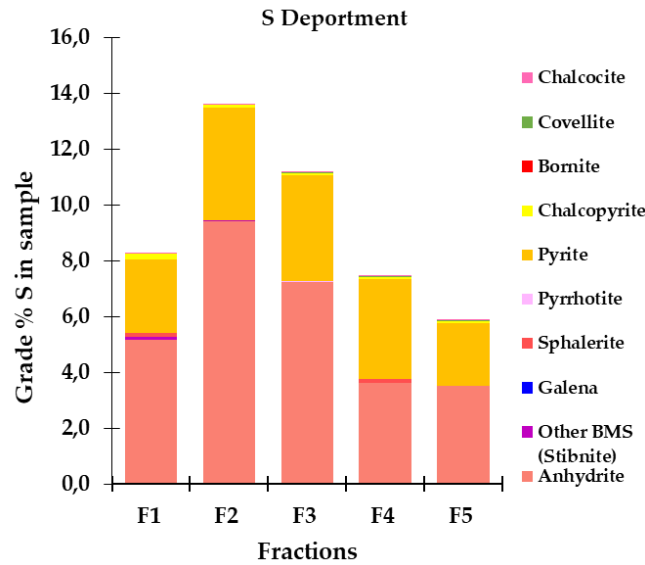


Figure D.4. S department per fractions.

Figure D.5 shows that the greatest abundance of total calcium is carried in anhydrite (77.2 to 92.6 %) with grades of 3.2 to 10 % Ca. Additionally, anorthite represents the second largest abundance (4.2 to 11.1 %), followed by carbonate (dolomite + calcite, 1.1 to 7.1 %) and apatite (1.7 to 4.9 %). These minerals represent Ca grades of 0.4 to 0.5 %, 0.1 to 0.3 % and 0.1 to 0.4 % Ca respectively. (Figure D.5). It can be concluded that the NP of the WR will be negligible due to the low content of carbonates (0.1 to 0.3 %).

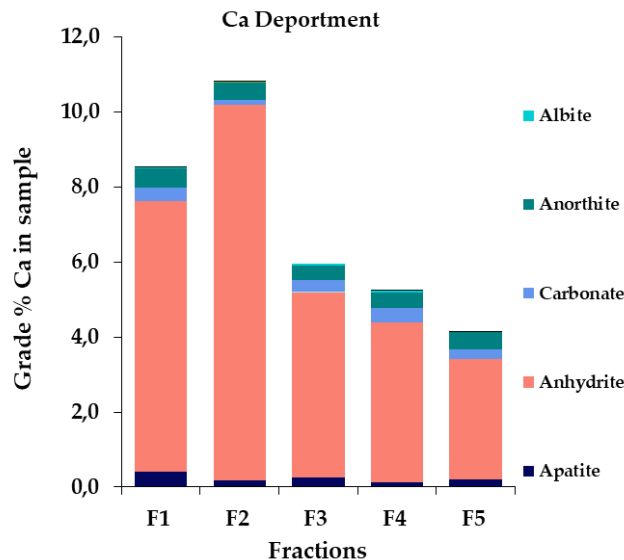


Figure D.5. Ca department per fractions.

Figure D.6 shows the comparison between the total sulfide and carbonate of the WR, which hints that all fractions will likely produce AMD. Nevertheless, this conclusion must be analyzed in conjunction with the minerals' degree of liberation to consider the surface exposure of the mineral per fraction, as well as to conduct the ABA test to get the DPLS.

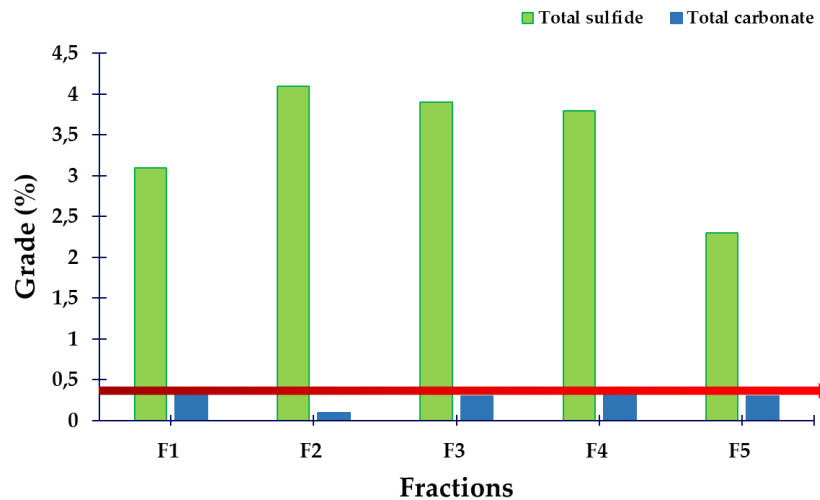


Figure D.6. Total sulfide and carbonate per fractions.

D.3.2.2 Relationship between pyrite degree liberation, ABA test, and textural analysis per fraction.

To assess and simplify liberation, individual pyrite, chalcopyrite, anhydrite, and carbonates, are presented in Figure D.7. Liberation in this context is defined as particles with greater than 95 % of their surface area exposed. The chalcopyrite is generally poorly liberated in the samples. Apart from F1 where chalcopyrite was 97 % liberated, the liberation degree of chalcopyrite decreases with an increase in particle size from F1 to F5. Pyrite was better liberated than chalcopyrite. F1 and F2 have high liberation of 96% and 92 % for both fractions, respectively. A decreasing degree of liberation is observed with an increase in particle size. Nevertheless, pyrite keeps higher liberation than chalcopyrite until F4 with around 50% of liberation. From these results, it can be concluded that from F1 to F4, acid generation is probable. F5 had only 9 % of liberation (it could be considered negligible), so this fraction could be non-acid generating; ABA tests will confirm this. Anhydrite is generally well liberated. Maximum liberation for this mineral is 93 %, and the minimum is 65 %. The same behavior was identified as liberation decreases with an increase in particle

size (see Figure D.7). Carbonate is well liberated; this mineral's maximum liberation is F1 (75%) and F2 (67%), and the minimum is 23 %. Despite the carbonates showing good liberation in F1 and F2, there is not enough carbonate available to be considered in the NP calculation. Also, F3 has the lower carbonate liberation (23%), with a pyrite liberation of around 69.2 %; therefore, AP is higher than NP, and the likelihood of acid generation is high.

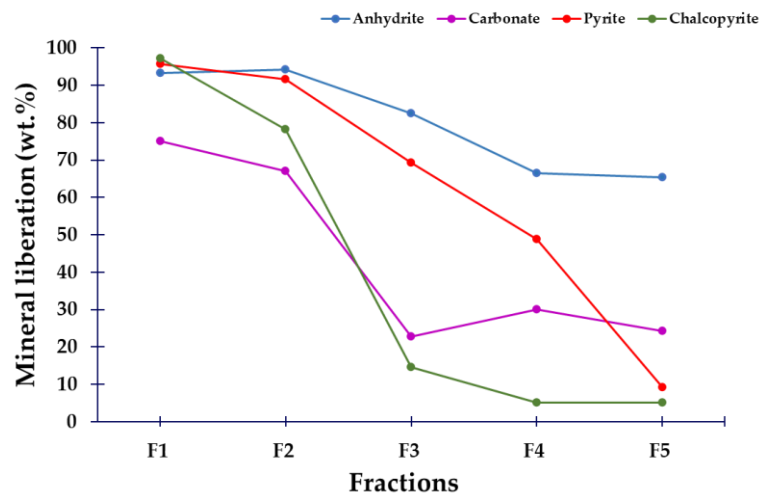


Figure D.7. Minerals liberation degree per fractions.

Prediction of acid generation potential for the five fractions was performed using the method proposed by Elghali et al. (2018) to calculate AP considering sulfide liberation and the method proposed by Lawrence, R. W., & Wang, 1997 to calculate NP. The ABA test results are shown in Figure D.8. The results using the NNP criterion show that most samples are acid-generating (F1 to F4), and F5 was in the uncertainty zone. In the case of the NPR criterion, F1 to F4 are considered potentially acid generating as well, but F5 is classified as non-acid generating. These results were expected due to the high pyrite content and its high degree of liberation of pyrite, combined with low carbonates content in the WR, as discussed in section 3.2.1. Table D.2 summarizes the results obtained.

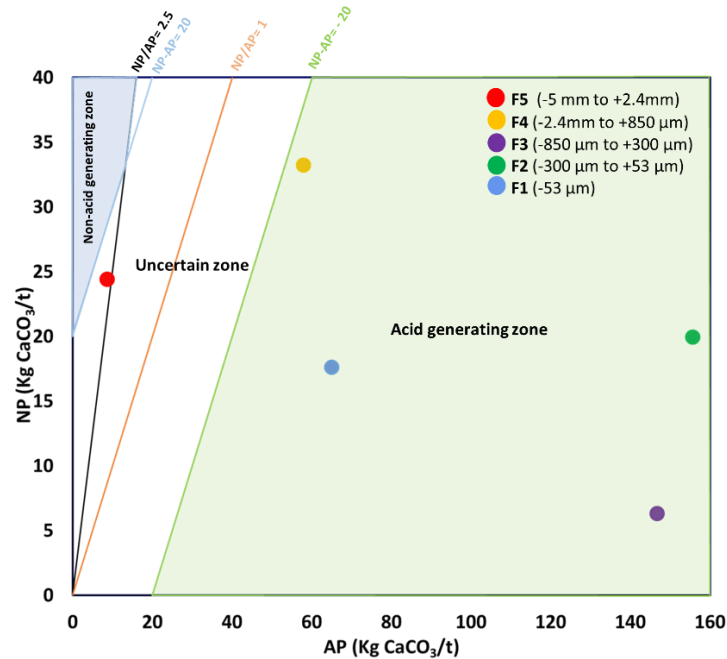


Figure D.8. ABA test results per fractions.

Nevertheless, although most of the fractions were in the AP generation category, the F2 and F3 have higher NNP and lower NPR than F1 and F4. Therefore, it seems like the DPLS for the WR is < 2.4mm (F4). However, as F5 was in UZ for NNP analysis and Non-AG in the NPR analysis, this introduces some uncertainty in defining the DPLS.

Table D.2. ABA test results

Fractions	AP (kg CaCO ₃ /t)	NP (kg CaCO ₃ /t)	NNP (kg CaCO ₃ /t)	NNP (RESULT)	NPR	NPR (RESULT)
F1	65.16	17.6	- 47.57	AG*	0.27	AG
F2	155.74	19.9	-135.82	AG	0.13	AG
F3	146.82	6.3	-140.52	AG	0.04	AG
F4	58.01	33.2	-24.82	AG	0.57	AG
F5	8.70	24.4	15.74	UZ	2.81	Non-AG

*AG (acid generating), UZ (uncertainty zone), and Non-AG (non-acid generating)


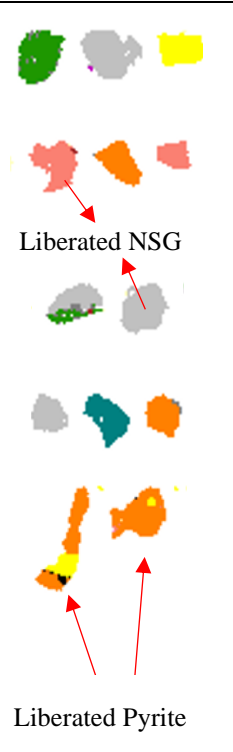
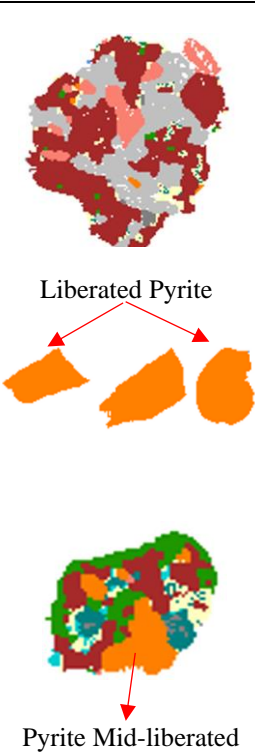
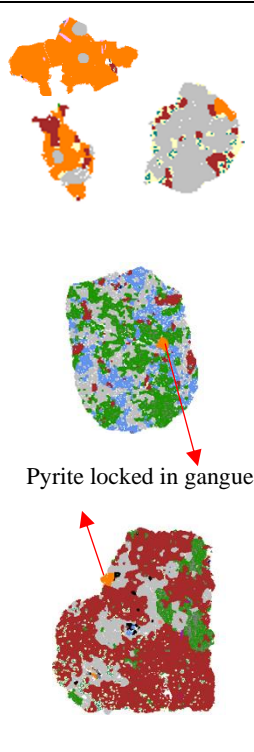
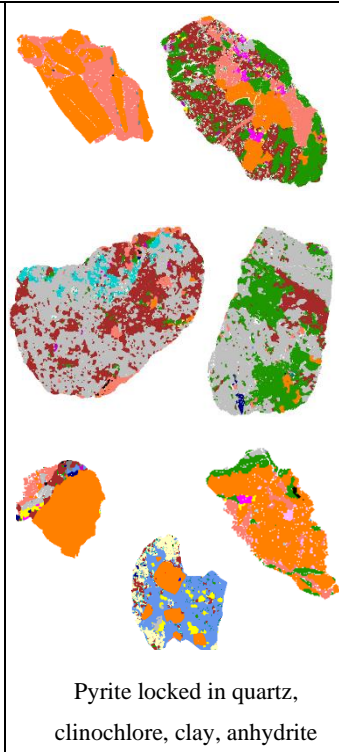
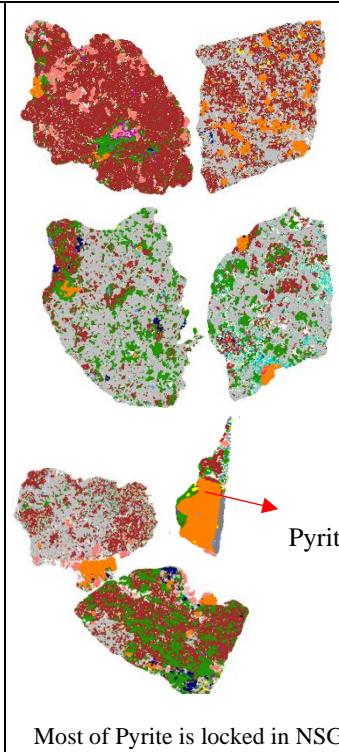
The mineralogical association has an essential role in conjunction with the liberation degree in the environmental assessment of WR. Table D.3 shows the particle sizes mapping of different textures of pyrite and chalcopyrite and their mineral association. The analysis of mineral texture and mineral association is divided into “liberated” when the mineral surface

area exposed is greater than 95 %. “Binaries” represent particles where >90% of the particle area is composed of the mineral of interest and Cu minerals, FeS, oxide, carbonate, silicate, anhydrite, or other. “Complex” particles represent particles with >90% of the particle area composed of three or more mineral phases, including the mineral of interest. These different textures were found among all five fractions.

F1 shows that all the particles, either pyrite, chalcopyrite, or NSG, are liberated by over 95 %. Pyrite binaries associated with copper are observed in well-liberated sample F1. This analysis is in accordance with the liberation degree in this fraction and with the ABA test, given that F1 is AG. F2 shows well-liberated pyrite, the chalcopyrite presence was less evident than in F1, and pyrite is better liberated than the chalcopyrite. Complex associations with chalcopyrite, including quartz, anhydrite, pyrite, and other NSG minerals, start appearing in this fraction. However, the degree of liberation of pyrite in F2 remains high (92%). F3 also shows well-liberated pyrite. Some binaries of pyrite with silicate, anhydrite, or other NSG were observed, as well as complex associations with quartz, anhydrite, clinocllore, and mica (muscovite), which are not limited to this WR fraction.

In overall conclusion, as the particle size increase, the pyrite has a stronger binary association with silicate and anhydrite and lower overall complex associations. This result has a direct relation with the degree of liberation, which was lower for fractions F4 and F5. Also, the ABA test reflects the effect of diminishing particle size liberation. It is worth mentioning that in the case of F4, the liberation degree was around 50%, and the mapping images show that even if the particles are coarser, there are also many pyrite particles that are almost liberated (see Table D.3, F4), which is a reason why F4 could be AG as well, according to the ABA test. Finally, the ABA test for F5 indicates uncertainty due to its different classification depending on the criteria (Non-AG with NPR or UZ with NNP). It could be explained using the mapping image for F5. Knowing that the liberation degree is around 9%, some pyrite particles are partially liberated, which could provoke AMD due to the high content of pyrite in this fraction (4 wt %) (see Figure D.3).

Table D.3. Textural analysis per fraction, relationship between pyrite degree liberation and ABA test.

Fractions	F1	F2	F3	F4	F5
	 <p>Liberated NSG</p> <p>Liberated Pyrite</p>	 <p>Liberated Pyrite</p> <p>Pyrite Mid-liberated</p>	 <p>Pyrite locked in gangue</p>	 <p>Pyrite locked in quartz, clinocllore, clay, anhydrite</p>	 <p>Pyrite</p> <p>Most of Pyrite is locked in NSG</p>
Pyrite liberation (wt. %)	95.7	91.6	69.2	48.8	9.1
ABA test	AG*	AG	AG	AG	UZ

*AG (Acid generating), UZ (Uncertain Zone)

D.4 Conclusions

The WR characterization by particle size fraction enables the identification of the DPLS of the WR, and provides information to help control AMD generation. Mineral characterization plays an essential role in assessing and predicting AP and NP since mineral associations, liberation degree, and mineral abundance in the WR significantly impact the AMD generation potential. It is worth mentioning that different works have been conducted using this methodology for other types of ores. Because ores and waste rock differ a lot in composition from one to another, each mining operation should implement a complete characterization as the first step of AMD assessment.

In this work, it was determined that the DPLS was $< 2.4\text{mm}$. The most problematic mineral was pyrite (high sulfide content and liberation degree), which was identified from F1 to F4. Nevertheless, F5 indicated uncertainty due to NNP giving uncertain acid generation potential, and NRP yielded non-acid generating. Therefore, these results must be corroborated by conducting kinetic tests of F5. On the other hand, the WR does not have intrinsic NP, since the carbonate content was low (maximum 0.3%). Therefore, the NP was measured directly using the method proposed by Lawrence and Wang (1997), and the concentrations obtained per fraction were not enough to significantly impact the NP. This could be one of the reasons why WR could be acid generating in almost all the fractions studied. Finally, introducing the parameter sulfide liberation (L_{sulfide}) in the AP calculation enabled to have a mineral texture indicator more accurate of the studied WR.

D.5 Ongoing research

Based on the concept of cleaner production, the assessment and prediction of AMD for WR (Chilean porphyry copper mine) in an early stage of the WR processing enable sustainability and lower operational costs. Therefore, reducing the sulfides' reactivity in the WR is necessary before deposition in the stockpile. Also, the valorization of WR can be a good approach in searching for alternative sources of valuable metals. This work identified copper (0.2%) and titanium (0.3%) as metals with economic value present in the WR. Accordingly, the desulfurization of WR using a flotation process is an alternative to treating the WR before stockpiling. However, an appropriate flotation technology must be considered to account for the large WR particle size. Ongoing work uses the fluidized bed flotation technology (hydrofloat), which allows the flotation of coarse particles larger than $250\ \mu\text{m}$, to separate sulfides from gangue minerals and reduce the acid

generation potential. The DPLS enables to know the particle size from which the WR must be desulfurized. Nevertheless, there is an issue concerning to the limit of particle size that can be floated using this technology. The size fraction that cannot be desulfurized will be evaluated using the kinetic test to orient decisions about how it should be stored.